1-1-1975

Static and dynamic studies of molecular orientation of semicrystalline polyethylene.

Su Don Hong
University of Massachusetts Amherst

STATIC AND DYNAMIC STUDIES OF MOLECULAR ORIENTATION OF SEMICRYSTALLINE POLYETHYLENE

A Dissertation Presented

By

Su Don Hong

Submitted to the Graduate Schcol of the
University of Massachusetts in partial fulfillment
of the requirements for the degree of

DOCTOR OF PHILOSOPHY

August 1975

Major Subject: Polymer Science & Engineering

STATIC AND DYNAMIC STUDIES OF MOLECULAR ORIENTATION OF SEMICRYSTALLINE POLYETHYLENE

A Dissertation

By

Su Don Hong

Approved as to style and content by:

R. S. Stein, Chairman of Committee

R. S. Porter, Member

W. J. MacKnight, Member

R. S. Porter, Head Department

August, 1975

DEDICATION

To my parents
who made many sacrifices for the
fulfillment of my education.

ACKNOWLEDGMENT

I wish to express my sincere thanks to Professor Richard S. Stein, thesis advisor, for his invaluable guidance, his continual inspiration and encouragement during the course of this work.

I also wish to extend my gratitude to the other members of my thesis committee, Professor Roger S. Porter and Professor William J. MacKnight, and Professor Fraser P. Price and Professor Howard D. Stidham who served on the committee before their sabbatical leave, for their invaluable comments and suggestions.

Appreciation is extended to Mr. Y. Uemura for his help during the first stage of the dynamic infrared experiment, Dr. Pierre Labarbe and Mr. Stanley Baczek for the LAXS measurements, Dr. John Maxfield for part of the IR measurements, Dr. Andrzej Wasiak for his help in light scattering measurements and Messrs. Daniel A. Keedy, Walter E. Clark and Roland LaBonte for their kind and coorperative technical assistance. Thanks also go to my colleagues in the Polymer Science and Enginnering Department for many helpful discussions, and for their collaboration in some of the work described in this thesis. In particular the x-ray results presented in Chapter 4 were made by Mr. Dennis Peiffer.

The author is grateful to the National Science Foundation and the Army Research Office (Durham) for financial support in the form of a research assistantship held by him during his course of study.

STATIC AND DYNAMIC STUDIES OF MOLECULAR ORIENTATION OF SEMICRYSTALLINE POLYETHYLENE

Su Don Hong, B.S., National Taiwan University

M.S., University of Waterloo

Directed by: Dr. Richard S. Stein

ABSTRACT

Values of the anisotropy of polarizability of methylene groups deduced from the refractive indices of n-paraffin crystals differ appreciably from those obtained from gas or liquid phase measurements. The differences are attributed to the erroneous application of the Lorenz-Lorentz internal field to the anisotropic crystal. A more detailed calculation of the internal field is carried out by detailed summation of the dipolar field over an idealized n-paraffin crystal in which the molecular chains are replaced by anisotropic rods. Based upon reasonable values of parameters and assumed crystal shape, the discrepancy in polarizability anisotropy is resolved.

The values of segment polarizability anisotropy obtained from the stress-optical coefficients for undiluted rubber networks are higher than those obtained for diluted rubber networks. The effect of swelling solvent on the stress-optical coefficient can be interpreted in terms of its role in separating chains from each

other and in itself being oriented by the polymer chain. The enhancement of the stress-optical coefficient for undiluted networks arises in part from mutual orientation of segments by their neighbors and in part from the anisotropy of the internal field arising from local order. All of these effects are interpretable in terms of relatively short range interactions and do not require the relatively long range ordering of a type proposed in some recent theories.

The effects of birefringence and internal field on optical dichroism was examined by solving the Maxwell's equation. The solution was applied to three morphologically different samples: (1) Single crystals, (2) Amorphous polymer and (3) Polycrystalline polymer for the consideration of the effect. The correction factors have been obtained and the processes of correction have been discussed.

The change in crystallinity accompanying stretching and the dynamic crystallinity change accompanying small amplitude variation have been followed by a modification of an x-ray method proposed for uniaxial orientation by Ruland. The change in crystallinity accompanying stretching and during relaxation at constant length have also been followed by infrared technique using crystalline sensitive bands. It was found that there was no significant variation in crystallinity up to 80 % sample elongation for both slowly and rapidly stretched samples. The infrared studies also found negligible changes in rotational isomer population.

The relationship between the molecular orientation and stress-strain relationship of polyethylene samples having different

morphology were investigated. It was found that, for the low density polyethylene which had spherulitic superstructure, stretching the quenched sample resulted in higher crystalline orientation and lower amorphous orientation as compared with the slowly cooled sample; while the medium density polyethylene, which had rodlike superstructure, gave rise to rather peculiar amorphous orientation. This orientational behavior of polyethylene was discussed in terms of the Yoon-Stein theory for crystalline orientation and the theories developed by Petraccone et al and Flory and Abe for the amorphous orientation. The stress-strain relationship was discussed with consideration of molecular orientation and deformation mechanisms.

The molecular orientation for quenched low density polyethylene during and after rapid stretching was investigated using infrared dichroism and birefringence techniques. It was found that for samples stretched at rates less than 500 % sec^{-1} the molecular orientation, as shown by infrared dichroism and birefringence, could follow the strain without any delay, but for samples stretched at rates in the range of 1100 % sec^{-1} and 1400 % sec^{-1}, the molecular orientation lagged the strain by about 10 msec for samples stretched about 40 %. The stress relaxation for samples stretched at a rate of 380 % sec^{-1} was measured. It was concluded that molecular orientation was not associated with stress relaxation. Various mechanisms of stress ralaxation were discussed.

TABLE OF CONTENTS

GENERAL INTRODUCTION

There has been great deal of work reported on the mechanical properties of crosslinked rubbery polymers and linear amorphous polymers (1-11). It has been found that, at small elongations and at temperatures above the glass transition of the polymers, a universal master curve can be obtained for stress relaxation data of amorphous polymers (3-8), and for dynamic properties of polymer solutions and bulk polymers (2,9-11) by applying the principle of time-temperature superposition. The master curves were obtained by using a reduced variable in place of time or frequency. The reduced variable, in turn, was obtained by dividing the time by a shift factor for relaxation data and by multiplying the frequency by the shift factor for dynamic data. Through use of the Doolittle equation (12) for the viscosity of liquids and the introduction of the concept of free volume, Williams, Landel and Ferry (WLF) (2) showed that the shift factor can be expressed as a function of temperature, in combination with the glass transition temperature and free volume of the polymer. Time-temperature superposition is also applicable to the glassy amorphous polymers provided that all the relaxation times concerned with a particular type of motion have the same temperature dependence (13-15). The temperature dependence of the shift factor follows an Arrhenius-type equation, with an

apparent activation energy independent of temperature (15). In general, a single shift factor will not be expected to apply for the entire spectrum in the glassy state because of the variety of molecular motions (16).

When the birefringence of amorphous polymers was measured along with the stress as a function of time, it was found that the stress-optical coefficient was independent of time (17). This can be explained on the basis of normal modes of motion of amorphous polymers (18,19), in which each of these normal modes has a characteristic relaxation time, and it can be shown that the stress-optical coefficient for each normal mode is identical (20).

Crystalline polymers show quite different behavior from those of amorphous polymers. The mechanical behavior are highly dependent on degree of crystallinity (21,22) and morphology of the polymer (23). The relaxation spectra are very broad compared to those of amorphous polymers and they are different for samples of different crystallization conditions (24). In general, many loss mechanisms are observed in the supposed rubbery regions and several shift factors, instead of a single one as in the case of amorphous polymers, are needed to obtain a master curve (25-33). The relaxation modulus or creep compliance changes within a quite narrow range and nothing

like the primary transition of the amorphous polymers is observed for highly crystalline polymers (21,23). As the degree of crystallinity decreases, the magnitude of the relaxation modulus diminishes and it changes more steeply with changes in temperature or frequency, and the transition zone corresponding to the primary transition in amorphous polymers appears (34,35).

Measurements of birefringence of crystalline polymers as a function of time (or frequency) and temperature again reveal the complicated behavior of these polymers. Multiple loss mechanisms are observed and horrizontal as well as vertical shift factors are needed to obtain a master curve (36-39). The shift factors generally follow a Arrhenius-type equation, which indicates that free volume is not a governing factor for activation energy.

This complicated behavior of crystalline polymers is attributable to the complexity of morphology of these materials. The current prevalent view concerning the morphology of crystalline polymers is that they can be represented as two-phase systems, in which crystals are interconnected by rubber-like amorphous phases (40-43). This concept of the two-phase model has gained more support in light of recent experimental observation on polymer single crystals as well as on bulk polymers. The most direct evidence come from the observations that both

polymer single crystals (44-47) and bulk polymer (48) have regions removable by nitric acid, indicating the existence of regions of selective reactivity. Further evidence from the absolute x-ray scattering power (49,50), from the correlation of density and long period of single-crystal mats (51) as well as from the observations of disappearance of an infrared absorption band arising in crystalline regions (52,53) and of the different orientation behaviors of chain segments supposedly residing in crystalline and amorphous regions, respectively, of bulk polymer (54) also point to the validity of the two-phase concept. Although most of these observations are made on single crystals, the postulation that the bulk crystalline polymers have similar morphology comes as a result of the observations in which from increasingly more concentrated solution (55) and from paraffin solutions of polyethylene (56) as well as from melts in the form of very thin films (46,56-58) all reveal the existence of single-crystal-type objects. The submicroscopic entities left from the selective oxidation of bulk polyethylene (48) also have the single-crystal-type texture.

There are different models proposed to describe the structure of crystalline polymers. Among them, Hosemann's kink model (62) represents an attempt to build a unified model to describe the polymer materials in all states; while the model

proposed by Keller (43) is based on the observations accumulated on polymer single crystals and embraces the concepts of regular fold surface and disordered one.

According to Keller's model, the crystals are lamellar; the polymer chains traverse the lamellae and fold back many times; the fold length depends on the crystallization temperature and thermal treatment. The amorphous regions consist of regular chain folds, large chain loops (irregular folds), chain ends (cilia) and tie chains which interconnect lamellae together. There also may be molecules which stay unattached to the crystals.

The crystalline units crystallized under the conditions of no external stress and of normal pressure are chain-folded lamellae. However when crystallized under stress or high pressure, they are extended-chain crystals (63-67). The crystals may, by repeated branching, lead to some sort of superstructure, like spherulitic or shish-kebab. It has been reported that the type of superstructure will affect the mechanical properties of the polymer (23). The crystal may not be entirely perfect, too. It is likely to contain such defects (42) as chain ends, kinks, jogs, chain torsions and isolated folds as well as disordered regions within the crystal. There are other kinds of defects like dislocations, twins and the mosaic block boundaries, etc. Some of these defects, like the mosaic block

boundaries (59,60) and the dislocations (61), may be responsible for some loss mechanisms observed in the crystalline polymers.

The viscoelastic properties of crystalline polymers will be related to their morphology, i.e. the structural elements in crystalline and amorphous regions, the topology of the individual phases, and the ultimate superstructure and so forth. Some of the loss mechanisms of crystalline polymers have been attributed to the motions of these structural elements.. For example, it has been suggested that the α loss peak of polyethylene results from the internal motion within the crystal as well as the motion of the chain folds on the surface (59,66,67), and the β loss peak from the interlamellar slip process (15,59).

The connections of the mechanical losses to the actual molecular motions of crystalline polymers, drawn from the viscoelastic functions observed under various conditions, are indirect inference and are not always without ambiguity. This is particularly difficult when the viscoelastic function is very complicated and it becomes necessary to resolve it into individual components representing particular molecular processes, because then one has to assume either homogeneous stress or homogeneous strain which in the real sample neither may be true (68-70). Thus it is desirable to have techniques

which could directly follow the motions of the structural elements in response to stress. For these reasons, various kinds of optical techniques have been devised (60,71-81) for direct measurements of molecular orientations.

This thesis presents some efforts made aiming at improving the fundamental basis for birefringence and infrared dichroism techniques, as well as at investigation of molecular orientation and relaxation of polyethylene crystallized under different conditions. Consequently, the thesis was literally organized into two parts: the first part including the first three chapters mainly deals with the theoretical endeavor, while the second part consisting of the rest three chapters is the experimental work looking into the morphology as well as the molecular orientation and relaxation of polyethylene.

Chapter 1 develops the theory of internal electric field polymer crystals. The theory represents an attempt to clarify the discrepancies concerning the optical anisotropy of methylene groups (CH_2) and presents a theoretical basis for the estimation of intrinsic birefringence of polymer crystals. The latter is of importance to the application of birefringence for investigation of molecular orientation because this may be the first theory of this kind. Chapter 2 is the application of the internal field theory to the explanation of stress-optical coefficient and ordering of amorphous polymers.

Chapter 3 investigates the effect of optical anisotropy of polymers on the optical dichroism; the theory supplements the theory developed by Fraser (82), which relates dichroic ratio and molecular orientation, and provides necessary corrections under special conditions. Chapter 4 investigates the change in crystallinity of low density polyethylene as a function of elongation and time. This represents an attempt to verify experimentally the assumption undertaken in almost all rheo-optical studies that the crystallinity of the polymer remains constant. Chapter 5 presents the investigation of the correlation between morphology, molecular orientation and stress-strain relation. While the relaxation behavior of polyethylene at various strain rates was presented in Chapter 6.

REFERENCES

1. L. R. G. Treloar, The Physics of Rubber Elasticity, Oxford, 2nd Ed., 1958.
2. J. D. Ferry, Viscoelastic Properties of Polymers, 2nd Ed., Wiley, 1969.
3. A. V. Tobolsky and R. D. Andrews, J. Chem. Phys., 13 3, (1945).
4. R. D. Andrews, N. Hoffman-Bang and A. V. Tobolsky, J. Polym. Sci., 3 669 (1948).
5. R. D. Andrews and A. V. Tobolsky, J. Polym. Sci., 7 221 (1951).
6. J. R. McLanghlin and A. V. Tobolsky, J. Colloid Sci., 7 555 (1952).
7. A. V. Tobolsky and J. R. McLanghlin, J. Polym. Sci., 8 543 (1952).
8. A. V. Tobolsky, Properties and Structure of Polymers, Wiley, New York, 1960.
9. J. D. Ferry, J. Am. Chem. Soc., 72 3746 (1950).
10. J. D. Ferry and E. R. Fitzgerald, J. Colloid Sci., 8 224 (1953).
11. J. D. Ferry, L. D. Grandine, Jr. and E. R. Fitzgerald, J. Appl. Phys. 24 911 (1953).
12. A. K. Doolittle and D. B. Doolittle, J. Appl. Phys., 28 901 (1957).
13. K. Sato, H. Nakane, T. Hideshima and S. Iwayanagi, J. Phys. Soc. Japan, 9 413 (1954).

14. S. Iwayanagi, J. Phys. Soc. Japan, 9 413 (1954).

15. N. G. McCrum and E. L. Morris, Proc. Roy. Soc., A281 258 (1964).

16. Y. Wada, Presented at 5th Intern. Cong. Rheology, Kyoto (1968).

17. R. S. Stein and A. V. Tobolsky, Textile Research J., 18 201, 302 (1948).

18. P. E. Rouse, J. Chem. Phys. 21 1272 (1953).

19. F. Bueche, J. Chem. Phys. 22 603 (1954).

20. B. E. Read, Polymer 3 143 (1962).

21. G. W. Becker, Kolloid-Z., 175 99 (1961).

22. M. Takayanagi, Pure and Appl. Chem., 15 555 (1967).

23. E. H. Andrews, Pure and Appl. Chem., 31 91 (1972).

24. S. Manabe, A. Sakoda, A. Katada and M. Takayanagi, Mem. Fac. Eng. Kyushu Univ., 28 277 (1969).

25. H. Nakayasu, H. Markovitz and D. J. Plazak, Trans. Soc. Rheology, 5 261 (1961).

26. K. Nagamatsu and Yoshitomi, J. Colloid Sci., 14 377 (1959).

27. K. Nagamatsu, T. Yoshitomi and T. Takemoto, J. Colloid Sci., 13 257 (1958).

28. S. Iwayanagi and H. Nakane. Proc. 5th Intern. Cong. Rheology, 3 203 (1968).

29. E. Catsiff, J. Offenbach and A. V. Tobolsky, J. Colloid Sci., 11 48 (1956).

30. J. A. Faucher, Trans. Soc. Rheology, 3 81 (1959).

31. K. Nagamatsu, Kolloid-Z., 172 141 (1960).

32. M. Takayanagi, Mem. Fac. Eng. Kyushu Univ., 23 No. 1, p41.

33. N. G. McCrum, B. E. Read and G. Williams, Anelastic and Dielectric Effects in Polymeric Solids, Wiley, New York, 1967.

34. K. Schemieder and K. Wolf, Kolloid-Z., 134 149 (1953).

35. N. G. McCrum, J. Polymer Sci., 34 355 (1959).

36. S. Onogi, T. Asada, Y. Fukui and T. Fujisawa, J. Polymer Sci., A2, 5 1067 (1967).

37. Y. Fukui, T. Sato, M. Ushirokawa, T. Asada and S. Onogi, J. Polymer Sci., A2, 8 1195 (1970).

38. S. Onogi, T. Sato, T. Asada and Y. Fukui, J. Polymer Sci., A2, 8 1211 (1970).

39. A. Tanaka, E. P. Chang, B. Delf, I. Kimura and R. S. Stein, J. Polymer Sci., A2 11 1891 (1973).

40. L. Mandelken, Crystallization of Polymers, McGraw-Hill, New York, 1964.

41. P. H. Geil, Polymer Single Crystals, Interscience, New York, 1963.

42. B. Wunderlich, Macromolecular Physics, Vol. 1, Academic Press, New York, 1973.

43. A. Keller, Rep. Progr. Phys., 31 623 (1968).

44. A. Peterlin and G. Meinel, J. Polymer Sci., B, 3 1059 (1965).

45. D. J. Blundell, A. Keller and T. Connor, J. Polymer Sci., A2,,5 991 (1967).

46. F. Winslow, M. Y. Hellman, W. Matreyek and R. Salovey, J. Polymer Sci., B, 5 89 (1967).

47. D. J. Blundel, A. Keller, I. M. Ward and I. J. Grant, J. Polymer Sci., B, 4 781 (1966).

48. R. P. Palmer and A. Cobbold, Makromolek. Chem., 74 174 (1964).

49. E. W. Fischer, H. Goddar and G. F. Schmidt, J. Polymer Sci., B, 5 619 (1967).

50. E. W. Fischer, H. Goddar and G. F. Schmidt, Proc. Conf. on Polymer Structure and Mechanical Properties, April, 1967 (U.S. Army, Natrick Laboratories, Natrick), pp. 148-182.

51. E. W. Fischer and G. F. Schmidt, Angrew. Chem., 74 551 (1969).

52. T. Okada and L. Mandelkern, J. Polymer Sci., A2, 5 239 (1969).

53. B. E. Read and R. S. Stein, Macromolecule, 1 116 (1968).

54. W. Glenz and A. Peterlin, J. Polymer Sci., A2, 9 1191 (1971).

55. D. C. Bassett, A. Keller and S. Mitsuhashi, J. Polymer Sci., A, 1 763 (1963).

56. H. D. Keith, J. Appl. Phys., 35 1270, 1286 (1964).

57. J. R. S. Waring and A. Keller, J. Polymer Sci., 17 447 (1955).

58. F. Danusso and F. Sabbioni, Rc. 1st Lomb. Sci. Lett. A, 92 435 (1958).

59. M. Takayanagi and T. Matsuo, J. Macromol. Sci., B1 407 (1967).

60. R. S. Stein, R. S. Finkelstein, D. Y. Yoon and C. Chang, J. Polymer Sci., Symposium No. 46, 15 (1974).

61. M. L. Williams, Ann. N.Y. Acad. Sci., 155 539 (1969).

62. R. Hosemann, J. Appl. Phys. 34 25 (1963).

63. A. J. Pennings and A. M. Kiel, Kolloid-Z. Polymere, 205 160 (1965).

64. P. H. Lindenmeyer, S. P. E. Trans., 4 1 (1964).

65. B. Lotz, A. J. Kovacs, G. Bassett and A. Keller, Kolloid-Z Polymere, 209 115 (1966).

66. K. H. Sinnot, J. Appl. Phys., 37 3385 (1966).

67. J. D. Hoffman, G. Williams and E. Passaglia, "Transitions and Relaxations in Polymers", J. Polymer Sci. C, 14, R. F. Boyer, Ed., Interscience, New York, 1966, pp. 173

68. K. Fujino, Y. Ogawa and H. Kawai, J. Appl. Polymer Sci., 8 2147 (1964).

69. M. Takayanagi, H. Harima and Y. Iwata, Mem. Fac. Eng. Kyushu Univ., 23, No. 1, p. 1 (1964).

70. M. Takayanagi, Proc. 4th Intern. Cong. Rheology, Part 1, Interscience, New York, 1965, p. 161.

71. R. S. Stein, in New Methods of Polymer Characterization, B. Ke, Ed., Interscience, New York, 1964, Chap. 4, pp. 155

72. R. S. Stein, Acc. Chem. Res., 5 121 (1972).

73. Y. Fukui, T. Asada and S. Onogi, Polymer J., 3 100 (1972).

74. S. Onogi and T. Asada, Prog. Polymer Sci., Japan, Vol. 2, pp. 261.

75. G. L. Wilkes, J. Macromol. Sci.-Revs. Macromol. Chem. C10 (2), 149 (1974).

76. V. J. McBrierty and I. M. Ward, Brit. J. Appl. Phys., 21 1529 (1968).

77. V. B. Gupta and I. M. Ward, J. Macromol. Sci., Phys., B4 (2), 453 (1970).

78. J. H. Nobbs, D. I. Bower, I. M. Ward and D. Patterson, Polymer, 15 287 (1974).

79. Y. Nishijima, Y. Onogi and T. Asai, J. Polymer Sci., C, 15 237 (1966).

80. J. Purvis, D. I. Bower and I. M. Ward, Polymer, 14 398 (1973).

81. R. S. Stein, J. Polymer Sci. C, 15 185 (1966).

82. R. D. B. Fraser, J. Chem. Phys., 24 89 (1956).

GENERAL INTRODUCTION TO CHAPTERS I AND II

The birefringence technique has been widely used in characterization of molecular orientation of amorphous polymers and crystalline polymers (1-4) as well as in the determination of crystallinity of crystalline polymers in their stretched state (5-8). This is made possible by the assumption of additivity of the birefringence of a multiphase system; thus the birefringence of a stretched crystalline polymer, Δ , can be described as follows (1,5)

$$\Delta = X_c \Delta_c + (1 - X_c) \Delta_a + \Delta_f \qquad (1)$$

where X_c is volume degree of crystallinity, Δ_c and Δ_a are the birefringence values of the crystalline and amorphous phases and Δ_f is the form birefringence. Form birefringence arises from the refractive index difference across the phase boundary between the phses. The value of Δ_f depends upon the refractive index difference between the two phases and upon the anisotropy of shape of the phase boundary (9). For polyethylene with spherulitic superstructure, the value of Δ_f is estimated to be 5 % to 10 % of the total birefringence (10,11).

For uniaxially oriental phases, the values of birefringence of the phases can be expressed in the form

$$\Delta_c = \Delta_c^\circ f_c \qquad (2)$$

$$\Delta_a = \Delta_a^\circ f_a \qquad (3)$$

where Δ_c° and Δ_a° are the intrinsic birefringence values of the perfectly oriented crystalline and amorphous phases, respectively. f_c and f_a are the orientation functions of the crystals and the amorphous phases, respectively where, for example, the orientation function of crystals is defined as (12)

$$f_c = \frac{3\langle \cos^2\theta_c \rangle_{av} - 1}{2} \qquad (4)$$

where θ_c is the angle between the optic axis of the crystal and the stretching direction.

The application of the birefringence technique to a crystalline polymer is possible if one can obtain the intrinsic birefringence of both phases from other sources. In principle, the intrinsic birefringence can be calculated by the methods of tensor additivity of bond polarizabilities (13,14) provided the bond polarizabilities and the internal field effect (see below) are known. It is the uncertain nature of the internal field effect which gives rise to the inconsistent values of bond polarizabilities on one hand, and, on the other hand,

to the contradictionary values of intrinsic birefringence of some polymer crystals; for instance, polypropylene has the same constituent chemical bonds as polyethylene, yet using the bond polarizabilities calculated from n-paraffin crystal to calculate its intrinsic birefringence, the calculated values is not in agreement with the experimental one (15).

The effect of internal field is illustrated in Fig. 1. The electric field of the incident radiation will disturb the distribution of electrons in the chemical bond and induce a dipole at each bond. The magnitude of the induced dipole depends on the bond polarizabilities and upon the electric field at the bond location. Moreover, the electric field at each bond, which is called the effective field, is the sum of the applied field, $\underset{\sim}{E}_o$, and the internal field, $\underset{\sim}{E}_{int}$, arising from the induced dipoles surrounding the particular bond in question. Thus the effective field, $\underset{\sim}{E}_j$, at bond j is given as

$$\underset{\sim}{E}_j = \underset{\sim}{E}_o + \sum_i E_{int,i} \qquad (5)$$

Therefore, the magnitude of the induced dipole moment of a sample will be affected by the internal field. Since the optical properties like refractive index are a measure of induced dipole per unit volume, the refractive index will depend on the internal field. For an anisotropic sample like a polyethylene crystal,

the internal field effect is also anisotropic, and this is one of the reasons which gives rise to different refractive indices along different crystallographic axes.

In Chapter I we try to develop a theory to estimate the internal field of polymer crystals, and to calculate the optical anisotropy of a methylene group in a polyethylene chain. The theory also provides a theoretical basis for the prediction of intrinsic birefringence of polymer crystals based on the knowledge of crystal structure, crystal size and shape, and bond polarizabilities.

REFERENCES

1. R. S. Stein and F. H. Norris, J. Polymer Sci., 21 381 (1956).
2. R. S. Stein, in Newer Methods of Polymer Characterization, B. Ke, Ed., Interscience, New York, 1964, Chapter 4, pp. 155.
3. R. S. Stein, R. S. Finkelstein, D. Y. Yoon and C. Chang, J. Polymer Sci., Symposium No. 46, 15 (1974).
4. G. L. Wilkes, J. Macromol. Sci. - Revs. Macromol. Chem., C10 (2), 149 (1974).
5. G. R. Taylor and S. R. Darin, J. Appl. Phys., 26 1075 (1955).
6. G. Kraus and J. J. Gruver, J. Polymer Sci., A2, 10 2009 (1972).
7. Y. Akana, Master Thesis, 1973, University of Massachusetts, Amherst, Mass.
8. M. Hashiyama, R. Gaylord and R. S. Stein, Macromol. Chem., in press.
9. O. Wiener, Abhandl. Kgl. Sachs Ges. Wiss., Math-Physik Klasse, 32 509 (1912).
10. D. Peiffer, C. Chang and R. S. Stein, J. Polymer Sci., Polym. Phys. Ed., 12 1441 (1974).
11. E. P. Chang, Ph.D. Thesis, University of Massachusetts, Amherst, Mass., 1973.
12. J. J. Hermans, P. H. Hermans, D. Vermaas and A. Weidynger, Rec. Trav. Chim. Pays-Bas, 65 427 (1946).

13. K. G. Denbigh, Trans. Faraday Soc., 36 936 (1940).

14. C. W. Bunn and R. D. P. Daubeny, Trans. Faraday Soc., 50 1173 (1954).

15. D. A. Keedy, J. Powers and R. S. Stein, J. Appl. Phys., 31 1911 (1960).

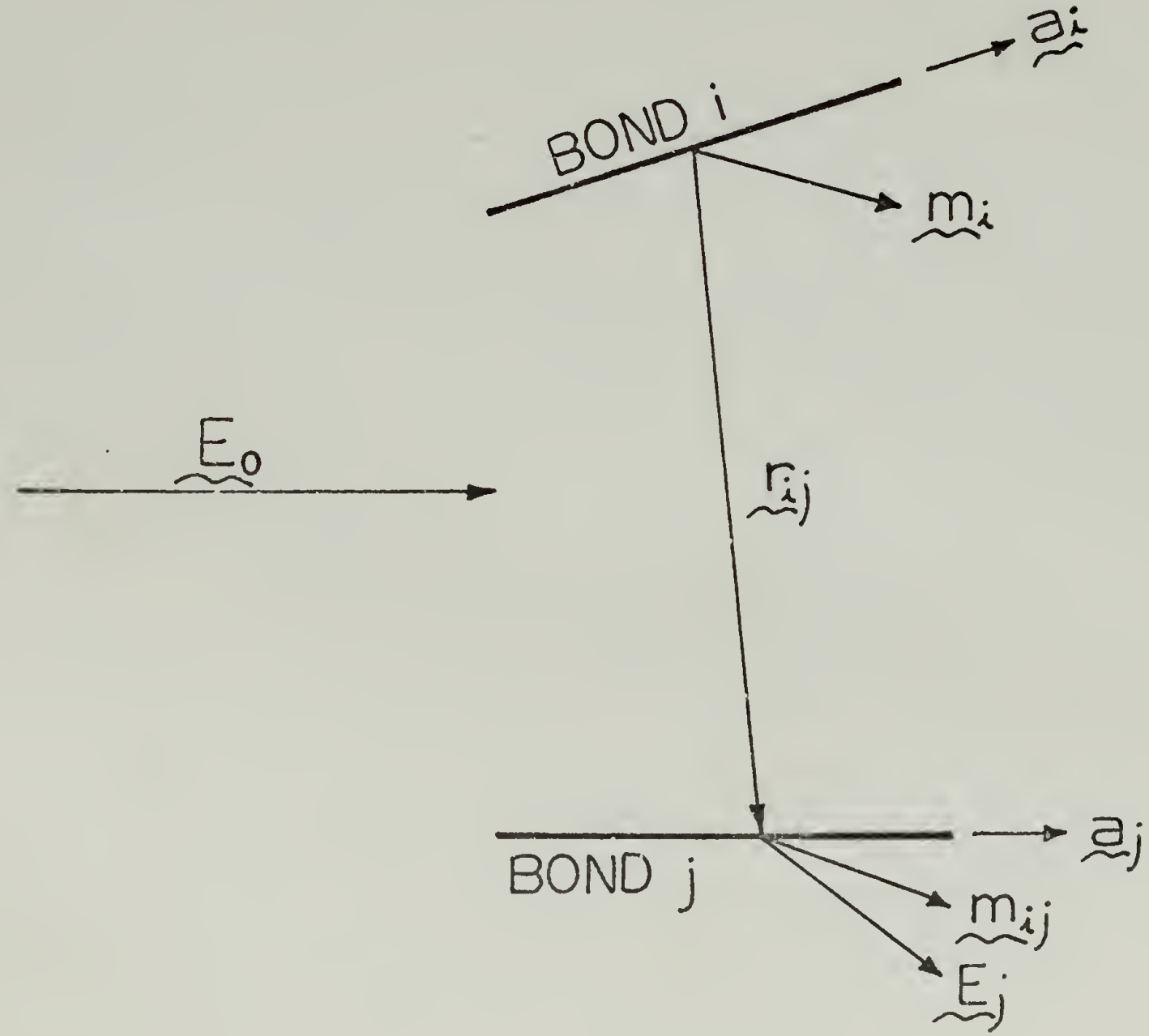

Fig. 1 Illustration of internal field. $\underset{\sim}{a}_i$ and $\underset{\sim}{a}_j$ are bond vectors of bond i and bond j. $\underset{\sim}{m}_i$ and $\underset{\sim}{m}_j$ are induced dipoles at bond i and bond j. $\underset{\sim}{E}_0$ is applied field and E_j is the effective field at bond j.

CHAPTER I

EFFECT OF INTERNAL FIELD ON THE BIREFRINGENCE OF POLYETHYLENE CRYSTALS AND ON THE ANISOTROPY OF POLYMER CHAINS

PART I: BIREFRINGENCE EFFECTS

S. D. Hong, C. Chang and R. S. Stein

Department of Polymer Science and Engineering,
Department of Chemistry, and
Polymer Research Institute
University of Massachusetts
Amherst, Massachusetts 01002

ABSTRACT

Values of the anisotropy of polarizability of methylene groups deduced from the refractive indices of n-paraffin crystals differ appreciably from those obtained from gas or liquid phase measurements. The differences is attributed to the erroneous application of the Lorenz-Lorentz internal field to the anisotropic n-paraffin crystal. A more detailed calculation of the internal field is carried out by detailed summation of the dipolar field over an idealized n-paraffin crystal in which the molecular chains are replaced by anisotropic rods. Based upon reasonable values of parameters and assumed crystal shape, the discrepancy in polarizability anisotropy is resolved.

INTRODUCTION

By assuming applicability of the principle of additivity of bond polariazbility tensors the bond polarizabilities of various kinds of chemical bonds have been determined from the Kerr constants and the depolarization ratios of solutions and vapors of organic molecules from light scattering as well as from the birefringence of n-paraffin crystal (1-3). The determined bond polarizabilities are not in reasonable agreement and some of the assumptions made in the calculation have been the subject of criticism (4). It has been shown that, for tetrahedrally bonded saturated hydrocarbons, the molecular anisotropy may be expressed in the form (4)

$$\gamma = C\Gamma \qquad (1)$$

where C is a geometric constant dependent upon the configuration of the molecular chain. Values of C have been calculated for small n-paraffin molecules (6,7) and for larger ones where rotational isomeric statistics are used (8-12). Values have also been calculated for cycloparaffins (13). Γ is the effective anisotropy of methylene group defined by

$$\Gamma = (b_1 - b_2)_{CC} - A(b_1 - b_2)_{CH} \qquad (2)$$

where b_1 and b_2 are the longitudinal and transverse polarizabilities of the C-C bond and C-H bond, respectively. For tetrahedrally bonded hydrocarbons, A = 2 (4) while if the bond angles differ from tetrahedral ones, A is slightly less than 2 (5,10).

The effective anisotropy Γ can be calculated directly from the determined bond polarizabilities by Eq. (2). Γ can also be determined from the experimental values of $\langle\gamma^2\rangle_{av}$, the mean square average of molecular anisotropy of vapors or solutions of n-paraffins determined from light scattering measurement (12,14). Γ has also been determined from the stress-optical coefficients of polyethylene networks (15-18). The estimation of Γ from the stress-optical coefficient is complicated by the fact that it depends upon the swelling of the network as well as upon the solvent used (16-19). This dependency may be attributed to the short-range ordering existing in the network and to orientation of the solvent by the oriented polymer (16,20).

The values of Γ determined from light scattering depolarization measurements of n-paraffin vapors [1.44 $\AA^3$ (1), 1.71 $\AA^3$ (6), 1.1-2.1 $\AA^3$ (21)] are much higher than those determined from the birefringence of n-paraffin crystals (0.288 $\AA^3$) (2), while the values of Γ determined from solutions of n-paraffins lie in between. Furthermore, it is found that Γ for a series of n-paraffin gases, from ethane through heptane, increases with the increase in molecular weight (21,24,25).

Pitzer (26) has indicated that the reported good agreement between experiment and theory of tensor additivity of polarizabilities (1-3) may be fortuitous. He has expressed the opinion that the effect of neighboring bonds on the effective polarizability of a given bond may be large. A quantitative calculation of such interaction by Rowell and Stein (27) has shown that the mean polarizabilities of C-C bond and C-H bond are indeed affected by the neighboring polarizable bonds. A more recent calcu-

lation by Stein (28), approximating the internal field of n-paraffin crystal as a cylindrical cavity with the ratio of the length and the radius of the cylinder as variable, shows that Γ is a function of this ratio having a value of 0.3 Å^3, corresponding to the value obtained by Bunn and Daubeny (2), when the ratio is one and is 2.7 Å^3 when the cavity is an infinite cylinder. The Bunn and Daubeny value of Γ was obtained from the birefringence of n-paraffin crystal by making the assumption that the internal field could be described by a spherical cavity (2). A similar calculation assuming an ellipsoidal cavity (29) yields results similar to, but somewhat lower than, those obtained from the cylindrical cavity calculation. These results clearly indicate that the bond polarizabilities are significantly influenced by the internal field and the Γ obtained depends on its specific effect.

It is apparent that a better understanding of the effect of internal field on the effective anisotropy of a methylene group is needed to give a reasonable explanation for the discrepancy among the various values of Γ. The purpose of present work is to calculate the internal field effect in a n-paraffin or a polyethylene crystal on the bases of a detailed model of interactions rather than by assumption of a cavity model. The calculation enables us to quantitatively estimate the effective anisotropy of a methylene group in an extended polyethylene chain and enables us to account for the forementioned discrepancies in terms of the internal field effect.

THEORY

The unit cell of polyethylene is shown in Fig. 1 (30) in which the polymer chains are in the planar zig-zag conformation and are located in the corners and center of the cell. This is idealized in Fig. 2 for purposes of simplifying the calculation, where the molecules are represented by thin anisotropic rods. We assume that these anisotropic rods have different polarizabilities, α_a, α_b and α_c in the directions of the a, b and c axes of the unit cell. Fig. 3 shows the case where the electric field of the incident radiation is parallel to the direction of chain axis while Fig. 4 shows the case when the field is perpendicular to the chain axis. $\underset{\sim}{M}_{ji}$ is an induced dipole moment element where j denotes the molecule on which the ith induced dipole resides.

We shall adopt a coordinate system such that the reference chain element p sits at the origin and x, y and z axes are coincident with the a, b and c axes of the unit cell, respectively.

The induced dipole moment $\underset{\sim}{M}_{ji}$ is defined by

$$\underset{\sim}{M}_{ji} = |\alpha_i| \, \underset{\sim}{E}_{eff,i} \tag{1}$$

where $|\alpha_i|$ is the polarizability tensor of the ith element and $\underset{\sim}{E}_{eff,i}$ is the effective field at i and is given by

$$\underset{\sim}{E}_{eff,i} = \underset{\sim}{E}_o + \underset{\sim}{E}_{int,i} \tag{2}$$

where $\underset{\sim}{E}_o$ is the applied field and $\underset{\sim}{E}_{int}$ is the internal field. From classical electrostatic theory, the electric potential at point p due to an

induced dipole moment $\underset{\sim}{M}_{ji}$ at distance r_{ji} is (31)

$$V_{ji} = \frac{M_{ji}}{\varepsilon_{ji} r_{ji}^2} \cos \theta_{ji} \qquad (3)$$

where θ_{ji} is the angle between the dipole moment $\underset{\sim}{M}_{ji}$ and $\underset{\sim}{r}_{ji}$. $\underset{\sim}{r}_{ji}$ is the displacement vector from the element i to the point p. ε_{ji} is the dielectric constant for the dielectric medium between $\underset{\sim}{M}_{ji}$ and p. In an anisotropic medium ε_{ji} is also anisotropic. We shall assume that for the jth chain, it has dielectric constants ε_{jc}, ε_{ja} and ε_{jb} in the directions of c-axis, a-axis and b-axis of the crystal. The internal field at p from all the induced dipoles in the neighboring molecules can be calculated by

$$E_{x,p} = \sum_j \sum_i \left(\frac{\partial V_{ji}}{\partial x}\right) \qquad (4)$$

$$E_{y,p} = \sum_j \sum_i \left(\frac{\partial V_{ji}}{\partial y}\right) \qquad (5)$$

$$E_{z,p} = \sum_j \sum_i \left(\frac{\partial M_{ji}}{\partial z}\right) \qquad (6)$$

There are no negative signs on the right hand sides of Eqs. (4), (5) and (6) because p is at the origin and the electric field at p is calculated from the change in V_{ji} when the position of M_{ji} is changed.

In the following section, we shall consider the cases where the applied fields are along c, a and b axes of the unit cell.

where

$$M_{ji} = M_c \, dz \tag{11}$$

$$C_j^2 = (x_j^2 + y_j^2) \tag{12}$$

$$\tan \omega_j = \frac{z_j}{C_j} \tag{13}$$

M_c is the induced dipole moment in the c axis direction per unit chain length. α_c is the polarizability of a methylene group in this direction. L is the projected length of C-C bond along the c axis. Thus the quantity $(\alpha_c L^{-1})$ represents the polarizability per unit length in the chain axis direction. (x_j, y_j) are the coordinates of the jth chain on the ab plane of the crystal and z_j is half the length of the jth chain.

Thus the internal field at p is in the same direction as the applied field. From Eq. 2 the effective field is the sum of the applied field and the internal field. However Eq. 8 shows that the internal field is proportional to the effective field. Therefore an iteration process must be carried out by first approximating the effective field as being equal to the applied field, then modifying the effective field for the calculation of the further corrected internal field. By iteration, it follows that

$$E_{eff,c} = \left(1 + \frac{K_c' \alpha_c}{L} + \left(\frac{K_c' \alpha_c}{L}\right)^2 + \ldots\right) E_o$$

$$= \left(1 - \frac{K_c' \alpha_c}{L}\right)^{-1} E_o = K_c E_o \tag{14}$$

K_c is the internal field factor in the direction of the c-axis.

For the applied field along the a-axis, one has from Fig. 4

$$\cos \theta_{ji} = - \frac{x_j}{r_{ji}} \tag{15}$$

and

$$E_{x,p} = \sum_j \sum_i \frac{1}{\varepsilon_{ja}} \left(\frac{3M_{ji}\, x_j^2}{(x_j^2 + y_j^2 + z_{ji}^2)^{5/2}} - \frac{M_{ji}}{(x_j^2 + y_j^2 + z_{ji}^2)^{3/2}} \right)$$

$$= \sum_j \int_{-z_j}^{z_j} \frac{1}{\varepsilon_{ja}} \left(\frac{3M_a\, x_j^2}{(x_j^2 + y_j^2 + z^2)^{5/2}} - \frac{M_a}{(x_j^2 + y_j^2 + z^2)^{3/2}} \right) dz$$

$$= \sum_j \left\{ \frac{2x_j^2}{\varepsilon_{ja} C_j^4} (3 \sin\omega_j - \sin^3\omega_j) - \frac{2\sin\omega_j}{\varepsilon_{ja} C_j^2} \right\} M_a$$

$$= K'_a M_a = K'_a \frac{\alpha_a}{L} E_{eff,a} \tag{16}$$

$$E_{y,p} = \sum_j \sum_i \frac{1}{\varepsilon_{jb}} \frac{3 M_{ji}\, x_j\, y_i}{(x_j^2 + y_j^2 + z_{ji}^2)^{5/2}} = 0 \tag{17}$$

$$E_{z,p} = \sum_j \sum_i \frac{1}{\varepsilon_{jc}} \frac{3 M_{ji}\, x_j\, z_{ji}}{(x_j^2 + y_j^2 + z_{ji}^2)^{5/2}} = 0 \tag{18}$$

where

$$M_{ji} = M_a d_z \tag{19}$$

The definitions of C_j and ω_j are the same as those given by Eqs. (12) and (13). M_a is the induced dipole moment per unit length of chain for the electric field in the a direction. α_a is the polarizability of a methylene group in the a direction, and L is the projected length of C-C bond along the a axis.

By iteration, one obtains

$$E_{eff,a} = \left[1 - \frac{K'_a \alpha_a}{L}\right]^{-1} E_o$$

$$= K_a E_o \tag{20}$$

where K_a is the internal field factor in the direction of the a-axis.

For the applied field along the b axis, we interchange x_j with y_j M_a with M_b and α_a with α_b in Eq. (16). Consequently we obtain

$$E_{y,p} = \sum_j \left\{ \frac{2 y_j^2}{\epsilon_{jb} C_j^4} (3 \sin\omega_j - \sin^3\omega_j) - \frac{2 \sin\omega_j}{\epsilon_{jb} C_j^2} \right\} M_b$$

$$= K'_b M_b = K'_b \frac{\alpha_b}{L} E_{eff,b} \tag{21}$$

$$Ex,p = Ez,p = 0 \tag{22}$$

where M_b is the induced dipole moment per unit length of chain for the electric field in the b direction. α_b is the polarizability of a methylene group in the b direction. The definitions of C_j, ω_j and L are the same as in the previous cases.

As in the previous cases, iteration gives

$$E_{eff,b} = \left[1 - \frac{K_b' \alpha_b}{L}\right]^{-1} E_o$$

$$= K_b E_o \qquad (23)$$

where K_b is the internal field factor in the direction of the b axis.

REFRACTIVE INDEX AND MOLECULAR POLARIZABILITY

For high frequency radiation, the refractive index, n, of a material is related to its polarization P by (33,34)

$$n^2 - 1 = 4\pi \frac{P}{E_o} \qquad (24)$$

where P is given by

$$P = N \alpha E_{eff} \qquad (25)$$

N is the number of molecules per unit volume and α the molecular polarizability. Combining Eqs. (14), (20), (23), (24) and (25), one has the general expression

$$n_i^2 - 1 = 4\pi N\alpha_i K_i \tag{26}$$

where i denotes the direction of the electric field of the radiation. By rearranging equation 26, one has

$$\alpha_i = \left[\frac{4\pi N}{(n_i^2 - 1)} + \frac{K_i'}{L}\right]^{-1} \tag{27}$$

From Eqs. (8), (16) and (21) one can visualize that the value of K_i' depends on the type of crystal structure, the crystal size, the shape of the crystal and the dielectric constants. For n-paraffin and polyethylene crystals, the crystal structure, L and N have been determined by x-ray diffraction (30). Thus the molecular polarizabilities can be calculated from the experimental data of x-ray diffraction and refractive indices of the crystal.

Although the theory is developed mainly for the purpose of calculating the molecular anisotropy of the polyethylene crystal, the general theory can be equally applied to the cases of other crystals provided the molecular chains are in their extended form. If the molecules inside the crystal have different configurations, for instance a helical chain rather than an extended one, the results from this theory are not immediately adoptive, but the general scheme is still applicable.

RESULTS AND DISCUSSION

Figure 5 shows K'_c, K'_a and K'_b as functions of R, the radius of a spherical region of the crystal within which all the induced dipoles are taken into account. Here we assume the dielectric constants ε_{jc}, ε_{ja} and ε_{jb} (see Eq. (3)) are equal to one. The unit cells of n-paraffin and polyethylene crystals have the dimensions a = 7.40 Å, b = 4.93 Å and c = 2.534 Å (30). The results indicate that the values of K'_c, K'_a and K'_b approach limiting values and change very slowly for R > 30 Å. Calculations for R > 10000 Å were not done because of the prohibitively long computation times required. We should point out that for an infinitely large crystal, K'_c will approach zero and K'_a and K'_b will be different from the values calculated for R = 10000 Å. However, as one can see from Eqs. (8), (16) and (21), K'_c, K'_a and K'_b will change very slowly for large R. Thus for the n-paraffin and polyethylene crystals of practical sizes, i.e., all the n-paraffin and polyethylene crystal so far have been grown in laboratories, the results may not be very different from the values calculated for R = 10000 Å.

We have also calculated the values of K'_c, K'_a and K'_b for a crystal cylinder with the ratio of the height and the diameter equal to one. The results are very close to, but slightly lower than those calculated from the crystal sphere.

In practice, the dielectric constants ε_{jc}, ε_{ja} and ε_{jb} for the jth chain will be one only for the chains in the vicinity of the reference chain p. For the molecules separated by long distances, the dielectric constants probably equal the macroscopic ones. For the chains at inter-

mediate distances, the values of the dielectric constants may lie in between. As an approximation, we use the macroscopic dielectric constants for the correction of dielectric effect.

From x-ray diffraction measurements, there are four methylene groups in each unit cell of an n-paraffin crystal (30). The refractive indices of the crystal are: $n_c = 1.575$, $n_a = 1.514$ and $n_b = 1.519$ (2). The subscripts c, a and b denote c, a and b axes of the crystal. The three molecular polarizabilities of a methylene group calculated from Eq. (27) are $\alpha_c = 5.363$ Å^3, $\alpha_a = 1.901$ Å^3 and $\alpha_b = 2.024$ Å^3 without corrections for dielectric effect and $\alpha_c = 3.392$ Å^3, $\alpha_a = 2.140$ Å^3 and $\alpha_b = 2.220$ Å^3 with correction for dielectric effect.

Using the bond angles $\angle CCC = 112^\circ$ and $\angle HCH = 109.5^\circ$, and the angle between the b axis of the unit cell and the molecular zig-zag plane equal to 41.2° (30), it can be shown that the effective anisotropy of a methylene group may be given by

$$\Gamma = 1.884 \left[\alpha_c - \tfrac{1}{2} (\alpha_a + \alpha_b)\right] \qquad (28)$$

and the value of A in Eq. 2 is 1.884.

Table I summarizes the calculated effective anisotropy of the methylene group and internal field factors of the n-paraffin crystal. For comparison, the results by Bunn and Daubeny and some experimental results from light scattering depolarization of n-paraffin vapors and solution are also included.

We note that the values of Γ with and without correction for dielectric effect differ substantially from each other. As we mentioned earlier, the real dielectric effect may be between these two extreme cases, and the value of Γ will be in between, too. Presumably the real value of Γ will be closer to 2.238 Å^3 rather than 6.407 Å^3 because only the few chains in the proximity of the reference chain have significantly different dielectric effect from the rest of the chains. The value of Γ corrected for dielectric effect seems to be in reasonable agreement with the experimental ones from the n-paraffin vapors. The fact that the theoretical Γ is higher than the experimental ones is expected and can be accounted for by the following arguments: (1) The CH_3 end groups of the n-paraffin molecules are not so anisotropic as are the CH_2 groups. Thus the end groups tend to diminish the anisotropy of the entire molecule. The end group effect may be dependent on molecular chain length and is more pronounced for shorter chains than for longer ones. One would expect the end group effect to level off as the chain length increases. (2) The theoretical values of Γ and the experimental ones from depolarization light scattering of n-paraffin molecules are not the Γ of an isolated bond but rather subject to the internal field of the rest of the molecule. The effect of the intramolecular internal field, in contrast to the intermolecular internal field effect, is to enhance the effective anisotropy of a methylene group. The reason for the enhancement effect of intramolecular internal field on the effective anisotropy arises from the fact that the intramolecular internal field effect comes from the polarization of parts of molecules residing in the same molecule. This intramolecular internal

field effect also depends upon the chain length. Since the internal field is inversely proportional to the third power of the distance separating the two interacting induced dipoles, this effect also levels off as the chain length increases. Thus from the above discussion, one would expect that the theoretical Γ calculated from the crystal may represent the high limit of that which one can obtain from the depolarization light scattering of n-paraffin vapors.

A comparison of the internal field factors K_c, K_a and K_b calculated by this theory and those by Bunn and Daubeny (2) indicates that while K_a and K_b are slightly different for the two cases, K_c is quite different. Bunn and Daubeny assumed that the internal field in a n-paraffin crystal could be approximated as a spherical cavity. Stein (28) has pointed out that the approximation of a spherical cavity for a n-paraffin crystal is unrealistic in the light of the molecular arrangement in the crystal. The calculated internal field factors from the present theory indicate that the effect of internal field in the crystal is to decrease its birefringence. Thus the n-paraffin molecules in the gaseous phase is expected to have higher optical anisotropy in agreement with observation (1, 20, 32).

The recent work of Patterson and Flory (12) seems to give strong support to the applicability of the principle of additivity of bond polarizability tensor for n-paraffin molecules in solution; this is in contradiction with the observations of gaseous molecules (20,23,24). We feel that the contradiction may be due to the methyl end group effect and the intramolecular internal field effect. The end group effect may

not be as significant as the intramolecular internal field for molecules of molecular weight higher than butane, as evidenced by the constant Γ from Patterson and Flory's work. But for molecules of ethane and propane, this end group effect may be important. The main cause for the contradiction may be due to the intramolecular internal field effect. In solution, the small solvent molecules are dielectrics and their presence will sharply decrease the intramolecular internal field effect. For instance, the dielectric constant of CCl_4 is 2.234 and the intramolecular internal field in CCl_4 medium will be only 45% of that in gaseous phase (free space). Thus the change in intramolecular internal field of n-paraffin molecules of molecular weight higher than that of butane with the change in chain length in CCl_4 medium may not be detectable. On the other hand, in the gaseous phase, this intramolecular internal field may be very significant and the measured Γ shows dependency on molecular weight for the low molecular weight n-paraffins. This intramolecular internal field effect argument may also explain the fact that the Γ determined from dilute solution is only 0.54 $\mathring{A}^3$ compared to the theoretical value of 2.283 $\mathring{A}^3$.

Although the values of K'_c, K'_a and K'_b for a cylindrical crystal with axial ratio, the ratio of the height and the diameter of the cylinder, equal to one is very close to those calculated for the spherical crystal, the results are quite different when the axial ratios are otherise. This is shown in Fig. 6, where R is the radius of the crystal cylinder and Z is its half height. Here the dielectric constants are assumed to be one. For Z = 50, 100, 500 and 1000 $\mathring{A}$, we found that the values of K'_c, K'_a, and

K_b' vs (R/Z) can be plotted into master curves with negligible deviation. This seems to indicate that for crystals of size larger than 30 Å in radius (see Fig. 5), the dependency of internal field upon the shape of the crystal may be described by the axial ratio.

The polyethylene crystals in the semicrystalline polyethylene solid were found to have thickness of the order of 100 Å. The shape of the crystals in this melt crystallized sample may be very different from that of n-paraffin crystals, which are diamond-shaped plates. From the results of Fig. 6, the internal field for this type of crystal is very different from what is in the n-paraffin crystal. Thus one may expect the birefringence of these polyethylene crystals to be different from that of the n-paraffin crystal. Detailed calculation on this subject is underway.

TABLE I

Effective Anisotropy of a Methylene Group and

Internal Field Factors of n-Paraffin Crystal

Present Work		Bunn-Daubeny	Experimental Values From n-Paraffins in Gaseous Phase
(a)	(b)		
$\Gamma = 6.407$ Å^3	$\Gamma = 2.283$ Å^3	$\Gamma = 0.288$ Å^3	1.44 Å^3 (1) 1.1-2.1 Å^3 (2) 1.71 Å^3 (32) 0.54 Å^3 (12) (from dilute solutions)
$K_c = 0.507$	$K_c = 0.801$	$K_c = 1.498$	
$K_a = 1.247$	$K_a = 1.108$	$K_a = 1.432$	
$K_b = 1.184$	$K_b = 1.080$	$K_b = 1.440$	

(a) Without correction for dielectric effect

(b) Correction for dielectric effect with macroscopic dielectric constants of the crystal

CAPTIONS FOR FIGURES

Fig. 1 Arrangement of molecules in unit cell of polyethylene and n-paraffin crystals.

Fig. 2 The thin rod model used for the calculation of the internal field.

Fig. 3 The dipole induced on the molecular chain when the electric field of the radiation is at the direction of chain axis.

Fig. 4 The dipole induced on the molecular chains when the electric field of the radiation is perpendicular to the chain axis.

Fig. 5 The coefficients of K'_c, K'_a and K'_b vs the radius of the crystal sphere R. The dielectric constants are taken to be one.

Fig. 6 The coefficients of K'_c, K'_a and K'_b vs the axial ratio of the crystal cylinder. The dielectric constants are taken to be one.

REFERENCES

1. K. G. Denbigh, Trans. Faraday Soc., 36, 936 (1940).
2. C. W. Bunn and R. de P. Daubeny, Trans Faraday Soc., 50, 1173 (1954).
3. Le Fevre and R. J. W. Le Fevre, Rev. Pure and Appl. Chem. (Austrialia), 5, 261 (1955).
4. R. P. Smith and E. M. Mortensen, J. Chem. Phys., 32, 502 (1960).
5. M. H. Liberman, Y. Abe and P. J. Flory, Macromolecules, 5, 550 (1972).
6. R. P. Smith and E. M. Mortensen, J. Chem. Phys., 32, 508 (1960).
7. R. S. Stein, J. Chem. Phys., 21, 1193 (1953).
8. R. P. Smith and E. M. Mortensen, J. Chem. Phys., 35, 714 (1961).
9. R. P. Smith, J. Chem. Phys., 44, 2543 (1966).
10. R. L. Jernigan and P. J. Flory, J. Chem. Phys., 47, 1999 (1967).
11. K. Nagai, J. Chem. Phys., 47, 4690 (1967).
12. G. D. Patterson and P. J. Flory, Trans. Faraday Soc., 68, 1098 (1972).
13. R. S. Stein, D. A. Keedy, J. Powers and A. Plaza, J. Polymer Sci., 62, 589 (1962).
14. I. L. Fabelinskii, Molecular Scattering of Light, Plenum Press, New York, 1968.
15. K. Nagai, J. Chem. Phys., 40, 2818 (1964).
16. K. Nagai, J. Chem. Phys., 49, 4212 (1968).
17. D. W. Saunders, D. R. Lightfoot and D. A. Parsons, J. Polymer Sci., A2, 6, 1183 (1968).
18. M. H. Liberman, Y. Abe and P. J. Flory, Macromolecules, 5, 550 (1972).

19. A. N. Gent and V. V. Vickroy, Jr., J. Polymer Sci., A-2, 5, 47 (1967).

20. R. S. Stein and S. D. Hong, to be published.

21. J. Powers, D. A. Keedy and R. S. Stein, J. Chem. Phys., 35, 376 (1961).

22. P. Bothorel, J. Colloid Interface Sci., 27, 529 (1968).

23. K. Nagai, J. Chem. Phys., 47, 4690 (1967).

24. G. M. Aval and R. Rowell, J. Chem. Phys., 57, 3104 (1972).

25. F. R. Dintzis and R. S. Stein, J. Chem. Phys., 40, 1459 (1964).

26. K. S. Pitzer, Advan. Chem. Phys., 2, 79 (1959).

27. R. L. Rowell and R. S. Stein, J. Chem. Phys., 47, 2985 (1967).

28. R. S. Stein, J. Polymer Sci., A2, 7, 1021 (1969).

29. C. Chang, Ph.D. Thesis, University of Massachusetts, Amherst, 1973.

30. C. W. Bunn, Trans. Faraday Soc., 35, 482 (1939).

31. R. S. Stein and R. L. Rowell, ONR Tech. Rept. 40 and NSF Progress Report. No. 1, Dept. of Chemistry, University of Massachusetts at Amherst.

32. R. F. Zurcher, J. Chem. Phys., 37, 2421 (1962).

33. H. A. Lorentz, The Theory of Electrons, Dover, New York, 1952; Ann. Physik, 9, 641 (1880).

34. L. Lorenz, Ann Physik, 11, 70 (1880).

Fig. 1

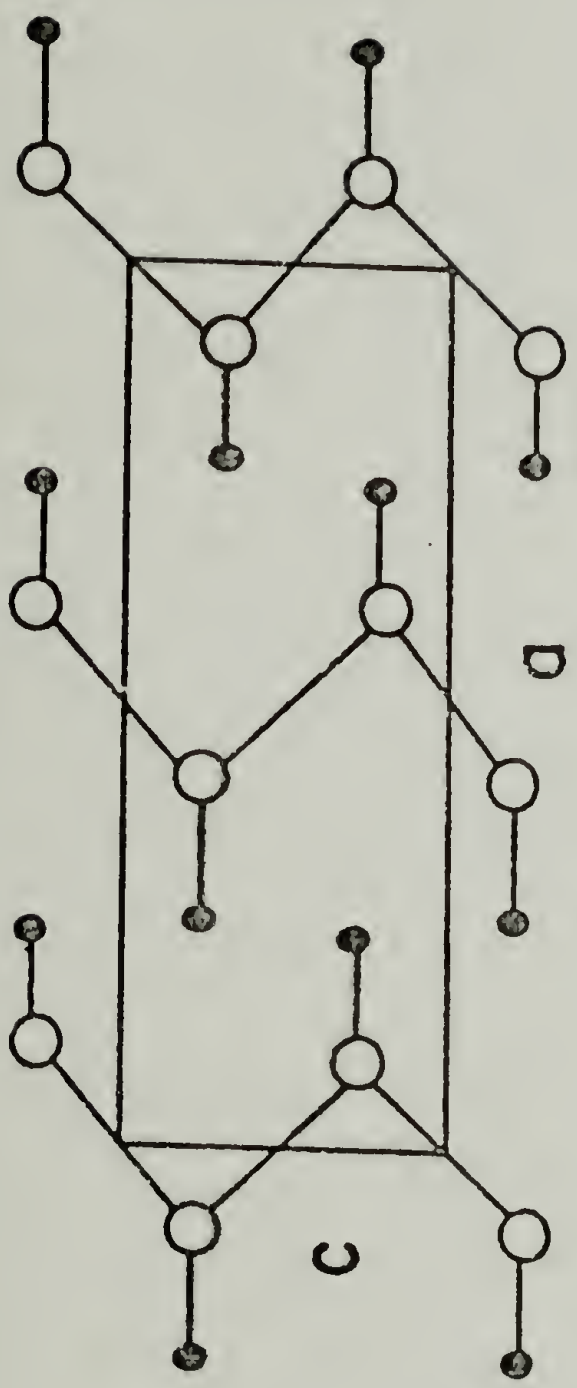

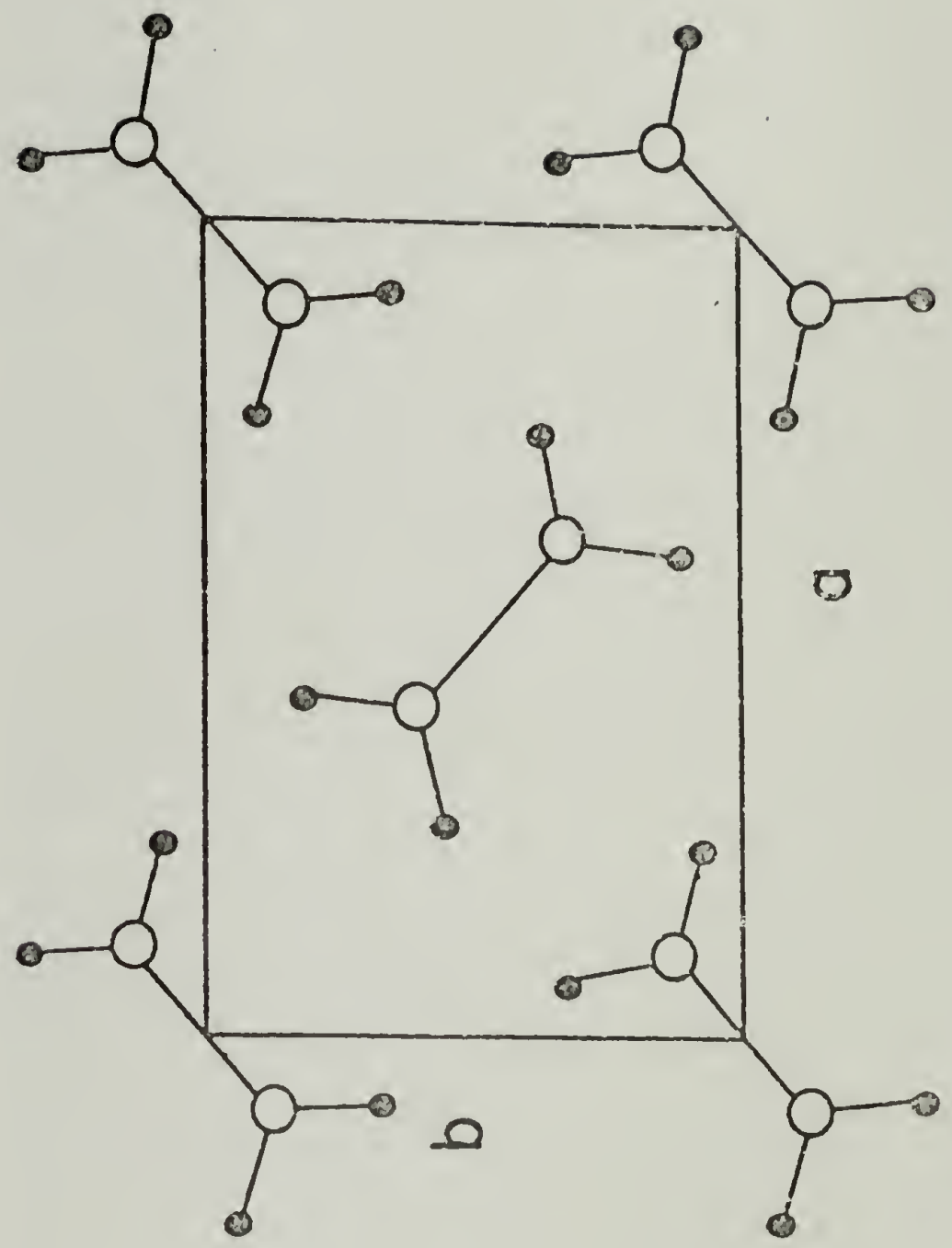

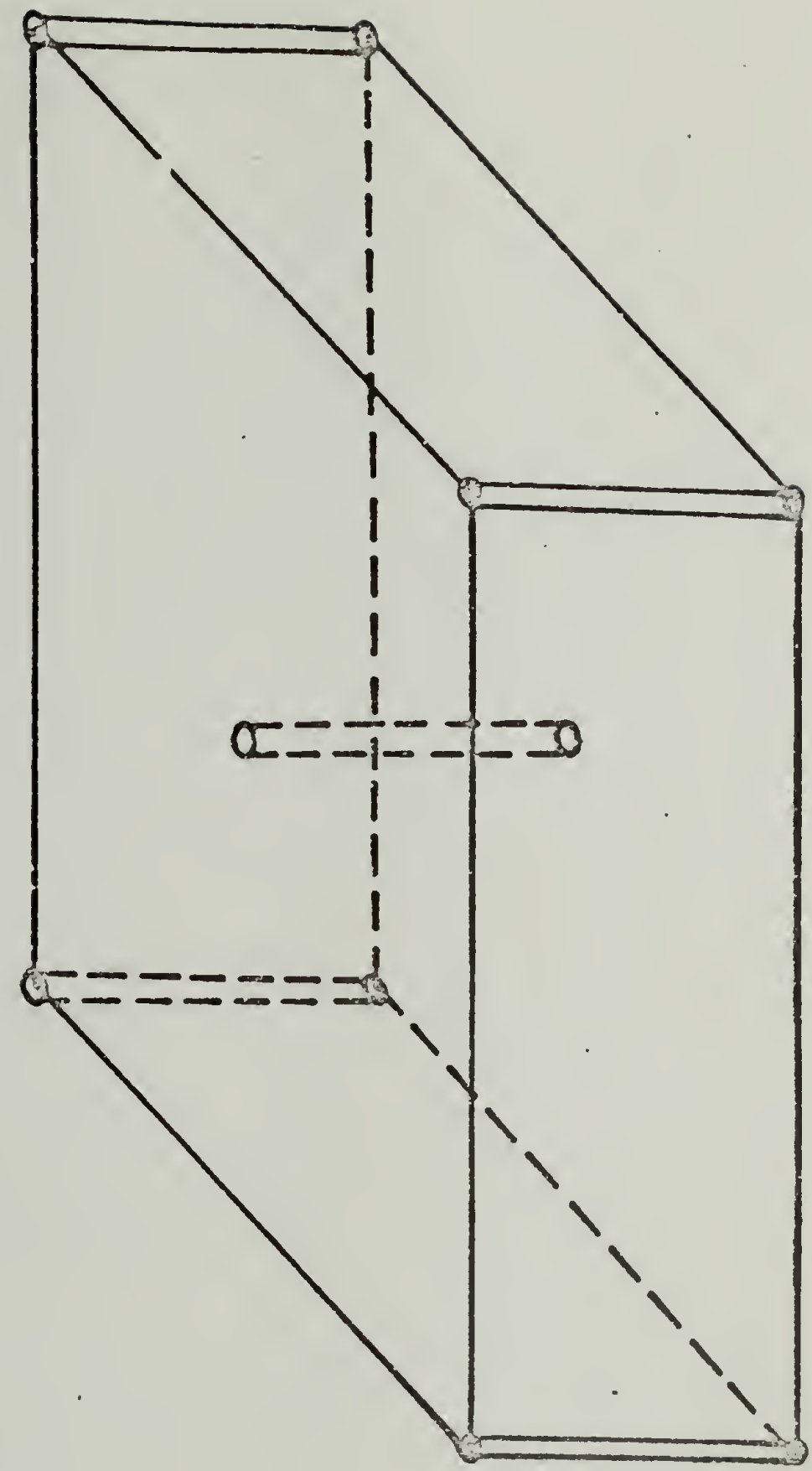

Fig. 2

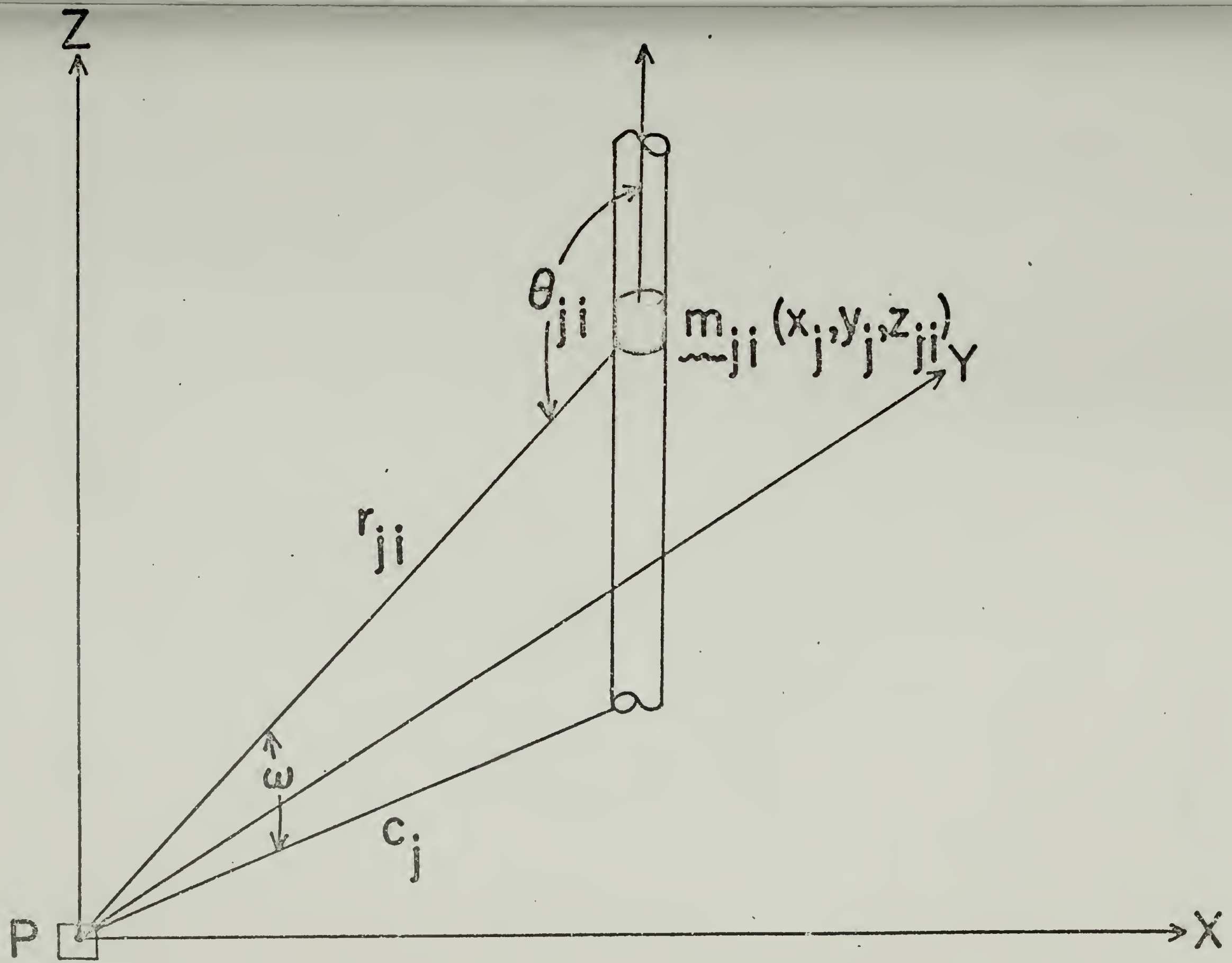

Fig. 3

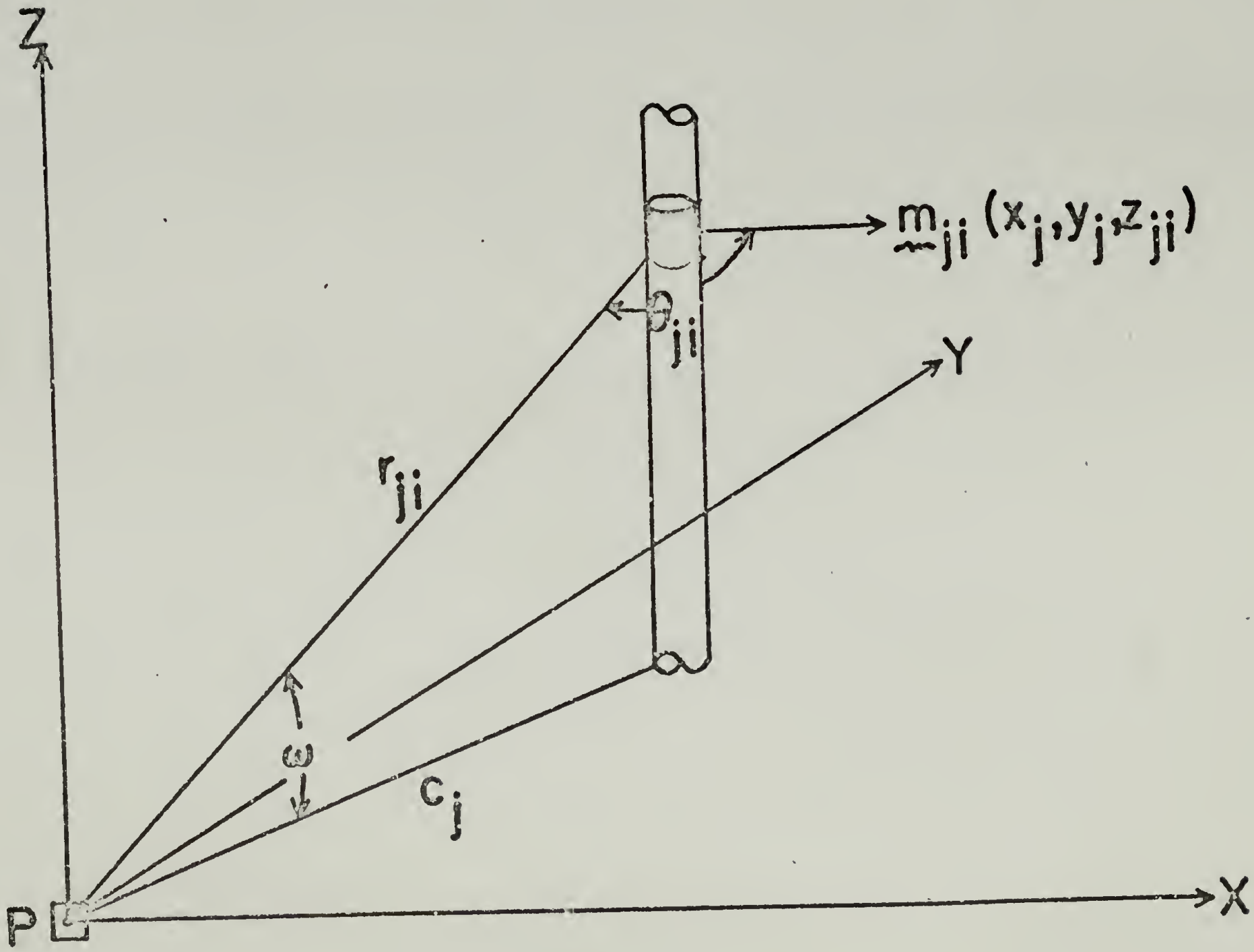

Fig. 4

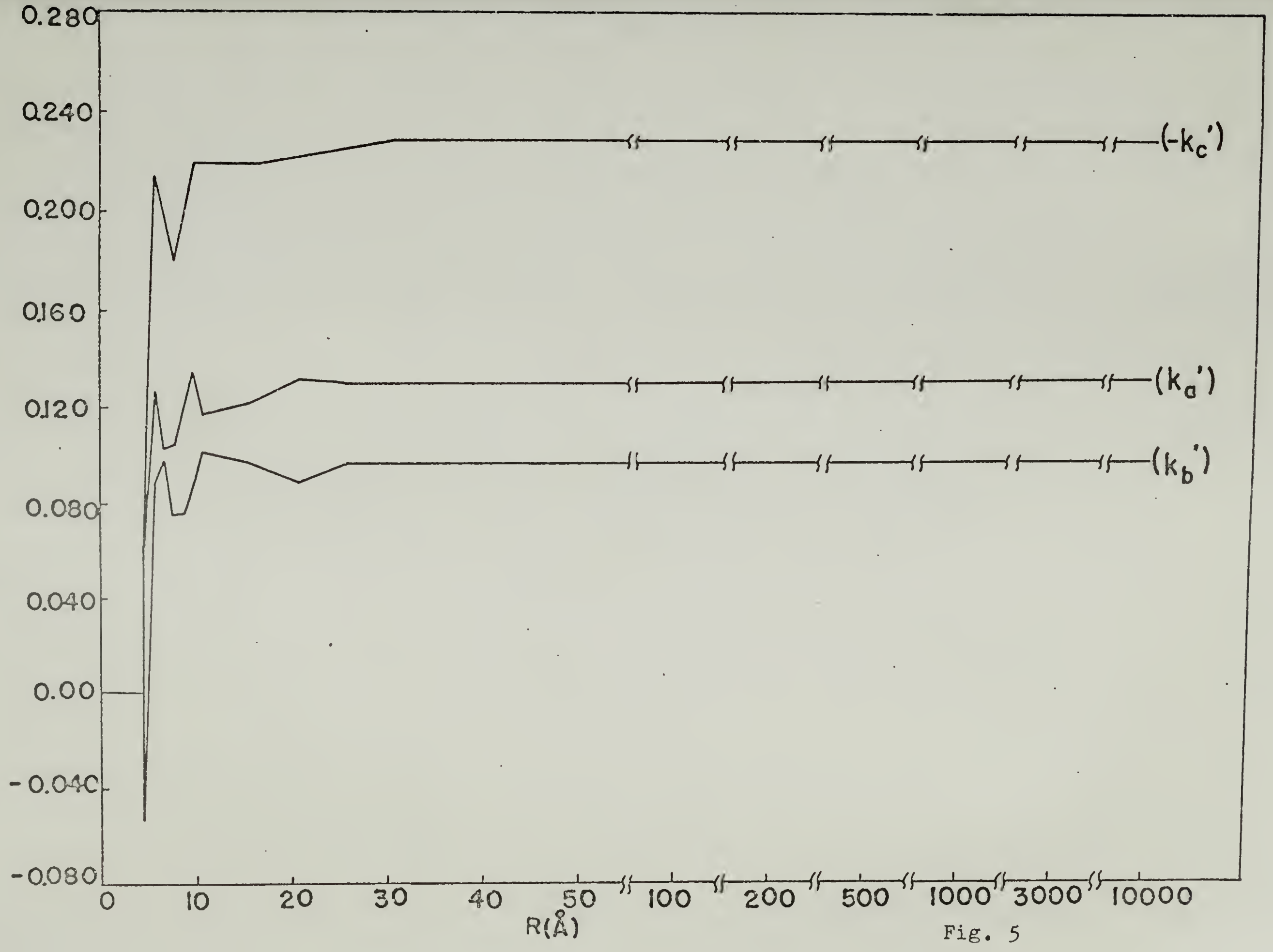
0.280
0.240
0.200
0.160
0.120
0.080
0.040
0.00
-0.040
-0.080
0
10
20
30
40
50
100
200
500
1000
3000
10000
R(Å)
(-k_c')
(k_a')
(k_b')

Fig. 5

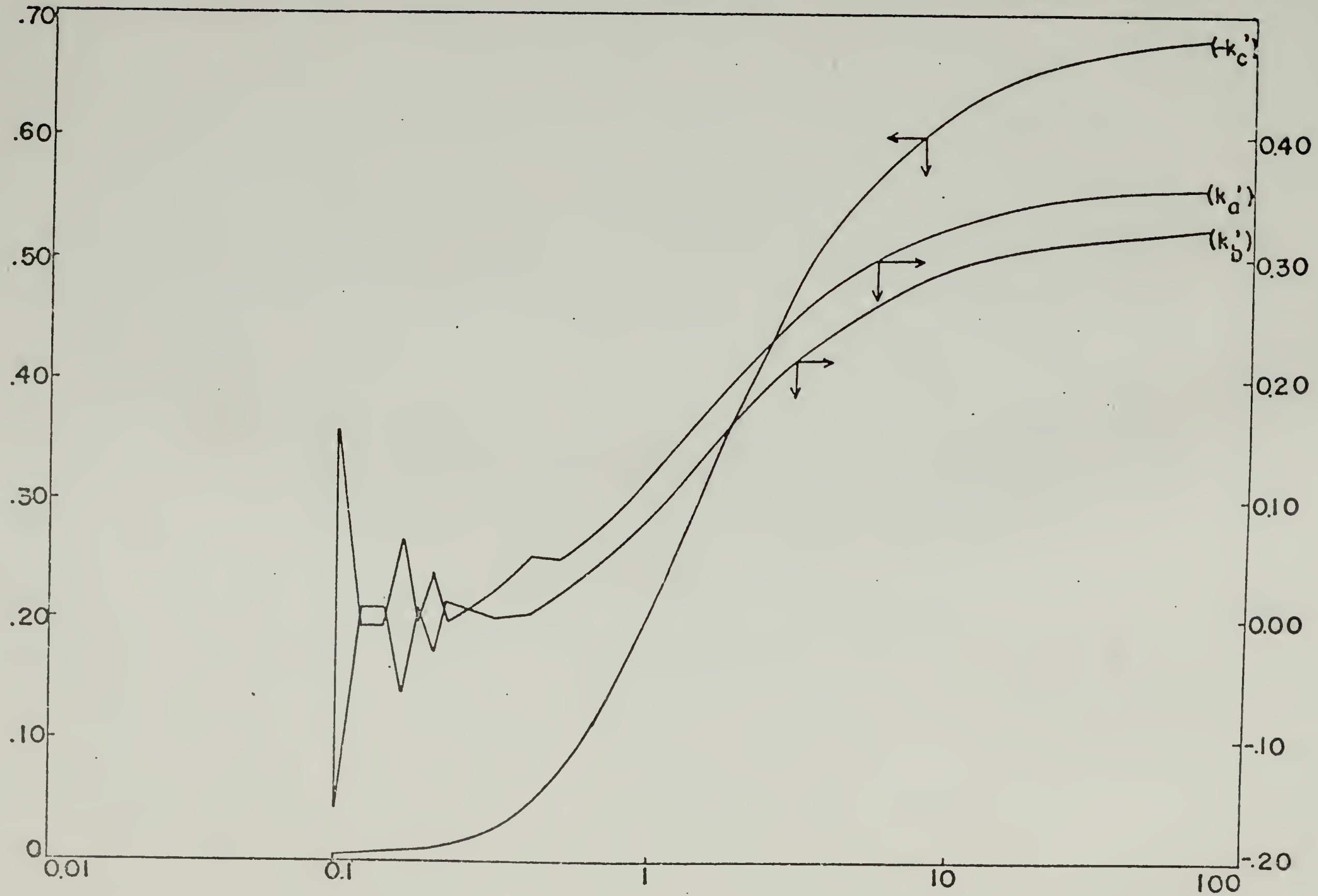
.70
.60
.50
.40
.30
.20
.10
0
0.01
0.1
1
10
100
R/Z
0.40
0.30
0.20
0.10
0.00
-.10
-.20
(k_c')
(k_a')
(k_b')

Fig. 6

CHAPTER II

THE STRESS-OPTICAL COEFFICIENT AND AMORPHOUS ORDER

by

R. S. Stein and S. D. Hong
Polymer Research Institute
and Department of Chemistry
University of Massachusetts
Amherst, Massachusetts 01002

SYNOPSIS

The calculated stress-optical coefficients obtained using the rotational isomer model and the principle of additivity of bond polarizability tensors give values of the segment polarizability anisotropy, $\Delta\Gamma_s$, in reasonable agreement with experimental values for swollen rubber networks. Furthermore, these values agree well with those obtained from streaming birefringence studies. Estimates of the effect of ordering in the amorphous state upon $\Delta\Gamma_s$ lead to values appreciably in excess of those found experimentally. The effect of swelling solvent on $\Delta\Gamma_s$ can be interpreted in terms of its role in separating chains from each other and in itself being oriented by the polymer chain. This model accounts for the observation that $\Delta\Gamma_s$ increases with increasing anisotropy of the swelling solvent. The value of $\Delta\Gamma_s$ found for networks swollen with an isotropic solvent is approximately, but not exactly equal to the intrinsic anisotropy of the segment, $\Delta\Gamma_s$. The enhancement of $\Delta\Gamma_s$ found for undiluted networks arises in part from mutual orientation of segments by

their neighbors. An additional cause comes from the anisotropy of the internal field arising from local order. All of these effects are interpretable in terms of relatively short range interactions and do not require the relatively long range ordering of a type proposed in some recent theories.

INTRODUCTION

The change in birefringence occurring when an amorphous polymer is deformed is an important observation which provides information concerning the state of order in amorphous solids. Since the presence of crystals appreciably affects the birefringence, we shall restrict our considerations to those polymers which show no equilibrium crystallinity at the temperature of study. Also, because of the poorer understanding of glassy polymers as compared with rubbery ones, we shall only consider systems above their T_g's.

The theory of birefringence of stretched rubbers was developed by Kuhn and Grün[1] and by Treloar[2] on the basis of the same procedure used for the development of the kinetic theory of rubber elasticity. The model adopted was that of a chain composed of anisotropic statistical segments which become oriented as the rubber is stretched in a manner describable by the Gaussian statistics of isolated chains in a crosslinked network, the crosslinking points of which are subject to an affine transformation. These theories lead to the expression for the stress-optical coefficient

$$C = \frac{\Delta n}{\sigma} = \frac{2\pi}{45kT} \frac{(\bar{n}^2 + 2)^2}{\bar{n}} \Delta\Gamma_s \qquad (1)$$

where Δn is the birefringence of the uniaxially stretched sample subjected to a stress σ (on unit area in the stretched state), k is Boltzmann's constant, T is the absolute temperature and $\bar{n}$ is the average refractive index of the rubber. The anisotropy of the statistical segment $\Delta\Gamma_s$ is given by

$$\Delta\Gamma_s = (b_1 - b_2)_s \qquad (2)$$

where b_1 and b_2 are the polarizabilities parallel and perpendicular respectively to the axis of the segment.

Equation (1) is derived upon the assumption of the local electrical field on a segment being given by the Lorenz-Lorentz equation which implies that the environment of a segment is optically isotropic. It also involves the assumption of tensor additivity of polarizabilities of non-interacting segments.

The anisotropy of a segment may be related to the anisotropy of the constituent bonds, again assuming polarizability additivity using

$$\Delta\Gamma_s = \sum_i \left\{(b_1 - b_2)_i \, [3\cos^2\theta_i - 1]/2\right\} \qquad (3)$$

where b_{1i} and b_{2i} are the polarizabilities of the i-th bond along and perpendicular to the bond axis and θ_i is the angle between the bond axis and the segment axis. Recently Flory[3] and Nagai[4] and coworkers have shown how to evaluate this sum in terms of the rotational isomer model giving rise to the equation

$$\Delta\Gamma_s = \frac{3}{2} \sum_i \langle \underset{\sim}{r}^T \underset{\sim}{\hat{\alpha}}_i \underset{\sim}{r} \rangle_o / \langle r^2 \rangle_o \qquad (4)$$

where $\underset{\sim}{r}^T$ is the transpose (i.e. the row form) of the end-to-end vector $\underset{\sim}{r}$ and $\underset{\sim}{\hat{\alpha}}$ is the traceless tensor representing the anisotropy of the polarizability of bond i defined by

$$\underset{\sim}{\hat{\alpha}}_i = \underset{\sim}{\alpha}_i - \bar{\alpha}_i \underset{\sim}{E}_3 \qquad (5)$$

where $\underset{\sim}{\alpha}_i$ is the polarizability tensor, $\bar{\alpha}_i$ is the mean polarizability and $\underset{\sim}{E}_3$ is the identity matrix. The symbol < > denotes averages over the free unperturbed chain. For hydrocarbons, this leads to the result that

$$\Delta\Gamma_s = A_{CC}(b_1 - b_2)_{CC} - A_{CH}(b_1 - b_2)_{CH} \qquad (6)$$

where $(b_1 - b_2)_{CC}$ and $(b_1 - b_2)_{CH}$ are anisotropies of the CC and CH bonds and A_{CC} and A_{CH} are constants dependent upon molecular geometry. For tetrahedrally bonded hydrocarbons[5], $A_{CH}/A_{CC} = 2$ while for the actual bond angles in polyethylene, it is 1.88. Thus

$$\Delta\Gamma_s = A_{CC}\, \Delta\Gamma_{PM} \qquad (7)$$

where $\Delta\Gamma_{PM}$ is the anisotropy of the polymethylene group given by

$$\Delta\Gamma_{PM} = (b_1 - b_2)_{CC} - 1.88\,(b_1 - b_2)_{CH} \qquad (8)$$

Statistical calculations for polyethylene give a value of $A_{CC} = 4.0 \pm 0.6$.

COMPARISONS BETWEEN EXPERIMENTAL AND THEORETICAL BIREFRINGENCE

Experimental measurements of $\Delta\Gamma_s$ of polyethylene have been reported[6-8]. It is found that values are higher for unswollen samples than for samples swollen with decalin, the latter giving $\Delta\Gamma_s$ = 4.0 Å^3 for ϕ_2 = 0.33 corresponding to a value of $\Delta\Gamma_{PM}$ = 1.0 Å^3. Theoretical values are dependent upon the choice of bond polarizabilities used in the calculation of $\Delta\Gamma_{PM}$ and are 1.47, 0.86 and 0.57 Å^3 for the bond polarizabilities of Denbigh[9], Clement and Botherel[10], and LeFevre, Orr and Ritchie[11] respectively. The latter value, which was considered most reasonable for the interpretation of light scattering depolarization measurements in n-paraffins[12] is somewhat small as compared with experimental measurements and may result partly from the fact that the concentration of polymer in the swollen gel used for the stress-optical measurements was relatively high, and partly because decalin is not an isotropic solvent. Similar measurements have been reported for poly(dimethylsiloxane)[8] but bond polarizability information was not available to compare with experiment.

A study of the stress-optical coefficients of cis-1,4-polyisoprene and cis-1,4-polybutadiene has been reported by Ishikawa and Nagai[13] who also find that the SOC for the dry rubbers is greater than that for the rubbers swollen with an isotropic solvent. For cis-PBD, calculated values of $\Delta\Gamma_s$ range from 5.33 to 5.58 Å^3 depending on the parameters used in the statistical weight matrices and using the Clement and Botherel polarizabilities[10] as compared with experimental values of 5.8 Å^3 on swollen samples and 7.5 Å^3 for unswollen samples. Considerably smaller values of 3.92 and 4.09 Å^3 are found using Denbigh's[9] or LeFevre's[11] values of bond polarizabilities, respectively.

For cis-PIP, calculated values[13] range from 0.152 to 0.764 Å^3 as compared with an experimental value of 0.72 Å calculated from data of Smith and Puett[14] on unswollen natural rubber.

For the above three cases, the agreement between experiment and theory is considered satisfactory, especially in view of the uncertainty concerning the values of anisotropic bond polarizabilities. It should be emphasized that the theory used is one which involves the orientation of an isolated chain with no correlation in orientation of segments on differing chains.

A systematic study of the stress-optical coefficients of samples of poly(1,4-butadienes) of differing cis content was undertaken by Fukuda, Wilkes and Stein[15] who confirmed the earlier reports of Ishikawa and Nagai[13] and Gent[16] that the values are appreciably affected by the swelling solvent used. For example, Figure 1 shows a typical result[15] for the variation of birefringence with stress for high-cis crosslinked 1,4-polybutadiene rubber swollen in a variety of solvents.

The value of the SOC increases with the anisotropy of the solvent and is least for the isotropic solvent, CCl_4. The values with CCl_4 are less than those for the unswollen polymer. It is suggested that adsorbed anisotropic solvents are oriented along with the polymer molecules and add to their anisotropy. Thus, for the unswollen polymers, the neighboring chains are adsorbed on each other and add to the SOC. This effect is diminished upon swelling with an isotropic solvent.

Another effect seen upon swelling is that both the stress and birefringence of the polymer obey Mooney-Rivlin type equations

$$\sigma\phi_2^{1/3}/[\lambda^2 - \lambda^{-1}] = 2C_1 + 2C_2/\lambda \qquad (9)$$

$$(\Delta n)\ \phi_2^{1/3}/\ [\lambda^2 - \lambda^{-2}] = B_1 + B_2/\lambda \qquad (10)$$

where λ is the elongation ratio ϕ_2 is the volume fraction of rubber and the constants C_2 and B_2 represent deviations from ideal behavior. It is found that both C_2 and B_2 diminish to essentially zero upon swelling and one might wonder whether this effect suggests chain packing or order. However, it has been found that both C_2[16-19] and B_2[19] are substantially decreased for unswollen networks which are crosslinked in the swollen state. Figure 2 shows a typical birefringence Mooney-Rivlin type plot[19] obtained from samples of cis 1-4-polybutadiene crosslinked in benzene solution at volume fractions ϕ_r designated in the figure. [v_r on the figure corresponds to ϕ_2 in Equations 9 and 10]. Curves are shown for measurements made on the subsequently dried polymer as well as for samples then swollen with CCl_4 to values of ϕ_2 in the range of 0.04-0.09. It is seen that even in the dry state, the slope of this plot is quite small indicating values of B_2 of the order of 0.2×10^{-4}. Since it is not likely that the molecular order in the dried network will depend upon the state of swelling at the time of crosslinking, it seems that this reduction is related to network topology differences dependent upon the state of swelling at the time of crosslinking. It has recently been suggested[20] that differences may be related to the greater number of intramolecular crosslinks occurring when crosslinking in solution. In any case, it does not appear that the finite values of C_2 and B_2 are directly related to amorphous order for these systems.

However, the dependence of B_1 upon the amount and kind of swelling solvent does suggest that its change may relate to amorphous structure.

A significant observation pointed out by Fukuda, et. al.[15] is the correspondence of the SOC's obtained both for cis and trans PBD from measurements on swollen networks and those obtained by streaming birefringence techniques with dilute solutions[21,22]. Figure 3 shows a comparison of some measurements by Fukuda, et. al.[15] of SOC's measured on some samples of crosslinked PBD samples of differing cis-1,4 content swollen with different solvents with values obtained by streaming birefringence by Poddubnyi, et. al.[21] and by Phillipoff[22]. The theory of streaming birefringence[23] indicates that it should give the same value of SOC as does the measurement on the crosslinked network. Since the streaming birefringence measurement is concerned with molecules in solution which are separated from each other, it is not likely that it can be affected by amorphous ordering. Thus, the correspondence of the values of SOC's measured by these two very different techniques suggests that the model based upon the orientation of isolated chains described by Gaussian statistics is appropriate for moderately swollen networks and is inconsistant with any ordered structure. The question remains as to whether there is any increase in ordering in going from a swollen to an unswollen network. It should be noted that the difference between the values of the SOC in the unswollen and isotropically swollen state is relatively small, usually less than a factor of two, and the enhancement of the SOC in the dry state is comparable with that produced by the ordering of a solvent such as toluene in the swollen state. Consequently, we feel that while

there may be some ordering in dry polymers, relatively short range ordering is sufficient to account for the observed result.

THE EFFECT OF AMORPHOUS ORDER ON THE STRESS-OPTICAL COEFFICIENT

In order to account for the possible effect of ordering on the SOC, we should examine the assumptions involved in the derivation of Equation (1). It is based upon the Lorenz-Lorentz equation for the relationship between the refractive index, n, and the polarizability per unit volume P

$$\frac{n^2 - 1}{n^2 + 2} = \frac{4}{3} \pi P \qquad (11)$$

which gives by differentiating

$$\Delta n = \frac{2}{9} \pi \frac{(\bar{n}^2 + 2)^2}{\bar{n}} (P_1 - P_2) \qquad (12)$$

The polarizability difference is then related to the anisotropy of the segment by

$$(P_1 - P_2) = N_s f_s \Delta r_s \qquad (13)$$

where N_s is the number of segments per unit volume and f_s is the orientation function of a segment defined as

$$f_s = [3 < \cos^2\theta_s >_{av} - 1]/2 \qquad (14)$$

where θ_s is the angle between the segment axis and the stretching direction. f_s may be given by the kinetic rubber elasticity theory in the Gaussian approximation as

$$f_s = \frac{1}{5} \frac{N_c}{N_s} [\lambda^2 - \lambda^{-1}] \qquad (15)$$

where N_c is the number of chains per unit volume.

Equation (1) results from combining Equations (12) through (15) with the kinetic elasticity equation for the stress

$$\sigma = N_c kT [\lambda^2 - \lambda^{-1}] \qquad (16)$$

Ordering in the amorphous state will affect the derivation at two points: in the use of Equation (11) for the internal field and in the use of Equation (15) for segment orientation. Equation (15) is obtained in the Kuhn-Grün treatment[1] by calculating the distribution function of segment orientations with respect to the displacement vector $\underset{\sim}{R}$ using the Lagrange method of undetermined multipliers subjecting the distribution to the constraints of a fixed number of segments and a fixed length of $\underset{\sim}{R}$. This leads to a value for the orientation function, f_R of segments with respect to R. The orientation function, f_s, is then obtained by convoluting this function with that of R with respect to the stretching direction. In this derivation, the segments are considered to have equal a-priori probability of any orientation, and no interaction between segments on different chains is considered. This is obviously not so for an

ordered amorphous phase. In a crystalline polymer, for example, a group of q segments on neighboring chains must be maintained parallel to each other. In this case, the segment orientation function will be q times that given by Equation (15). In the case of intermediate order, an average, $\bar{q}$ may be used which represents the number of segments surrounding a given segment whose orientation is correlated with that of the first segment. Since the SOC of the dry polymer was generally less than two times that of the swollen polymer, the factor q must be less than two if it is attributable to this cause. This is smaller by an order of magnitude or two than what would be expected on the basis of models which would have been proposed[24,25] for ordered amorphous polymers.

The theory for the SOC for a swollen network of non-interacting chains[2] requires that the SOC should not vary with degree of swelling, provided that $\Delta\Gamma_s$ is not affected. If solvent molecules are oriented along with the polymer segment, the value of $\Delta\Gamma_s$ will be enhanced to give

$$\Delta\Gamma_s = \Delta\Gamma_s^o + \Delta\Gamma_\ell \tag{17}$$

where $\Delta\Gamma_s^o$ is the anisotropy of the isolated polymer segment and $\Delta\Gamma_\ell$ is the additional anisotropy resulting from the orientation of the surrounding solvent. This is given by

$$\Delta\Gamma_\ell = \Delta\Gamma_\ell^o N_\ell \int f_\ell(\underset{\sim}{r}_{s\ell})\, d\underset{\sim}{r}_{s\ell} \tag{18}$$

Δr_ℓ^o is the intrinsic anisotropy of the solvent molecule N_ℓ is the number of solvent molecules per unit volume given by

$$N_\ell = (\rho_\ell N_o)/M_\ell \qquad (19)$$

where ρ_ℓ is the density of the solvent, N_o is Avagardro's number and M_ℓ is the molecular weight of the solvent. $f_\ell(\underset{\sim}{r}_{s\ell})$ is the orientation function of the solvent molecules at a distance $\underset{\sim}{r}_{s\ell}$ from the segment with respect to the segment axis defined by

$$f_\ell(r_{s\ell}) = [3 \langle \cos^2\theta_{s\ell} \rangle_{\underset{\sim}{r}} - 1]/2 \qquad (20)$$

where $\theta_{s\ell}$ is the angle between the segment axis and the optic axis of the solvent. The integral is over all lengths and orientations of $\underset{\sim}{r}_{s\ell}$. The symbol $\langle\ \rangle$ designates averaging at constant $\underset{\sim}{r}_{s\ell}$.

$$\langle \cos^2\theta_{s\ell} \rangle_{\underset{\sim}{r}} = \frac{\int_o^\pi P(\theta_{s\ell}, \underset{\sim}{r}_{s\ell}) \cos^2\theta_{s\ell} \sin\theta_{s\ell} d\theta_{s\ell}}{\int_o^\pi P(\theta_{s\ell}, \underset{\sim}{r}_{s\ell}) \sin\theta_{s\ell}\, d\theta_{s\ell}} \qquad (21)$$

where $P(\theta_{s\ell}, \underset{\sim}{r}_{s\ell})$ is the probability of orientation at angle $\theta_{s\ell}$ for a solvent molecule separated from the segment by distance $\underset{\sim}{r}_{s\ell}$. This may be described by a Boltzmann distribution

$$P(\theta_{s\ell}, \underset{\sim}{r}_{s\ell}) = K \exp\,[-V(\theta_{s\ell}, \underset{\sim}{r}_{s\ell})/kT] \qquad (22)$$

where $V(\theta_{s\ell}, \underset{\sim}{r}_{s\ell})$ is the potential for interaction between the polymer segment and the solvent molecule which depends upon intermolecular forces and decreases rapidly with their separation.

It is evident from this treatment that $\Delta\Gamma_s$ should increase with increasing solvent anisotropy, $\Delta\Gamma_\ell$, and should be a minimum for isotropic solvents. However, it must be realized that

$$\Delta\Gamma_\ell^o = (\Delta\Gamma_\ell^o)_{inh} + (\Delta\Gamma_\ell^o)_{ind.} \qquad (23)$$

where $(\Delta\Gamma_\ell^o)_{inh}$ is the inherent anisotropy of the isolated solvent molecule and $(\Delta\Gamma_\ell^o)_{ind}$ is the induced anisotropy arising from the dipole moment induced in the solvent by the dipole moment of the segment. This, of course depends upon the solvent polarizability. Consequently, even if $(\Delta\Gamma_\ell^o)_{inh} = 0$ as with CCl_4, it may be that there is a finite $(\Delta\Gamma_\ell^o)_{ind}$ so that $\Delta\Gamma_s$ may not equal $\Delta\Gamma_s^o$ as is usually assumed.

To some extent, the enhancement of $\Delta\Gamma_s$ for unswollen polymers which arises from local order may be treated in the above manner in which the segments of neighboring chains play the role of ordered solvent molecules.

EFFECT OF INTERNAL FIELD

The refractive index of a material is related to its polarization by

$$n^2 - 1 = 4\pi P/E \qquad (24)$$

where E is the applied field. P in turn is given by

$$P = N\alpha E_{eff} \tag{25}$$

where N is the number of molecules/cm^3 having polarizability α and E_{eff} is the effective field acting on the molecule. This is related to the applied field by

$$E_{eff} = E + E_{int.} \tag{26}$$

where $E_{int.}$ is the internal field arising from the polarization of surrounding molecules. Lorentz calculates this as the field arising from the polarization charge on the surface of a spherical cavity of a dielectric which leads to the result

$$E_{eff} = \frac{n^2 + 2}{3} E \tag{27}$$

The use of this Lorentz field in Equations (24) and (25) leads to the Lorenz-Lorentz-Equation. This equation is satisfactory for gases or isotropic liquids but its application to an anisotropic crystal is incorrect. We believe that its erronious use in relating the polarizabilities to the refractive index of n-paraffin crystals has led to the very low value of r_{PM} of 0.3 Å^3 as compared with the higher value of 1.47 obtained by Denbigh[9] from gas phase light scattering depolarization measurements[27]. It is not reasonable to accomodate an elongated polyethylene chain within a

spherical cavity and Stein has proposed[27] an alternate approach utilizing a cylindrical cavity within which the internal field factor κ_i is defined by

$$(E_{eff})_i = \kappa_i E_o \qquad (28)$$

is different parallel and perpendicular to the axis of the cylinder and depends upon its axial ratio. It was shown that with reasonable values of the axial ratio, the difference between the two values of $\Delta\Gamma_{PM}$ may be understood.

More recently, Hong and Stein[28] have developed a theory for the internal field within a polyethylene crystal based upon a summation over the contribution from dipolar fields of neighboring molecules. A polyethylene chain in a crystal is replaced by a cylinder with differing longitudinal and transverse polarizabilities located at the position of the real chains in the unit cell of the polyethylene crystal. The induced field at position p within a crystal arising from a point dipole at position $\underset{\sim}{r}_{ip}$ removed from p is given by

$$\underset{\sim}{E}_{ip} = \frac{3(\underset{\sim}{m}_i \cdot \underset{\sim}{r}_{ip})}{r_{ip}^5}\ \underset{\sim}{r}_{ip} - \frac{\underset{\sim}{m}_i}{r_{ip}^3} \qquad (29)$$

The total internal field at p is then given by

$$(\underset{\sim}{E}_{int})_p = \sum_i \underset{\sim}{E}_{ip} \qquad (30)$$

The dipole moment, $\underset{\sim}{m}_i$ is obtained from the total field at i from

$$\underset{\sim}{m}_i = |\alpha_i| \underset{\sim}{E}_i \tag{31}$$

where $|\alpha_i|$ is the polarizability tensor at i. For a uniaxially polarizable element, Equation (31) becomes

$$\underset{\sim}{m}_i = \delta_i (\underset{\sim}{E}_i \cdot \underset{\sim}{a}_i) \underset{\sim}{a}_i + \alpha_{2i} \underset{\sim}{E}_i \tag{32}$$

where δ_i is the anisotropy of polarizability of the ith volume element, $(\alpha_{1i} - \alpha_{2i})$, and $\underset{\sim}{a}_i$ is a unit vector along the principal polarizability axis. E_i is obtained in turn by adding to the external field, the internal field at i of the molecules surrounding point i.

This procedure is carried out by summing over an infinite crystal using iteration. In this way, the ratio of the dipole moment to the externally applied field may be determined leading to an expression for the internal field factor

$$\kappa_i = \frac{\underset{\sim}{m}_i}{\underset{\sim}{E}_0 |\alpha|} \tag{33}$$

This procedure is extended to a disordered structure, using the statistical segment modification. For this purpose Equations (29) and (30) are replaced by an integration over a segment distribution function

$$\underset{\sim}{E}_p = \int P(\underset{\sim}{r}_p, \underset{\sim}{a}) \left\{ \frac{3(\underset{\sim}{m} \cdot \underset{\sim}{r}_p)}{r_p^{\,5}} \underset{\sim}{r}_p - \frac{\underset{\sim}{m}}{r_p^{\,3}} \right\} d\underset{\sim}{r}_p \tag{34}$$

where $P(\underset{\sim}{r}_p, \underset{\sim}{a})$ is the probability that a segment will lie at a distance $\underset{\sim}{r}_p$ from p and be oriented in the direction $\underset{\sim}{a}$. The solution of this equation requires assuming some form for the segment distribution function. This function could be expanded in spherical harmonics where the coefficients serve as correlation functions in a manner similar to that used in the theory of light scattering from systems having non-random orientation correlations[29,30]. The coefficients in this expansion serve as correlation functions which describe how molecular order decreases with increasing molecular separation. These contain correlation distances which serve as measures of the sizes of ordered regions. In this manner, it would be possible to account for the internal field effects.

Let the reference molecule at position p be oriented in the Z direction and consider the effect of a second molecule, i, located at a vector distance $\underset{\sim}{r}_{ip}$ having angular coordinates ω and ψ (Figure 4) which is oriented with its principal polarizability axis $\underset{\sim}{a}_i$ at angles β and γ. For an applied field in the Z direction, Equation (29) gives for the components of internal field at p

$$
\begin{aligned}
E_{ix,p} = (E/r^3) \{ & 3\delta_i (\sin\omega \cos\psi)^2 (\sin\beta \cos\beta \cos\gamma) \\
& + 3 \delta_i (\sin^2\omega \sin\psi \cos\psi)(\sin\beta \cos\beta \sin\gamma) \\
& + 3 [\bar{\alpha}_i + \delta_i (\cos^2\beta - (1/3))] \sin\omega \cos\omega \cos\psi \\
& - \delta_i \sin\beta \cos\beta \cos\gamma \}
\end{aligned}
\tag{36}
$$

$$E_{iy,p} = (E/r^3) \left\{ 3\,\delta_i(\sin^2\omega\,\sin\psi\,\cos\psi)(\sin\beta\,\cos\beta\,\cos\gamma) \right.$$

$$+ 3\,\delta_i(\sin\omega\,\sin\psi)^2\,(\sin\beta\,\cos\beta\,\sin\gamma)$$

$$+ 3\,[\bar{\alpha}_i + \delta_i(\cos^2\beta - (1/3))]\,\sin\omega\,\cos\omega\,\sin\psi$$

$$\left. - \delta_i\,\sin\beta\,\cos\beta\,\sin\gamma \right\} \qquad (37)$$

and

$$E_{iz,p} = (E/r^3) \left\{ 3\,\delta_i(\sin\omega\,\cos\omega\,\cos\psi)(\sin\beta\,\cos\beta\,\sin\gamma) \right.$$

$$+ 3\,\delta_i(\sin\omega\,\cos\omega\,\sin\psi)(\sin\beta\,\cos\beta\,\cos\gamma)$$

$$\left. + [\bar{\alpha}_i + \delta_i(\cos^2\beta - (1/3))]\,[3\,\cos^2\omega - 1] \right\} \qquad (38)$$

The average internal field components at the origin is then found by averaging over angles. It is convenient to define the averages

$$F_1 = \langle \sin\beta\,\cos\beta\,\cos\gamma \rangle = \int_0^{2\pi}\int_0^{\pi} P(\beta,\gamma)\,\sin^2\beta\,\cos\beta\,\cos\gamma\,d\beta d\gamma \qquad (39)$$

$$F_2 = \langle \sin\beta\,\cos\beta\,\sin\gamma \rangle = \int_0^{2\pi}\int_0^{\pi} P(\beta,\gamma)\,\sin^2\beta\,\cos\beta\,\sin\gamma\,d\beta d\gamma \qquad (40)$$

and

$$F_3 = \langle \cos^2\beta \rangle = \int_0^{2\pi}\int_0^{\pi} P(\beta,\gamma)\,\cos^2\beta\,\sin\beta\,d\beta d\gamma \qquad (41)$$

The function $P(\beta,\gamma)$ expresses the probability that the polarizability axis $\underline{a}$ of the ith bond will be oriented at angles β and γ with respect to the first bond. We shall assume that this is cylindrically symmetrical and independent of γ so that $F_1 = F_2 = 0$. Thus the average field strengths

will be given by

$$\underset{\sim}{\bar{E}}_{i,xp} = \frac{3E}{r^3} \left[\alpha_i + (2/3)\ \delta_i\ F_{ij}\right] \sin\omega \cos\omega \cos\psi \qquad (42)$$

$$\underset{\sim}{\bar{E}}_{i,yp} = \frac{3E}{r^3} \left[\alpha_i + (2/3)\ \delta_i\ F_{ij}\right] \sin\omega \cos\omega \sin\psi \qquad (43)$$

and

$$\underset{\sim}{\bar{E}}_{i,zp} = \frac{E}{r^3} \left[\alpha_i + (2/3)\ \delta_i\ F_{ij}\right] \left[3\cos^2\omega - 1\right] \qquad (44)$$

where

$$F_{ij} = \left[3 \langle \cos^2\beta \rangle - 1\right]/2 \qquad (45)$$

The function F_{ij} characterizes the correlation of orientation of two molecules separated by vector distance $\underset{\sim}{r}_{ij}$ and diminishes with increasing magnitude of r.

The total average field at point p is then found by summing over all contributions from bonds i to give

$$\underset{\sim}{\bar{E}}_p = \sum_i \underset{\sim}{E}_{ip} = \bar{E}_{xp}\ \underset{\sim}{i} + \bar{E}_{yp}\ \underset{\sim}{j} + \bar{E}_{zp}\ \underset{\sim}{k} \qquad (46)$$

If we further assume that there is cylindrical symmetry of bond distribution in ψ, then $\bar{E}_{xp} = \bar{E}_{yp} = 0$ so

$$\underset{\sim}{\bar{E}}_p = \bar{E}_{zp}\ \underset{\sim}{k} \qquad (47)$$

where

$$\bar{E}_{zp} = \sum_i (E/r^3) \left\{\left[\bar{\alpha}_i + (2/3)\ \delta_i\ F_{ij}\right] \left[3\cos^2\omega - 1\right]\right\} \qquad (48)$$

A similar treatment for the case where the applied field is along the X (or the Y) axis leads to

$$\bar{\underset{\sim}{E}}_p = \bar{E}_{xp}\, \underset{\sim}{i} \tag{49}$$

where

$$\bar{E}_{xp} = \sum_i (E/r^3)\left\{[\bar{\alpha}_i - (1/3)\,\delta_i\, F_{ij}][3\sin^2\omega\cos^2\psi - 1]\right\} \tag{50}$$

The evaluation of the internal field then requires the assumption of some form for F_{ij}. Rather than assuming an empirical function to represent correlation in a partially ordered amorphous structure such as that portrayed in Figure 5, we shall idealize it as a two-phase model shown in Figure 6 consisting of (1) cylindrical domains within which there is crystal-like order where $F_{ij} = 1$ surrounded by (2) a random phase where there is complete disorder where $F_{ij} = 0$. Consequently Equation (48) becomes

$$\bar{E}_{zp} = E\left\{\sum_{ord.}[(1/r^3)(3\cos^2\omega - 1)\,\alpha_{||}] + \sum_{dis.}[(1/r^3)(3\cos^2\omega - 1)\,\bar{\alpha}]\right\}$$

$$= (\bar{E}_{zp})_{ord.} + (\bar{E}_{zp})_{dis.} \tag{51}$$

while Equation (50) gives

$$\bar{E}_{xp} = E\left\{\sum_{ord.}[(1/r^3)(3\sin^2\omega\cos^2\psi - 1)\,\alpha_{\perp}] + \sum_{dis.}[1/r^3)\right.$$

$$\left.(3\sin^2\omega\cos^2\psi - 1)\bar{\alpha}]\right\} = (\bar{E}_{xp})_{ord.} + (\bar{E}_{xp})_{dis.} \tag{52}$$

where all of the molecules are considered identical and

$$\alpha_{||} = \bar{\alpha}_i + (2/3)\ \delta_i \tag{53}$$

$$\alpha_{\perp} = \bar{\alpha}_i - (1/3)\ \delta_i \tag{54}$$

To evaluate $(\overline{E}_{zp})_{ord.}$ and $(\overline{E}_{xp})_{ord.}$, we may use the results of the previous treatment[28] for crystalline polyethylene which gives

$$(\overline{E}_{zp})_{ord.} = E \sum_i \left\{ (2/\varepsilon_{zi}\ C_i^2)(\sin^3\omega_i - \sin\omega_i)\ \alpha_{||} \right\}$$

$$= K_z'\ E\ \alpha_{||} \tag{55}$$

and

$$(\overline{E}_{xp})_{ord.} = E \sum_i \left\{ (2\ x_i^2/\varepsilon_{xi}\ C_i^4)(3\ \sin\omega_i - \sin^3\omega_i) - 2\ \sin\omega_i/\varepsilon_{xi}\ C_i^2 \right\} \alpha_{\perp}$$

$$= K_x'\ E\ \alpha_{\perp} \tag{56}$$

where ε is the dielectric constant (assumed constant as ε_z and ε_x) and C_i is defined as

$$C_i = (x_i^2 + y_i^2)^{1/2} \tag{57}$$

where x_i and y_i are the coordinates of the ith molecule and K_z' and K_x' are the internal field factors. In Equations (55) and (56), the angle ω_i is defined as $\tan\omega_i = H/C_i$ according to our previous treatment, where 2H is the height of the cylindrical cavity. The summation was carried out over the volume of the cylindrical cavity of height 2H and radius R.

The internal field from the disordered phase is evaluated utilizing the previously published calculation of the internal field within a cylindrical cavity[27] giving

$$(\bar{E}_{zp})_{dis.} = (n^2 - 1)[1 - f/(1 + f^2)^{1/2}]\, E_o$$

$$= K_z''\, E_o \qquad (58)$$

and

$$(\bar{E}_{xp})_{dis.} = [(n^2 - 1)/2][f/(1 + f^2)^{1/2}]\, E_o$$

$$= K_x''\, E_o \qquad (59)$$

where

$$f = H/R \qquad (60)$$

is the axial ratio of the cavity. n is the average refractive index of the polymer.

The total internal field at p is then

$$\bar{E}_{xp} = K_z'\, \alpha_{||}\, \bar{E}_{eff,z} + (K_z''/\varepsilon_z)\, E_o \qquad (61)$$

and

$$\bar{E}_{xp} = K_z'\, \alpha_{\perp}\, \bar{E}_{eff,x} + (K_z''/\varepsilon_x)\, E_o \qquad (62)$$

The dielectric constants must be introduced into the second terms to account for the modification of the polarization field of the disordered amorphous phase by the medium within the cavity. Since the effective field is the sum of the applied field and internal field, it must be

evaluated by an iteration process leading to

$$E_{eff,z} = \left[\frac{1}{1 - K_z' \alpha_{||}}\right]\left[1 + \frac{K_z''}{\varepsilon_z}\right] E_0 \qquad (63)$$

$$= K_z E_0$$

and

$$E_{eff,x} = \left[\frac{1}{1 - K_x' \alpha_{\perp}}\right]\left[1 + \frac{K_x''}{\varepsilon_x}\right] E_0 \qquad (64)$$

$$= K_x E_0$$

The effective anisotropy may then be calculated from

$$\Lambda = K_z \alpha_{||} - K_x \alpha_{\perp} \qquad (65)$$

This calculated anisotropy will include the total contribution of all the molecules within the ordered region which are subjected to the internal field which is modified by the ordering. Thus, the increase in anisotropy from ordering obtained in this way is a consequence of both enhancement of anisotropy arising from the association of molecules within the aggregates as well as the effects arising from the influence of ordering upon the internal field.

The anisotropy has been calculated taking the dimensions of the ordered region as an adjustable parameter. We have modified the preceding procedure in that we have allowed for some disorder in the ordered region, taking it as a paracrystal in which the chains are parallel to each other

but where they may deviate from their ideal lattice points in a direction perpendicular to the chain (cylinder) axis. Two cases were considered: one where the fluctuation in the x and y directions (parallel to the a and b crystal axes of the polyethylene unit cell) was $\pm$ 1 Å and $\pm$ 0.5 Å respectively, and a second where the fluctuations are assymetric and are between -1 Å and +2 Å in the a-axis direction and -0.75 Å to +1.25 Å in the b-axis direction. The paracrystalline lattices possessing such fluctuations were generated using a random number routine with a computer assuming that all values of lattice parameters within the prescribed limits may occur with equal probability. Polarizabilities were calculated for the parameters of the polyethylene unit cell where a = 7.40 Å, b = 4.93 Å and c = 2.534 Å. The values of bond polarizabilities for the bonds within a crystal, corrected for the internal field effect, which were proposed in our earlier publication were employed. The dielectric constant was assumed to be equal to the macroscopic dielectric constant of the crystal along each of the three crystal axes.

In this way the curves of Figure 7 were obtained which show the variation of the effective anisotropy of the statistical segment defined by Equation (65) as a function of the diameter of the cylindrical ordered region for various values of its axial ratio. As expected, the anisotropy increases with the size of the ordered region and does so more rapidly as the axial ratio of the ordered region becomes greater. The increase is more pronounced for a more disordered lattice.

The values are compared with the range of values calculated from experimental stress-optical coefficients. In making such a comparison, one

must consider that the value of $\Delta\Gamma_s$ obtained from the stress-optical coefficient using Equation (1) involves the assumption of the Lorentz field of Equation (27) and is therefore not strictly comparable with that given by Equation (65). Thus, one should actually compare the quantity

$$\Lambda_{exp} = \frac{(\bar{n}^2 + 2)^2}{9} \quad (\Delta\Gamma_s)_{exp} \tag{66}$$

which is the product of the experimental segment anisotropy and the internal field correction factor with Equation (65) rather than $\Delta\Gamma_s$ itself. The range of experimental values of Λ_{exp} obtained in this way is indicated in Figure 7.

It is noted that for reasonable values of axial ratios, the diameter of the ordered region would have to be less than 10 Å in order that the theoretically predicted values of Λ lie within the range of those obtained experimentally.

CONCLUSIONS

It is evident that experimental values of Γ obtained from SOC measurements are not consistent with long range ordering in the amorphous phase. Consideration of the effects of mutual orientation of amorphous segments and internal field effects are consistent with an orienting region in the dry polymer containing a small number of amorphous segments and having dimensions in the range of 5-10 Å. These dimensions are comparable with the range of ordering found for low molecular weight liquids

and are much smaller than the dimensions of ordered regions postulated in some recent discussions[24,25].

REFERENCES

1. W. Kuhn and F. Grün, Kolloid Z., 101, 248 (1942).
2. L. R. G. Treloar, Trans. Faraday Soc., 43, 277 (1947); 50, 881 (1954); The Physics of Rubber Elasticity, Oxford Univ. Press., 2nd Ed., 1967.
3. P. J. Flory, Statistical Mechanics of Chain Molecules, Interscience Publishers, New York, 1969; P. J. Flory, R. L. Jernigan and A. Tonelli, Macromolecules, 5, 550 (1972)
4. K. Nagai, J. Chem. Phys., 40, 2818 (1964); 49, 4212, (1960); K. Nagai and T. Ishikawa, J. Chem. Phys. 45, 3128 (1966).
5. R. P. Smith and E. M. Mortensen, J. Chem. Phys., 32, 502 (1960).
6. A. N. Gent and V. V. Vickroy, Jr., J. Polym. Sci., A2, 5, 47 (1967); A. N. Gent and T. H. Kuan, J. Polym. Sci., A2, 9, 927 (1971).
7. D. W. Saunders, D. R. Lightfoot and D. A. Parsons, J. Polym. Sci., A2, 6, 1183 (1968).
8. M. H. Liberman, Y. Abe and P. J. Flory, Macromolecules, 5, 550 (1972).
9. K. G. Denbigh, Trans. Faraday Soc., 36, 936 (1940).
10. C. Clement and P. Botherel, J. Chim. Phys. Physicochim. Biol., 61, 878, 1262 (1964); C. R. Acad. Sci. (Paris), 258, 4757 (1964).
11. R. J. W. LeFevre, B. J. Orr, and G. L. D. Ritchie, J. Chem. Soc. B, 273 (1966); R. L. W. LeFevre, Advances in Physical Orgnaic Chemistry, Academic Press, New York, (1965), Vol. 3, p. 1.
12. G. D. Patterson and P. J. Flory, Trans. Faraday Soc., 68, 1098 (1972).
13. T. Ishikawa and K. Nagai, J. Polym. Sci., A-2, 7, 1123 (1969).
14. K. J. Smith and D. Puett, J. Appl. Phys., 37, 364 (1966).
15. M. Fukuda, G. L. Wilkes and R. S. Stein, J. Polym. Sci., A-2, 9, 1417 (1971).

16. A. N. Gent, Macromolecules, 2, 262 (1961).

17. C. Price, G. Allen, F. deCandia, M. C. Kirkham and A. Subramanian, Polymer, 11, 486 (1970); C. Price, K. A. Evans and F. deCandia, Polymer, 14, 338 (1973).

18. J. E. Mark, J. Am. Chem. Soc., 92, 7252 (1970); C. U. Yu and J. E. Mark, Macromolecules, 6, 751 (1973).

19. C. S. M. Ong and R. S. Stein, J. Polym. Sci., (Polym. Phys. Ed.), 12, 1599 (1974).

20. A. E. Tonelli and E. Helfand, Macromolecules, 7, 59 (1974).

21. I. Ya. Poldubnyi, Ye. G. Erenburg and M. A. Yeremina, Vysokomol. Soedin, A10, 1381 (1968).

22. W. Phillipoff, private communication, 1970.

23. K. Nagai, J. Phys. Chem., 74, 411 (1970).

24. C. S. Y. Yeh, Pure and Applied Chem., 31, 65 (1972); CRC Critical Reviews in Macromolecular Science, April, 1972, p. 173.

25. W. Pechold, IUPAC Preprints 789 (1971); W. Pechold, M. E. T. Hauber and E. Liska, Koll. Z., J. Z. Polymers, 251, 818 (1973).

26. C. W. Bunn and R. Daubeny, Trans. Faraday Soc., 50, 1173 (1954).

27. R. S. Stein, J. Polym. Sci., A-2, 7, 1021 (1969).

28. S. D. Hong, C. Chang and R. S. Stein, Bull. Am. Phys. Soc., 19, 311 (1974); submitted for publication.

29. R. S. Stein, P. F. Erhardt, S. B. Clough and G. Adams, J. Appl. Phys., 37, 3980 (1966).

30. J. J. van Aartsen, Polymer Networks, Structure and Mechanical Properties, ed. A. J. Chompff and S. Newman, Plenum Press, N.Y., 1971, p. 307.

FIGURES

1) The variation of birefringence with stress for high cis crosslinked 1,4-polybutadiene rubber swollen in a variety of solvents (From Ref. 15, Fig. 15).

2) Mooney-Rivlin type plots for the birefringence-strain relationship for solution vulcanized cis-1,4-polybutadiene. Samples were vulcanized in solution containing a volume fraction of rubber designated by ϕ_r in the figure. (The symbol v_r in the figure corresponds to ϕ_2 in the text). (From Ref. 19, Fig. 2).

3) The variation of the stress-optical coefficient of samples of crosslinked 1,4-polybutadiene with cis content and for a number of swelling solvents as compared with streaming birefringence data. (From Ref. 15, Fig. 21).

4) The angles ω and ψ defining the orientation of the vector $\underset{\sim}{r}_R$ and the angles β and γ defining the orientation of the principal polarizability axis of the ith bond.

5) The partially ordered amorphous phase in which closely spaced chains tend to lie parallel to each other.

6) The idealized two-phase model consisting of cylindrical ordered regions imbedded in a disordered matrix.

7) The variation of the effective anisotropy of the statistical segment of polyethylene with the diameter of the cylindrical ordered region for several values of its axial ratio. Calculations are carried out for paracrystalline structure of the ordered region assuming a) $\Delta a = \pm 1$ Å and $\Delta b = \pm 0.5$ Å (dashed line) and b) -1 Å $> \Delta a > 2$ Å and $-0.75 > \Delta b > 1.25$ Å (solid line). Values are compared with the range of calculated experimental values of Λ.

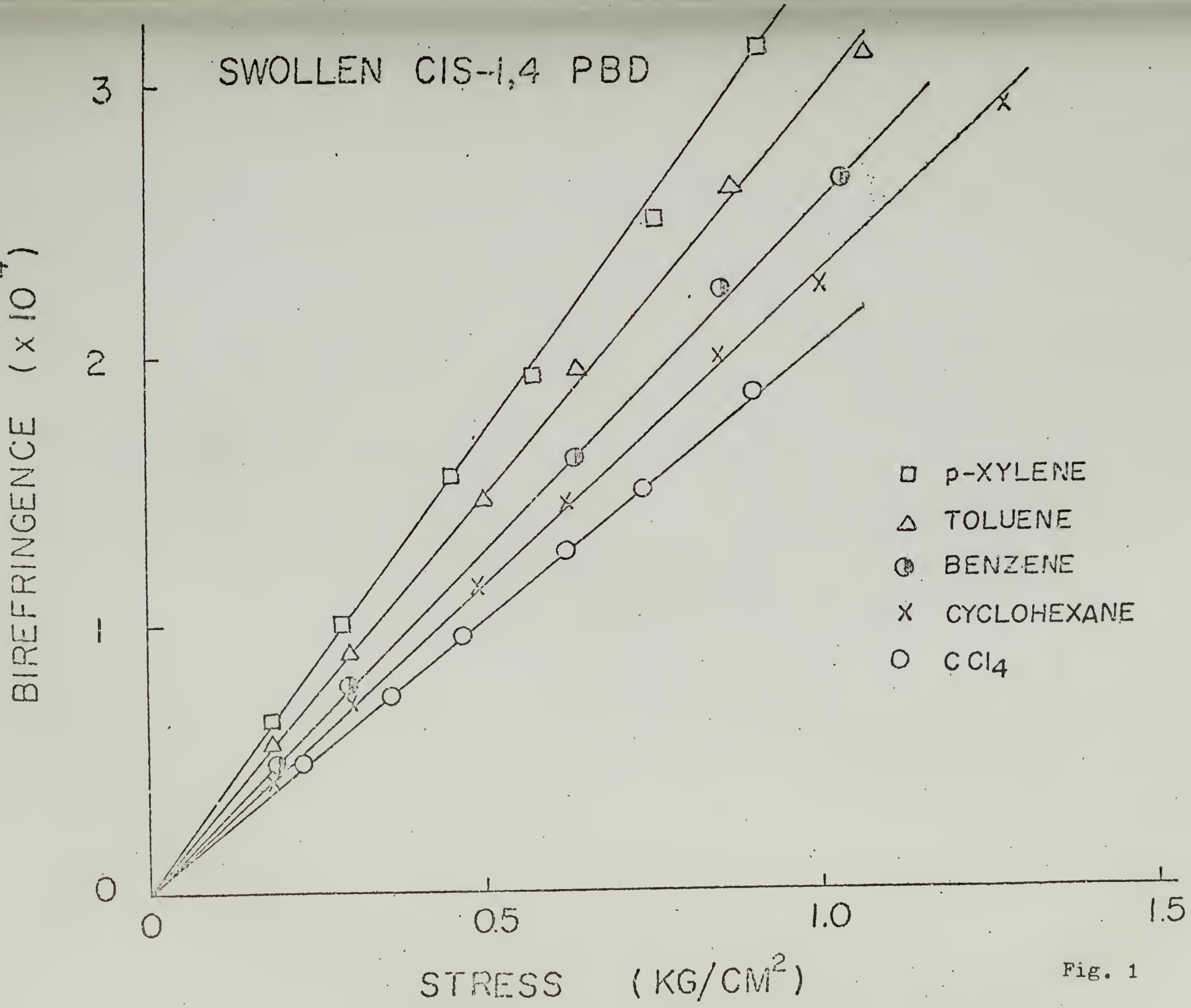
SWOLLEN CIS-1,4 PBD
BIREFRINGENCE (x 10^-4)
3
2
1
0
0
0.5
1.0
1.5
STRESS (KG/CM^2)
p-XYLENE
TOLUENE
BENZENE
CYCLOHEXANE
CCl4

Fig. 1

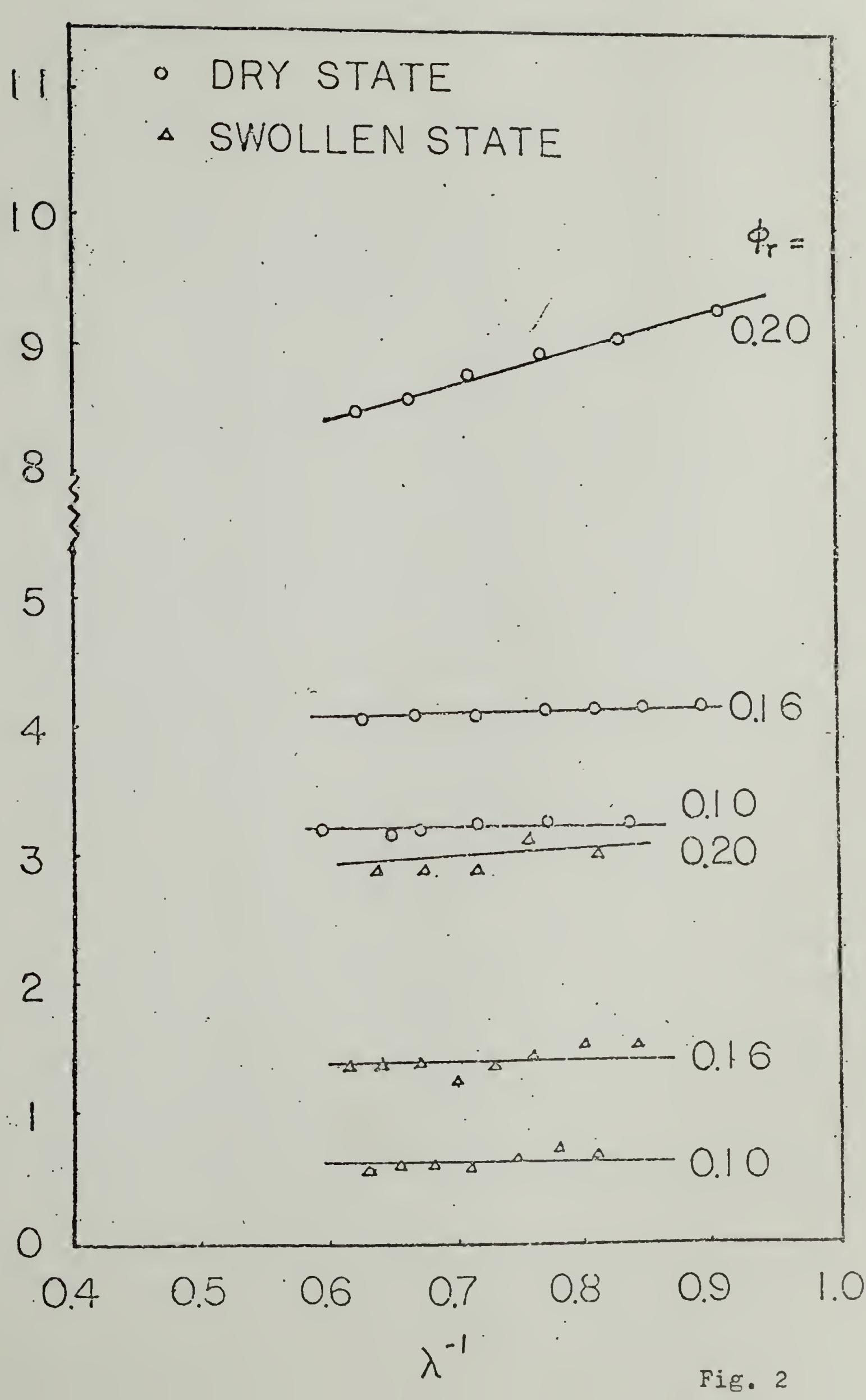
DRY STATE
SWOLLEN STATE
ϕ_r =
0.20
0.16
0.10
0.20
0.16
0.10
$\Delta\pi v_r^{-1/3}/(1\lambda^2 - \lambda^{-1}) \times 10^4$
λ^{-1}
0
1
2
3
4
5
8
9
10
11
0.4
0.5
0.6
0.7
0.8
0.9
1.0

Fig. 2

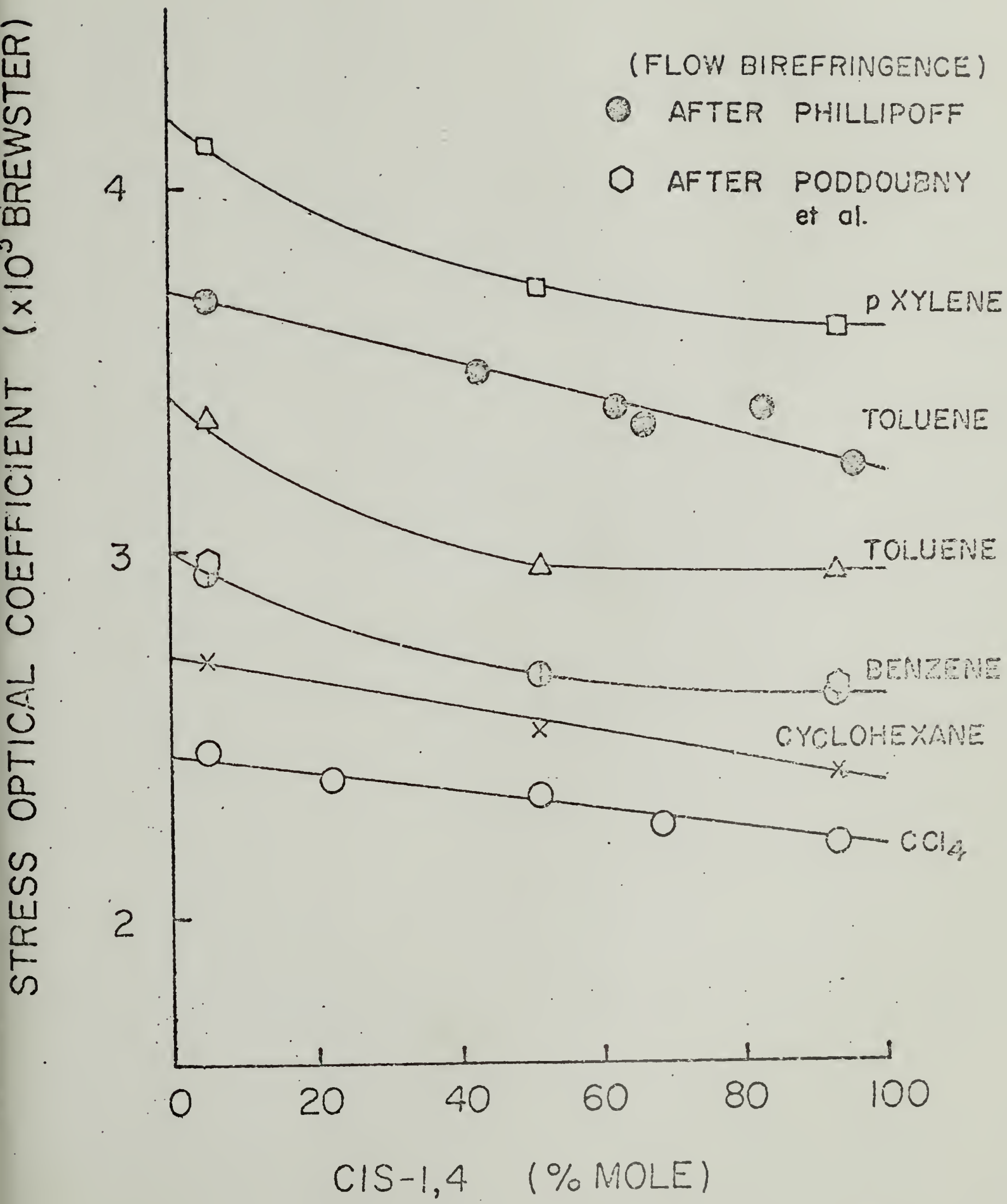
(FLOW BIREFRINGENCE)
AFTER PHILLIPOFF
AFTER PODDOUBNY et al.
p XYLENE
TOLUENE
TOLUENE
BENZENE
CYCLOHEXANE
CCl4
STRESS OPTICAL COEFFICIENT (x10^3 BREWSTER)
4
3
2
0
20
40
60
80
100
CIS-1,4 (% MOLE)

Fig. 3

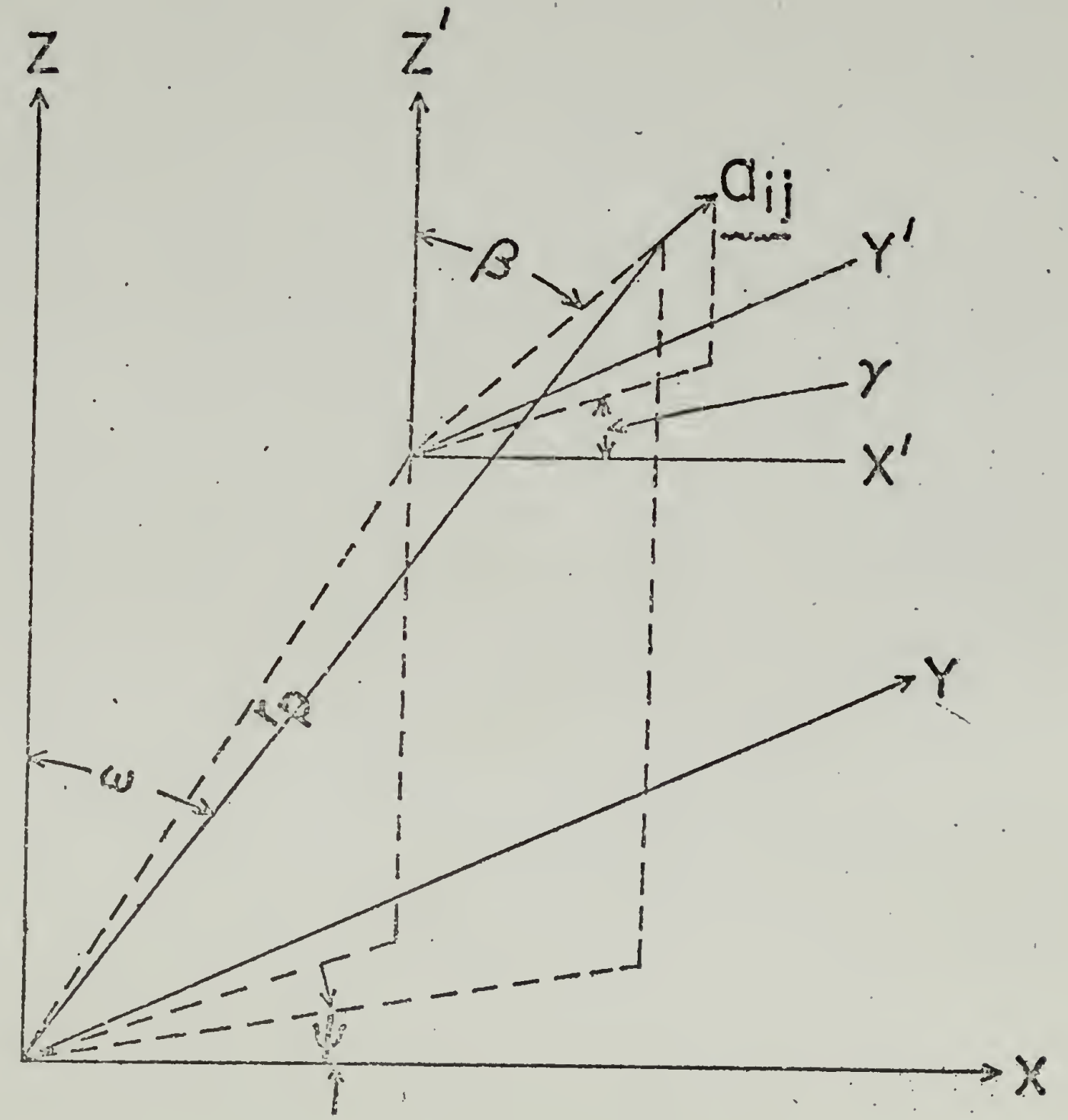

Fig. 4

Fig. 5

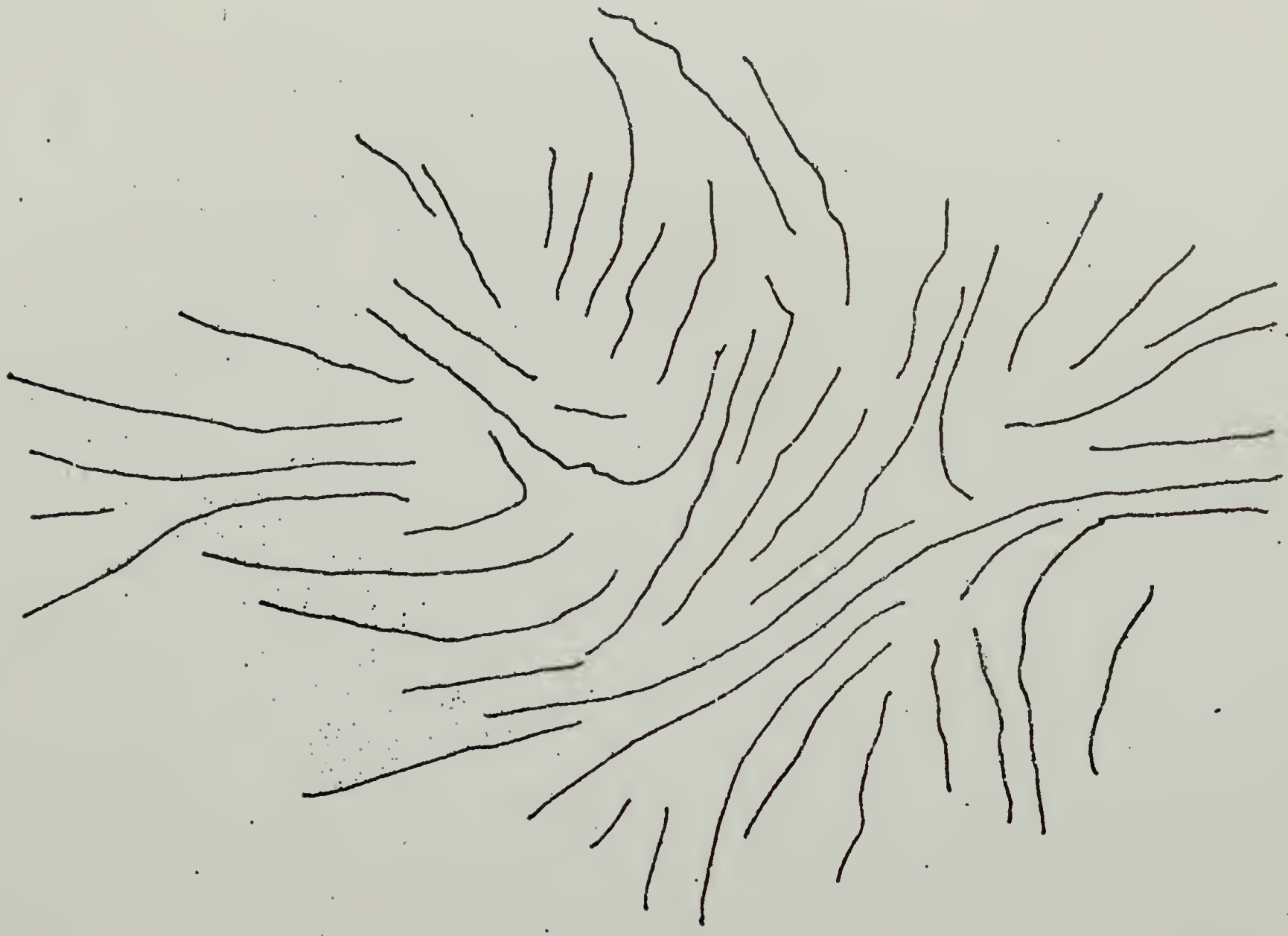

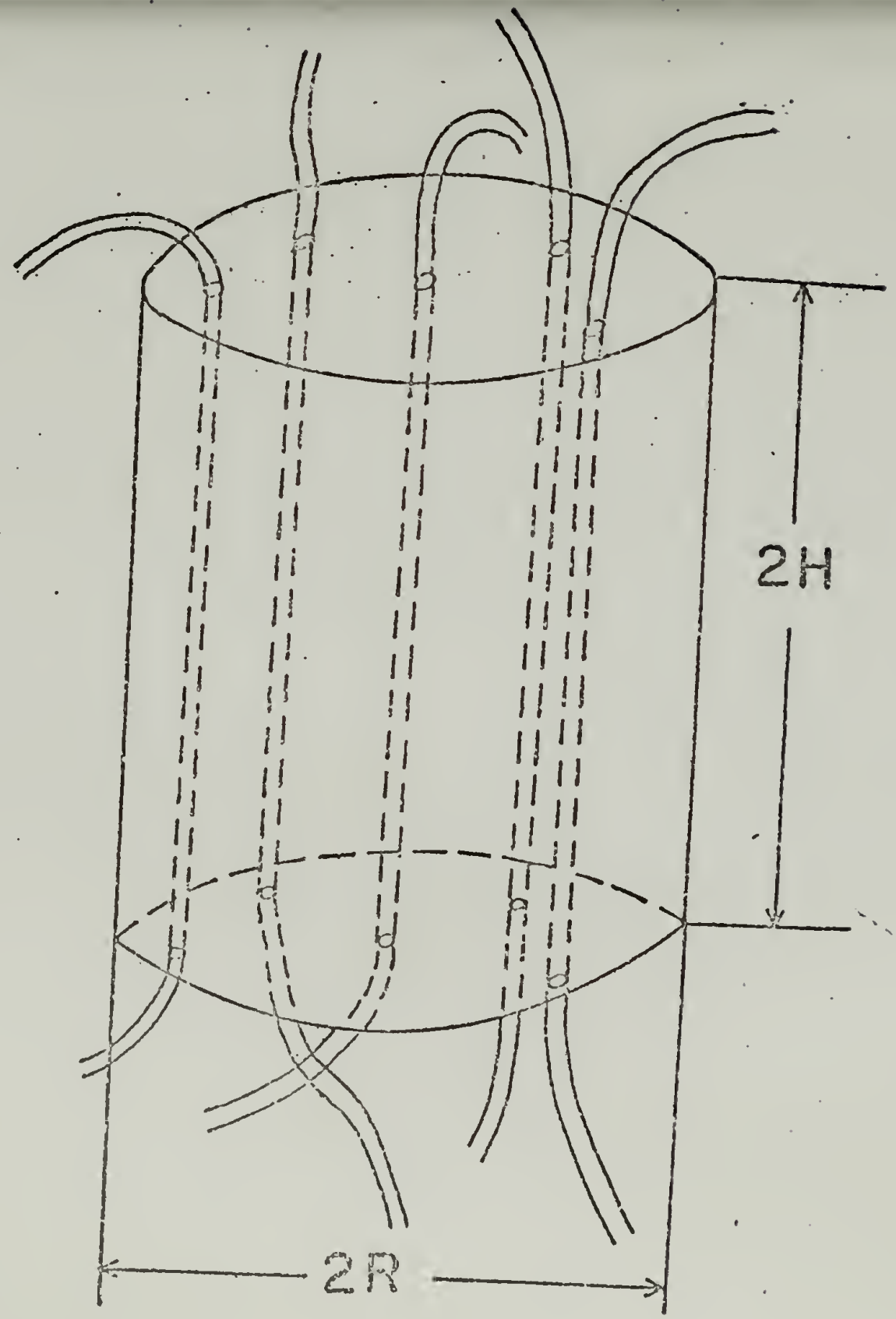

Fig. 6

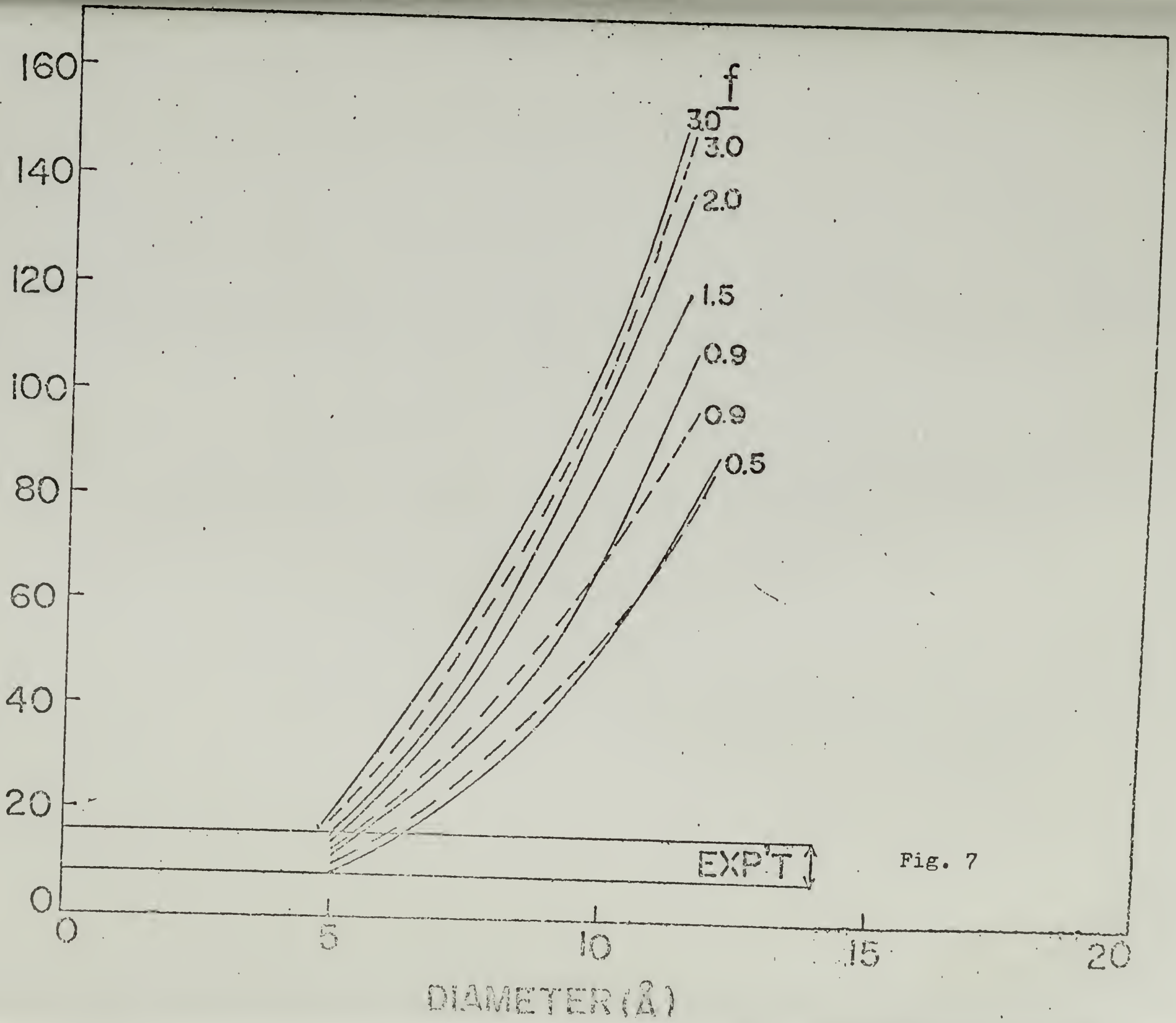
160
140
120
100
80
60
40
20
0
A (Å^3)
f
3.0
3.0
2.0
1.5
0.9
0.9
0.5
EXPT
0
5
10
15
20
DIAMETER (Å)

Fig. 7

CHAPTER III

EFFECTS OF BIREFRINGENCE AND INTERNAL FIELD ON OPTICAL DICHROISM

ABSTRACT

The effects of birefringence and internal field on optical dichroism was examined by solving the Maxwell's equation. The solution was applied to three morphologically different samples: (1) Single crystals, (2) Amorphous polymer and (3) Polycrystalline polymer for the consideration of the effect. The correction factors have been obtained and the processes of correction have been discussed. The results also reveal that the experimental results measured by installing the polarizer before the sample or after the sample are identical. It is also concluded that a single crystal is the better sample for the purpose of structure studies by polarized radiation technique. Comparison with the theory developed by Cunningham et al is discussed.

INTRODUCTION

Optical dichroism, e.g. ultraviolet dichroism, visible dichroism and infrared dichroism, have been utilized in the determination of molecular structure as well as in the characterization of molecular orientation of polymers (1-5). The use of this

technique comes from the fact that optical absorption arises from the interaction between the electric field of incident radiation and the transition moments associated with the vibration modes of particular molecular groups. Consequently, as molecular chains are oriented, the absorption will show dichroic effect with a polarized incident beam.

The molecular orientation can be expressed as a function of dichroic ratio, which is the ratio of absorbance with incident beam polarized parallel to the fiber axis and that with incident beam polarized perpendicular to the fiber axis (6). However, the assumption underlying the derivation is that absorption is the only interaction between the matter and radiation as the beam passes through the sample. This is not true because there are other interactions like polarization of the dielectrics occurring. Particularly, in an anisotropic sample these interactions are not identical in all directions, thus their effects will affect the dichroic ratio and obscure the interpretation of molecular orientation based on dichroism measurement. For instance some peptide single crystals show that the direction of maximum absorption always coinciding with a principal optic axis direction regardless of the orientation of the transition moment (1).

The problem of the effect of birefringence on optical dichroism of some organic single crystals has been examined by Ward (1). More recently, Cunningham, Davies and Ward (7) have developed a theory to account for the internal field effect (local field effect)

on the infrared dichroism of polyethylene terephthalate. The latter approach employed the Lorentz-Lorenz or Clausius-Mosotti equation to account for the internal field effect.

The purpose of this Chapter is to re-examine the relationship between molecular orientation and dichroic ratio, taking account of the effects of birefringence and internal field. Our approach is similar to that of Ward ___ except that while Ward only considered the birefringence effect, we try to take account of both the birefringence effect and the internal field effect ___ in which Maxwell's electromagnetic equations are rederived with consideration of birefringence and internal field effects. Furthermore, an anisotropic sample, i.e. a stretched polymer film, will be considered as a general case and the derivation of the theory will be done with consideration of the present experimental set-up.

The theory will be applied to calculate the molecular orientation from the experimental results on PET obtained by Cunningham et al (8). It will be shown, by adopting the Lorentz-Lorenz equation to account for the internal field effect, that the results are in reasonable agreement with those obtained from the theory of Cunningham, Davies and Ward (7).

THEORY

As the radiation passes through the medium, its electric field will interact with the absorbing groups and with the chemical

bonds of the medium. The former interaction gives rise to absorption and the latter gives rise to polarization of the chemical bonds. We shall only consider nonconducting nonferromagnetic materials which include perhaps all the synthetic organic polymers. In such a medium, it is the absorption, rather than conduction, to be the function of dissipating the electric energy. By adopting the analogy between conduction and absorption in terms of energy dissipation, one may express the energy dissipated by absorption in the form (1,9)

$$-\dot{\omega} = \sum_{ij} \sigma_{ij} E_{eff,i} E_{eff,j} \qquad (1)$$

where $-\dot{\omega}$ is the rate of dissipation of electrical energy per cubic centimeter per second. σ_{ij} are the components of the absorptivity tensor. $E_{eff,i}$ represents the i^{th} component of the effective electric field. The effective electric field is introduced in place of the applied electric field because the actual electric field interacting with the absorbing groups inside the sample is this effective electric field which includes the applied electric field of the radiation and the internal electric field arising from the surrounding induced dipoles resulting from polarization of the chemical bonds of the medium. The effective electric field may be expressed in the form

$$E_{eff,i} = \sum_{p} k_{ip} E_{p} \qquad (2)$$

for an anisotropic medium. Where k_{ip} are the components of the internal field factor tensor and E_p is the component of the applied field. Combining equs. (1) and (2), one obtains

$$\begin{aligned} -\dot{\omega} &= \sum_{i,j,p,q} \sigma_{ij}\, k_{ip}\, k_{jq}\, E_p\, E_q \\ &= \sum_{p,i,j,q} E_p\, k_{pi}\, \sigma_{ij}\, k_{jq}\, E_q \\ &= \sum_{p,q} E_p\, b_{pq}\, E_q \\ &= \underset{\sim}{E} \cdot |b_{pq}|\, \underset{\sim}{E} \\ &= \underset{\sim}{E} \cdot \underset{\sim}{\mathbb{E}} \end{aligned} \qquad (3)$$

where $$b_{pq} = k_{pi}\, \sigma_{ij}\, k_{jq} \qquad (4)$$

and $$\underset{\sim}{\mathbb{E}} = |b_{pq}|\, \underset{\sim}{E}$$

$\underset{\sim}{E}$ is the applied electric field of the radiation.

In the case of an isotropic medium, the internal field factor can be expressed as a scalar by adopting, for example, the Lorentz-Lorenz spherical cavity model (10). It has also been shown that, for an orthorhombic crystal, the three k_{ii}'s which associate with the three optic axes can be calculated based on knowledge

of the crystal structure (11). In the case of a deformation-induced anisotropic medium such as a stretched polymer, it is difficult to calculate k_{jp} based on the structure because the exact structure is usually not known. The k_{jp} can still be estimated by the assumption of some sort of model (10,12). In order to simplify the treatment, we shall assume that the internal field factor tensor can be diagonalized with the three mutual perpendicular optical axes as reference coordinates. Consequently, we need consider only the three diagonal components, k_{ii}, of the internal field factor tensor and eq.(4) becomes

$$b_{ij} = k_{ii}\, \sigma_{ij}\, k_{jj} \qquad (5)$$

The components of σ_{ij} can be expressed as

$$\sigma_{ij} = \sigma \sum_k l_{ik}\, l_{kj} \qquad (6)$$

where l_{ik} is the direction cosine of the k^{th} transition moment in the i^{th} direction. σ can be shown to be related to the square of the transition moment as follows. The rate of dissipation of electrical energy per second due to the absorption of a perfectly oriented transition moment may be given as (13)

$$-\frac{\dot{w}}{N} = \frac{8\pi^3 \nu}{3h}\, \mu^2\, \rho(\nu) \qquad (7)$$

where h is Planck's constant, ν the frequency of radiation, N the net number of absorbing groups per unit volume eligible for transition and μ the transition moment. $\rho(\nu)$ is the radiation density, which can be expressed as (9)

$$\rho(\nu) = \frac{1}{8\pi} E_{eff}^2 \qquad (8)$$

Substituting eq. (8) into eq. (7) and by comparing with eq. (1) for the case of a perfectly oriented transition moment, this yields

$$\sigma = \frac{\pi^2 \nu}{3h} \mu^2 \qquad (9)$$

or σ can be related to the absorption coefficient obtained from experiment, K_{exp}, by (13)

$$\sigma = \frac{c K_{exp}}{8\pi N}$$

where C is the velocity of light in vacuum.

The vector of the dielectric displacement can be expressed as (1,9)

$$\underset{\sim}{D} = |\epsilon_{ij}| \underset{\sim}{E} \qquad (11)$$

where $|\epsilon_{ij}|$ is the dielectric tensor.

By consideration of the law of conservation of energy, it can be shown (9) that

$$\text{Curl}\ \underset{\sim}{H} = \frac{|\epsilon_{ij}|}{c}\frac{\partial \underset{\sim}{E}}{\partial t} + \frac{4\pi}{c}\,|k_{ii}\,\sigma_{ij}\,k_{jj}|\,\underset{\sim}{E} \qquad (12)$$

$$\text{Curl}\ \underset{\sim}{E} = -\frac{1}{c}\frac{\partial \underset{\sim}{H}}{\partial t} \qquad (13)$$

where $\underset{\sim}{H}$ is the magnetic field of the radiation and C the velocity of light in vacuum.

In optical dichroism measurement, one is considering only the interaction between the electric field of the radiation and the transition moment. Thus by eliminating $\underset{\sim}{H}$ from eqs. (12) and (13), it yields (1)

$$c^2\left(\nabla^2 E_i - \sum_j \frac{\partial}{\partial x_i}\frac{\partial E_j}{\partial x_j}\right) = \frac{\partial}{\partial t}\left(\sum_{ij} 4\pi\, k_{ii}\,\sigma_{ij}\,k_{jj}\,E_j + \sum_j \epsilon_{ij}\frac{\partial E_j}{\partial t}\right) \qquad (14)$$

Eq. (14) is identical to the one obtained by Ward (1) except for the inclusion of k_{ii} and k_{jj} to account for the internal field effect.

The electric field of the radiation propagates through the medium must satisfy eq. (14). To solve eq. (14), one may assume a solution of the form

$$E_i = a_i \exp\left[ip\left\{t - \frac{q}{c}(l x_1 + m x_2 + n x_3)\right\}\right] \qquad (15)$$

This represents a plane wave propagating in the direction given by the direction cosines l, m and n.

$$
\left.\begin{aligned}
&a_1\{q^2(l^2-1)-4\pi i(k_{11}^2\sigma_{11}/p)+\epsilon_{11}\}+a_2\{q^2lm-4\pi i(k_{11}k_{22}\sigma_{12}/p)+\epsilon_{12}\}\\
&\qquad+a_3\{q^2ln-4\pi i(k_{11}k_{33}\sigma_{13}/p)+\epsilon_{13}\}=0\\
&a_1\{q^2lm-4\pi i(k_{11}k_{22}\sigma_{21}/p)+\epsilon_{21}\}+a_2\{q^2(m^2-1)-4\pi i(k_{22}^2\sigma_{22}/p)+\epsilon_{22}\}\\
&\qquad+a_3\{q^2mn-4\pi i(k_{22}k_{33}\sigma_{23}/p)+\epsilon_{23}\}=0\\
&a_1\{q^2nl-4\pi i(k_{11}k_{33}\sigma_{13}/p)+\epsilon_{31}\}+a_2\{q^2nm-4\pi i(k_{22}k_{33}\sigma_{32}/p)+\epsilon_{32}\}\\
&\qquad+a_3\{q^2(n^2-1)-4\pi i(k_{33}^2\sigma_{33}/p)+\epsilon_{33}\}=0
\end{aligned}\right\}\qquad(16)
$$

To solve eq. (14), one substitutes eq. (15) into eq. (14) and obtains eq. (16). The determinant of the coefficients of the a_i in eq. (16) must vanish in order for the a_i to be consistent, consequently one obtains eq. (17).

$$
\begin{vmatrix}
q^2(l^2-1)-4\pi i(k_{11}^2\sigma_{11}/p)+\epsilon_{11} & q^2lm-4\pi i(k_{11}k_{22}\sigma_{12}/p)+\epsilon_{12} & q^2ln-4\pi i(k_{11}k_{33}\sigma_{13}/p)+\epsilon_{13}\\
q^2ml-4\pi i(k_{11}k_{22}\sigma_{21}/p)+\epsilon_{21} & q^2(m^2-1)-4\pi i(k_{22}^2\sigma_{22}/p)+\epsilon_{22} & q^2mn-4\pi i(k_{22}k_{33}\sigma_{23}/p)+\epsilon_{23}\\
q^2nl-4\pi i(k_{11}k_{33}\sigma_{13}/p)+\epsilon_{31} & q^2nm-4\pi i(k_{22}k_{33}\sigma_{32}/p)+\epsilon_{32} & q^2(n^2-1)+4\pi i(k_{33}^2\sigma_{33}/p)+\epsilon_{33}
\end{vmatrix}=0
\qquad(17)
$$

It can be shown, as in the case obtained by Ward (1), that the coefficient of q^6 in eq. (17) always vanishes on account of the condition

$$\ell^2 + m^2 + n^2 = 1 \qquad (18)$$

and eq. (17) is a quadratic equation in q^2. To further simplify the problem, one may consider the case as shown in Fig. 1, where x_1, x_2 and x_3 are the principal optic axes and a polarized radiation propagates along x_2 with its electric field $\underset{\sim}{E}$ vibrating in the x_1x_3 plane and forming an angle θ with x_1. We may further assume that the incident radiation is normal to the sample surface, thus there is no complication of refraction, consequently m = 1 and ℓ = n = 0. The transition moment of the medium has a component residing in the plane x_1x_3 and this component makes an angle ϕ with x_1. The other component of the transition moment need not be considered because it is perpendicular to the electric field of the radiation and thus there is no interaction. It follows from eq. (6) that

$$\sigma_{11} = \sigma' \cos^2\psi \cos^2\phi, \quad \sigma_{13} = \sigma_{31} = \sigma' \cos^2\psi \sin\phi \cos\phi, \quad \sigma_{33} = \sigma' \cos^2\psi \sin^2\phi \qquad (19)$$

where $\sigma' = N\sigma$. Furthermore, since we define the optic axes as the reference coordinates, then

$$\epsilon_{13} = \epsilon_{31} = 0 \qquad (20)$$

Eq. (17) now reduces to

$$\begin{vmatrix} 4\pi i(\sigma' k_{11}^2/p)\cos^2\psi\cos^2\phi - \epsilon_{11} + q^2 & 4\pi i(\sigma' k_{11}k_{33}/p)\cos^2\psi\sin\phi\cos\phi \\ 4\pi i(\sigma' k_{11}k_{33}/p)\cos^2\psi\sin^2\phi\cos\phi & 4\pi i(\sigma' k_{33}^2/p)\cos^2\psi\sin^2\phi - \epsilon_{33} + q^2 \end{vmatrix} = 0 \qquad (21)$$

The solution of eq. (21) is

$$q_1^2 = \epsilon_{11} - \frac{4\pi\sigma'\cos^2\psi\cos^2\phi\, k_{11}^2}{p}\, i + \frac{4\pi^2\sigma'^2\cos^2\psi\sin^2 2\phi\, k_{11}^2 k_{33}^2}{p^2(\epsilon_{33}-\epsilon_{11})} - \cdots$$

$$q_3^2 = \epsilon_{33} - \frac{4\pi\sigma'\cos^2\psi\sin^2\phi\, k_{33}^2}{p}\, i - \frac{4\pi^2\sigma'^2\cos^2\psi\sin^2 2\phi\, k_{11}^2 k_{33}^2}{p^2(\epsilon_{33}-\epsilon_{11})} + \cdots \qquad (22)$$

or

$$q_1 \simeq \sqrt{\epsilon_{11}} - \frac{2\pi\sigma'\cos^2\psi\cos^2\phi\, k_{11}^2}{p\sqrt{\epsilon_{11}}}\, i$$

$$q_3 \simeq \sqrt{\epsilon_{33}} - \frac{2\pi\sigma'\cos^2\psi\sin^2\phi\, k_{33}^2}{p\sqrt{\epsilon_{33}}}\, i \qquad (23)$$

Substituting eq. (22) into eq. (16), one obtains the ratios of the amplitudes

$$\frac{a_1}{a_3} = 1\Big/\left(\frac{2\pi\sigma'\sin 2\phi\cos\psi\, k_{11}k_{33}}{p(\epsilon_{33}-\epsilon_{11})}\, i\right) = -\frac{1}{\eta}\, i \qquad (24)$$

for $q^2 = q_1^2$, called type I waves, and

$$\frac{a_1}{a_3} = \frac{2\pi\sigma'\sin 2\phi\cos\psi\, k_{11}k_{33}}{p(\epsilon_{33}-\epsilon_{11})\, i} = -\eta\, i \qquad (25)$$

for $q^2 = q_3^2$, called type III waves.

The electric field of the incident beam in the boundary plane can be resolved into three components (see Fig. 1)

$$E_1 = E_0 \cos\theta \, e^{i\rho t} \quad , \quad E_2 = 0$$

$$E_3 = E_0 \sin\theta \, e^{i\rho t} \tag{26}$$

Continuity must be maintained as the radiation across the boundary. If we neglect the loss of reflection, then it can be shown that the two types of waves in the medium are

Type I

$$E_1 = E_0(\cos\theta - i\eta \sin\theta)\, e^{i\rho(t - \beta_1 x_2/c)}$$

$$E_3 = E_0 \, i\eta \cos\theta \, e^{i\rho(t - \beta_1 x_2/c)}$$

Type III

$$E_1 = E_0 \, i\eta \sin\theta \, e^{i\rho(t - \beta_3 x_2/c)}$$

$$E_3 = E_0(\sin\theta - i\eta\cos\theta)\, e^{i(t - \beta_3 x_2/c)} \tag{27}$$

Because $\sigma'/\rho \ll 1$ (for instance, $\frac{\sigma'}{\rho} = 6.42 \times 10^{-5}$ for the band of 1894 cm^{-1} of polyethylene using the absorption coefficient obtained by Read et al (14)), therefore, the higher order terms of η were neglected. The solution is identical to that obtained by Ward (1), as to be expected, except the inclusion of k_{11} and k_{33} (Note : eqs. (24) and (25) are not the same as those obtained by Ward, the latter appears to be in error. Furthermore, $\sigma' = N\sigma$ instead of σ

is used because σ is defined to arise from a single transition moment according to eq. (6). Assume the thickness of the sample is $x_2 = d$, if the higher order terms of η are neglected, then the intensity of the beam emerged from the sample will be

Type I

$$I_1 = \frac{1}{8\pi} E_1 E_1^* = \frac{E_0^2}{8\pi} \cos^2\theta\, e^{-K_1 d}$$

$$I_3 \cong 0$$

Type III

$$I_1 \simeq 0$$

$$I_3 = \frac{1}{8\pi} E_3 E_3^* = \frac{E_0^2}{8\pi} \sin^2\theta\, e^{-K_3 d} \qquad (28)$$

and the total intensity of the radiation emerged from the sample is

$$I = \frac{1}{8\pi} E_0^2 \left(\cos^2\theta\, e^{-K_1 d} + \sin^2\theta\, e^{-K_3 d} \right) \qquad (29)$$

where

$$K_1 = \frac{4\pi\sigma' k_{11}^2 \cos^2\phi \cos^2\psi}{c\sqrt{\epsilon_{11}}}$$

$$K_3 = \frac{4\pi\sigma' k_{33}^2 \sin^2\phi \cos^2\psi}{c\sqrt{\epsilon_{33}}} \qquad (30)$$

Since $\frac{\sigma'}{p}$ and in turn η are very small, one may neglect the terms containing η and eq. (27) becomes

Type I

$$E_1 = E_0 \cos\theta\, e^{ip(t - \beta_1 d/c)}$$

and Type III

$$E_3 = E_0 \sin\theta \, e^{ip(t - \beta_3 d/c)} \tag{31}$$

For the convenience of further discussion, we shall consider the case in which the electric vector of the incident beam is at an angle θ to x_1 and the electric vector of the exit beam at an angle θ_0 to x_1. The electric field of the exit beam, E_x' and that perpendicular to E_x', E_y', can be shown to be

$$E_x' = E_0 \cos\theta_0 \cos\theta \, e^{ip(t - \beta_1 d/c)} + E_0 \sin\theta_0 \sin\theta \, e^{ip(t - \beta_3 d/c)}$$

$$E_y' = E_0 \cos\theta_0 \sin\theta \, e^{ip(t - \beta_3 d/c)} + E_0 \sin\theta_0 \cos\theta \, e^{ip(t - \beta_1 d/c)} \tag{32}$$

Combining eqs. (23), (30) and (32), one obtains

$$E_x' = E_0 \left[\cos\theta_0 \cos\theta \, e^{-(K_1/2)d} + \sin\theta_0 \sin\theta \, e^{-\left(\frac{K_3}{2}\right)d} e^{-i\delta}\right] e^{ip\left(t - \sqrt{\epsilon_{11}}\frac{d}{c}\right)}$$

$$E_y' = E_0 \left[\cos\theta_0 \sin\theta \, e^{-\left(\frac{K_3}{2}\right)d} - \sin\theta_0 \cos\theta \, e^{-\left(\frac{K_1}{2}\right)d} e^{-i\delta}\right] e^{ip\left(t - \sqrt{\epsilon_{11}}\frac{d}{c}\right)} \tag{33}$$

where K_1 and K_3 are absorption coefficients as defined in eq. (30). δ is the retardation defined as

$$\delta = p\frac{d}{c}\left(\sqrt{\epsilon_{33}} - \sqrt{\epsilon_{11}}\right) = p\frac{d}{c}\Delta \tag{34}$$

The intensity of the beam is

$$I_x' = \frac{1}{8\pi} E_x' \cdot E_x'^{*} = \frac{E_0^2}{8\pi} \left[\cos^2\theta_0 \cos^2\theta\, e^{-K_1 d} + \sin^2\theta_0 \sin^2\theta\, e^{-K_3 d} \right.$$
$$\left. + 2\cos\theta_0 \sin\theta_0 \cos\theta \sin\theta\, e^{-(K_1+K_3)\frac{d}{2}} \cos\delta \right]$$

$$I_y' = \frac{1}{8\pi} E_y' \cdot E_y'^{*} = \frac{E_0^2}{8\pi} \left[\cos^2\theta_0 \sin^2\theta\, e^{-K_3 d} + \sin^2\theta_0 \cos^2\theta\, e^{-K_1 d} \right.$$
$$\left. - 2\cos\theta_0 \sin\theta_0 \cos\theta \sin\theta\, e^{-(K_1+K_3)\frac{d}{2}} \cos\delta \right] \qquad (35)$$

In the event that the incident beam is unpolarized and the polarizer is placed behind the sample, then the intensity measured by the detector is

$$I_x = \frac{2\int_0^{\pi} I_x' \, d\theta}{\int_0^{\pi} d\theta} = \frac{E_0^2}{8\pi} \left[\cos^2\theta_0\, e^{-K_1 d} + \sin^2\theta_0\, e^{-K_3 d} \right]$$

$$I_y = \frac{2\int_0^{\pi} I_y' \, d\theta}{\int_0^{\pi} d\theta} = \frac{E_0^2}{8\pi} \left[\sin^2\theta_0\, e^{-K_1 d} + \cos^2\theta_0\, e^{-K_3 d} \right] \qquad (36)$$

If the optical density is small, i.e. $K_1 d \ll 1$ and $K_3 d \ll 1$, eq. (36) can be expanded in the form

$$I_x \cong \frac{E_0^2}{8\pi} e^{-\frac{4\pi\sigma' \cos^2\psi}{c} \left(\frac{k_{11}^2 \cos^2\theta_0 \cos^2\phi}{\sqrt{\epsilon_{11}}} + \frac{k_{33}^2 \sin^2\theta_0 \sin^2\phi}{\sqrt{\epsilon_{33}}} \right) d}$$

$$I_y \cong \frac{E_0^2}{8\pi} e^{-\frac{4\pi\sigma' c_{us}^2 \psi}{c}\left(\frac{k_{11}^2 \sin^2\theta_0 c_{us}^2\phi}{\sqrt{\epsilon_{11}}} + \frac{k_{33}^2 c_{us}^2\theta_0 \sin^2\phi}{\sqrt{\epsilon_{33}}}\right)d} \qquad (37)$$

and the optical density

$$A_x = \log \frac{I_0}{I_x} = \frac{4\pi\sigma' c_{us}^2\psi}{2.303\, C}\left(\frac{k_{11}^2 c_{us}^2\theta_0 c_{us}^2\phi}{\sqrt{\epsilon_{11}}} + \frac{k_{33}^2 \sin^2\theta_0 \sin^2\phi}{\sqrt{\epsilon_{33}}}\right)d$$

$$A_y = \log \frac{I_0}{I_y} = \frac{4\pi\sigma' c_{us}^2\psi}{2.303\, C}\left(\frac{k_{11}^2 \sin^2\theta_0 \cos^2\phi}{\sqrt{\epsilon_{11}}} + \frac{k_{33}^2 c_{us}^2\theta_0 \sin^2\phi}{\sqrt{\epsilon_{33}}}\right)d \qquad (38)$$

where $I_0 = \frac{E_0^2}{8\pi}$

DISCUSSION

The conditions we set for the derivation of the theory are : (1) The incident beam is normal to the sample surface, therefore no refraction arises. (2) The beam propagates along a principal optic axis. This restriction can be met in the cases of single crystal and amorphous polymer. In the case of a semicrystalline polymer, this condition cannot be satisfied because the crystals of the sample have different orientation and thus the optic axis of the sample does not coincide with the optic axes of the crystals. (3) The internal field factor tensor can be diagonalized

with the optic axes of the sample as reference coordinates. (4) Another assumption underlying in the derivation of the theory is that the optic properties, i.e. birefringence, etc. of the sample along the beam path is homogeneous. This assumption is not valid in the case of semicrystalline polymer because the optical properties of the amorphous regions and the crystalline ones may be different.

The result of eq. (29) is obtained by passing a linearly polarized beam through the sample with the electric field of the incident beam vibrates in the direction which makes an angle θ with x_1 , while I_x of eq. (36) is obtained by passing an unpolarized beam through the sample and by placing a polarizer behind the sample with the plane of vibration of the polarizer making an angle θ_o with x_1 . The only difference in these two cases is the position of the polarizer, i.e. in the former case the polarizer is in front of the sample while in the latter case the polarizer is behind the sample. As one can see the results are exactly the same. This means, in contrast to the prevalent view (15), that the position of the polarizer does not affect the result.

The results of eq. (30) indicate that the absorption coefficients include the refractive index and the internal field factors. The inclusion of refractive index in the absorption coefficient has been mentioned by Ward (1). This is the first evidence of the effect of birefringence on optical dichroism.

In the following discussion, we shall consider separately

three cases with regard to the effect of optical anisotropy on dichroism, namely (1) Single crystal. (2) Amorphous polymer. (3) Semicrystalline polymer.

(1) Single Crystal

For a single crystal, one can always choose the principal optic axis as the direction of the incident beam. The optical density measured with the beam polarized in the directions at angles θ_o and $90^o + \theta_o$ to the optic axis x_1 is shown in eq. (38). The dichroic ratio is

$$D_{exp} = \frac{A_x}{A_y} = \frac{\left(\frac{\epsilon_{33}}{\epsilon_{11}}\right)^{0.5}\left(\frac{k_{11}}{k_{33}}\right)^2 \cot^2\phi \cos^2\theta_o + \sin^2\theta_o}{\left(\frac{\epsilon_{33}}{\epsilon_{11}}\right)^{0.5}\left(\frac{k_{11}}{k_{33}}\right)^2 \cot^2\phi \sin^2\theta_o + \cos^2\theta_o} \qquad (39)$$

when $\theta_o = 0$ in which the plane of vibration of polarizer coincides with the optic axis

$$D_{exp} = \left(\frac{\epsilon_{33}}{\epsilon_{11}}\right)^{0.5}\left(\frac{k_{11}}{k_{33}}\right)^2 \cot^2\phi$$

or

$$D = \cot^2\phi = \left(\frac{\epsilon_{11}}{\epsilon_{33}}\right)^{0.5}\left(\frac{k_{33}}{k_{11}}\right)^2 D_{exp} \qquad (40)$$

D represents the true dichroic ratio with respect to the optic axis x_1. The result of eq. (40) indicates that a correction factor, $\left(\frac{\epsilon_{11}}{\epsilon_{33}}\right)^{0.5}\left(\frac{k_{33}}{k_{11}}\right)$, should be included to estimate the molecular orientation from the measured dichroic ratio. The results of eq. (39) also indicate that, in the case of an anisotropic crystal, one will not observe $D = \infty$, as one does with the isotropic materials, when the absorption is measured with the beam polarized in the directions parallel and perpendicular to the transition moment except in the case when the transition moment coincides with the optic axis.

If the transition moment is along an optic axis, say x_3, when $\sin\phi = 0$ and $\cos\phi = 1$ and eq. (39) becames

$$D_{exp} = \frac{\cos^2\theta_o}{\sin^2\theta_o} = \cot^2\theta_o \qquad (41)$$

Under this circumstance the dichroic ratio represents the molecular orientation with respect to the plane of vibration of the radiation.

The result of eq. (41) indicates that the internal field has no effect on dichroism if the transition moment is along the optic axis. The same conclusion has been reached for a crystal in another approach (16), in which we considered only the effect of internal field, neglecting the birefringence effect, on the absorption.

(2) Amorphous Polymers

In the case of amorphous polymers, optical anisotropy developed

because of the deformation. The anisotropy could be uniaxial or biaxial dependent upon the mode of deformation, i.e. uniaxial or biaxial deformation. As far as the effect of optical anisotropy is concerned, there is no difference between the uniaxial anisotropy and the biaxial anisotropy as long as the beam propagates along a principal optic axis.

Here we shall consider only uniaxially stretched polymers, which are the materials we have studied. The principal optic axes are in the directions parallel and perpendicular to the stretching direction. The dichroism is measured with the beam polarized along the directions parallel and perpendicular to the stretching direction. This condition corresponds to that of $\theta_o = 0$ of eq. (38), thus

$$A_x = \frac{4\pi\sigma' c_4 \cos^2\phi}{2.303\, C} \frac{k_{11}^2 \cos^2\phi}{\sqrt{\epsilon_{11}}} d$$

$$A_y = \frac{4\pi\sigma' c_4 \cos^2\phi}{2.303\, C} \frac{k_{33}^2 \sin^2\phi}{\sqrt{\epsilon_{33}}} d \qquad (42)$$

Since in an uniaxially oriented polymer all orientations of the transition moment around the stretching direction are equally probable, it can be shown (6) that

$$D_{exp} = \frac{2A_x}{A_y} = 2\left(\frac{\epsilon_{33}}{\epsilon_{11}}\right)^{0.5}\left(\frac{k_{11}}{k_{33}}\right)^2 \cot^2\phi \qquad (43)$$

and the orientation function of the polymer chain can be expressed as (6)

$$F = \frac{D_o + 2}{D_o - 1} \frac{D - 1}{D + 2} \qquad (44)$$

if the orientations of the transition moment around the polymer chain are equally probable. Where

$$D = 2\cot^2\phi = \left(\frac{\epsilon_{11}}{\epsilon_{33}}\right)^{0.5} \left(\frac{k_{33}}{k_{11}}\right)^2 D_{exp} \qquad (45)$$

and $D_o = 2\cot^2\alpha$ where α is the angle between the polymer chain and the transition moment.

(3) Polycrystalline Polymers

The situations in polycrystalline polymers are far more complicated. Here there are amorphous regions and crystalline regions. The anisotropy of the amorphous regions is dependent upon the extent of deformation and is different from that of the crystal. Furthermore, the crystal are partially oriented, which means each crystal has its own orientation with respect to the incident beam. It is obvious then that the local anisotropy is different throughout the entire sample. Under these circumstances it is very difficult to have a good estimate of the effect of anisotropy on the optical dichroism. One may consider, as an approximation, only the macroscopic anisotropy and neglect the

local heterogeneity, then the results obtained for amorphous polymers, eq. (45), are applicable for both the crystal orientation and the amorphous orientation. However, one must bear in mind that this is only an approximate solution and a difference in the values of orientation function measured by optical dichroism and other techniques is expected to exist even with the correction of the anisotropy effect.

For a deformed polymer, the refractive indices, $\sqrt{\epsilon_{11}}$ and $\sqrt{\epsilon_{33}}$, are measurable quantities. However the internal field factors, k_{11} and k_{33}, are difficult to estimate as we mentioned earlier. However, for the crystal orientation of the polycrystalline polymers, one may use the internal field factors of the crystals instead of the internal field factors of the sample because the induced dipoles in the amorphous regions contribute negligibly to the internal field if the crystals are not too small (11). Consequently, if the transition moment is along the optic axis, then eq. (45) becomes

$$D = \left(\frac{\epsilon_{11}}{\epsilon_{33}}\right)^{0.5} D_{exp} \qquad (46)$$

where $\sqrt{\epsilon_{11}}$ and $\sqrt{\epsilon_{33}}$ are the refractive indices of the sample (not the crystal).

The values of refractive indices of a stretched polyethylene in the infrared region are not available in the literature at

present. However, one may use the refractive indices of a highly oriented polyethylene in the visible region to estimate the effect of birefringence on the dichroic ratio. The values of refractive indices of such a highly oriented polyethylene were found to be (17) $\sqrt{\epsilon_{11}} = 1.58$ and $\sqrt{\epsilon_{33}} = 1.52$. Thus according to eq. (46), the correction results in about 4 % difference in the dichroic ratio.

There have been attempts (18) to determine the direction of the transition moment by comparing the orientation functions of crystals measured by infrared dichroism and x-ray techniques. From the above discussions, it appears likely that the results may be subject to considerable error without taking account of the effects of birefringence and internal field, particularly the latter when the transition moment is not along the optic axis. The single crystal appears to be the desirable sample for such structure determination according to the previous discussion. Furthermore, theory has been developed (11) to estimate the internal field factors for the single crystal; the internal field effect appears to be the dominant factor as one can see from eq. (40).

(4) Comparison With The Theory Developped By Cunningham et al

Recently a similar theory of the effect of internal field on the infrared dichroism has been developed by Cunningham et al (7).

Their approach is based on the Lorentz-Lorenz equation in which both refractive index and the molecular polarizability are assumed to be complex. The real parts of the refractive index and the polarizability are related to the electronic polarization process and the imaginary parts of the refractive index and the polarizability are related to absorption. By solving the Lorentz-Lorenz equation, the dichroic ratio can be expressed as a function of refractive indices and absorption coefficients of the sample measured with linear polarized radiation.

The difficulty involved with the use of Lorentz-Lorenz equation is, as pointed out by Stein (10), that for a highly oriented sample this equation may not be adequate to describe the internal field. Other models, for instances the cylindrical cavity model (10) and the ellipsoidal cavity model (12), have been proposed to describe the internal field of a highly oriented sample. Recently, a theory has been developed to calculate the internal field of a polyethylene crystal on the bases of a detailed model of interaction rather than by assumption of a cavity model (11). The results indicate that the internal field factors estimated from this theory are very different from those calculated from the Lorentz-Lorenz equation.

The present theory does not involve any specific modeling of the internal field. The theory is developed with the assumption, among others, that the internal field factor tensor can be diagonalized with the optical axes as reference coordinates as discussed previously. In order to test the theory, we have used eqs. (45) and (44) to calculate the molecular orientation of PET, using the

experimental data kindly supplied to us by Prof. I. M. Ward of the University of Leeds in England. Here we use the Lorentz-Lorenz equation to calculate the internal field factors. Thus

$$f_{kii'} = \frac{n_{ii'}^2 + 2}{3} = \frac{\epsilon_{ii'} + 2}{3} \qquad (47)$$

The results are shown in Figs. 2 and 3. Where

$$P_2(\theta_m) \langle P_2(\theta) \rangle_{ir} = \frac{D - 1}{D + 2}$$

and $\langle P_2(\theta) \rangle_{opt}$ is the molecular orientation from birefringence and is taken directly from Ref. 8. For the purpose of comparison, the uncorrected results of the 795 cm^{-1} band are also shown in Fig. 2.

The results calculated from the present theory are in good agreement with those obtained by Cunningham et al (8). This seems to mean that, for the state of orientation of the PET sample, the Lorentz-Lorenz equation is adequate in describing the internal field of the sample.

We would like to point out that the present theory can be applied in a very general way by solving Maxwell's equation (eq. (14)) without imposing any restriction on the internal field factor tensor. Furthermore, the internal field factor can be expreseed as complex number to include the contribution to the internal field from the transition moments of the vibrating absorbing groups.

REFERENCES

1. J. C. Ward, Proc. Roy. Soc., A228 205 (1955).
2. D. Patterson and I. M. Ward, Trans. Faraday Soc., 53 1516 (1957).
3. F. P. Chappel, Polymer, 1 409 (1960).
4. E. J. Ambrose and A. Elliot, Proc. Roy. Soc. (Loncon), A205 47 (1951).
5. B. E. Read and R. S. Stein, Macromolecules, 1 116 (1968).
6. R. B. D. Fraser, J. Chem. Phys., 21 1511 (1953); ibid, 28 1113 (1958).
7. A. Cunningham, G. R. Davies and I. M. Ward, Polymer, 15 743 (1974).
8. A. Cunningham, I. M. Ward, H. A. Willis and Veronica Zichy, Polymer 15 749 (1974).
9. G. Joos and I. M. Freemen, Theoretical Physics, Hafner Publishing Company, New York, 1958, Chap. 13, Chaps. 18 and 19.
10. R. S. Stein, J. Polymer Sci., A2, 7 1021 (1969).
11. S. D. Hong, C. Chang and R. S. Stein, J. Polymer Sci., Polymer Physics Ed., 13 1447 (1975).
12. C. Chang, Ph.D. Thesis, University of Massachusetts, Amherst, 1973.
13. E. B. Wilson, J. C. Decius and P. C. Cross, Molecular Vibrations, McGraw-Hill, New York, 1955, Chap. 7.
14. B. E. Read and R. S. Stein, Macromolecules, 1 116 (1968).
15. R. Zbinden, Infrared Spectroscopy of High Polymers, Academic Press, New York, 1964, Chap. 5.
16. S. D. Hong and R. S. Stein, unplished work.
17. W. M. D. Bryant, J. Polym. Sci., 2 547 (1947).
18. R. J. Samuels, J. Polym. Sci., Part A, 3 1741 (1965).

CAPTIONS TO THE FIGURES

1. Diagram showing the reference coordinates of the sample. x_1, x_2 and x_3 are the three optical axes. $\underset{\sim}{\mu}$ is the transition moment of an absorbing band and $\underset{\sim}{E}$ is the electric field of the incident beam.
2. Values of $P_2(\theta_m)\langle P_2(\theta)\rangle_{ir}$ for the 795 cm^{-1} band as a function of $\langle P_2(\theta)\rangle_{opt}$. The solid points are corrected results and the open points express the uncorrected results.
3. Values of $P_2(\theta_m)\langle P_2(\theta)\rangle_{ir}$ for the 875 cm^{-1} band as a function of $\langle P_2(\theta)\rangle_{opt}$. The results are corrected.

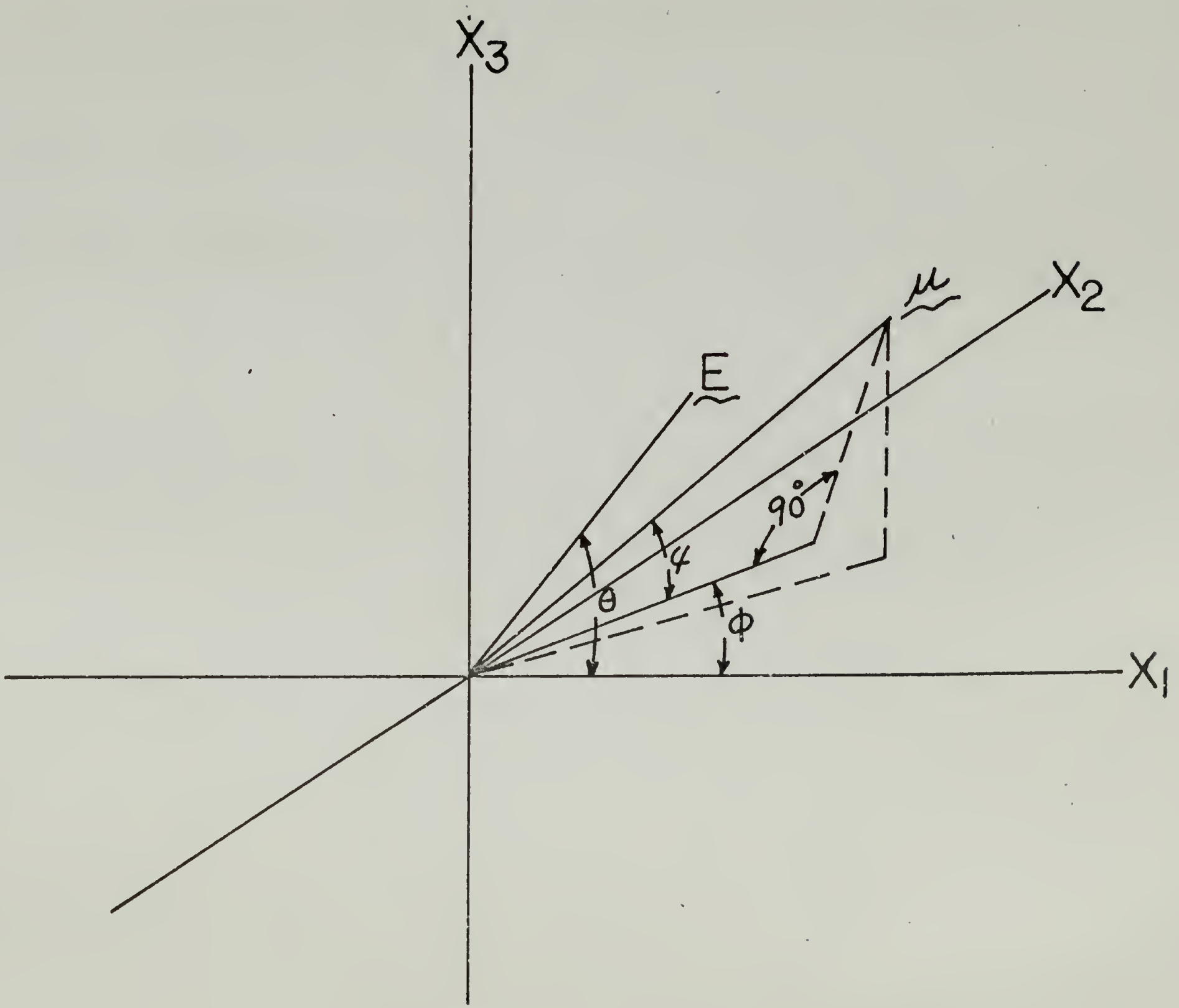

Fig. 1

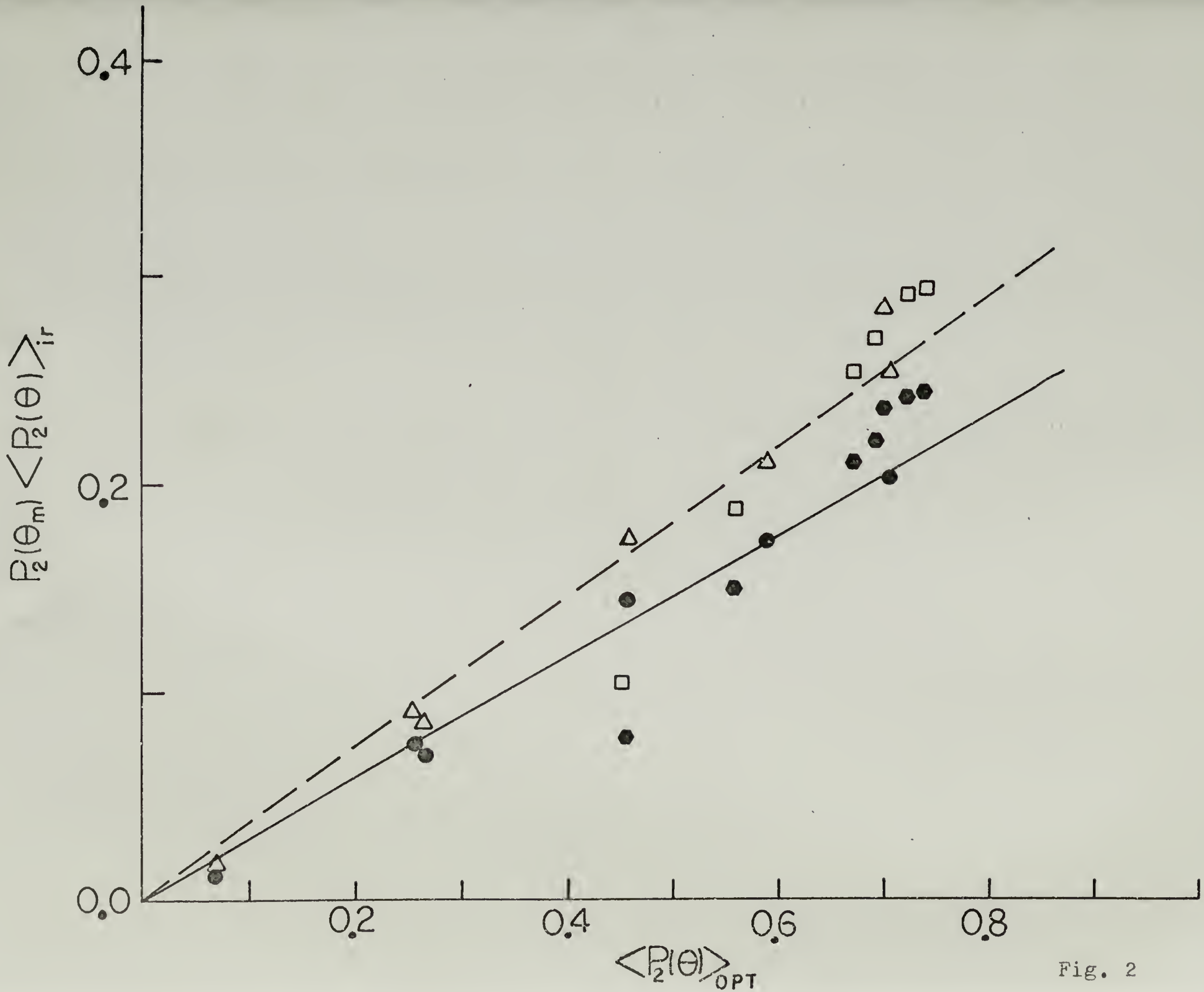
0.4
0.2
0.0
0.2
0.4
0.6
0.8
$P_2(\theta_m) \langle P_2(\theta) \rangle_{ir}$
$\langle P_2(\theta) \rangle_{OPT}$

Fig. 2

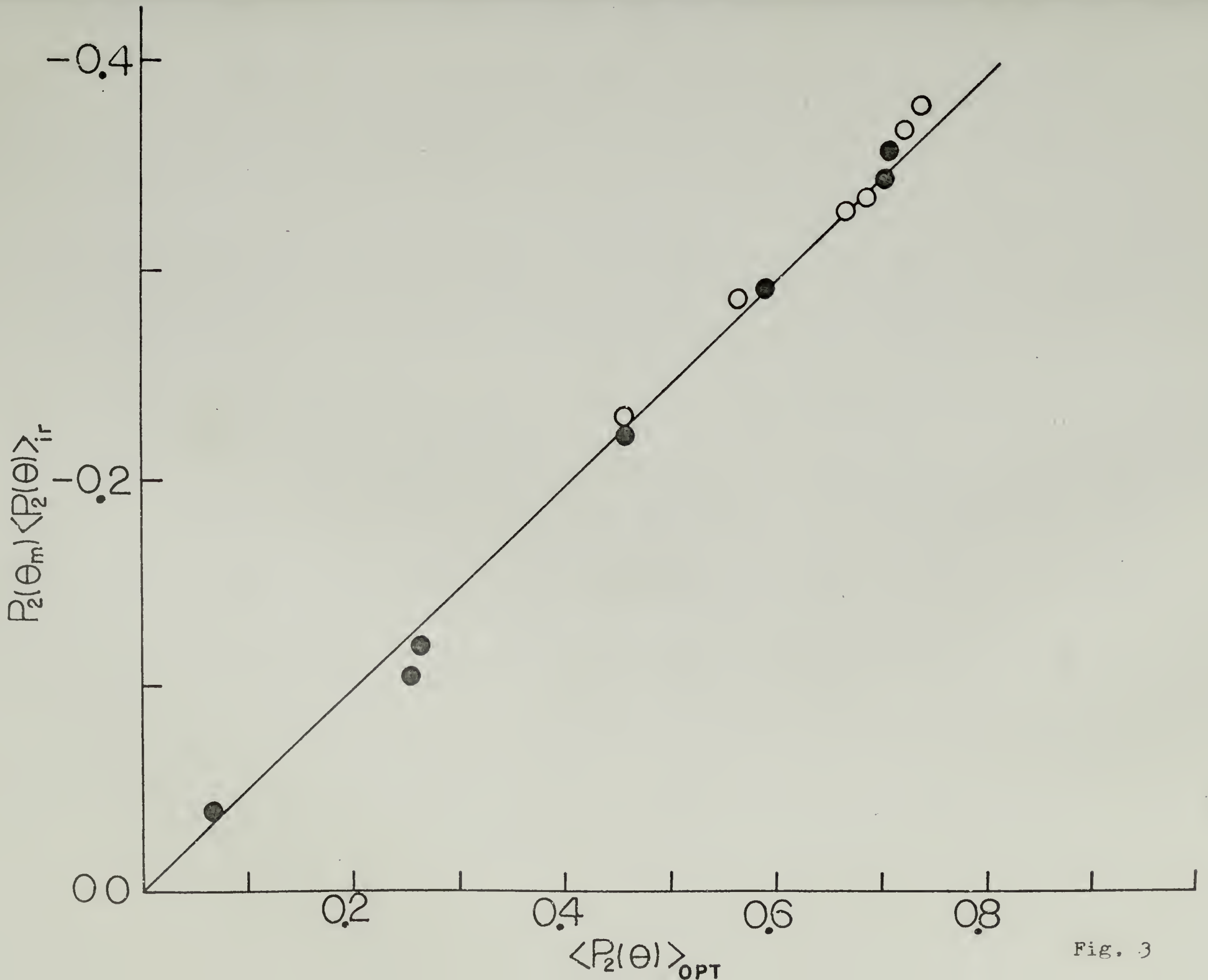
0.4
0.2
0
0
0.2
0.4
0.6
0.8
$P_2(\theta_m)\langle P_2(\theta)\rangle_{ir}$
$\langle P_2(\theta)\rangle_{OPT}$

Fig. 3

CHAPTER IV

THE ELONGATION AND TIME DEPENDENCE OF THE CRYSTALLINITY OF LOW DENSITY POLYETHYLENE

D. Peiffer, S. D. Hong and R. S. Stein
Polymer Research Institute and
Department of Chemistry
University of Massachusetts
Amherst, Massachusetts 01002

SYNOPSIS

It has been presumed in studies of the orientation of low density polyethylene and its time dependence that the degree of crystallinity remained constant with elongation and did not vary with time following elongation. This paper represents a test of this hypothesis by several methods. Ths change in crystallinity accompanying stretching has been followed by a modification of an x-ray method proposed for uniaxial orientation by Ruland in which diffraction peaks are resolved into crystalline and amorphous components and their respective areas are determined by two-dimensional integration over both the Bragg angle and the azimuthal angle of diffraction. The weight fraction crystallinity is then determined from the ratio of the weighted crystalline area to the total area. There appears to be no significant variation in crystallinity up

to 50% sample elongation for both slowly and rapidly stretched samples at room temperature. The dynamic crystallinity change accompanying small amplitude vibration has also been determined by the dynamic x-ray diffraction technique and found to be negligible over a wide range of frequency. The degree of crystallinity has also been evaluated from the absolute infrared absorbence of crystalline sensitive bands and has also been found to be independent of elongation at room temperature up to 80% elongation. Changes have also been observed by this method during relaxation at constant length following rapid extension and have also been found to be negligible. These results also indicate negligible changes in rotational isomer population. Consequently, we conclude that changes observed during relaxation and vibration arise from orientational changes rather than changes in the degree of crystallinity.

INTRODUCTION

The birefringence change occurring upon elongating a crystalline polymer has been separated into crystalline and amorphous contributions using the equation[1,2]

$$\Delta = \phi_c \Delta_c + (1 - \phi_c)\, \Delta_a + \Delta_f \qquad (1)$$

where ϕ_c is the volume fraction crystallinity, Δ_c and Δ_a are the values of birefringence of pure crystalline and amorphous polymer and Δ_f is the form birefringence. The change in birefringence with elongation has been ascribed to the change in orientation of crystalline and amor-

phous polymer using, for uniaxial crystals

$$\Delta_c = \Delta_c^o \ f_c \tag{2}$$

$$\Delta_a = \Delta_a^o \ f_a \tag{3}$$

where Δ_c^o and Δ_a^o are the intrinsic birefringence values for the perfectly oriented phases, and f_c and f_a are the orientation functions of these phases defined, for example, by

$$f_c = [3 < \cos^2\theta_c > - 1]/2 \tag{4}$$

where θ_c is the angle between the crystal optic axis and the stretching direction.

It is presumed in the application of these equations to the analysis of the static and dynamic orientational changes[2-6] that ϕ_c remains constant. It is the purpose of this paper to investigate whether this assumption is correct.

X-RAY STUDIES

Crystallinity is determined by a number of methods, including density studies[7], calorimetry[8], x-ray diffraction[9] and infrared spectrometry[10]. For study of the time dependence of the degree of crystallinity for samples subjected to stress, the x-ray and infrared methods are most convenient. The conventional method[11,12] using x-ray diffraction is to

determine the relative areas of crystalline to total diffraction of a plot of corrected diffracted intensity vs. Bragg angle. A more correct approach has been described by Ruland[13] who has proposed the equation

$$X_c = \frac{\int_0^\infty s^2 I_{cr}\, ds}{\int_0^\infty s^2 I\, ds} \cdot \frac{\int_0^\infty s^2 \overline{f}^2_{cr}\, ds}{\int_0^\infty Ds^2 \overline{f}^2\, ds} \qquad (5)$$

where X_c is the weight fraction crystallinity, s is the magnitude of the reciprocal space vector. $(2/\lambda) \sin \theta$, θ is the Bragg angle, I_{cr} is the part of the coherent scattering at s under the crystalline peak and I is the total area under the total coherent diffraction. $\overline{f}^2$ is defined by

$$\overline{f}^2 = \Sigma N_i f_i^2 / \Sigma N_i \qquad (6)$$

where N_i is the number of atoms of type i having scattering factors, f_i. D(s) is a disorder function which takes into account the loss of intensity concentrated at reciprocal lattice points due to deviations of the atoms from their ideal positions. To a first approximation for unoriented systems, this may be taken as $\exp(-ks^2)$, where k is a parameter characterizing the extent of disorder which includes the effects of both thermal fluctuations as well as lattice imperfections.

In practice, the integrations of Equation (5) are usually taken over a finite range (from s_o to s_p) so that it may be written in the form

$$X_c = K(s_o, s_p, D, \bar{f}) \frac{\int_{s_o}^{s_p} s^2 I_{cr}(s)\, ds}{\int_{s_o}^{s_p} s^2 I(s)\, ds} \qquad (7)$$

where

$$K = \frac{\int_{s_o}^{s_p} s^2 \bar{f}^2\, ds}{\int_{s_o}^{s_p} s^2 \bar{f}^2 D\, ds} \qquad (8)$$

A value of k is chosen to evaluate K such that a value of X_c is obtained which is independent of the integration limits.

For a uniaxially oriented sample, the diffracted intensity is dependent upon the azimuthal as well as the Bragg angle in which case

$$I(s) = (1/4\,\pi)\int_0^{4\pi} I(s)\, d\omega$$

$$= \int_0^{\pi/2} I(s,\alpha) \sin\alpha\, d\alpha \qquad (9)$$

where ω is the solid angle and α is the azimuthal scattering angle (Figure 1). It should be noted that the sin α weighting factor is necessary in Equation (9) so, as has been pointed out[14], the often used procedure of randomizing orientation by spinning a film about its normal may lead to error. Either randomization in three dimensions is necessary or else the integration of Equation (9) must be carried out numerically or by mechanically including an attenuator in the diffractometer to introduce the sin α weighting factor[15].

Experiments were carried out on a Monsanto low density experimental polyethylene (M_n = 1.67 x 10^4, M_w = 6.20 x 10^5, melt index 7.0) identical with that used in our preceding rheo-optical investigations[4-6]. Samples were prepared by molding films 600 μm thick in a laboratory press at 10,000 psi and 155°C for 5 min. after which they were quenched in an ethanol-dry ice bath. Statically drawn samples were homogeneously stretched at room temperature in a hand operated stretcher and were clamped at constant length for x-ray studies. X-ray measurements were made using our dynamic diffractometer[16] in a static mode using CuKα radiation. Measured relative intensities were corrected using[17]

$$I(2\theta, \alpha) = \left[I_{exp.} - I_{back.}\, e^{-\mu d \sec\theta}\right]\left[\frac{2}{1 + \cos 2\theta}\right] \times \left[\frac{e^{\mu d \sec\theta}}{\sec\theta}\right]\left[\frac{1}{\sin 2\theta}\right] - I_{incoh.} \tag{10}$$

where $I_{back.}$ is the background intensity obtained without a sample in the apparatus, μ is the absorption coefficient of the sample of thickness d, and $I_{incoh.}$ is the incoherent scattering of the sample obtained by assuming that the diffraction at an angle of 2θ = 55° was entirely incoherent. (While a somewhat greater angle would have been desirable, this angle was chosen because of instrument limitations.)

It is noted that $s^2\, I(s)\, ds = (8/\lambda^3)\, I(2\theta, \alpha) \sin^2\theta \cos\theta\, d\theta$. A typical plot of $I(2\theta, \alpha) \sin^2\theta \cos\theta$ vs θ for several values of α for a

sample stretched 30% is given in Figure (2). Each of these plots is resolved into its crystalline and amorphous components and the areas under the plots of the total intensity and the amorphous parts are plotted against the azimuthal angle, α as shown in Figure (3). The area under the crystalline contribution is then determined by difference. The ratios of these areas then gives the ratios of the integrals of Equation (7). It has been arbitrarily assumed that K = 1 so that the values of X_c are relative values. Thus, conclusions concerning the variation of X_c with elongation are dependent upon whether K varies with elongation. It is conceivable of course that the degree of disorder may vary with elongation and lead to a variation of K.

The variation of X_c with elongation for a sample stretched to 50%, in a stepwise manner, holding the sample at each elongation for 24 hours is plotted in Figure (4). After stretching was completed the strain was relaxed by steps. It is noted that upon release of the stress, the sample recovers to about 20% elongation. There appears to be a slight decrease in crystallinity from 46 to 43% on stretching with no further change upon relaxation. Subsequent stretching to 50% strain produces no further change of crystallinity. The density of films used in the static strain experiments were measured by the floatation method in a water-ethanol mixture at room temperature and indicated weight fraction crystallinities of 0.474 for the unstretched sample and 0.453 for the stretched and totally relaxed sample.

We then applied a similar analysis to a sample stretched at high speed as described by Stein and Finkelstein[5,6]. The sample was elongated

to its ultimate elongation in about 10 msec. using a spring loaded stretching device. In this case, diffracted intensities were obtained using a high intensity rotating anode generated providing AgKα radiation. Since the equipment only involved single channel recording it was necessary to carry out a separate experiment using a new sample at each pair of diffracting angles. Intensity data were displayed and photographed from an oscilloscope trace.

Data were analyzed using similar procedures to those for the static experiments. A typical variation of X_c with strain obtained with high speed elongation is shown in Figure (5). In this case, X_c is observed to decrease from 46 to 40% during the elongation. The subsequent change in X_c with time following high speed stretching is shown in Figure (6). No appreciable change in crystallinity was detected.

The third study involved the determination of the variation of crystallinity during the oscillatory strain of the sample following the technique described by Tanaka, et al.[4] using the data obtained by Chang[18]. In this work, measurements had been made at positions of intensity peaks at various azimuthal angles. For each intensity peak, an integral over azimuthal angle defined by

$$A_i = \int_0^{\pi/2} I_i(\alpha) \sin\alpha \, d\alpha \qquad (11)$$

may be calculated. In this case, the approximate equation for the fraction crystallinity used

$$X_c = \frac{A_{110} + A_{200}}{A_{110} + A_{200} + A_{am}} \tag{12}$$

where A_{110}, A_{200} and A_{am} are the integrated areas under the 110, 200 and amorphous peaks. Then by differentiating with respect to strain

$$\frac{\Delta X_c}{\Delta \varepsilon} = \frac{A_{am}\left(\frac{\Delta A_{am}}{\Delta \varepsilon} + \frac{\Delta A_{200}}{\Delta \varepsilon}\right) - \left(\frac{\Delta A_{am}}{\Delta \varepsilon}\right)(A_{110} + A_{200})}{(A_{110} + A_{200} + A_{am})^2} \tag{13}$$

where

$$\frac{\Delta A_i}{\Delta \varepsilon} = \int_0^{\pi/2} \left(\frac{\Delta I_i}{\Delta \varepsilon}\right) \sin\alpha \, d\alpha \tag{14}$$

The quantities $(\Delta I_i/\Delta\varepsilon)$ were determined experimentally for the 110, 200 and amorphous peaks. These are frequency dependent, and typical values of $\Delta I'_{200}$ are plotted as a function of azimuthal angle at various frequencies in Figure (7). The prime indicates the component of $\Delta I'$ which is in phase with the strain.

The values of $(\Delta A_i/\Delta\varepsilon)$ for the 110, 200 and amorphous peaks are plotted in Figure (8) as a function of frequency. The variation of the values of $(\Delta X_c/\Delta\varepsilon)$ with frequency calculated from these values using Equation (13) are also plotted in this figure. The value is relatively independent of frequency and has a value of about -0.3. This may be compared with a value of -0.16 as measured in the high speed stretching equipment.

INFRARED STUDIES

Infrared measurements present an alternate means for following crystallinity changes during slow or rapid extension. Furthermore, they present a means for following changes in conformation with stretching. Samples for infrared studies were prepared in a similar manner to those for x-ray studies with the exception that samples were usually thinner in order that the absorbence be in a region where the precision of measurements is good. Static measurements were made using a Perkin-Elmer Model 180 Spectrometer equipped with a Perkin-Elmer Model 186-0240 silver bromide wire grid polarizer. Samples were stretched in a direction 45° to the vertical. Measurements were made with the polarizer in the common beam (in front of the entrance slit) of the spectrometer so that both beams were subject to the same machine polarization. By having the sample oriented at 45° the intensities of the beams polarized parallel and perpendicular to the sample stretching direction was equalized. Absorbences were calculated using

$$A = \ell n(100/T) \qquad (15)$$

where T is the percent transmission. Measurements are carried out for polarization parallel ($A_{||}$) and perpendicular ($A_{\perp}$) to the stretching direction.

Typical absorption spectra in various regions for oriented quenched low density polyethylene samples are given in Figure (9). The assignment of the principal absorption bands are indicated in Table I in which references for the assignments are given.

The determination of the percent transmission (100 I_t/I_o, where I_t and I_o are the transmitted and incident intensities) requires the establishment of the baseline intensity. The procedure for specifying this in an absorption spectrum involving overlapping contributions is somewhat arbitrary. The procedure which we used is indicated in Figure 10 showing absorption spectra in two regions. We have measured our intensities from baselines indicated by the solid lines in this Figure which differ from baselines used by some other workers[10,25] shown as the dashed lines in this Figure. Read and Hughes[26] have shown that the assignment of baseline (e) may be a better choice for the 2016 cm^{-1} band for amorphous polyethylene. In order to check errors that may arise from baseline choice, we have calculated A_o for the 1894 cm^{-1} band as a function of elongation using the two different baselines labeled (c) and (d) in the figure. Although the absolute values of absorbence calculated using these two different baselines are different, the change in A_o with λ is not appreciably affected by the choice. The same conclusions follow for the bands at 1375 cm^{-1}, 1368 cm^{-1}, 1352 cm^{-1} and 1303 cm^{-1} where the baseline (b) was suggested by Witenhafer and Koenig[27]. The use of the horizontal baselines simplifies our dynamic experiments in that measurements are only required at two different wavelengths for each band rather than three as would be required for sloping baselines.

It is noted that the absorbence for oriented samples is dependent upon polarization. The dichroism ($D = A_{\parallel}/A_{\perp}$) serves as a measure of orientation which is of interest in other studies[21,28]. For purposes

of determining the amount of crystalline phase, the average absorbence is of interest, defined as

$$A_o = (A_1 + A_2 + A_3)/3 \qquad (16)$$

where A_1, A_2 and A_3 are the absorbences for radiation polarized parallel to the three principal axes of the sample. For uniaxial orientation, $A_1 = A_{||}$ and $A_2 = A_3 = A_{\perp}$ so that

$$A_o = (A_{||} + 2A_{\perp})/3 \qquad (17)$$

It is noted that in order to determine A_o, it is necessary to measure $A_{||}$ and $A_{\perp}$ separately. A measurement with unpolarized radiation gives A_u which is

$$A_u = (A_{||} + A_{\perp})/2 \qquad (18)$$

which differs from A_o.

A_o is proportional to the thickness of the sample, d, according to the equation

$$A_o = \varepsilon_o d \qquad (19)$$

where ε_o is the extinction coefficient. For uniaxial orientation, d varies with the elongation ratio, λ, according to the equation

$$d = d_o/\lambda^{1/2} \tag{20}$$

where d_o is the initial thickness. Thus

$$A_o \lambda^{1/2} = \varepsilon_o d_o \tag{21}$$

Hence, if the amount of absorbing material remains constant, $A_o \lambda^{1/2}$ should be a constant, independent of elongation.

This prediction may be tested through measurement of the 1375 cm^{-1} band which arises from a CH_3 symmetrical bending vibration and is independent of crystallinity. A plot of $\lambda^{1/2} A_o$ vs. elongation for this band is given in Figure (11) which confirms this constancy and verifies the assumption of uniaxial extension.

For a band which arises from crystalline absorption, such as the 1894 cm^{-1} band, it follows that

$$(A_o)_c \lambda^{1/2} = (\varepsilon_o)_c d_o X_c \tag{22}$$

A plot of $\lambda^{1/2} A_o$ vs. elongation ratio for this band is shown in Figure (12). It is seen that there is little variation with extension, confirming the constancy of X_c.

The constancy of crystallinity may be further studied by examining bands arising from amorphous absorption. Plots of $A_o(v)/A_c$ (1375 cm^{-1}) for three such bands are given in Figure (13). Dividing normalizes the absorbence and corrects for the thickness changes. While this procedure

is superior to that given previously using Equation (22), it is not always possible to employ it because of the large differences of absorbence of the band to be studied and the reference band.

Figure (13) suggests that the relative amount of amorphous phase is independent of elongation. Furthermore, as is seen from Table I, the conformational dependence of these three amorphous bands is different. The 1354 cm^{-1} band is believed to arise from gg sequences while the 1303 and 1368 cm^{-1} bands are believed to arise from gtg or gtg' sequences. Consequently, the similar independence of elongation for those three bands suggests that the relative population of these sequences does not change with elongation. This is not surprising in view of the relatively small range of elongation.

Thus in agreement with the x-ray results, the static infrared measurements demonstrate little dependence of X_c on elongation. The infrared technique may also be used to follow crystallinity changes during and after high speed elongation. This may be done using the high speed spectrometer previously described[28] in which samples are elongated in millisecond time periods using a pneumatic-hydraulic device.

Data obtained in this way is shown in Figure (14) for the 1894 cm^{-1} crystalline band which again indicated little change in crystallinity with elongation or during the subsequent relaxation. Data for one of the amorphous bands at 1354 cm^{-1} is shown in Figure (15) which indicates some increase in amorphous content with time. However, the precision of these results is low.

CONCLUSIONS

It is seen that static and dynamic x-ray diffraction and static and dynamic infrared studies indicate that the change in crystallinity during extension of quenched low density polyethylene at room temperature is small, perhaps amounting to a 5% decrease. This result may be compared for example with that shown in Figure (16)[5] in which the total birefringence change is resolved into components arising from crystalline and amorphous contributions using equations like Equations (1) and (2). The five-fold increase in crystalline birefringence contribution was calculated from x-ray measurements of crystalline orientation functions obtained by assuming that the x-ray intensity changes represent a change in crystalline orientation rather than a change in amount of crystalline material. The results of this paper, calculated in part from the same data strongly demonstrate that the intensity changes leading to this conclusion of a large increase in crystal orientation would not be appreciably affected by the small decrease in X_{cr} that may simultaneously occur. Similar conclusions would apply to the measurement of orientation changes by the infrared technique in this[21,28] and other laboratories[29].

We[4] and others[30] have concluded that the alpha mechanical loss mechanism is primarily a process associated with changes in crystal orientation. It has been assumed[31-33] that these processes involve inter and intracrystalline slip processes depending upon such phenomena as rotations about crystal axes and slipping of chains within crystals along their c-axes. It has been suggested[34], that because of the correspondence of the temperature of the alpha loss process and that at which

crystal melting begins, that this process may involve a melting of crystals and a recrystallization in a new orientation. Our measurements do not preclude this possibility. However, such recrystallization processes would have to conform to our observations that the total degree of crystallinity remains constant, so that the melting and growth of crystals would produce compensating changes in X_c. This requirement imposes strong restrictions on the kinetics of the recrystallization processes in that this compensation must be maintained over a 10^4 range of extension rates. Also the recrystallization processes must be such as to lead to different kinetics of orientation change with respect to different crystal axes.

ACKNOWLEDGEMENT

The authors appreciate receiving comments and suggestions from Professor Paul J. Flory and Professor Leo Mandelkern which motivated us to undertake this study.

TABLE I

Principal Absorption Bonds for Polyethylene

Frequency	Phase	Assignment
2016 cm^{-1}	A,C	Combination between the raman-active twisting mode and the IR-active rocking mode of CH_2 group[19,20]
1894 cm^{-1}	C[10,21]	Combination between the raman-active and the IR-active rocking mode of CH_2 group[19,20,22]
1375 cm^{-1}	A	CH_3 symmetric bending mode[19,23]
1368 cm^{-1}	A	CH_2 wagging (symmetric with respect to the center trans bond) in gtg or gtg‘ conformation[23]
1352 cm^{-1}	A	CH_2 wagging mode in the gauche conformation or in gg conformation[22]
1303 cm^{-1}	A	CH_2 twisting mode in the gauche conformation[19,24] or CH_2 wagging mode (antisymmetric with respect to the center trans bond) in gtg or gtg' conformation[23]

REFERENCES

1. J. J. Hermans, P. Hermans, D. Vermaas and A. Weidinger, Rec. Trav. Chim., 65 427 (1946).
2. R. S. Stein and F. H. Norris, J. Polym. Sci., 21 381 (1956).
3. R. S. Stein, Accounts Chem. Res., 5 121 (1972).
4. A. Tanaka, E. P. Chang, B. Delf, I. Kimura and R. S. Stein, J. Polym. Sci., Polym. Phys. Ed., 11 1891 (1973).
5. R. S. Stein, R. S. Finkelstein, D. Y. Yoon and C. Chang, J. Polym. Sci., C46 in press.
6. R. S. Stein, A. Tanaka and R. S. Finkelstein, Appl. Polym. Symp., 20 335 (1973).
7. L. Mandelkern, F. A. Quinn, Jr., and P. J. Flory, J. Appl. Phys., 25 830 (1954); L. Mandelkern, Crystallization of Polymers, McGraw-Hill, New York, 1964.
8. J. M. G. Fatou and J. M. Barrales-Riendu, J. Polym. Sci., A2, 7 1755 (1969).
9. S. Hoshino, E. Meineke, J. Powers, R. S. Stein and S. Newman, J. Polym. Sci., A, 3 3041 (1956).
10. T. Okada and L. Mandelkern, J. Polym. Sci., A2, 5 239 (1967).
11. H. Hendus and G. Schnell, Kunstoffe 51 69 (1960).
12. M. R. Gopalan and L. Mandelkern, J. Polym. Sci., 5 925 (1967).
13. W. Ruland, Acta Crystallographica, 14 1180 (1961).
14. C. R. Desper and R. S. Stein, J. Polym. Sci., B, 5 893 (1967).
15. Z. W. Wilshinsky, French Pat., 1,459,172; Filed U.S. Oct. 4, 1964.
16. T. Ito, T. Oda, H. Kawai, T. Kawaguchi, D. A. Keedy and R. S. Stein, Rev. Sci. Instr., 39 1847 (1968).

17. L. E. Alexander, X-Ray Diffraction Methods in Polymer Science, Wiley-Interscience, New York, 1969.

18. C. S. H. Chang, Ph.D. Thesis, University of Massachusetts, Amherst, Mass., 1973.

19. S. Krimm, Fortschr. Hochpolym.-Forsch., 2 51 (1960).

20. J. R. Nielsen and A. H. Wollett, J. Chem. Phys., 26 1391 (1957).

21. B. E. Read and R. S. Stein, Macromolecules, 1 116 (1968).

22. J. R. Nielsen, J. Polym. Sci., C7 19 (1964).

23. R. G. Snyder, J. Chem. Phys., 47 1316 (1967).

24. J. R. Nielsen and R. F. Holland, J. Molec. Spectros., 6 394 (1961).

25. W. Glenz and A. Peterlin, J. Macromol. Sci., B3 473 (1971).

26. B. E. Read and D. A. Hughes, Polymer, 13 495 (1972).

27. D. E. Whitenhafer and J. L. Koenig, Makromol. Chem., 99 193 (1966).

28. Y. Uemura and R. S. Stein, J. Polym. Sci., A2, 10 1691 (1972).

29. Y. Fukui, T. Asada and S. Onogi, Polym. J. (Japan), 3 100 (1972).

30. N. Saito, K. Okano, S. Iwayanagi and T. Hideshima, in Solid State Physics, Vol. 14, F. Seitz and D. Turnbull, Eds., Academic Press, New York, 1963, p. 343.

31. M. Takayanagi, T. Arakami, M. Yoshino and K. Hoashi, J. Polym. Sci., 46 531 (1960).

32. N. G. McCrum and E. L. Morris, Proc. Roy. Soc. (London), A292 506 (1966).

33. T. Kajiyama, T. Okada, A. Sakoda and M. Takayanagi, J. Macromol. Sci., (Phys.), B7 (3) 583 (1973).

34. L. Mandelkern, private communication.

FIGURES

1) The angles for x-ray diffraction.
2) The variation of $I(2\theta,\alpha)\ \sin^2\theta\ \cos\theta$ with θ for a 30% stretched quenched polyethylene sample at several azimuthal angles.
3) The variation the area under the amorphous contribution to Figure (2) $S_{am}(\alpha)$ and the total area $S(\alpha)$ with α for a quenched polyethylene sample stretched 30%.
4) The variation of X_c with percent strain and subsequent relaxation for a slowly stretched sample of quenched polyethylene.
5) The variation of X_c with percent strain for a rapidly stretched sample of quenched polyethylene.
6) The variation of X_c with time following the high speed stretching of quenched polyethylene.
7) The variation of $\Delta I'_{200}$ and $\Delta I''_{200}$ with azimuthal angle at several frequencies at strain amplitude $\Delta\varepsilon = 0.01$ for a quenched sample of polyethylene.
8) The variation of $(\Delta A_i/\Delta\varepsilon)$ with frequency for the 110, 200, and amorphous peaks for a quenched sample of polyethylene, and the variation of $(\Delta X_c/\Delta\varepsilon)$ with frequency calculated from those values.
9) Absorption spectra for oriented quenched polyethylene films in various spectral regions. Elongation ratios and sample thicknesses are indicated.
10) The choice of baselines in the measurement of infrared absorbences.
11) The variation of $\lambda^{1/2}\ A_o$ with elongation ratio for the 1375 cm^{-1} methyl deformation band.

12) The variation of $\lambda^{1/2} A_0$ with elongation ratio for the 1894 cm^{-1} crystalline band.

13) The variation on $A_0(v)/A_0$ (1375) with elongation ratio for the 1303, 1354 and 1368 cm^{-1} bands.

14) The variation of $\lambda^{1/2} A_0$ with elongation at 1894 cm^{-1} during and following high speed stretching of quenched polyethylene.

15) The variation of $\lambda^{1/2} A_0$ with elongation at 1354 cm^{-1} during and following high speed stretching of quenched polyethylene.

16) The variation in total birefringence and in the amorphous and crystalline contribution during and following the rapid stretching by 10% of a quenched low density polyethylene at 20°C. [From Ref. (5)].

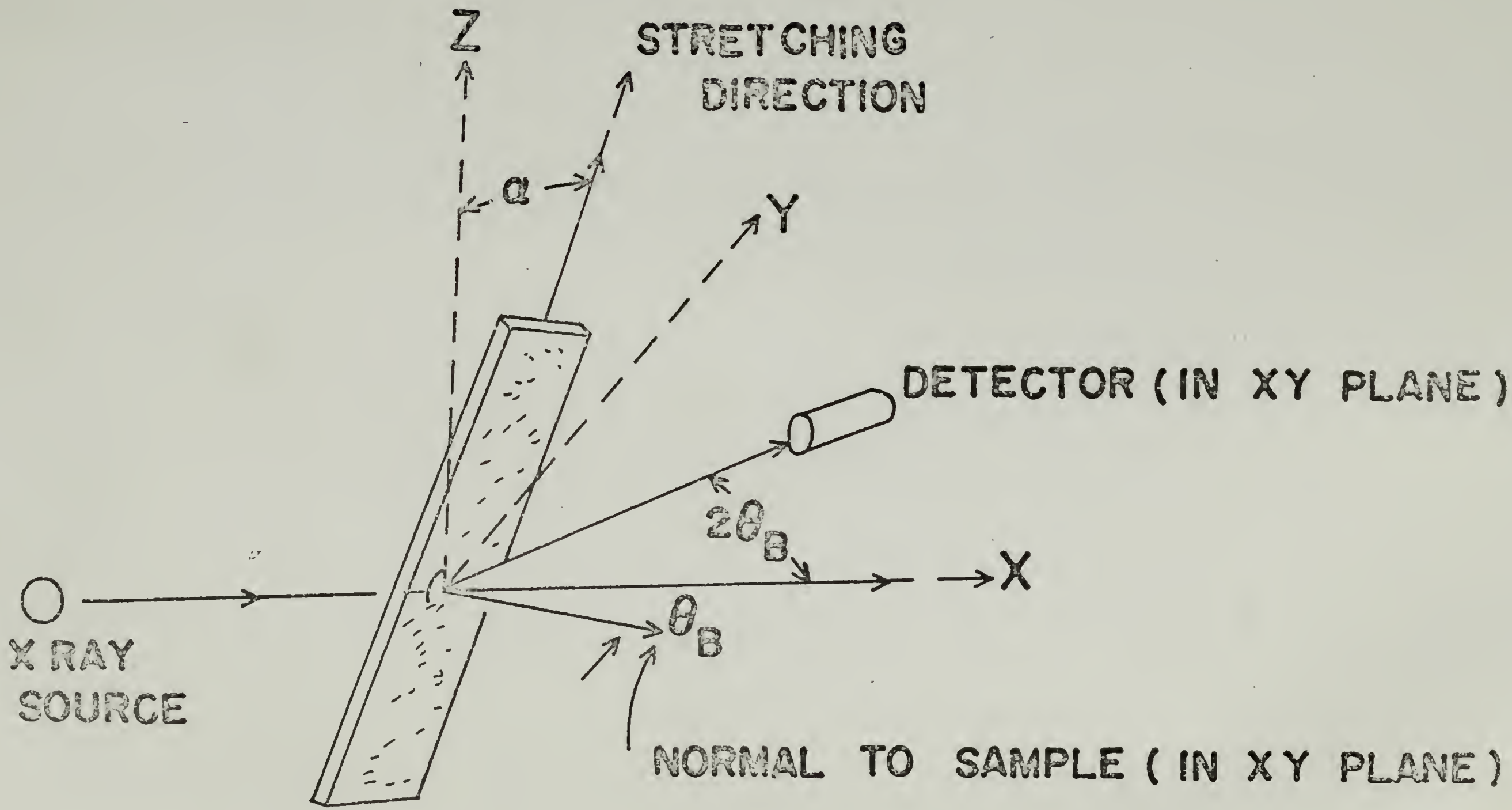
Z
STRETCHING DIRECTION
α
Y
DETECTOR (IN XY PLANE)
2θB
X
θB
X RAY SOURCE
NORMAL TO SAMPLE (IN XY PLANE)

Fig. 1

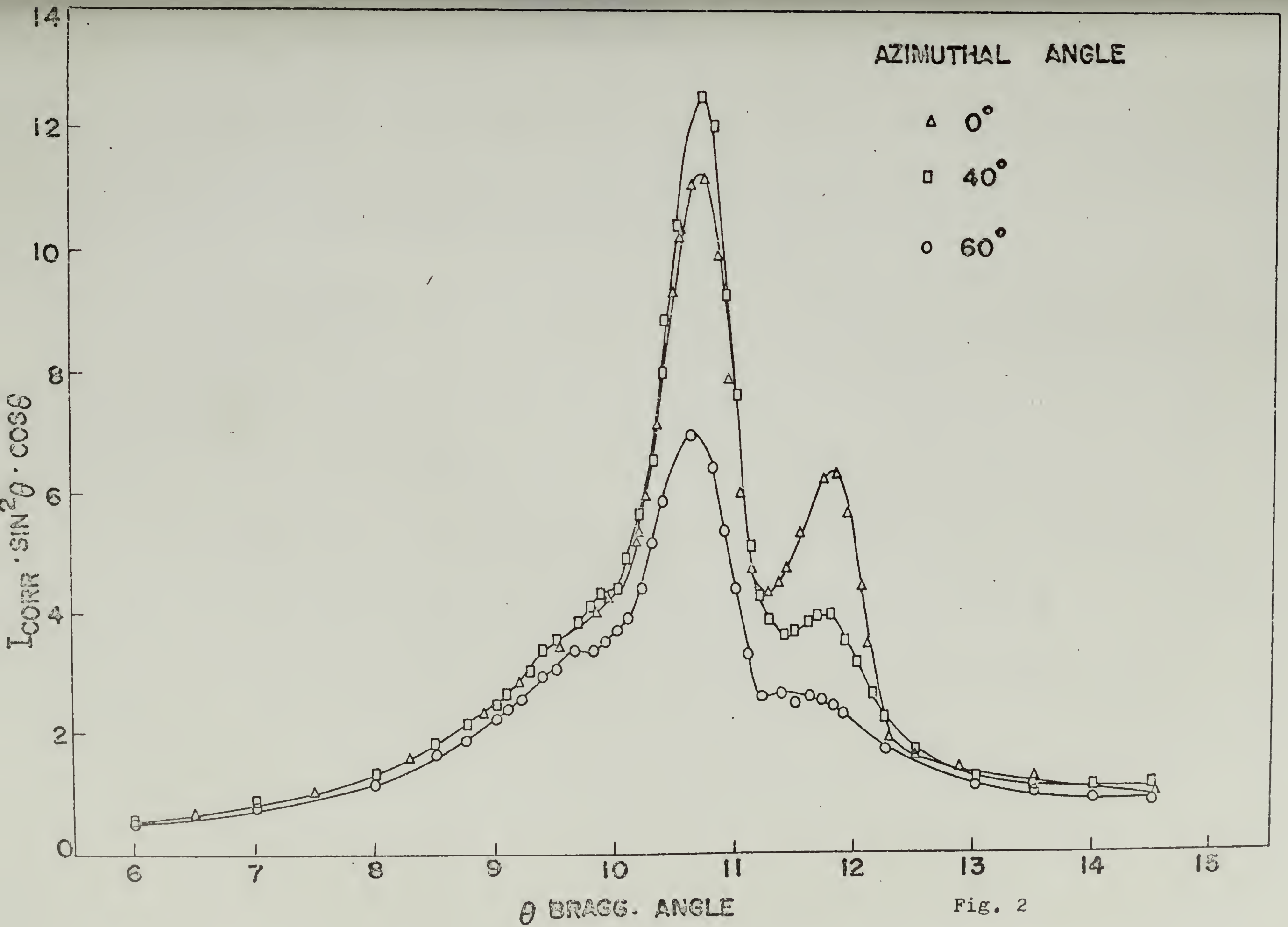
AZIMUTHAL ANGLE
0°
40°
60°
$I_{CORR} \cdot SIN^2\theta \cdot COS\theta$
θ BRAGG. ANGLE
0
2
4
6
8
10
12
14
6
7
8
9
10
11
12
13
14
15

Fig. 2

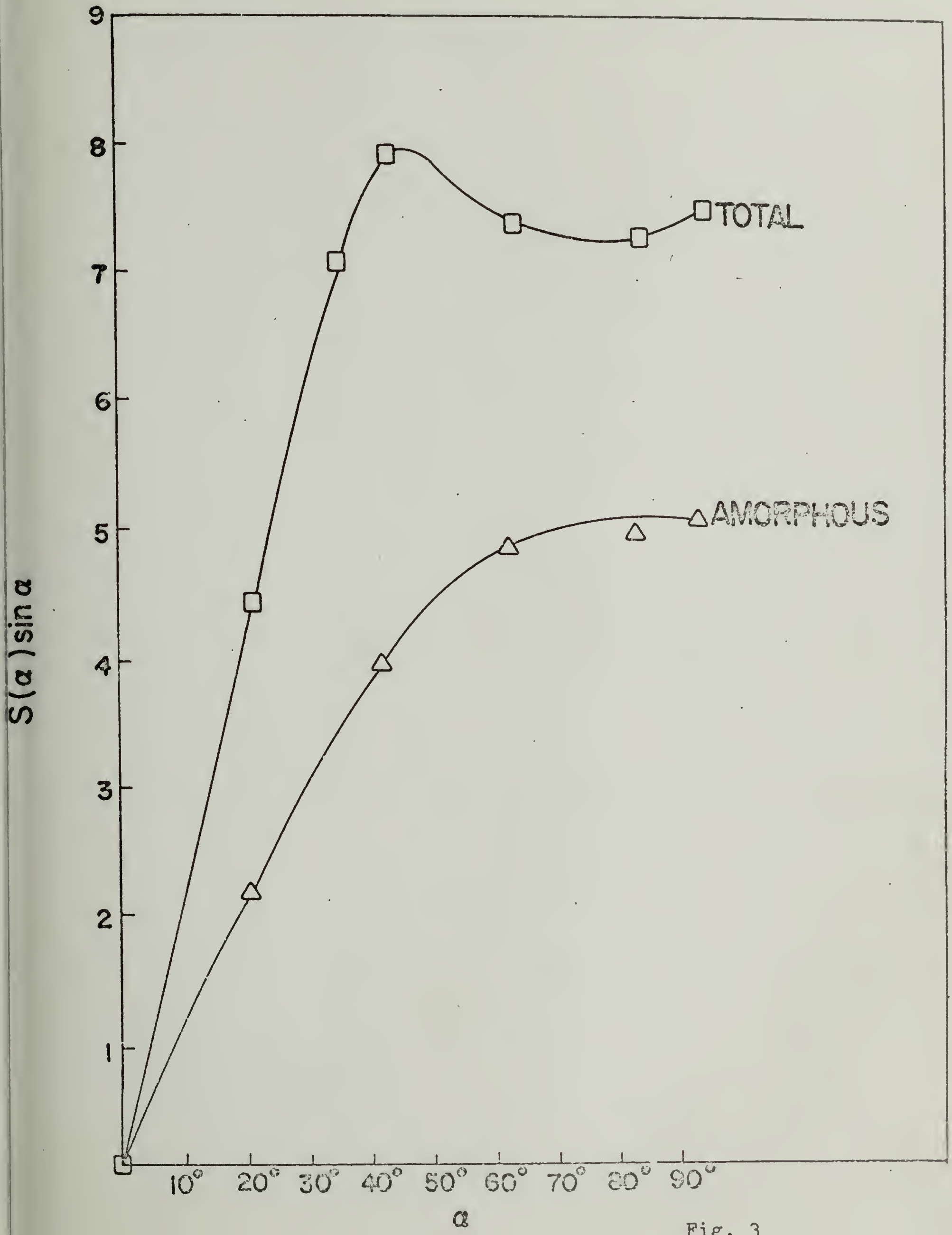

Fig. 3

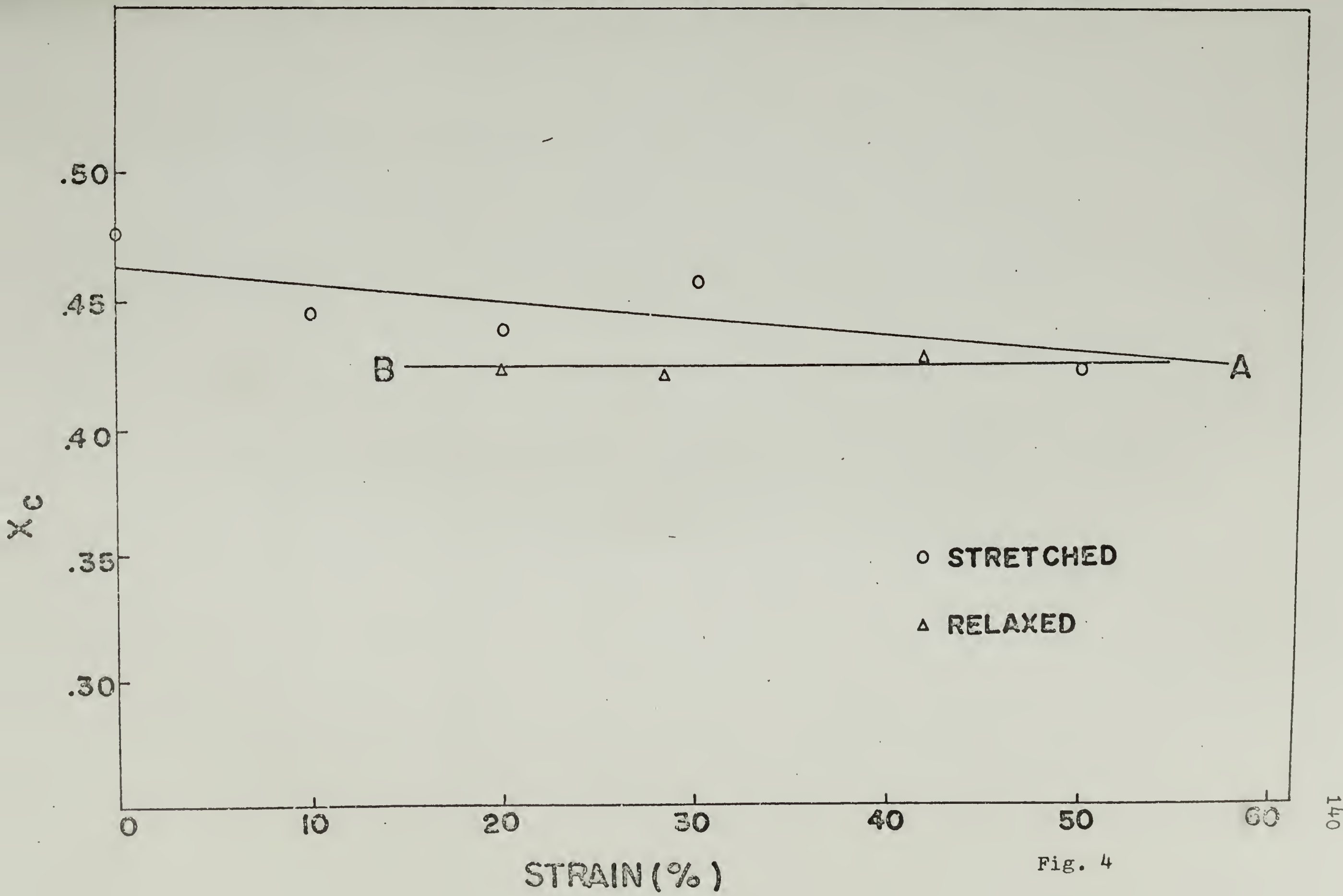
Quenched Low Density Polyethylene at 20°C
.50
.45
.40
.35
.30
Xc
B
A
o STRETCHED
Δ RELAXED
0
10
20
30
40
50
60
STRAIN (%)

Fig. 4

HIGH SPEED STRETCHING

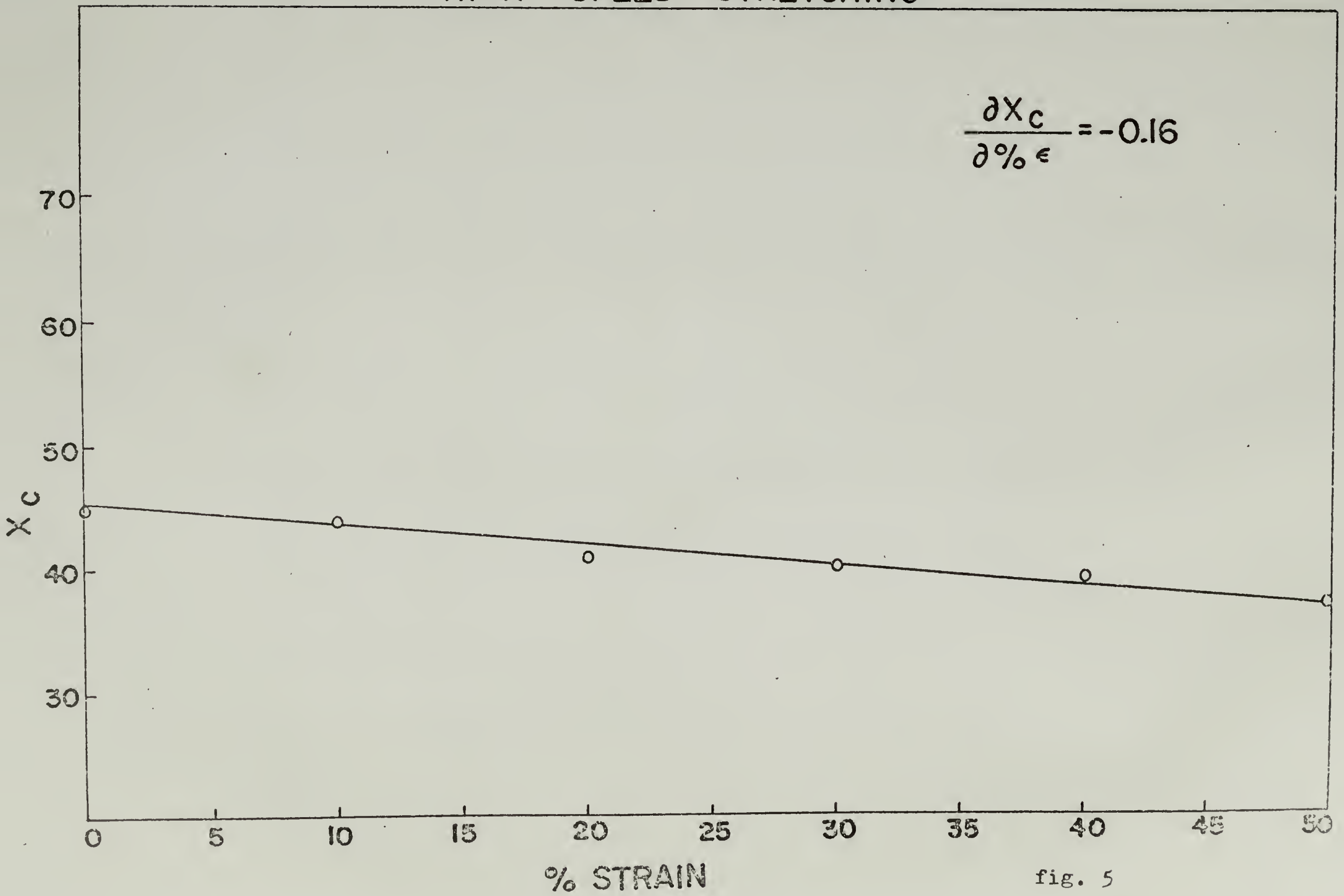

fig. 5

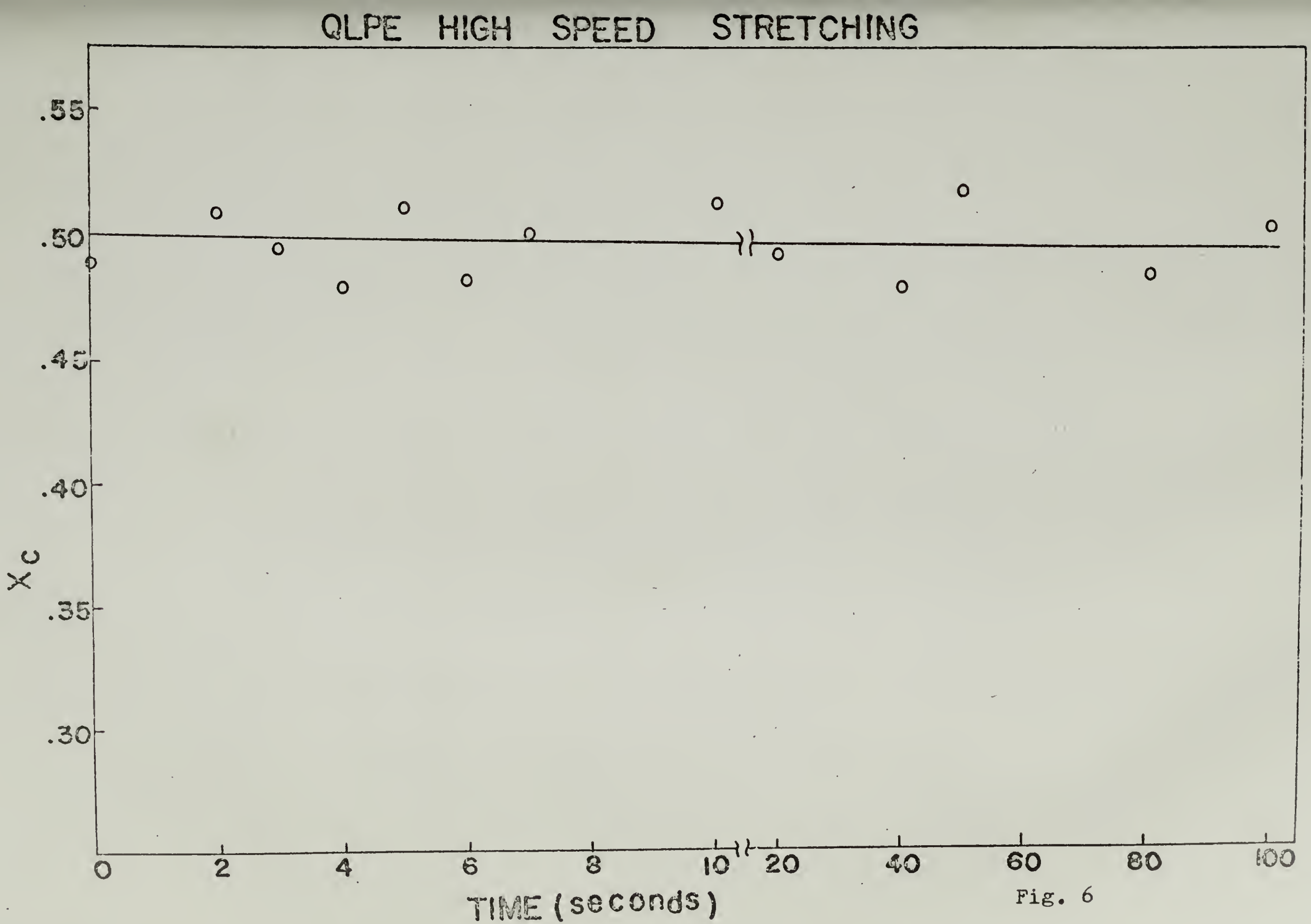
QLPE HIGH SPEED STRETCHING
.55
.50
.45
.40
.35
.30
Xc
0
2
4
6
8
10
20
40
60
80
100
TIME (seconds)

Fig. 6

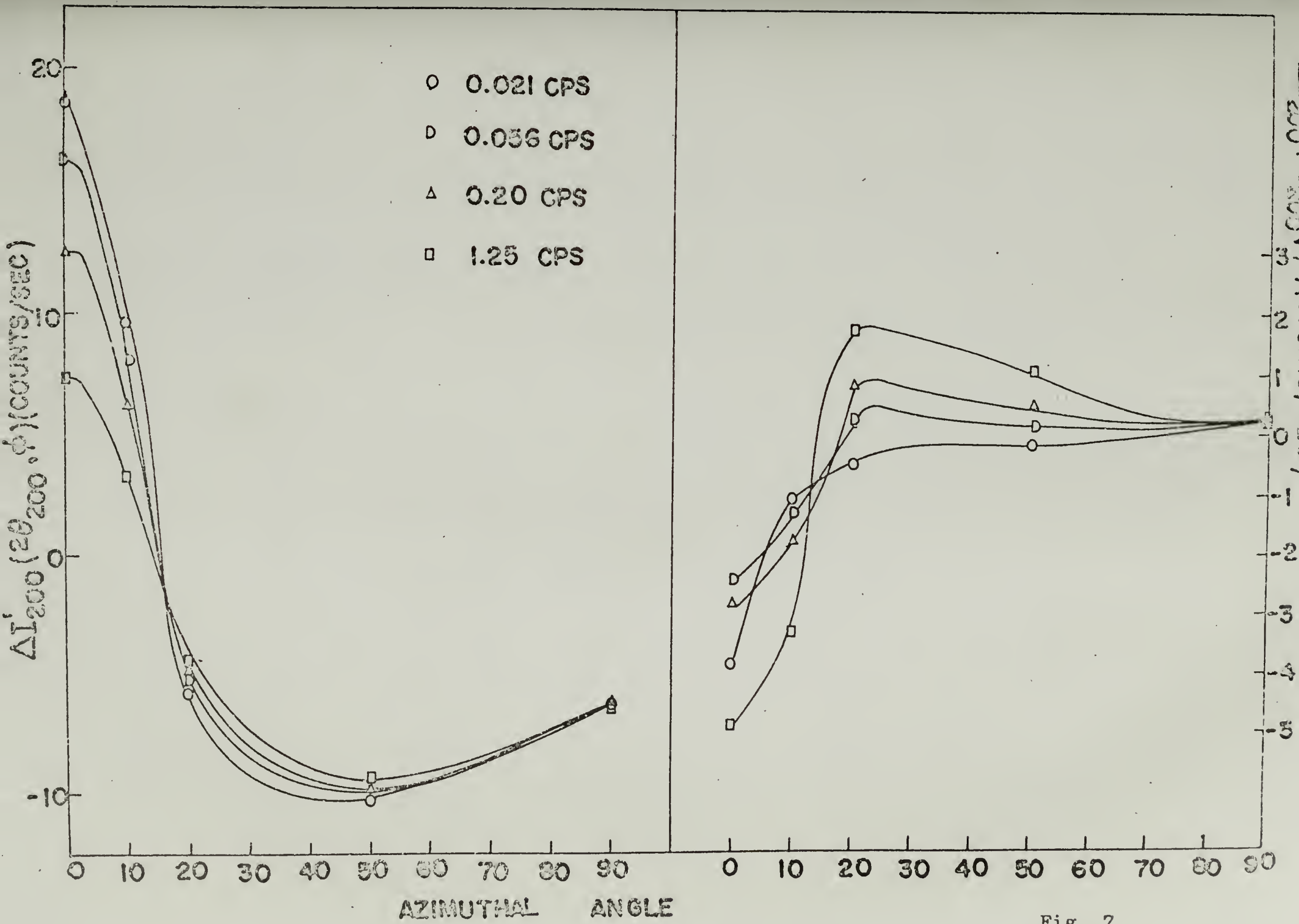
0.021 CPS
0.056 CPS
0.20 CPS
1.25 CPS
$\Delta I'_{200}(2\theta_{200})$ (COUNTS/SEC)
$\Delta I''_{200}(2\theta_{200})$ (COUNTS/SEC)
AZIMUTHAL ANGLE
20
10
0
-10
3
2
1
0
-1
-2
-3
-4
-5
0 10 20 30 40 50 60 70 80 90

Fig. 7

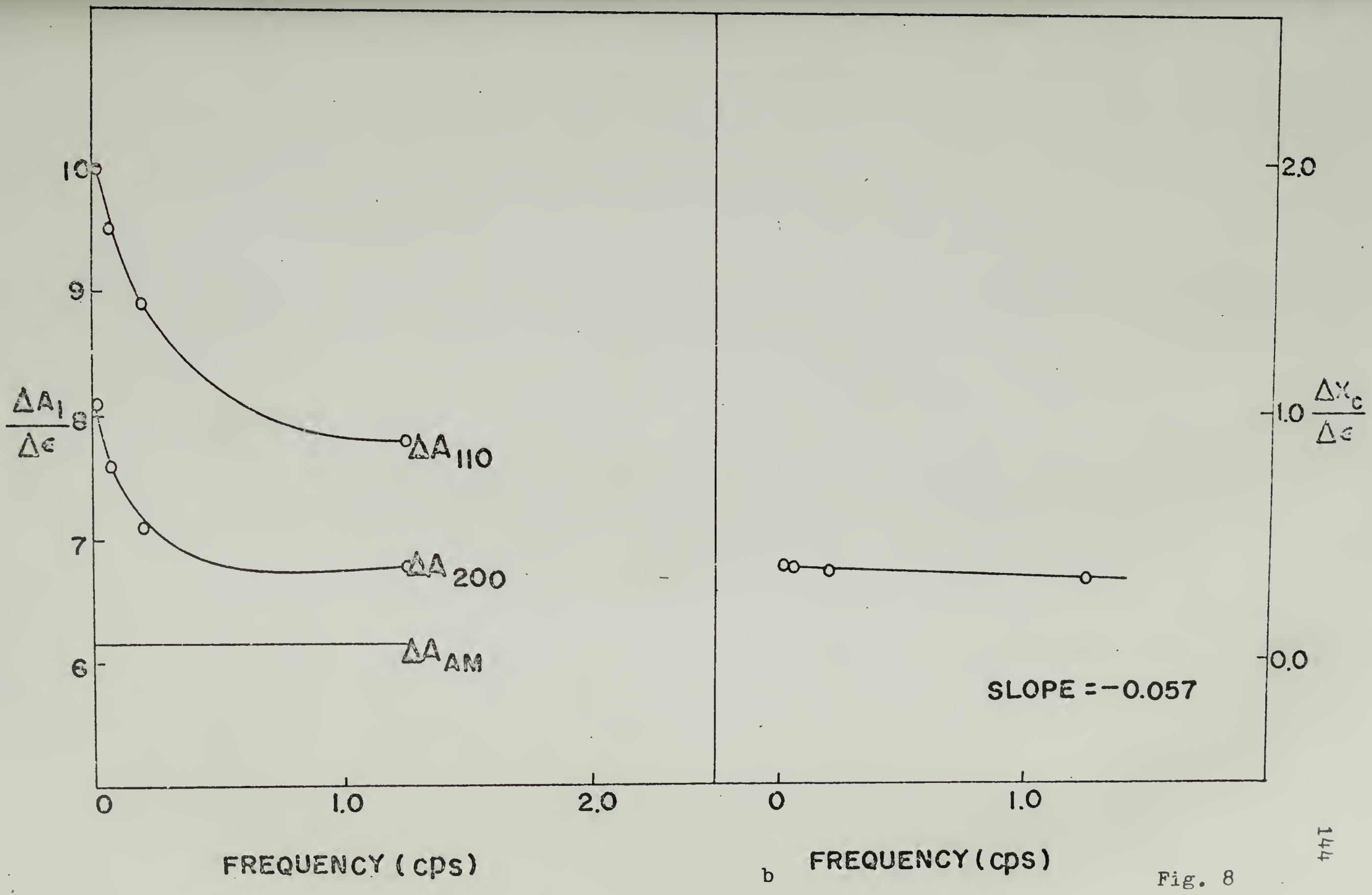
10
9
8
7
6
$\frac{\Delta A_1}{\Delta \epsilon}$
ΔA_{110}
ΔA_{200}
ΔA_{AM}
0
1.0
2.0
FREQUENCY (cps)
2.0
1.0
0.0
$\frac{\Delta X_c}{\Delta \epsilon}$
SLOPE = −0.057
0
1.0
FREQUENCY (cps)

b

Fig. 8

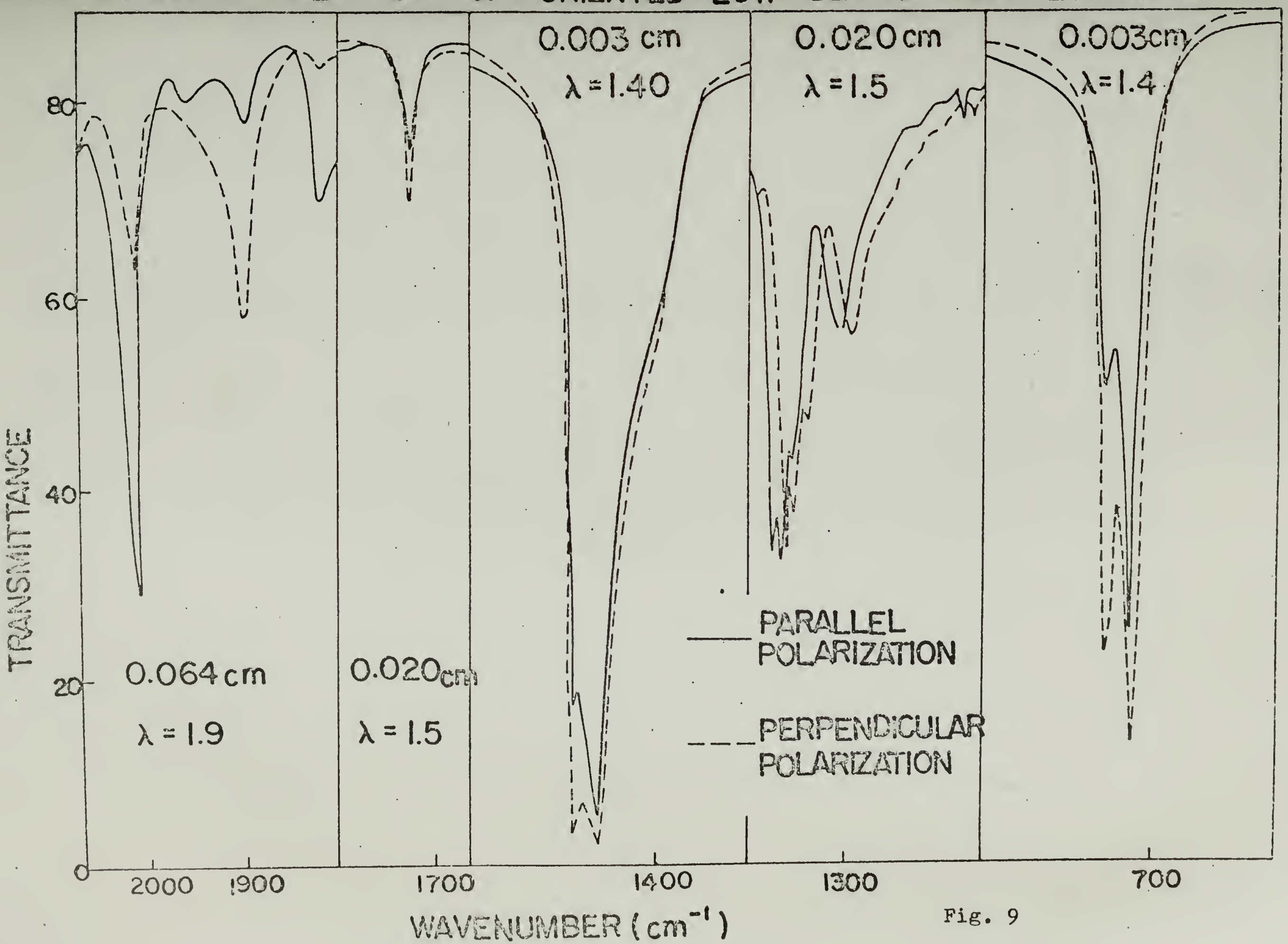
INFRARED SPECTRUM OF ORIENTED LOW DENSITY POLYETHYLENE
0.003 cm
λ = 1.40
0.020 cm
λ = 1.5
0.003cm
λ = 1.4
0.064 cm
λ = 1.9
0.020cm
λ = 1.5
PARALLEL POLARIZATION
PERPENDICULAR POLARIZATION
TRANSMITTANCE
80
60
40
20
0
2000
1900
1700
1400
1300
700
WAVENUMBER (cm⁻¹)

Fig. 9

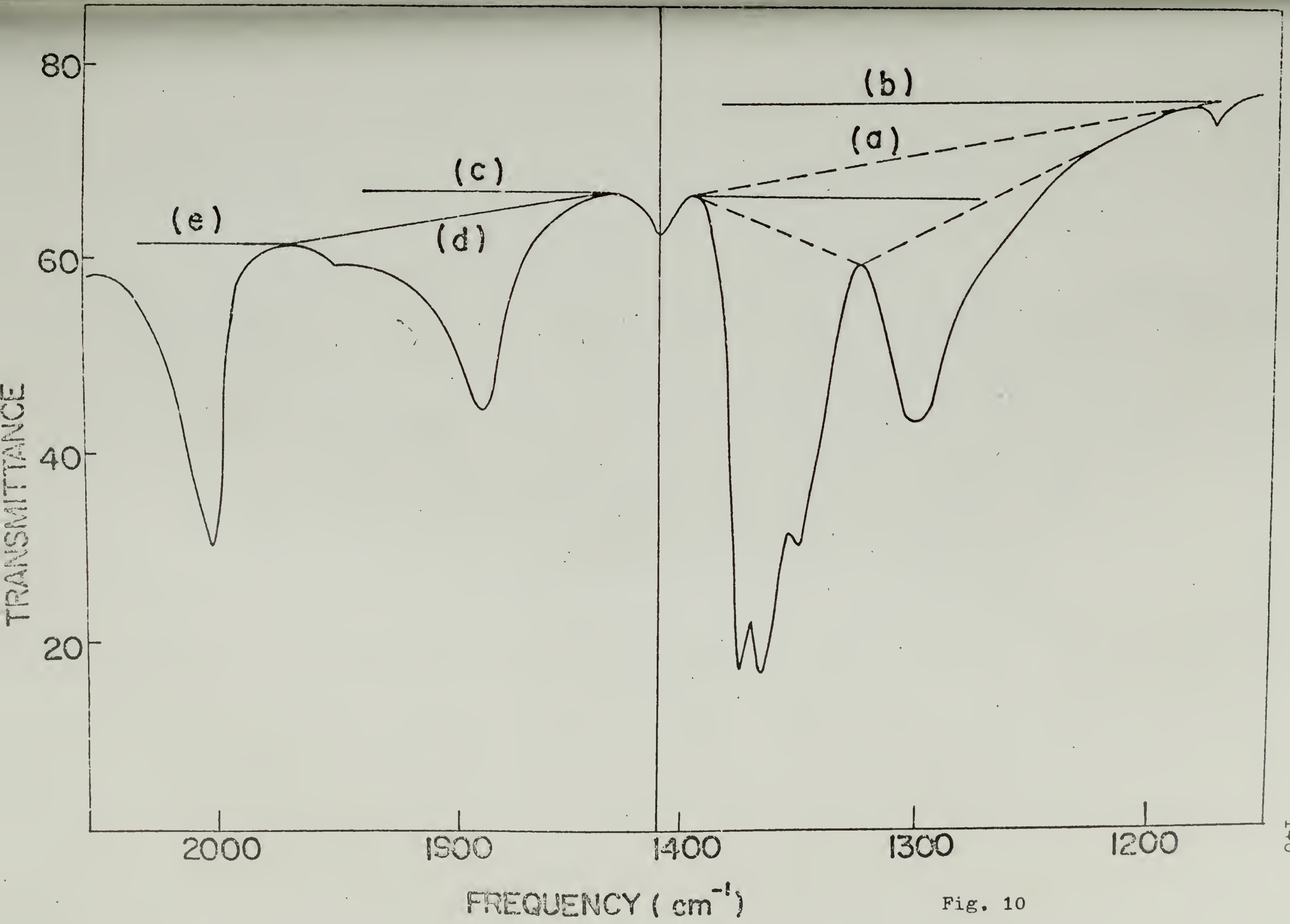
80
60
40
20
TRANSMITTANCE
(a)
(b)
(c)
(d)
(e)
2000
1500
1400
1300
1200
FREQUENCY (cm^{-1})

Fig. 10

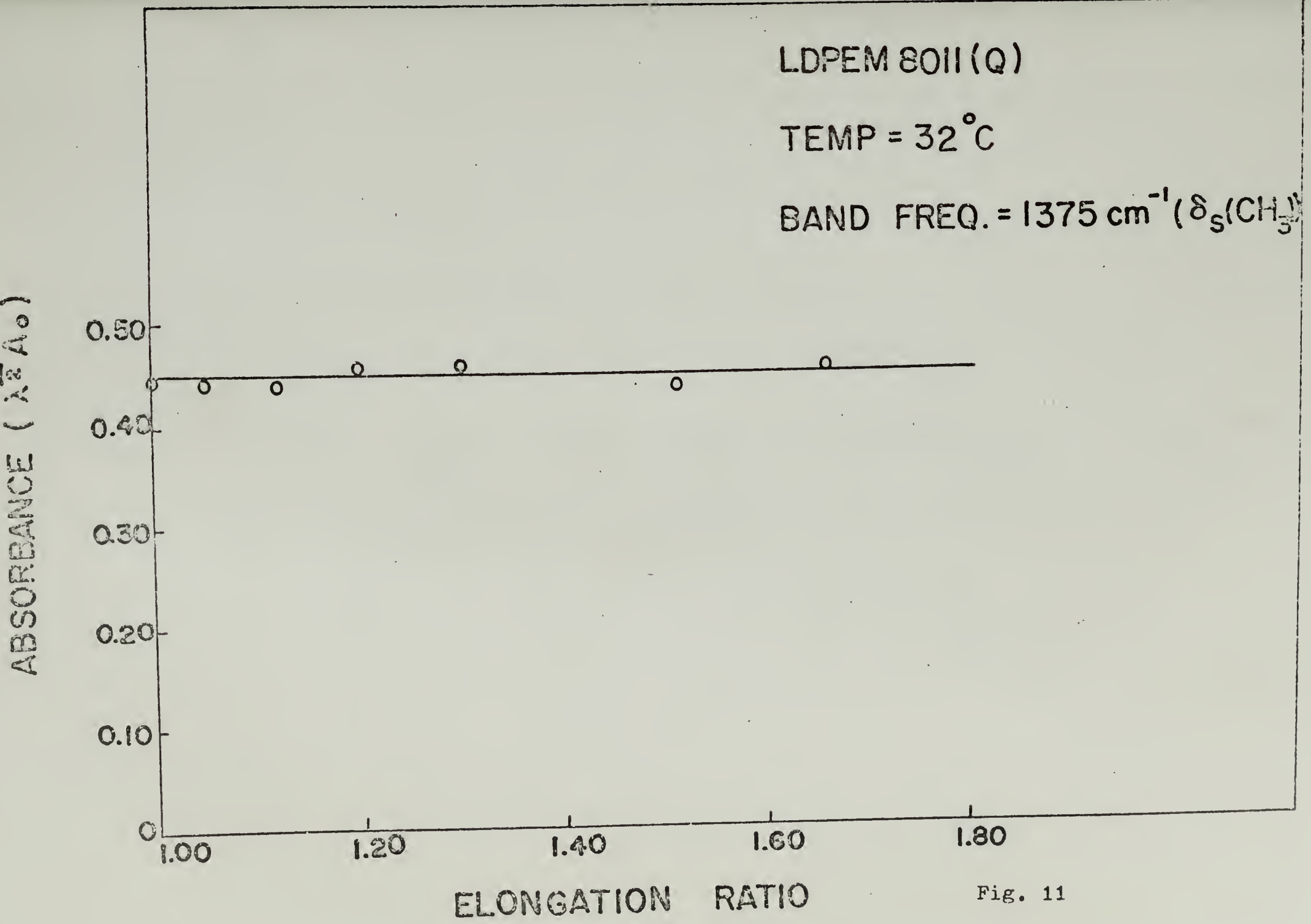
LDPEM 8011(Q)
TEMP = 32°C
BAND FREQ. = 1375 cm⁻¹ (δs(CH3))
ABSORBANCE (λ⁻² Å₀)
0.50
0.40
0.30
0.20
0.10
0
1.00
1.20
1.40
1.60
1.80
ELONGATION RATIO

Fig. 11

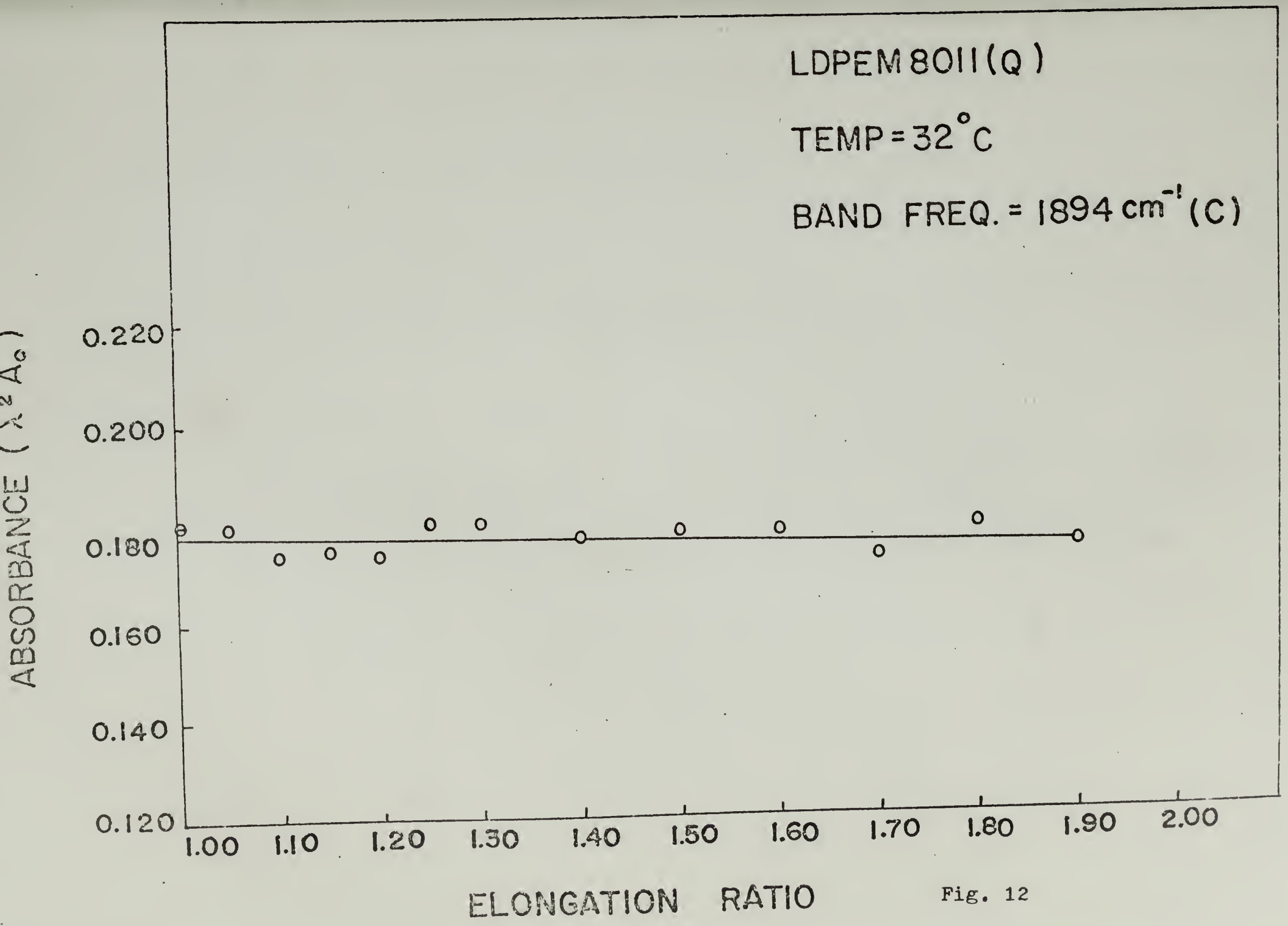
LDPEM8011(Q)
TEMP=32°C
BAND FREQ.=1894 cm⁻¹(C)
ABSORBANCE ($\lambda^{\frac{1}{2}} A_0$)
0.220
0.200
0.180
0.160
0.140
0.120
1.00
1.10
1.20
1.30
1.40
1.50
1.60
1.70
1.80
1.90
2.00
ELONGATION RATIO

Fig. 12

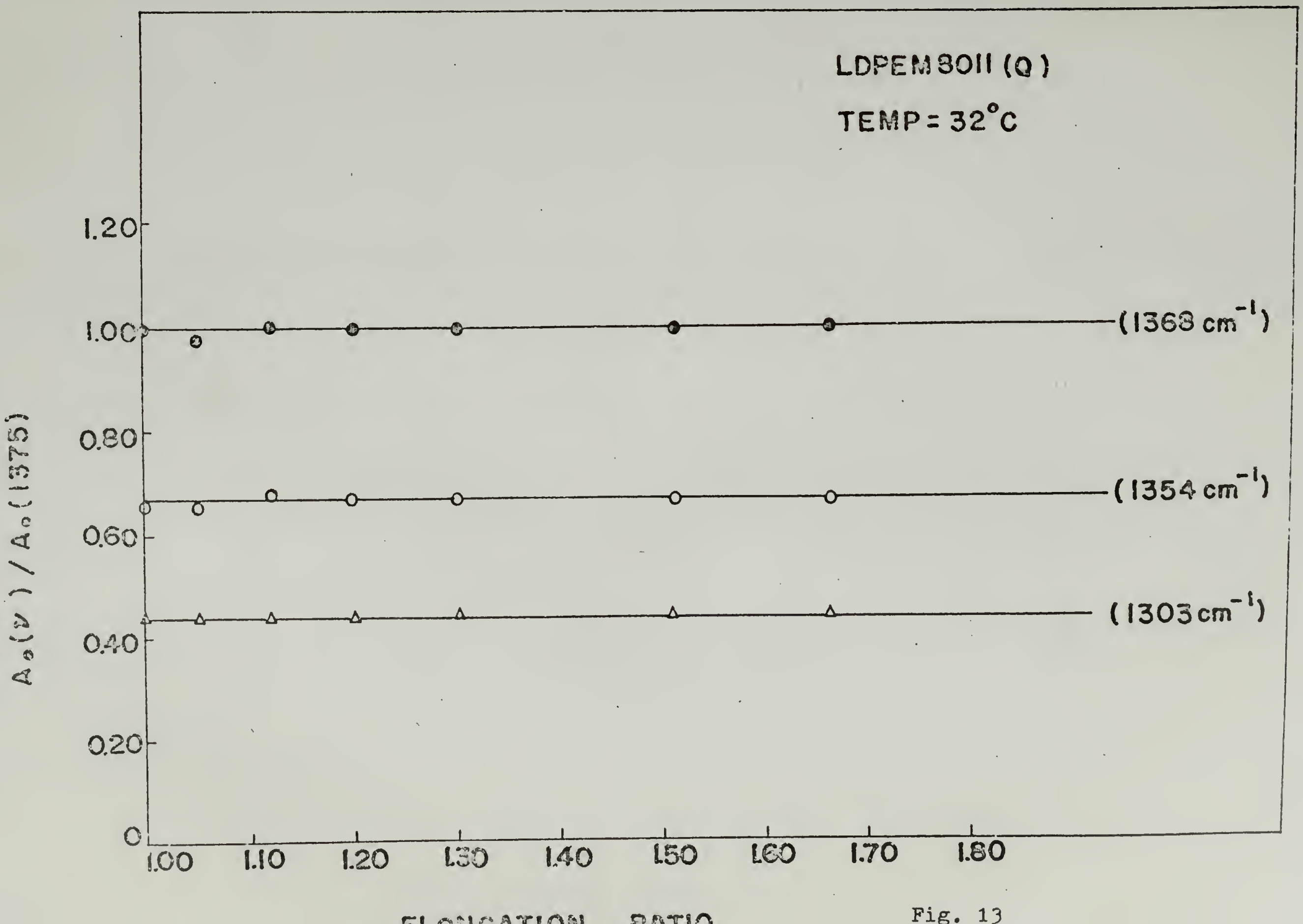
LDPEM3011 (Q)
TEMP = 32°C
1.20
1.00
0.80
0.60
0.40
0.20
0
(1368 cm⁻¹)
(1354 cm⁻¹)
(1303 cm⁻¹)
A₀(ν) / A₀(1375)
1.00
1.10
1.20
1.30
1.40
1.50
1.60
1.70
1.80
ELONGATION RATIO

Fig. 13

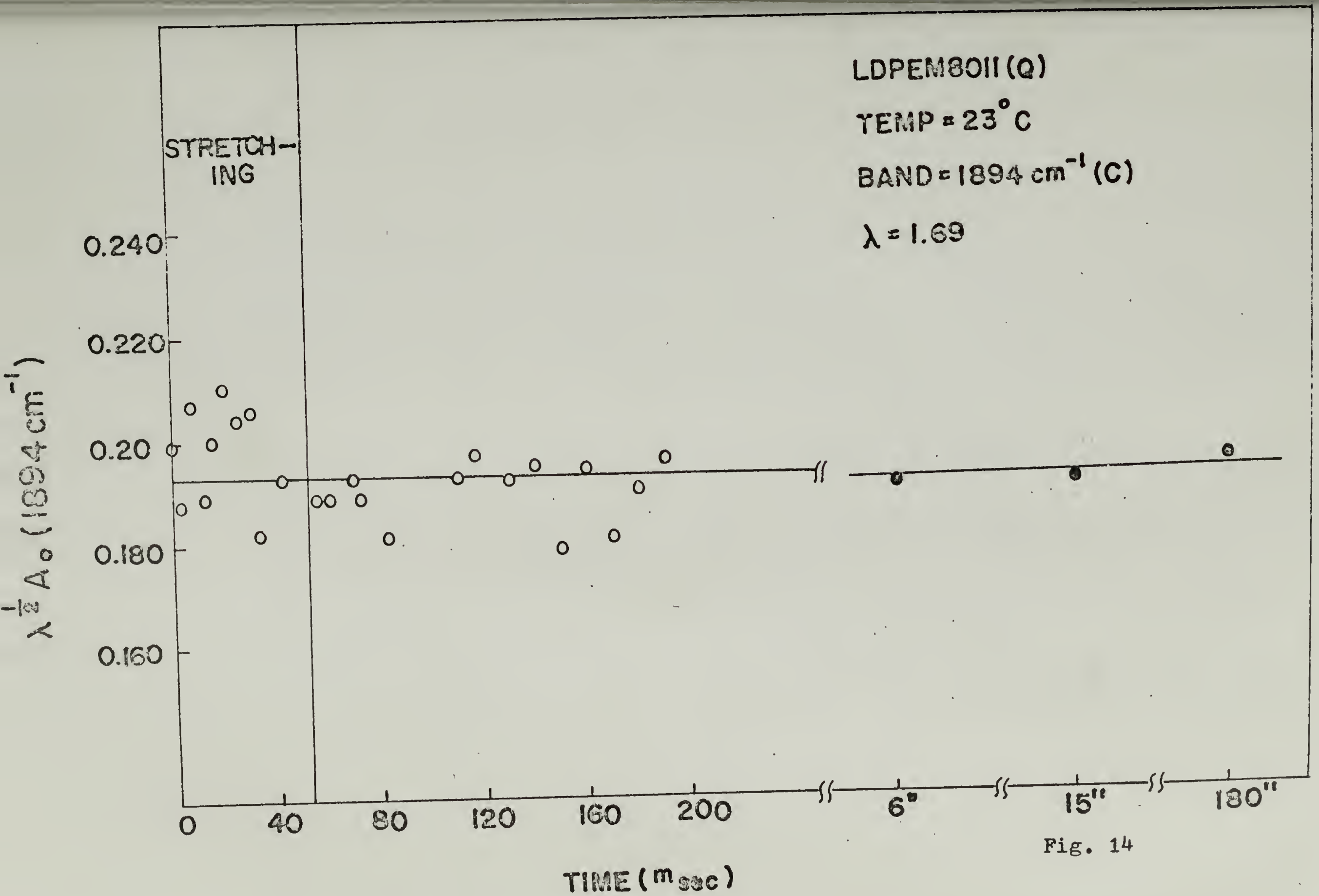
LDPEM8011(Q)
TEMP = 23°C
BAND = 1894 cm⁻¹ (C)
λ = 1.69
STRETCH-
ING
0.240
0.220
0.20
0.180
0.160
λ^½ A₀ (1894 cm⁻¹)
0
40
80
120
160
200
6"
15"
180"
TIME (m sec)

Fig. 14

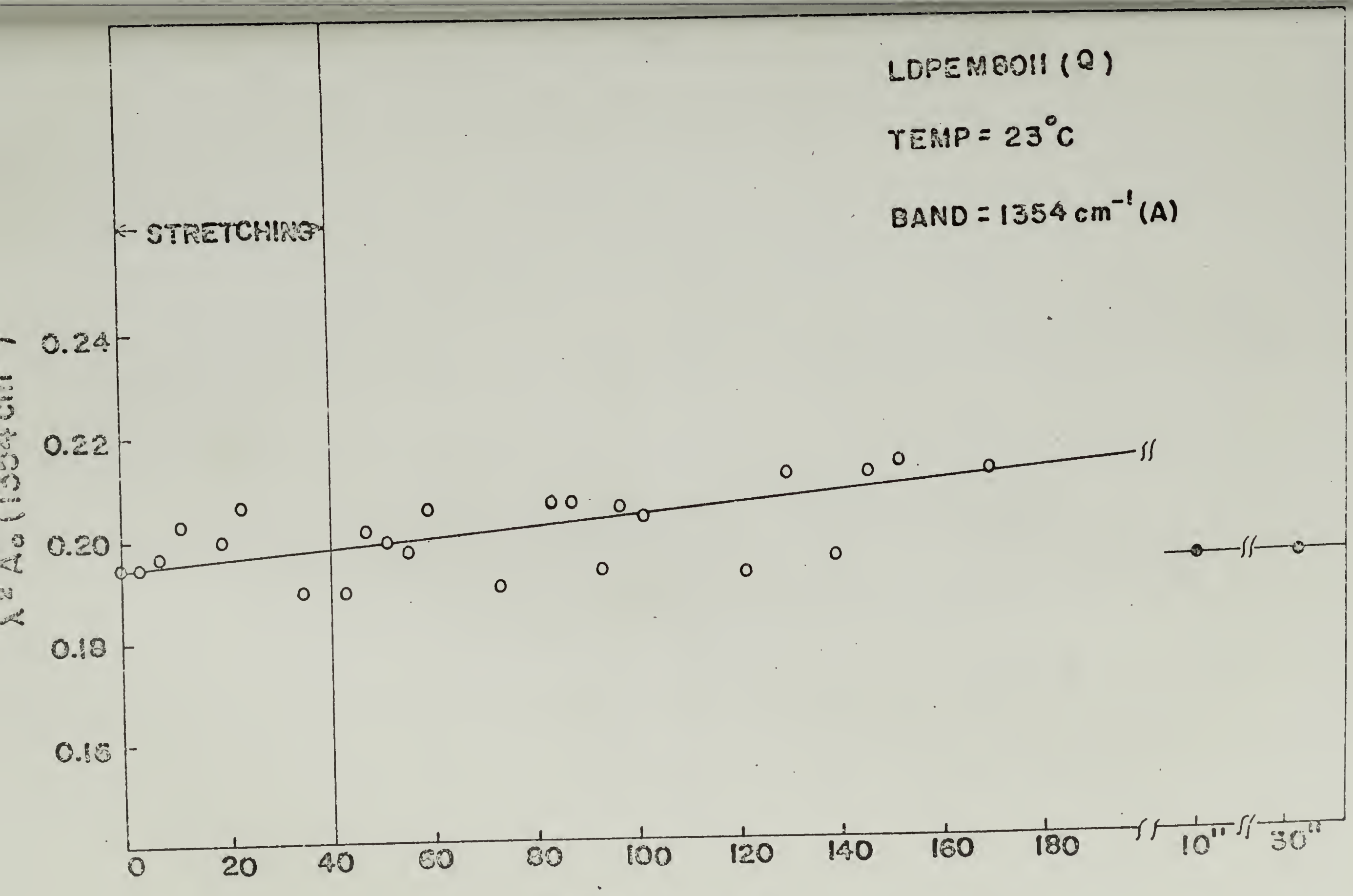
LDPEM6011 (Q)
TEMP = 23°C
BAND = 1354 cm⁻¹ (A)
STRETCHING
0.24
0.22
0.20
0.18
0.16
0
20
40
60
80
100
120
140
160
180
10"
30"
TIME (m sec)

Fig. 15

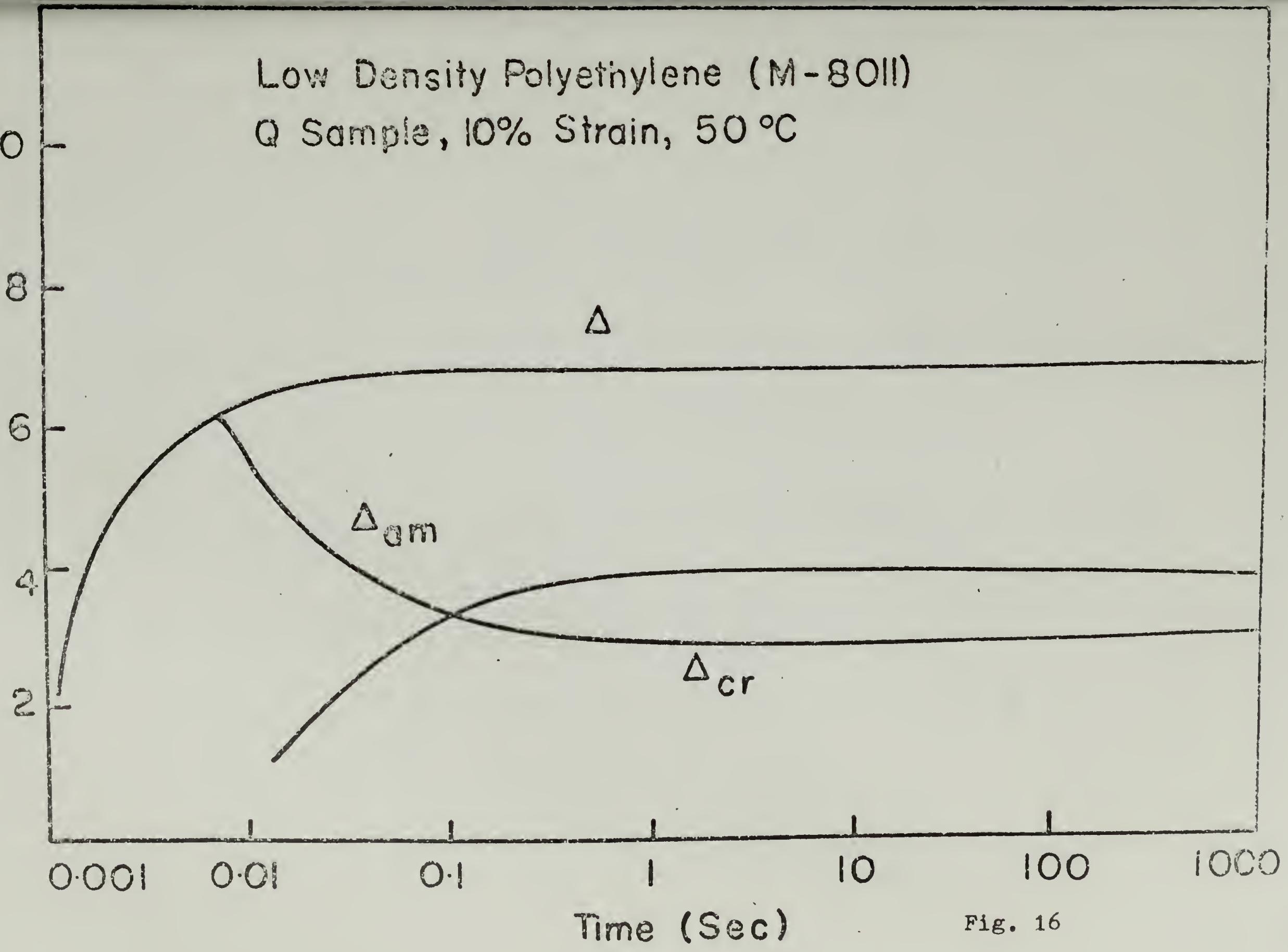
Low Density Polyethylene (M-8011)
Q Sample, 10% Strain, 50 °C
Δ
Δ_{am}
Δ_{cr}
Δ X 10³
10
8
6
4
2
0·001
0·01
0·1
1
10
100
1000
Time (Sec)

Fig. 16

CHAPTER V

STUDIES OF THE RELATIONSHIP BETWEEN ORIENTATION AND MECHANICAL PROPERTIES OF POLYETHYLENE

SYNOPSIS

The relationship between the molecular orientation and stress-strain relationship of polyethylene samples having different morphology were investigated. Polarized infrared and x-ray techniques were employed for the studies of molecular orientation, and small angle x-ray and small angle light scattering were applied for the characterization of long period and superstructure of samples, respectively. It was found that, for the low density polyethylene which had spherulitic superstructure, stretching the quenched sample resulted in higher crystalline orientation and lower amorphous orientation as compared with the slowly cooled sample; while the medium density polyethylene, which had rodlike superstructure, gave rise to rather peculiar amorphous orientation. This orientational behavior of polyethylene was discussed in terms of the Yoon-Stein theory for crystalline orientation and the theories developed by Petraccone *et al* and Flory and Abe for the amorphous orientation. Also there was no good correlation between stress-strain relationship and molecular orientation. The stress-strain relationship was discussed with consideration of molecular orientation and deformation mechanisms.

INTRODUCTION

As we discussed briefly in the Chapter of General Introduction, crystalline polymers may be represented as two-phase systems in which crystals are interconnected by amorphous phases. The crystals may be chain-folded lamellae or extended-chain crystals, depending upon the crystallization conditions. The crystals are not entirely perfect and may contain various kinds of defects such as kinks, dislocations, surface defects like mosaic boundaries and amorphous defects which are inclusions of disordered regions within the crystal or at the surface of the crystal (1). The amorphous regions may include regular chain folds, large chain loops (irregular folds), chain ends (cilia) and tie chains which interconnect lamellae together. Moreover, the lamellae may form aggregates which in many cases have superstructure of spherulitic or shish-kebab type.

When under stress, the structural elements of the crystalline polymer, i.e., the lamellae and the various kinds of chains in the amorphous regions, must reorient themselves to accomodate the imposed strain. The processes of response of these structural elements to the stress will deeply affect the mechanical properties of the crystalline polymers. Thus the understanding of the deformation processes of crystalline polymers has not only scientific but also technological importance because of the

important roles of these polymers play in the manufacturing of fibers, films and construction materials.

There have been a number of studies investigating the mechanisms involved in the deformation of crystalline polymers. These include work on the deformation of single polymer crystals (2-5) and of spherulites (6-7), studies of viscoelastic properties and anisotropic mechanical properties of crystalline polymers (8-13), and studies of rheo-optical properties of crystalline polymers (14). The studies of the deformation of single polymer crystals and of spherulites reveal various processes of deformation of the crystal and the spherulites as a whole. The studies of viscoelastic properties and anisotropic mechanical properties enable the interpretation of various mechanical losses in terms of molecular processes such as interlamellar slip, intermosaic deformation and shear deformation of the lamellae according to Takayanagi et al (8-9), or such as interlamellar shear and c-axis shear of the crystals by Ward et al (10-13). The rheo-optical studies generally confirm the conclusions of viscoelastic studies, but they provides more information concerning the detailed orientation of the crystals and of the amorphous regions (14).

The direct consequence of the stress (or the strain) is the orientation of polymer molecules along the stretching direction. This orientation of molecules reflects in changes in the

mechanical properties (15) and in the viscoelastic properties (10-13) of the polymers. There also have been reports on the good correlation between the stress-strain and the crystalline orientation of low density polyethylene (16-17).

Since the lamellae of crystalline polymers are interconnected by amorphous chains, the crystalline and the amorphous orientation of crystalline polymers of moderately high degree of crystallinity may be very important in connection with the mechanical and viscoelastic properties. This is because in these samples the amorphous regions do not serve only as a matrix for crystalline regions but rather both the crystalline and the amorphous regions are actively participating in responding to the stress. Thus to understand the structure-property relationship of these samples, it is necessary to investigate both the crystalline orientation and the amorphous orientation in response to deformation.

In order to get more understanding about the complex relationships of the morphology, the degree of crystallinity, the orientation and the stress-strain, crystalline and amorphous orientations of samples of low density polyethylene with different heat treatment and samples of high density polyethylene were measured by x-ray and infrared techniques. The infrared technique has the advantages of rendering not only the crystalline orientation but also orientation of chain segments of various

conformations in amorphous regions. In order to correlate with orientation with the mechanical properties, the stress-strain relationship of these samples was also determined.

EXPERIMENTAL

SAMPLES AND SAMPLE PREPARATION

Monsanto experimental low density polyethylene (LDPE), M8011, and Monsanto medium density polyethylene (HDPE), MPE 220/27007, were used. The M8011 sample has $\overline{Mn} = 1.38 \times 10^4$, $\overline{Mw} = 1.72 \times 10^5$, melt index = 2.9, 1.4 long chain branches/100C and the MPE 220/27007 has $\overline{Mn} = 1.85 \times 10^4$, $\overline{Mw} = 1.974 \times 10^5$, melt index = 0.78, and 0.12 CH_3/100C.

Pellets of polyethylene were melted between two photoferrotype plates in a Carver Laboratory Press at 165°C for ten minutes and were subsequently pressed at 12,000 psi at the same temperature for ten minutes. The melt was then either quenched in a dry ice-methanol bath or allowed to cool to room temperature at 5000 psi in the press. The quenched samples will be designated as Q-sample while the slowly cooled ones as SC-sample and the medium density sample as the HDPE sample.

The characterization of the prepared films is summarized in Table I. The density of films was measured by a density gradient column of ethanol-water mixture at room temperature.

The weight fraction crystallinity was calculated from the density using the density of pure crystal and that of pure amorphous material of polyethylene determined by Okada et al (18). The spherulite size was determined from Hv low angle light scattering patterns using the equation (19)

$$4\pi (R/\lambda) \sin (\theta_{max}/2) = 4.1 \qquad (1)$$

where R is the radius of spherulite, λ is the wavelength of the incident beam and θ_{max} the position of maximum intensity of the Hv scattering pattern at 45^{o} of azimuthal angle. The long periods were ontained according to Bragg's equation from small angle x-ray scattering using a Rigaku-Denki camera with slit collimation, where the intensity was desmeared and Lorentz corrected.

Infrared Measurement

Measurements were made on a Perkin-Elmer Model 180 IR Spectrophotometer. Perkin-Elmer silver bromide wire grid polarizers were used for the polarized investigation. The differential method (double-polarizer technique) and, when the absorption of the sample film was too high to use the differential method because the recorder was malfunctioned due to low intensity of the refrence beam, the conventional single-polarizer method was used to determine the dichroic ratio.

Details of the differential method were presented elsewhere (20). In adopting this technique to the Perkin-Elmer Model 180 IR Spectrophotometer, polarizers were placed in the sample chamber and the reference beam chamber, respectively. The polarizers were set at 45^{o} to the entrance slit of monochromater; this was achieved by using another polarizer, Perkin-Elmer Model 186-0240 which was mounted in front of the entrance slit, as reference. The orientation of the reference polarizer can be rotated by a dial. The ara arrangement of the polarizers at 45^{o} to the entrance slit was intended to have both beams subject to same machine polarization. Contrary to the usual case where the two polarizers were set at 90^{o} to each other, the two polarizers were arranged parallel to each other. This arrangement was necessary because the sample beam reflected one more time before both beams passed through the polarizers, thus the component of the electric field of the sample beam at 45^{o} to the entrance slit was rotated 90^{o} from that of the reference beam. A schematic diagram showing the modification is shown in Fig. 1. The differential method directly measured the difference of absorbance of both beams, thus it has higher sensitivity than the usual single-polarizer technique (20)..

The sample films were mounted on a stretcher which was capable of extending both ends simultaneously, thus the same part of the film was maintained in the beam at all elongations.

The stretcher was placed at the site inside the compartment housing the source where the image of the source was focused. A stream of cool air was blown at the sample to cool it. The temperature of the sample was measured to be about 32°C.

For the bands of 730 cm^{-1} and 1473 cm^{-1}, even using films of thickness about 0.0015-0.0025 cm, the absorption is still too high to use the differential method. Therefore, the conventional single-polarizer method was used to make the measurement. The polarizer was mounted in a holder in front of the entrance slit, thus both the sample beam and the reference beam passed through polarizer and were subject to the same machine polarization. The polarizer can be rotated by a dial. The stretcher was placed at the sample compartment. Different scans were made with the polarization parallel and perpendicular to the stretching direction.

Strips of film of the size 3cm X 6cm and of various thickness (0.0015-0.075 cm) were used for the investigation. The films were stretched slowly in a stepwise fashion. Ten minutes were allowed for relaxation before measurements were made. Lines 0.5 cm apart were ruled on the undeformed samples; these lines were used to determine the elongation ratio. For the Q-sample of LDPE the deformation was quite uniform at all elongation ratios. For the SC-samples of LDPE and the HDPE sample, the deformation was quite uniform at elongation ratios less

than 1.5 for the former and 1.3 for the latter. The actual elongation ratio was determined in the region where the beam was transimitted.

The spectra were scanned at a speed of about 30 cm^{-1}/min. The resolution was set at better than 4 cm^{-1}. In the cases of 730 cm^{-1} and 1473cm^{-1}, resolution was set at 2 cm^{-1}.

In determining the dichroic ratio from the differential spectra, the average absorbance for the unstrained polymer was needed. The average absorbance of the undeformed sample, A_o, was measured with unpolarized light (the polymer in the undeformed state was randomly oriented, at least in the plane parallel to the sample surface as indicated by IR studies). Since the elongation was uniaxial and there were no changes in crystallinity and in conformation populations as shown by the results of Chapter 4, the average absorbance of the sample at extension ratio λ was estimated by the relation

$$A_o(\lambda) = A_o(\lambda=1.0) / \sqrt{\lambda} \qquad (2)$$

Figure 2 shows the bands investigated in LDPE. The base lines selected for various bands are also indicated. There is different choice of the base lines for different bands, as indicated by the dotted lines (18, 21-23). We have measured the absorbance of 1894 cm^{-1}, 1375 cm^{-1}, 1368 cm^{-1}, 1354 cm^{-1}

and 1303 cm^{-1} as a function of the sample thickness using the selected base lines. The results are shown in Figures 3 and 4. The plots of absorbance against thickness are linear and pass through the origin; this is a good indication that the choice of base lines is reasonable for these bands. While the orientation function will somewhat depend on the choice of the base line, the trend of change should not be greatly affected.

Figure 3 shows typical absorption spectra in various regions for oriented low density polyethylene and Fig. 4 shows the differential spectra. The base lines in the differential spectra were obtained by scanning the spectra with an undeformed sample in the beam; it was found that the base line so obtained well coincided with that obtained with no sample in the beam if the sample had no preorientation and had a very good surface. In some cases, the base line of the sample in the deformed state changed because of changes in surface texture of the sample which affects the reflectivity of the beam. Under these circumstances, the base line was established by drawing a line connecting the two points on the spectrum which were predetermined as base line.

We did not correct for the effects of insufficient resolution arising from finite mechanical slit width. The corrections for band overlapping were made only for the bands of 730 cm^{-1} and 720 cm^{-1} as well as 1463 cm^{-1} and 1473 cm^{-1} by

assuming the band shape could be represented by a Lorentz curve

$$\ln\left(I_o/I\right)_\nu = \frac{a}{(\nu - \nu_o)^2 + b^2} \qquad (3)$$

where ν is the frequency in cm^{-1}, ν_o the frequency of the peak maximum and a and b are constants. The bandwidth at half peak intensity is

$$\Delta\nu_{1/2} = 2b \qquad (4)$$

The measured half bandwidth was used as first approximation. The results did show improvement, but since the process was quite arbitrary, we only made the first correction and did not pursue it further.

The reflection from the sample surface was also considered. According to the equation derived by Cunningham et al (25), it was estimated that for the 1473 cm^{-1} band, the effect was about 10 %. for the other bands whose absorption are less intense, the effect is not very significant. Therefore, the reflection effect was neglected.

The absorption bands investigated for the dichroism are listed in Table II. More detailed summary of the band assignments is presented in Ref. 26.

X-RAY STUDIES

The crystal orientation were determined by the x-ray technique. The apparatus, operation procedures, intensity corrections and data treatments are described elsewhere (24). There is an uncertainty about the contributions from amorphous phase scattering to the intensities of various crystalline peaks. Therefore three different procedures for correcting the amorphous contributions were undertaken. The amorphous halo was assumed to be symmetry with intensity peaked at 19.4^{o} of the scattering angle (which is twice the Bragg angle), as shown in Fig. 5. These three procedures included : (1) Assuming no amorphous contributions; the orientation function so obtained was designated as f^{I}. (2) Assuming the ratio of I_o to I_1 and that of I_o to I_2 were constant and independent of elongation; the orientation function obtained was expressed as f^{II}. (3) Assuming $I_1 = I_3$ and $I_2 = I_4$, where I_1 and I_3 as well as I_2 and I_4 were intensity at symmetric position with respect to the amorphous peak at I_o . I_3 and I_4 were directly measured along with the crystalline peak intensity. The orientation function obtained by this procedure was indicated as f^{III}.

STRESS-STRAIN MEASUREMENT

Tensile stress was measured on a table model instron (Instron Engineering Corp., Model TM). Sample were stretched at about 3 % per min. in a stepwise fashion. Enough time was allowed

for the stress to relax to constant value (about 1.5 min.) . For the Q-sample of LDPE, there was no sign of stress relaxation for the sample stretched up to about 5 %. When relaxation did occur, the change in the magnitude of the stress was relatively small. In the cases of the SC-sample of LDPE and of the HDPE sample, stress relaxation occurred at very small strain. Typical stress relaxation for these three samples was shown in Fig. 6. Attempts were not undertaken to determine the exact strain where relaxation started to appear.

The sample were ruled with lines of 0.5 cm apart. The strains of a small area were determined. True tensile stress was estimated from the total load and the sample cross-section with consideration of change in cross-section due to deformation. It was assumed the sample being uniaxially deformed and having constant volume.

ORIENTATION FROM INFRARED AND X-RAY MEASUREMENTS

1. Infrared

For a uniaxially oriented sample, the absorbance ($A_{//}$) measured with radiation polarized in the stretching direction may differ from the absorbance ($A_{\perp}$) determined for radiation polarized perpendicular to this direction. The dichroic ratio, D, is defined as

$$D = \frac{A_{//}}{A_{\perp}} \qquad (5)$$

The dichroic ratio can also be expressed as (20)

$$D = \frac{2(A_{//} - A_{\perp}) + 3A_o(\lambda)}{3A_o(\lambda) - (A_{//} - A_{\perp})} \qquad (6)$$

where $A_o(\lambda)$ is the average absorbance at extention ratio λ defined as

$$A_{//} + 2A_{\perp} = 3A_o \qquad (7)$$

The quantity $(A_{//}-A_{\perp})$ is directly measurable from the differential method.

The second order orientation function of polymer chains in the stretched sample is defined as (34)

$$f = (3\langle \cos^2\theta \rangle - 1)/2 \qquad (8)$$

where θ is the angle between the stretching direction and the axis of the chain segments. The relationship between f and the dichroic ratio for a particular absorption band is (35)

$$f = \frac{D_o + 2}{D_o - 1}\,\frac{D - 1}{D + 2} \qquad (9)$$

Here D_o is defined as

$$D_o = 2\cot^2\phi \qquad (10)$$

where ϕ is the angle between the chain axis and the transition moment direction for the vibrational mode responsible for the infrared absorption.

The crystalline infrared bands at 730 cm^{-1} and 1473 cm^{-1} have their transition moments along the a-axis of the crystal, so the orientation function of a-axis (f_a) is

$$f_a = \frac{D_{730} - 1}{D_{730} + 2} \qquad (11)$$

and

$$f_a = \frac{D_{1473} - 1}{D_{1473} + 2} \qquad (12)$$

because $\phi = 0^o$. Similarly, the band 1176 cm^{-1} has its transition moment along the c-axis of the crystal, consequently the orientation function of c-axis is

$$f_c = \frac{D_{1176} - 1}{D_{1176} + 2} \qquad (13)$$

The transition moment direction of the crystalline band 1894 cm^{-1} is perpendicular to the c-axis, but its exact direction is uncertain. One can express the orientation of the transition moment as

$$f_{1894} = \frac{D_{1894} - 1}{D_{1894} + 2} \qquad (14)$$

If the transition moment is along the crystal a-axis as some suggested (see Table II), the f_{1894} is equivalent to f_a.

The amorphous bands at 1368 cm^{-1}, 1352 cm^{-1} and 1303 cm^{-1} are each reported to have transition moments along the chain axis (see table II), the amorphous orientation functions from these bands can be expressed as

$$f_{1368}^{am} = \frac{D_{1368} - 1}{D_{1368} + 2} \qquad (15)$$

$$f_{1352}^{am} = \frac{D_{1352} - 1}{D_{1352} + 2} \qquad (16)$$

$$f_{1303}^{am} = \frac{D_{1303} - 1}{D_{1303} + 2} \qquad (17)$$

According to current assignments (see Table II), f_{1352}^{am} should characterize the orientation of amorphous gauche conformations and f_{1368}^{am} and f_{1303}^{am} should be related to the orientation of amorphous trans units, probably those isolated trans units flanked by gauche units.

The amorphous band at 1078 cm^{-1} has a transition moment lying perpendicular to the chain axis. Since it may be rea-

sonable to assume that the transition moment has equally probable orientation around the chain axis, we have from eqs. 9 and 10

$$f_{1078}^{am} = -2\,\frac{D_{1078}-1}{D_{1078}+2} \qquad (18)$$

f_{1078}^{am} probably characterizes some average orientation of both gauche and trans sequences.

The band at 2016 cm^{-1} has been attributed to both crystalline and amorphous phases. The crystalline component has transition moment along the c-axis. It has been shown that, for a uniaxially stretched sample, the dichroic ratio of the amorphous component is given as (26)

$$D_{2016}^{am} = \frac{(A_{2016})_{\parallel} - (A_{1894})_{\perp}\left(\frac{\epsilon^{o}_{c,2016}}{\epsilon^{o}_{c,1894}}\right)(1+2f_c)/(1-f_{1894})}{(A_{2016})_{\perp} - (A_{1894})_{\perp}\left(\frac{\epsilon^{o}_{c,2016}}{\epsilon^{o}_{c,1894}}\right)(1-f_c)/(1-f_{1894})} \qquad (19)$$

and

$$f_{2016}^{am} = \frac{D_{2016}^{am}-1}{D_{2016}^{am}+2} \qquad (20)$$

where $\epsilon^{o}_{c,2016}$ and $\epsilon^{o}_{c,1894}$ are extinction coefficients of pure crystal. The value of $(\epsilon^{o}_{c,2016} / \epsilon^{o}_{c,1894})$ is found to be 1.27 for polyethylene (26).

2. X-ray

The orientation function of the crystallites in uniaxially deformed polyethylene, following eq. (8), can be expressed as

$$f_a = \frac{3\langle \cos^2\theta_a \rangle - 1}{2} \qquad (21)$$

$$f_b = \frac{3\langle \cos^2\theta_b \rangle - 1}{2} \qquad (22)$$

$$f_c = \frac{3\langle \cos^2\theta_c \rangle - 1}{2} \qquad (23)$$

where θ_a, θ_b and θ_c are the angle which a, b and c axes, respectively, make with the stretching direction. It has been shown (34) that

$$f_a + f_b + f_c = 0 \qquad (24)$$

Therefore anly the orientation functions of two crystal axes are needed to characterize the crystll orientation. The quantity $\langle \cos^2\theta \rangle$, refered to as orientation parameter, can be evaluated from pole figure data by the relationship (36)

$$\langle \cos^2\theta \rangle = \frac{\int_0^{\frac{\pi}{2}} I(\theta) \cos^2\theta \sin\theta \, d\theta}{\int_0^{\frac{\pi}{2}} I(\theta) \sin\theta \, d\theta} \qquad (25)$$

where $I(\theta)$ is the intensity of the diffraction peak for the selected crystal plane when the fiber axis is at an angle θ. In the case of polyethylene, generally only the intensity of

110 and 200 peaks is high enough for a convenient measurement. It has been shown, however, that the orientation parameter of b-axis, $\langle \cos^2\theta_b \rangle$, can be determined by the relation (36)

$$\langle \cos^2\theta_b \rangle = 1.445 \langle \cos^2\theta_{110} \rangle - 0.445 \langle \cos^2\theta_{200} \rangle \qquad (26)$$

and since

$$\langle \cos^2\theta_a \rangle = \langle \cos^2\theta_{200} \rangle$$

then $\langle \cos^2\theta_c \rangle$ can be obtained by

$$\langle \cos^2\theta_c \rangle = 1 - \langle \cos^2\theta_a \rangle - \langle \cos^2\theta_b \rangle \qquad (27)$$

RESULTS

1. Superstructure of Undeformed and Deformed Sample

The small angle light scattering patterns (Hv) of the undeformed and deformed samples are shown in Figs. 7, 8 and 9. The Hv scattering patterns of Q-sample (Fig. 7) and SC-sample (Fig. 8) of LDPE have the characterization four-leaf clover appearance, each leaf having a maximum intensity. This indicates that the superstructure is spherulitic (37), while the Hv patterns of the HDPE sample (Fig. 9) also have the four-leaf clover appearance, but it appears that the intensity maximum is at the center of the clover with decreasing intensity at larger scattering angles. This indicates that the superstructure

of the HDPE sample appears to be either highly disordered spherulitic or rodlike (38).

When these samples are deformed up to 40 % for the LDPE samples and up to 20 % for the HDPE sample, the four-leaf clover characteristic still remains. For the LDPE samples, the patterns correspond to an affine deformation of the spherical spherulite to an ellipsoid of revolution (39,40). While for the HDPE sample, the pattern seems to indicate that the superstructure as a whole was deformed.

These results from light scattering give a fairly good indication that, at least within the mentioned deformation range, the superstructures of the samples still maintain their entities. Thus the orientation of structural elements must occur by the deformation of the superstructure and by the orientation of the structural units within the superstructure.

2. Effect Of Sample Thickness On Orientation

Figs. 10 and 11 show the plots of D_{2016} vs. elongation of the ratio of the Q-sample and SC-sample of various thickness, respectively, and Fig. 12 show the orientation function of the band 1894 cm^{-1}, f_{1894} , of the Q-samples of different thickness at various elongation. Fig. 13 shows f_{730} , f_{1473} and f_{1894} vs. elongation ratio; the slight difference in f_{730} , f_{1473} and f_{1894} will be discussed later. One may conclude from these results that in the case of the Q-sample, the orientational behavior for

samples of thickness in the range of 0.003 cm-0.064 cm are the same. For the SC-samples, although less evidence is available, from the results of Fig. 11, it may be reasonable to assume that the sample thickness does not affect the orientation. Perhaps these results give a good indication that the thickness of these samples does not affect their morphology.

3. Orientation of Crystallites

(a) Infrared Measurements

The crystalline orientation determined by the absorption bands 730 cm^{-1}, 1473 cm^{-1} and 1894 cm^{-1} is shown in Fig. 13. The 730 cm^{-1} and 1473 cm^{-1} are reported to have transition moments along the a-axis of the crystal unit cell (32, 33). While the transition moment of 1894 cm^{-1} band is in the direction perpendicular to the c-axis (28), it has been suggested that the transition moment is in the a-axis direction (26, 27, 29). The results of Fig. 13 seems to be in agreement with the latter assignment. The values of orientation function measured by the 730 cm^{-1} band and 1473 cm^{-1} band are not in exact agreement. This is mainly due to overlapping with neighboring bands. After correcting for band overlapping, using the procedures described above, the orientation functions determined from 730 cm^{-1} and 1473 cm^{-1} are in better agreement with that obtained from the 1894 cm^{-1} band as shown in Fig. 14.

Fig. 15 shows the orientation function of the c-axis,

measured from the band 1172 cm^{-1} , and that of the a-axis, measured from the band 1894 cm^{-1}, of Q-sample and SC-sample of LDPE. Fig. 16 shows the crystal orientation functions of the HDPE sample. These results indicate that, while there are slight differences in crystal orientations of these samples, the general trend of crystal orientation is similar despite the difference in morphology of these samples.

(b) X-ray Measurements

The crystal orientation functions of the c-axis and a-axis measured by x-ray, using the three methods described above for correcting amorphous contribution, are plotted against those measured by infrared dichroism in Figs. 17 and 18. I, II and III correspond to the results obtained by applying the correcting method 1, 2 and 3, respectively. f^{I} may represent the lower limit of the orientation function obtained by x-ray technique because of the neglect of the amorphous contribution to the scattering intensity. It appears that the crystalline orientation obtained by the x-ray technique is higher than that obtained by IR technique. This will be discussed later.

4. Orientation of Amorphous Phases

(a) Infrared Measurement

The amorphous orientations of Q-sample and SC-sample of LDPE, determined from the dichroic ratios of 2016 cm^{-1}, 1368 cm^{-1}, 1352 cm^{-1}, 1303 cm^{-1} and 1078 cm^{-1} bands are shown in Figs. 19 and 20, and the amorphous orientations of HDPE, obtained from the dichroic ratios of 2016 cm^{-1} and 1078 cm^{-1} bands, are shown

in fig. 21. The orientations obtained from the bands 1368 cm^{-1}, 1352 cm^{-1} and 1303 cm^{-1} are generally relatively small, and thus the orientations from these bands were not measured in the case of HDPE.

(b) X-ray Measurement

The fact that molecular chains in the amorphous phase are orientated on the deformed state is shown in Fig. 22, in which scattering intensity measured from the amorphous halo of the x-ray scattering at the scattering angles 17.8° and 15.6° and at various azimuthal angles was plotted for sample of different elongations. One can see that the intensity curves measured at 17.8° are different from those measured at 15.6°. It is evident that the effect of amorphous orientation affects the shape of the intensity distribution of the amorphous halo, which is no longer symmetric in the deformed state. Therefore any procedure for correcting for the amorphous contribution to the intensity measured at the crystalline peak with the assumption of a symmetric amorphous halo will not be correct.

5. Stress-strain Relationship

The stress-strain data for the LDPE and HDPE samples are shown in Figs. 23 , 24 and 25. The stress shows a steep increase at elongation less than 10 %, then the stress increases almost

linearly with the elongation. The initial slopes are 6×10^5 g/cm^2 and 18×10^5 g/cm^2 for the Q-sample and SC-sample of LDPE, respectively, and 24×10^5 g/cm^2 for the HDPE sample, wnile the yield stresses are 0.7×10^5 g/cm^2 and 1.0×10^5 g/cm^2 for the Q-sample and SC-sample of LDPE and 1.2×10^5 g/cm^2 for the HDPE sample. The slope of the stress-strain curve after yield is approximately the same for these three samples.

DISCUSSION

1. Comparison of Crystalline Orientations Obtained by Infrared Dichroism and X-Ray Diffraction

The results of Figs. 13 and 14 seems to lend support for the assignment that the transition moment of 1894 cm^{-1} lies in the direction of the crystal a-axis. The evidence also indicates along with the results shown in Figs. 10, 11, that sample thickness does not affect the molecular orientation in these samples. Thus the disagreement between the crystalline orientations measured by polarized infrared and x-ray diffraction, as shown in Figs. 17 and 18, needs another explanation.

According to the theory developed in Chapter 4, corrections must be made for experimentally measured dichroic ratic for internal field and birefringence effects. In the case of polyethylene crystal, the internal field effect can be neglected for

the bands having transition moments along the crystallographic axes, assuming the internal field is only a local effect. Consequently, only the birefringence must be considered. Using the refractive indices of polyethylene crystal, which may represent the limit of the refractive indices of the deformed polyethylene, it is estimated that the correction for birefringence effect amounts to only 4 % change in dichroic ratio.

On the other hand, the crystal orientation functions from x-ray greatly depend on how the amorphous contribution was corrected, as illustrated by the results of Figs. 17 and 18. The difficulty involved in correcting the amorphous contribution is that one is not able to directly measure the amorphous contribution, rather one has to use the indirect correcting method as described. These indirect correcting method may not be valid because the amorphous phase is oriented in the deformed state, as shown by Fig. 22; thus even though the amorphous halo is symmetry in the undeformed state, it may not be so in the deformed state because of the orientation of molecular axes having different correlation distances are not equal.

From this discussion, it appears likely that the crystal orientation measured by polarized infrared is closer to the true value of crystal orientation. However, one must also bear in mind the possibility that the transition moments of these crystalline absorption bands may not be exact along the

axes of the unit cell, particularly for the bands 730 cm^{-1}, 1473 cm^{-1} and 1894 cm^{-1}. In this respect, it may be desirable to measure the orientation function of a nitric-acid-etched single crystal mat which contains only the crystal core, thus the amorphous contribution is negligible. Comparison of the crystal orientation of such a single crystal mat measured by polarized infrared andby x-ray may be able to determine experimentally the direction of the transition moments of the absorbands.

2. Morphology and Orientation

(a) Crystalline Orientation

The crystal orientation, particularly for a spherulite, is a composite process involving the deformation of the superstructure and various crystal reorientation processes occurring within the superstructure. The orientation, then, will certainly be affected by the morphology of the sample.

Figs. 15 and 16 show the crystal orientation vs. elongation. The HDPE sample has a shish-kebah or rod-like superstructure, as indicated by the light scattering pattern (Fig. 9). To describe the orientation of such a sample, the Kratky floating-rod model (41) may be used; however, in view of the high crystallinity of this sample, this model may not be sufficient to describe the crystal orientation under deformation because the

crystallites are not individually embeded in the amorphous matrix, rather they may form complicated aggregates. Thus we shall not elaborate further on the orientation of this sample in terms of various crystal reorientation processes, except pointing out the observations that, at low elongation (40 %), f_a and f_b are about equal, this seems to contrast the behavior of the spherulite, in which in general the orientation of b-axis is less than that of a-axis at low elongation.

The orientation of the LDPE samples, which have spherulitic superstructure as indicated by the light scattering patterns of Fig. 7 and 8 is shown in Fig. 15. The magnitude of f_c is always positive and those of f_a and f_b are negative. This indicates that, upon deformation, the c-axis tends to align along the stretching direction and the a-axis and b-axis incline to align perpendicularly to the stretching direction. f_a seems to be higher than f_b for both samples, and the orientation of the Q-sample of LDPE is higher than that SC-sample.

As we mentioned earlier, the crystal orientation is a composite process involving the deformation of the superstructure (spherulite) and various reorientation processes occurring within the superstructure. Yoon and Stein (42) have developed a theory in which they included three crystal reorientation processes along with an affine spherulite deformation. These three crystal reorientation processes are: (1) The interlamellar slip

involving twisting of the lamellae about the spherulite radial direction. (2) The chain tilting process in which the lamellae are tilted with respect to the crystal plane. (3) The rotation of b-axis toward the plane defined by the c-axis and the spherulite radius. The theory demonstrated that with proper choice of parameters associated with each process, the orientation behavior of the spherulite can be described by the theory very well (42).

Since the b-axis originally aligns along the radial direction of the spherulite, the deformation of spherulite without crystal reorientation processes occurring will result in a positive orientation function of b-axis. Thus the reorientation processes are to increase the orientation of c-axis in the direction of stretching and to bring the orientation of b-axis back to the direction perpendicular to the stretching direction. Based on these considerations, it is apparent that if the effects of the crystal reorientation processes are lower than that of the spherulite deformation, the magnitueds of f_c and f_a will be smaller, and that of f_b will be smaller, too, with negative sign or even becomes positive in the case that the spherulite deformation is the dominating process. Thus the influence of the morphology will be reflected in the magnitude of f_c , f_a and f_b .

One can see from Fig. 15 that the Q-sample has higher absolute values of f_c , f_a and f_b , this seems to be a good indication that the spherulite deformation has greater effect in the SC-sample than in the Q-sample. In other words, the crystals in the SC-sample are less able to reorient, and this results are in agreement with the results from dynamic x-ray studies (43,44), in which different orientation behaviors of the Q-sample and the SC-sample (designated as H-sample in Ref. 43 and 44) were demonstrated. The conclusion that the crystals are less able to reorient in the SC-sample is expected as a consequence of sample heat treatment, which results in a more perfect superstructure. Using these arguments, one may also conclude from the fact that f_a and f_b are about equal for the HDPE sample, as shown by Fig. 16, that the crystal orientation processes are the dominating factors.

Based on the above discussions, one may expect that values of the three parameters associated with the crystal reorientaion processes in the Yoon-Stein formulation may depend on the morphology.

(b) Amorphous Orientation

The orientation in the amorphous phase is highly conformation sensitive as shown by the results in Figs. 19-21. These observations have been qualitatively confirmed by a theory by

Flory and Abe (45), in which the strain-dichroism of various chain segments having different conformations in a single chain was calculated by employing the rotational isomeric statics. More recently, Petraccone et al (46) have calculated the amorphous orientations in spherulites, using a Monte Carlo computer simulation on a tetrahedral lattice. The Petraccone et al's formulation is believed to be more appropriate in explaining the present results, becsuse it takes into account the effect of crystallinity, initial lamellar separation, mole fraction of bonds in amorphous chains of each type and chain lengths of each type of amorphous chain. It should be pointed out that in these theories, the orientation of C-C bonds, rather than the orientation of chain axis or transition moment as in the case of experimental results, was calculated. The latter theory indicates that tie chains are the principal contributions to amorphous orientation, and the chain segments of a trans sequence conformation has the highest orientation.

The theory of Flory and Abe (45) has been applied for the study of the dichroism of the 2033 cm^{-1} band of crosslinked polyethylene at temperatures above the crystalline melting point (21). They arrived at the conclusion that this band may arise from a sequence of seven trans conformations. In the crss crystalline polyethylene, the absorption band occurs at 2016 cm^{-1} rather than at 2033 cm^{-1}. It is not certain about the reason of

the shift in the frequency at present, assuming these two bands arise from the same conformation.

Thus the high value of f_{2016} may be attributed to the fact that this band arise from chain segments containing a trans sequence. Moreover, it is estimated that a great fraction of the trans sequences will be tie chains if the tie chain's total length is equivalent to 100-150 C-C bonds (46). This is anotner factor contributing to the high value of f_{2016}, because the orientation of the trans sequences in the loop and cilia is smaller as compared with that in the tie chains.

Flory and Abe (45) have the opinion that the band 1078 cm^{-1} may preponderantly arise from gauche bonds because of the small transition moment from the vibration of the trans bonds. We feel that due to the high dichroism of the trans-sequence conformation, the contribution to f_{1078} from the trans bonds may be significant; this may also explain the fact that f_{1078} is much higher than f_{1352}, which is due to the orientation of the GG bonds. The fact that the trans bonds and the gauche bonds may have different transition moment at 1078 cm^{-1} means that f_{1078} can not be uniquely related to molecular orientation.

The value of f_{1303} is very small at all elongations and f_{1352} and f_{1368}, while higher than f_{1303}, are about equal. The 1352 cm^{-1} and 1368 cm^{-1} are strongly overlapped; this may be the reason that f_{1368} and f_{1352} are equal. The 1368 cm^{-1} and

1303 cm^{-1} bands are assigned to the same (GTG) chain conformation. Flory and Abe (45) have shown that, assuming the transition moment is in the direction perpendicular to the planes of two CH_2 groups on either side of the trans bond, the 1303 cm^{-1} band has almost zero dichroism with respect to the chain end-to-end vector despite a fairly high negative dichroism of the trans bond in the GTG conformation (Petraccone et al have also arrived at the similar negative dichroism for the GTG conformation (46)). Thus one may expect a very small f_{1303} in the deformed spherulite. This also suggests that the 1368 cm^{-1} has its transition moment in a direction different from that of the 1303 cm^{-1} band and results in a higher dichroism in the deformed spherulite.

The effect of morphology on the amorphous orientation is shown by the higher amorphous orientation of the SC-sample of LDPE than that of Q-sample, as shown in Figs. 19 and 20. The difference is most eminently shown by f_{2016} and f_{1078} of the two samples.

According to the theory developed by Petraccone et al (46), the orientation in the amorphous phase is related to the mole fraction of bonds of each amorphous type, i.e. tie chain, cilia and loop, etc., the chain length of each of these type, the cyrstallinity of the spherulite, and the initial interlamellar spacing. Practically, for the orientation of bonds in a trans sequence conformation, it increases as the number of C-C bonds

in the amorphous chain decreases.

The crystallinity of the SC-sample is slightly higher than that of Q-sample. However, since the difference is only 2 %, one does not expect that this will have great effect on the orientation. Similarly, the initial interlamellar spacings for the two samples are about the same as having been confirmed by small angle x-ray results.

The LDPE is highly branched, as evidenced by the high absorbance of the band 1375 cm^{-1}, which is assigned to the mode of CH_3 group (27) as shown in Fig. 2. The fact that the Q-sample and the SC-sample have almost the same crystallinity seems to indicate that branching is the factor limiting the crystallinity, because in the case of high density polyethylene, different thermal treatment generally results in significantly different crystallinities (for example, see the results in Ref. 47). This means that the sections of polyethylene chain which are branched form folded-chain crystals with difficulty, thus putting a limiting factor for increasing crystallinity by thermal treatment. Those sections of polyethylene chain which have sufficient length without branching will be capable of forming folded-chain crystal and give rise to the slight increase in crystallinity by thermal treatment. The tie chains formed by these chain sections are expected to be tauter in the SC-sample than in the Q-sample, because in the SC-sample, each chain may form more folds and the fold length

may be longer. A consequence of the taut chain is that the population of chain segments of trans sequence conformation will increase (46). The number of the tie chains, cilia and loops may not be very different in tne SC-sample and the Q-sample.

Thus it seems reasonable to conclude that the higher value of f_{2016} for the SC-sample is the result of the taut tie chain, while the relatively high value of f_{1078} may be attributed to the higher orientation of bands in the trans sequence conformation of the taut tie chains and the higher population of these chain segments.

The amorphous orientation of the HDPE sample shows the peculiar negative f_{2016} at elongation less than 30 %. As shown by Petraccone's theory,(46), the bonds in a trans sequence conformation in the tie chains and in the cilia will contribute to a positive f_{2016} while those in the loops will contribute to a negative f_{2016}. One may speculate that this is the reason for the negative f_{2016}.

3. Orientation and Stress-Strain Relationship

There has been reported a good correlation between molecular orientation and the stress-strain relationship of polyethylene (16). However, these samples probably had a special morphology due to the processing as shown by the orientation measured in the undeformed state.

Andrews and coworkers (15) have investigated the deformation of irradiated polyethylene single crystal, unirradiated and irradiated bulk polyethylene. They came to the conclusion that (1) the initial slope of the stress-strain curve before yield for samples of intermediate crystallinity depends on the crystallinity and the morphology, and for samples of low crystallinity (less than 30 %) and high crystallinity (higher than 65 %) it depends on the crystallinity; (2) there is a good correlation between the crystallinity and the yield stress, thus the yield point may represent the point of breakdown of areas of mechanical attachment between lamellar surfaces or the breakdown of interlamellar attachment; (3) beyond the yield point, the deformation is largely controlled by the rubber-like amorphous regions for samples of low crystallinity, and by lamellar deformation for those of high crystallinity.

For the three samples we have investigated, the stress, as shown in Figs. 23-25, rises steeply before the yield. Beyond the yield, the stress rises quite gradually with the elongation. On the other hand, the crystalline orientation and the amorphous orientation, except the peculiar f_{2016} of the HDPE sample, show monotonical increase with elongation and there is no change in orientation parallel to that in stress-strain, as one can see from Figs. 15, 16, 19-21.

The initial slopes of the stress-strain curves for these three

samples increase as the crystallinity of the sample increases. However, although the crystallinity of the SC-sample is only 2 % higher than that of the Q-sample, the value of initial slope for the SC-sample is about 3 times higher than that for the Q-sample. Thus the effect of morphology on the magnitude of the initial slope is clearly demonstrated. The yield stress shows similar dependency upon the crystallinity and the morphology; the increase in yield stress follows the order of increase in sample crystallinity and the increase in the yield stress of the SC-sample of 14 % over that of the Q-sample is far greater than can be expected from the consideration of increase in crystallinity alone.

The molecular orientation function expresses the average orientation of the molecular elements within the superstructure. Thus it is likely that, while the local molecular orientation is very high, the average molecular orientation is still quite low. This is to be expected, particularly in the equatorial regions of the spherulite where the lamellae have to come apart in response to the stress as has been experimentally observed (6). The amorphous orientation in the equatorial regions may be very high even at fairly low elongations. At further elongation, plastic deformation in the lamellae in this region will occur because the tie chains in the amorphous regions are highly extended. In the meridian regions, probably crystal plastic deformation

will occur along with the amorphous deformation as the deformation starts. According to Kajiyama and Takayanagi (9), deformation in the intermosaic regions is the dominant mechanism occurring in the lamellae at 30°C.

Thus the initial slope of the stress-strain curve may be related to amorphous orientation, particularly the orientation of the tie chains, and the deformation in the intermosaic regions. This may explain the fact that the initial slope of stress-strain curve of the Q-sample is much lower than that of the SC-sample, although the crystallinities of these two samples are about the same, because the orientation of the tie chains is higher and the crystal is less able to reorient in the SC-sample, as discussed previously. The fact that the crystal in the SC-sample has lower orientation also reflects the fact that the lamellae are more perfect and it is less easy for the intermosaic regions to slip past each other. Moreover, the HDPE has the highest initial slope of the stress-strain curve because this sample has the highest crystallinity, thus quite extensive plastic deformation in the lamellae may be expected in the range of deformation before yield.

The yield point may represent the point at which the lamellae are broken into smaller mosaic blocks, at least in the equatorial regions. Consequently, the yield stress depends not only on the crystallinity but also on the thermal treatment of the

sample. This may also be the reason that the slope of the stress-strain curve after the yield point is approximately the same for these three samples despite difference in crystallinity and thermal treatment.

One may conclude that, while there is no simple correlation between the stress-strain relationship and the average molecular orientation, the stress-strain curve of polyethylene can be explained satisfactorily in terms of the local orientation with consideration of the deformation mechanisms. In this connection, it may be fruitful to measure the local molecular orientation as a function of elongation, and to measure the sizes of mosaic blocks by low angle x-ray and to observe the sizes of the broken small crystalline blocks in the deformed state by the detachment replica technique, thus one can have solid experimental evidences to reveal the complicated structure-property relationship of spherulite.

REFERENCES

1. B. Wunderlich, Macromolecular Physics, Vol. 1, Academic Press, 1973, Chap. 4, pp. 380
2. P. H. Geil, J. Polymer Sci., A2 3813 (1964).
3. H. Kiho, A. Peterlin and P. H. Geil, J. Appl. Phys., 35 1599 (1964).
4. H. Kiho, A. Peterlin and P. H. Geil, J. Polymer Sci., B3 257 (1964).
5. E. H. Andrews and I. G. Voigt-Martin, Proc. Roy. Soc., A 327 251 (1972).
6. I. L. Hay and A. Keller, Kolloid Z. Z. Polymere, 204 43 (1965).
7. P. Predecki and A. W. Thornton, J. Appl. Phys., 41 4342 (1970).
8. T. Kajiyama, T. Okada, A. Sakoda and M. Takayanagi, J. Macromol. Sci.-Phys. B7 577 (1973).
9. T. Kajiyama and M. Takayanagi, J. Macromol. Sci.-Phys., B10 (1) 131 (1974).
10. I. M. Ward, Polymer, 15 379 (1974).
11. Z. H. Stachurski and I. M. Ward, J. Polym. Sci., A2, 6 1817 (1968).
12. Z. H. Stachurski and I. M. Ward, J. Macromol. Sci.-Phys., B3 445 (1969).
13. I. M. Ward, Phys. Bull. 21 71 (1970).

14. R. S. Stein, R. S. Finkelstein, D. Y. Yoon and C. Chang, J. Polym. Sci., Symposium No. 46, 15 (1974).

15. E. H. Andrews, Pure and Appl. Chem. 31 91 (1972).

16. S. Onogi and T. Asada, Progr. in Polymer Science, Japan, Vol. 2, pp. 261

17. V. B. Gupta, A. Keller and I. M. Ward, J. Macromol. Sci., B4 453 (1970).

18. T. Okada and L. Mandelken, J. Polym. Sci., A-2, 5 239 (1967).

19. R. S. Stein, P. Erhardt, J. J. Van Aartsen, S. Clough and M. Rhodes, J. Polym. Sci., 13 1 (1966).

20. B. E. Read, D. A. Hughes, D. C. Barues and F. W. M. Drury, Polymer, 13 485 (1972).

21. B. E. Read and D. A. Hughes, Polymer, 13 495 (1972).

22. W. Glenz and A. Peterlin, J. Macromol. Sci., B3 473 (1971).

23. D. E. Whitenhafer and J. L. Koenig, Makromol. Chem., 99 193 (1966).

24. C. Chang, Ph. D. Thesis, University of Massachusetts, Amherst, Mass. , 1973.

25. A. Cunningham, G. R. Davies and I. M. Ward, Polymer, 15 743 (1974).

26. B. E. Read and R. S. Stein, Macromolecules, 1 116 (1968).

27. S. Krimm, Fortschr. Hachpolymer-Forsch., 2 52 (1960), Advances in Polymer Science.

28. J. R. Nielsen and A. H. Woollett, J. Chem. Phys., 26 1391 (1957).

29. J. R. Nielsen, J. Polym. Sci., C, 7 19 (1964).

30. R. G. Snyder, J. Chem. Phys., 47 1316 (1967).

31. J. R. Nielsen and R. F. Holland, J. Mol. Spectrosc., 6 394 (1961).

32. M. Shen, W. N. Hansen and P. C. Romo, J. Chem. Phys., 51 425 (1969).

33. R. S. Stein, J. Chem. Phys., 23 734 (1954).

34. R. S. Stein, J. Polym. Sci., 31 327 (1958).

35. R. D. B. Fraser, J. Chem. Phys., 21 1511 (1953).

36. Z. W. Wilchinsky, Advan. X-Ray Anal., 6 231 (1962).

37. R. S. Stein, P. Erhardt, J. J. Van Aartsen, S. Clough and M. Rhodes, J. Polym. Sci., Pt. C, 13 1 (1966).

38. M. B. Rhodes and R. S. Stein, J. Polym. Sci., A2, 7 1539 (1969).

39. J. J. Van Aartsen and R. S. Stein, J. Polym. Sci., A2, 9 295 (1971).

40. R. Samuels, J. Polym. Sci., Pt. C, 13 37 (1966).

41. O. Kratky, Kolloid Z., 84 149 (1938).

42. D. Y. Yoon and R. S. Stein, J. Polym. Sci., Polym. Phys. Ed., 12 2019 (1974).

43. A. Tanaka, Ph.D. Thssis, University of Massachusetts, (Amherst, 1971).

44. R. S. Stein, R. S. Finkelstein, D. Y. Yoon and C. Chang, J. Polym. Sci., Symposium No 46, 15 (1974).

45. P. J. Flory and Y. Abe, Macromolecules, 2 335 (1969).

46. V. Petraccone, I. C. Sanchez and R. S. Stein,

47. W. Glenz and A. Peterlin, J. Macromol. Sci., (Phys.) B4 473 (1970).

TABLE I CHARACTERIZATION OF SAMPLES

	Thermal Treatment	Density (g/cm^3)	Crystal-linity (%)	Spherulite Size (μm)	Long * Period (A^o)	Lamellar** Thickness (A^o)
M8011	Slowly Cooled from 165°C	0.923	48	5.4	132	71
	Quenched in Dry-ice Methanol Bath	0.920	46	2.5	116	72
MPE220/27007	Quenched in Dry-ice Methanol Bath	0.931	53	—	—	—

* Slit desmeared and Lorentz corrected.

** Tsvankin corrected lamellar thickness.

TABLE II ASSIGNMENTS OF IR BANDS OF POLYETHYLENE

Frequency (CM^{-1})	Phase	Assignments
2016	A,C(26)	Combination between the Raman active twisting mode and IR active rocking modes of CH_2 (27-28). The crystalline component has a transition moment parallel to C axis (27,28). The amorphous component may be due to extended trans sequences (21,27) and the transition moment is parallel to the chain axis (28).
1894	C(18,26)	Combination between the Raman active and the IR active rocking modes of CH_2 (27-29). The band is polarized perpendicular to C axis (28). It has been suggested more recently that the transition moment is along a-axis (26,27,29).
1368	A	CH_2 wagging in GTG or GTG' conformation. The transition moment direction is uncertain from the assignment (30).
1352	A	CH_2 wagging mode in the gauche conformation (27) or in the GG conformation (29). The transition moment is perpendicular to the plane of CH_2 group.

(Continued)

TABLE II ASSIGNMENTS OF IR BANDS OF POLYETHYLENE (CONTINUED)

Frequency (CM^{-1})	Phase	Assignments
1303	A	CH_2 twisting mode in the gauche conformation (27) or CH_2 antisymmetric wagging in GTG or GTG' with the trans bond as center (30). The transition moment is parallel to the chain axis.
1078	A	Stretching mode of skeletal C-C bonds of both trans and gauche conformations (27). The transition moment direction is perpendicular to the chain axis (31).
1473	C	CH_2 in phase bending mode (27,32). The transition moment direction is parallel to a axis.
1176	C	CH_2 wagging mode (27,31). The transition moment direction is parallel to c axis.
731	C	CH_2 in phase rocking mode (27,32). The transition moment is along a axis.

CAPTIONS TO THE FIGURES

1. Schematic diagram of the infrared spectrophotometer. The sample is placed at the position of P-3 or P-2 and the polarizer is placed at P-4 for the single-polarizer technique. The sample is placed at P-1 and the two polarizers are placed at P-2 and P-3, respectively for the differential technique.
2. Infrared spectrum of low density polyethylene. The sample thickness used, and the base lines, are indicated for the different spectral regions.
3. Infrared spectra for oriented quenched polyethylene films in various spectral regions. Elongation ratios and sample thickness are indicated.
4. Differential spectra for an oriented polyethylene film stretched by 40 % in various spectral regions. The ordinate expresses the ratio of the transmitted intensity with the beam polarized parallel ($I_{\parallel}$) and perpendicular ($I_{\perp}$) to the stretching direction. The dotted line represents the base line.
5. The intensity of x-ray diffraction of a quenched polyethylene film as a function of scattering angle (2θ). The amorphous halo is assumed to be symmetric with respect to the peak maximum (I_o). I_1 and I_3 as well as I_2 and I_4 are intensity on opposite side of the amorphous peak maximum but at equal distances from it.

6. Stress relaxation of polyethylene samples stretched at a rate of 3 % per min.
7. H_v light scattering patterns of LDPE-Q sample.
   (a) Undeformed sample. (b) Sample stretched 40 %.
   P is the direction of polarizer and A the direction of analyzer. S is the stretching direction.
8. H_v light scattering pattern of LDPE-SC sample.
   (a) Undeformed sample. (b) Sample stretched 40 %.
   P is the direction of polarizer and A the direction of analyzer. S is the stretching direction.
9. H_v light scattering pattern of HDPE sample.
   (a) Undeformed sample. (b) Sample stretched 20 %.
   P is the direction of polarizer and A the direction of analyzer. S is the stretching direction.
10. Dichroic ratio of LDPE-Q samples of various thickness as a function of elongation ratio. The absorption band is 2016cm^{-1}.
11. Dichroic ratio of LDPE-SC samples of various thickness as a function of elongation ratio. The absorption band is 2016cm^{-1}.
12. Orientation function of LDPE-Q samples of various thickness as a function of elongation ratio. The absorption band is 1894 cm^{-1}.
13. Orientation function of LDPE-Q samples as a function of elongation ratio. The absorption bands used are 730 cm^{-1}, 1473 cm^{-1} and 1894 cm^{-1}. The absorption coefficients were not corrected for bandoverlapping.

14. Orientation function of LDPE-Q samples as a function of elongation ratio. The absorption bands used are 730 cm^{-1}, 1473 cm^{-1} and 1894 cm^{-1}. The absorption coefficients of these bands 730 cm^{-1} and 1473 cm^{-1} were corrected for band overlapping as described.

15. Crystalline orientation functions of LDPE-Q and LDPE-SC samples measured by infrared dichroism technique. The 1176 cm^{-1} band was used to determine f_c and the 1894 cm^{-1} band to determine f_a. Solid points represent LDPE-SC and open points represent LDPE-Q.

16. Crsystlline orientation functions of HDPE samples measured by infrared dichroism technique. The 1176 cm^{-1} was used to determine f_c and the 1894 cm^{-1} to determine f_a.

17. Orientation function of c-axis of LDPE-Q and LDPE-SC samples measured by x-ray diffraction plotted against that obtained by infrared dichroism. Solid points represent LDPE-SC and open points represent LDPE-Q. f_c^{I}, f_c^{II}, and f_c^{III} indicate that f_c is obtained by x-ray diffraction using method (1), (2) and (3) to correct the amorphous contribution to the scattering intensity as described. The straight line represents the line $f_c = f_c$ (1176 cm^{-1}).

18. Orientation function of a-axis of LDPE-Q and LDPE-SC samples measured by x-ray diffraction plotted against that obtained by infrared dichroism. Solid points represent LDPE-SC and open points represent LDPE-Q. f_a^{I}, f_a^{II} and f_a^{III} indicate that f_a is obtained by x-ray diffraction using method (1),

(2) and (3) to correct the amorphous contribution to the scattering intensity as described. The straight line represents the line $f_a = f_a$ (1894).

19. Amorphous orientation of LDPE-Q samples obtained by infrared dichroism technique as a function of elongation ratio.
20. Amorphous orientation of LDPE-SC samples obtained by infrared dichroism technique as a function of elongation ratio.
21. Amorphous orientation of HDPE samples obtained by infrared dichroism technique as a function of elongation ratio.
22. The intensity of x-ray scattering from the amorphous regions of LDPE-Q samples as a function of azimuthal angle at varoous elongation ratios. The intensity was measured at two scattering angles (2θ): 17.8° and 15.6°. The intensity is normalized to same sample thickness.
23. True stress of LDPE-Q sample as a function of elongation ratio.
24. True stress of LDPE-SC sample as a function of elongation ratio.
25. True stress of HDPE samples as a function of elongation ratio.

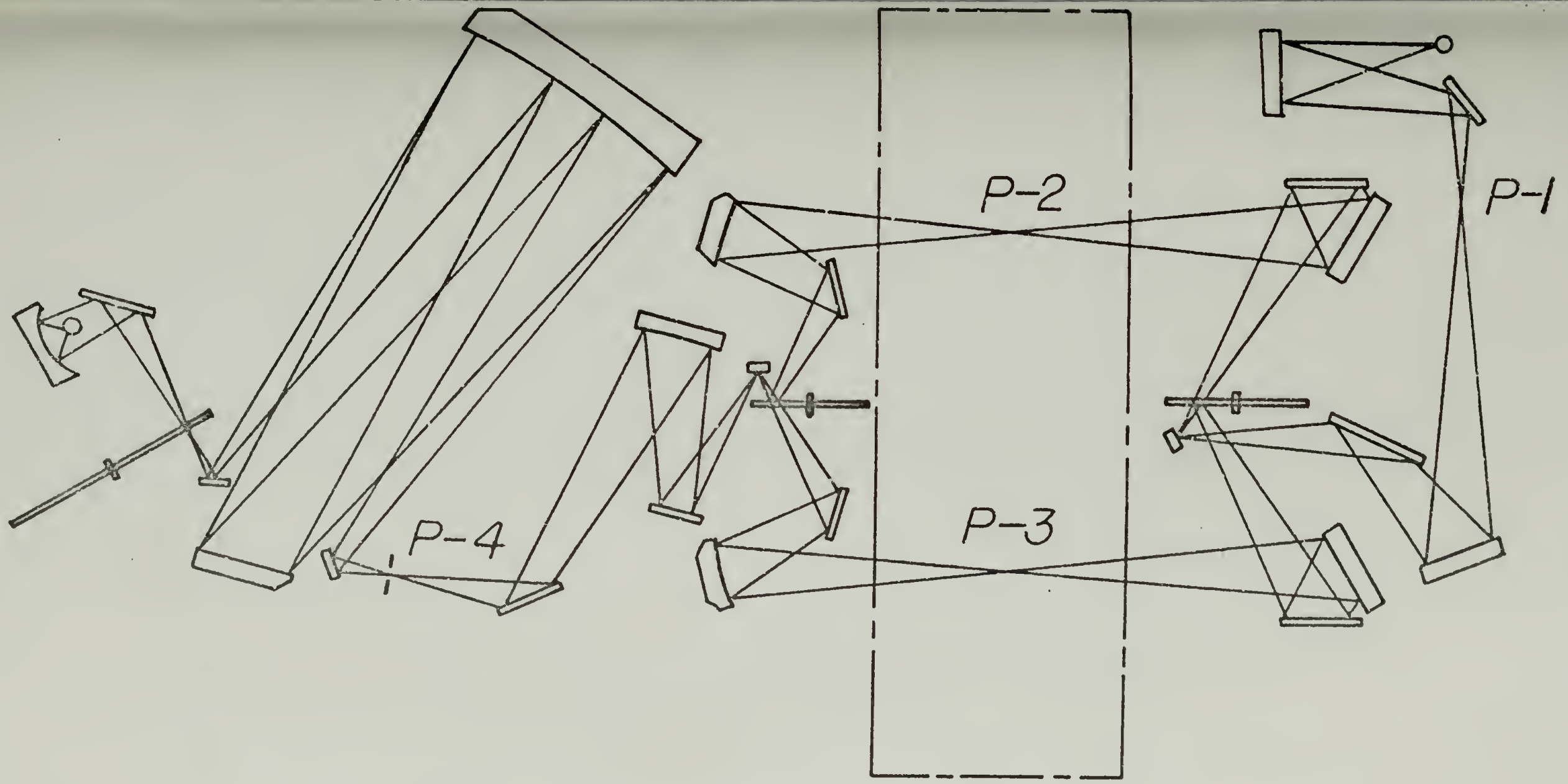

1 CONVENTIONAL METHOD SAMPLE AT P-2 POLARIZER AT P-4

2 DIFFERENTIAL METHOD AT P-2 AND P-3 SAMPLE AT P-1 AND POLARIZERS

Fig. 1

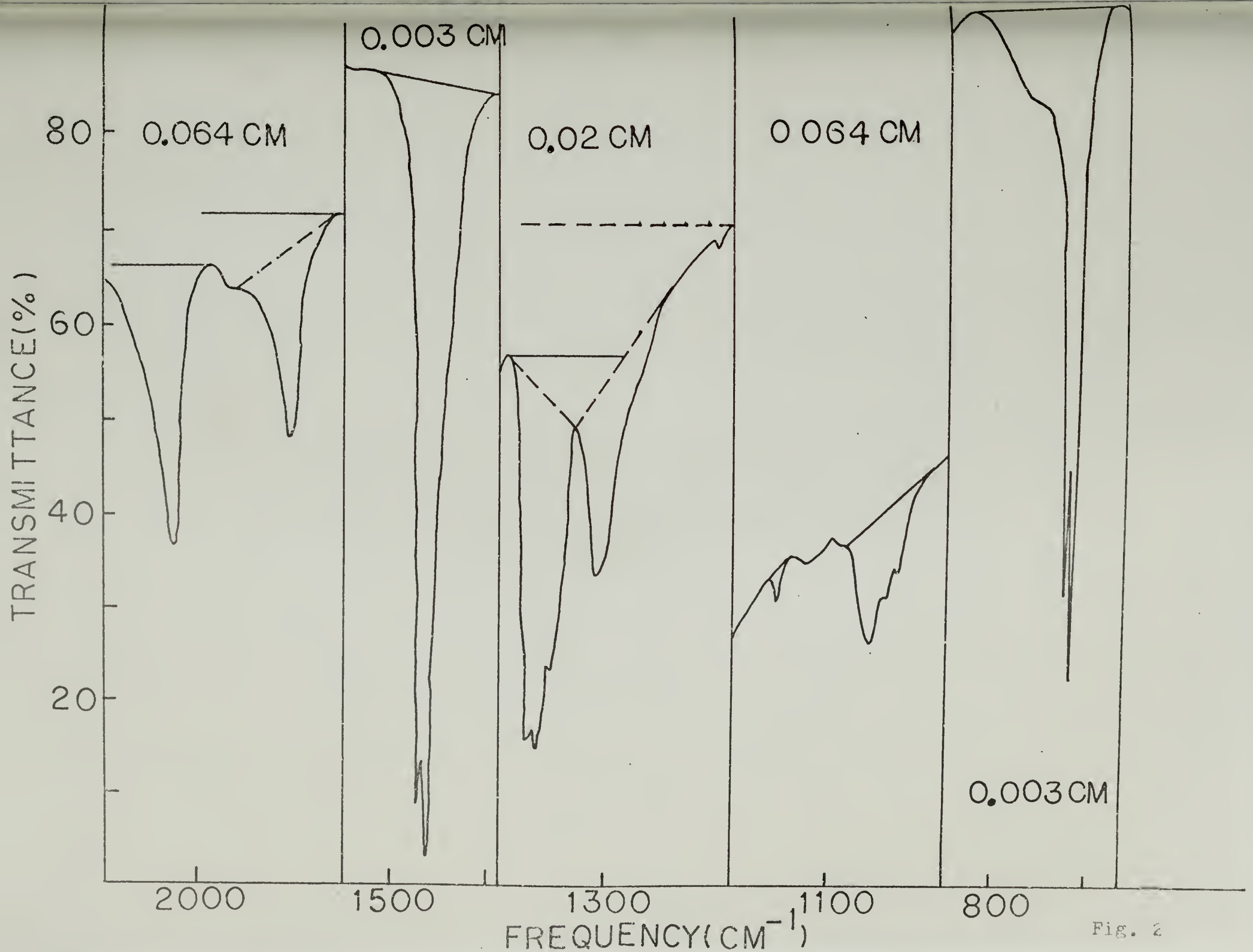
0.003 CM
0.064 CM
0.02 CM
0 064 CM
80
60
40
20
TRANSMITTANCE(%)
0.003 CM
2000
1500
1300
1100
800
FREQUENCY(CM^{-1})

Fig. 2

INFRARED SPECTRUM OF ORIENTED LOW DENSITY POLYETHYLENE

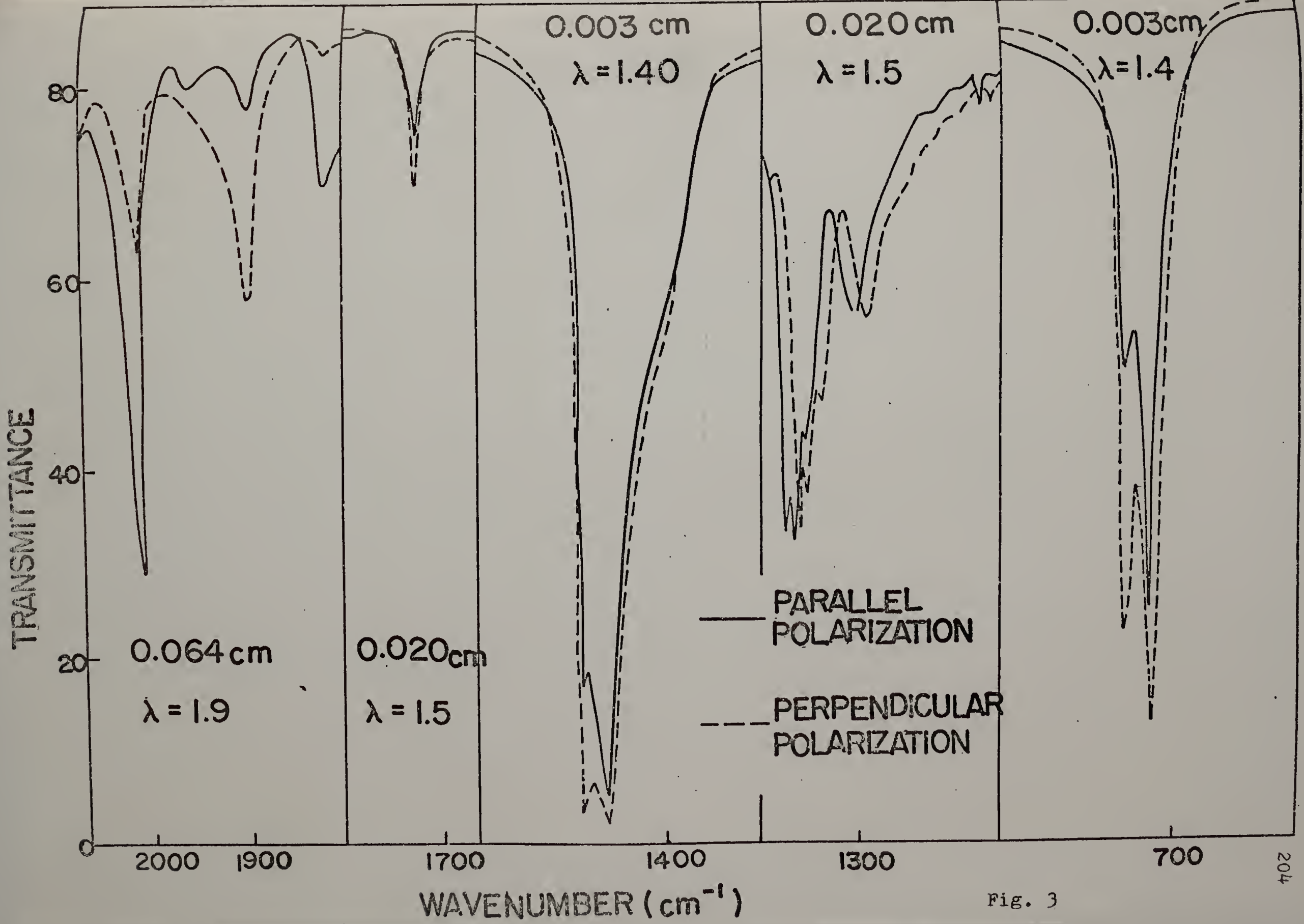

Fig. 3

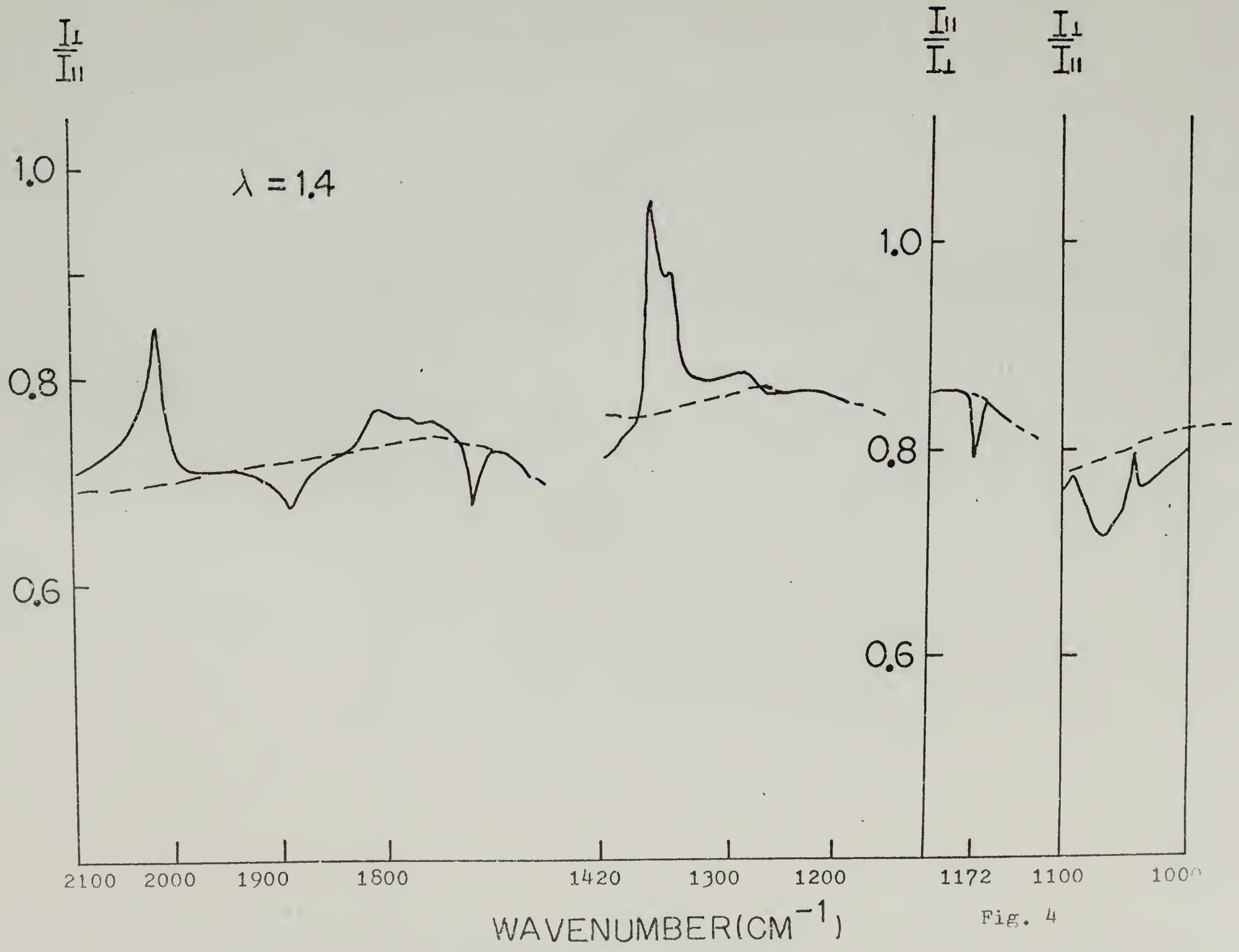
$\frac{I_\perp}{I_\parallel}$
$\frac{I_\parallel}{I_\perp}$
$\frac{I_\perp}{I_\parallel}$
λ = 1.4
1.0
0.8
0.6
1.0
0.8
0.6
2100
2000
1900
1800
1420
1300
1200
1172
1100
1000
WAVENUMBER(CM^{-1})

Fig. 4

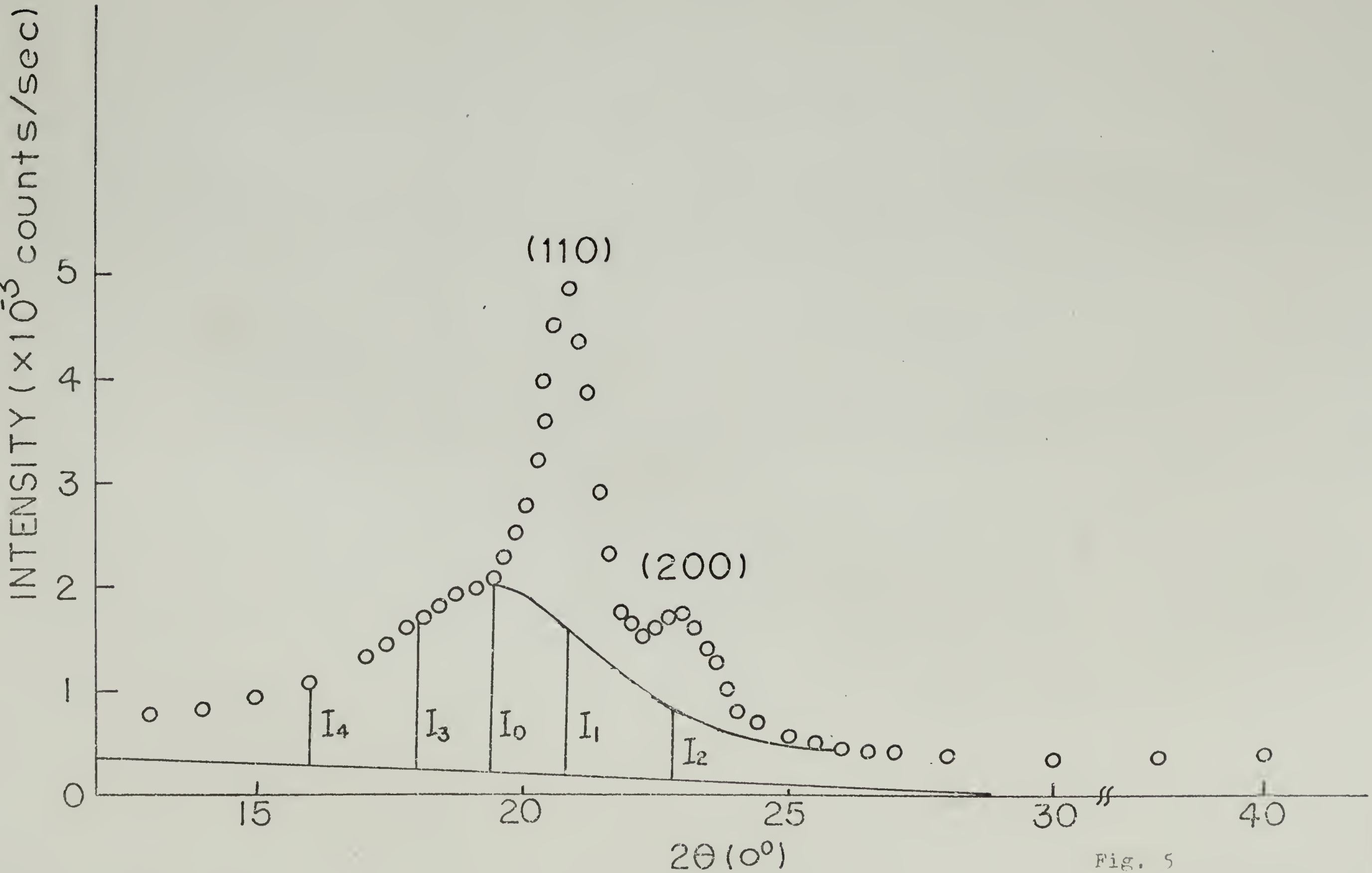
INTENSITY (x10⁻³ counts/sec)
0
1
2
3
4
5
(110)
(200)
I4
I3
I0
I1
I2
15
20
25
30
40
2θ(0°)

Fig. 5

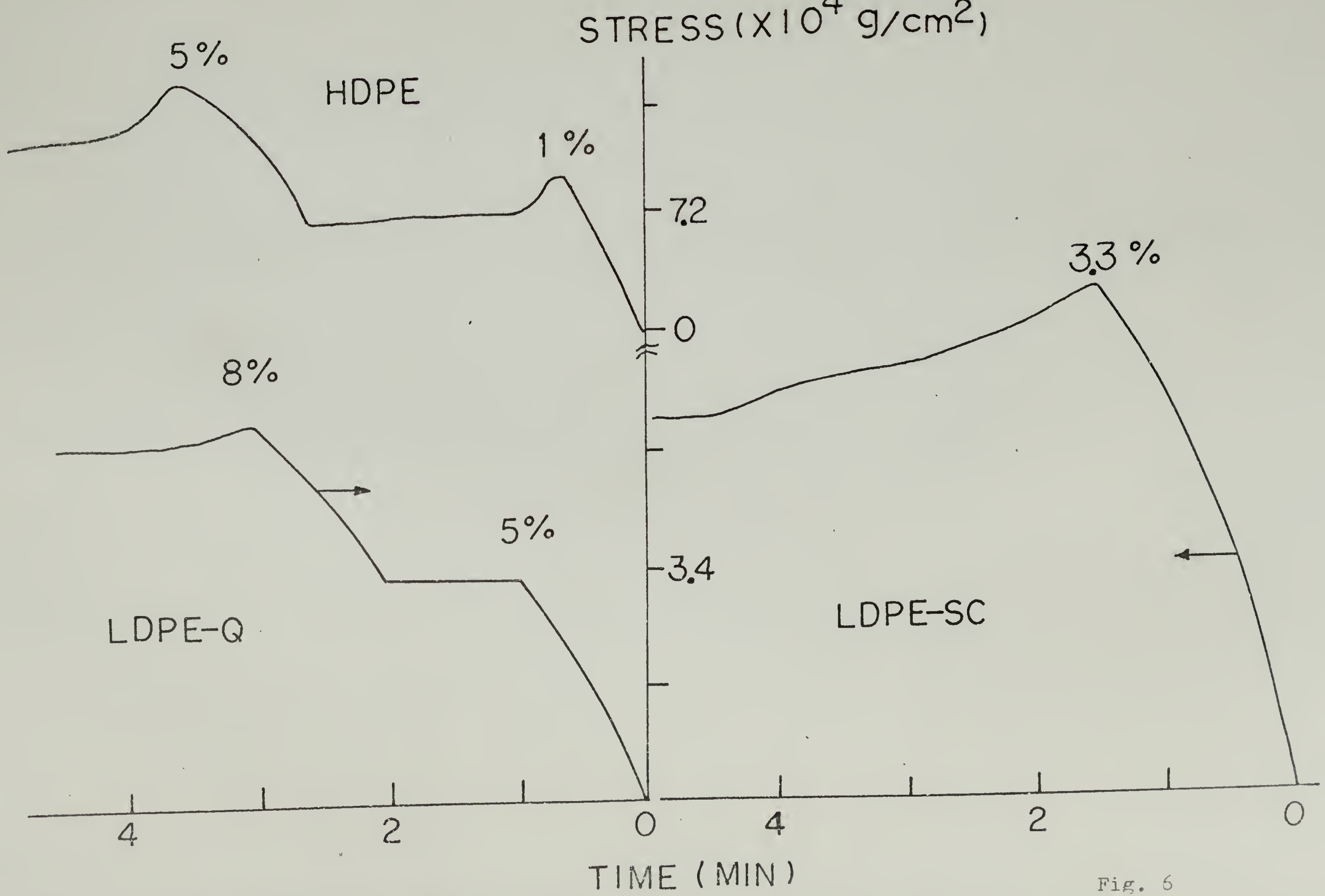
STRESS (X 10⁻⁴ g/cm²)
5%
HDPE
1%
7.2
0
3.3%
8%
5%
3.4
LDPE-Q
LDPE-SC
4
2
0
4
2
0
TIME (MIN)

Fig. 6

LDPEM8011 (Q)

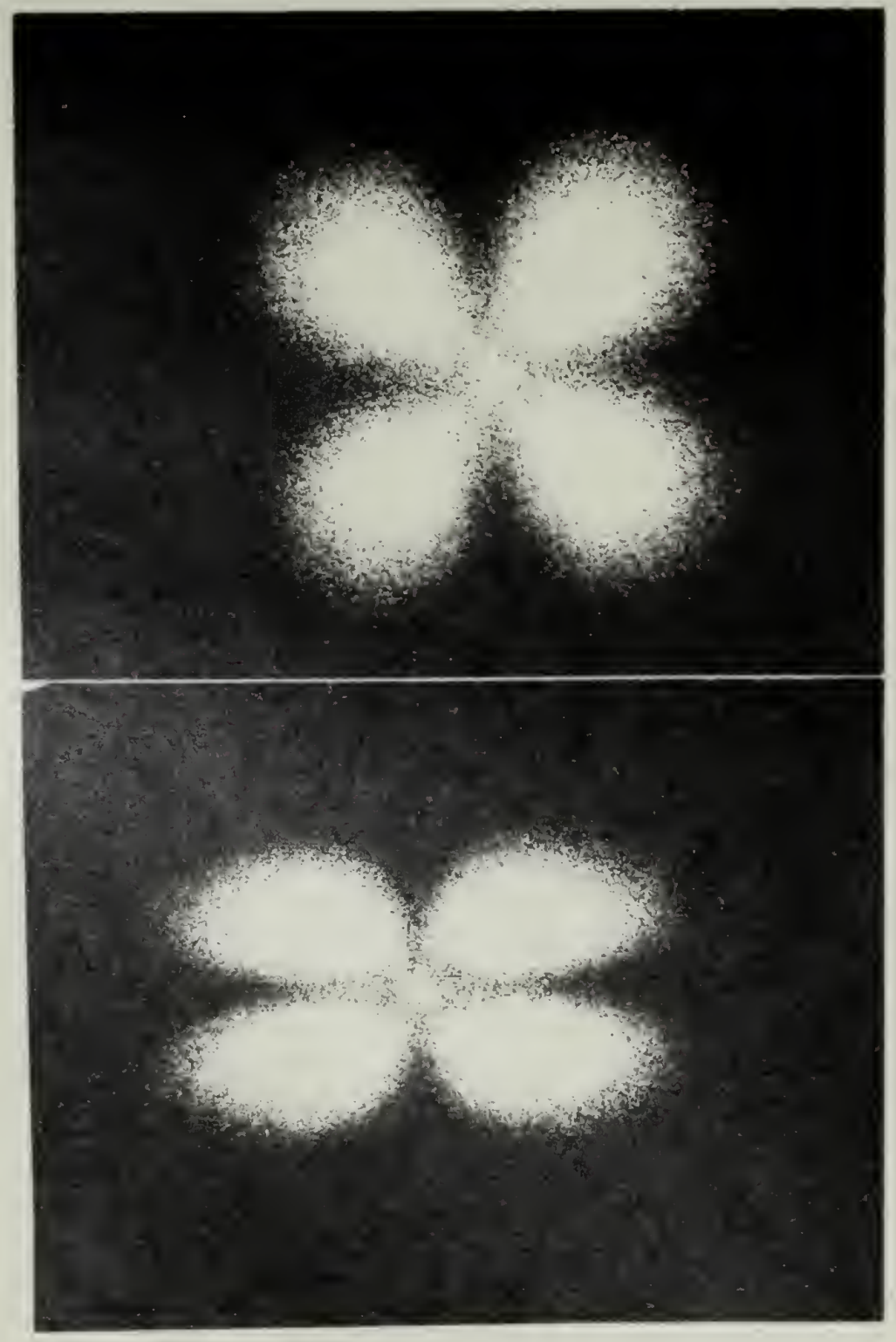

(a)

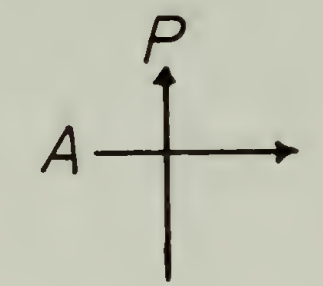

λ=1.0

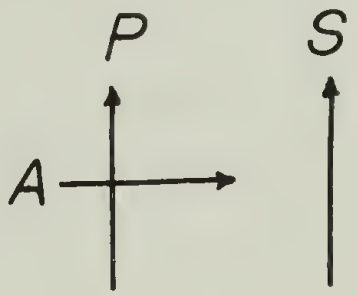

λ=1.4

(b)

Fig. 7

LDPEM8011(SC)

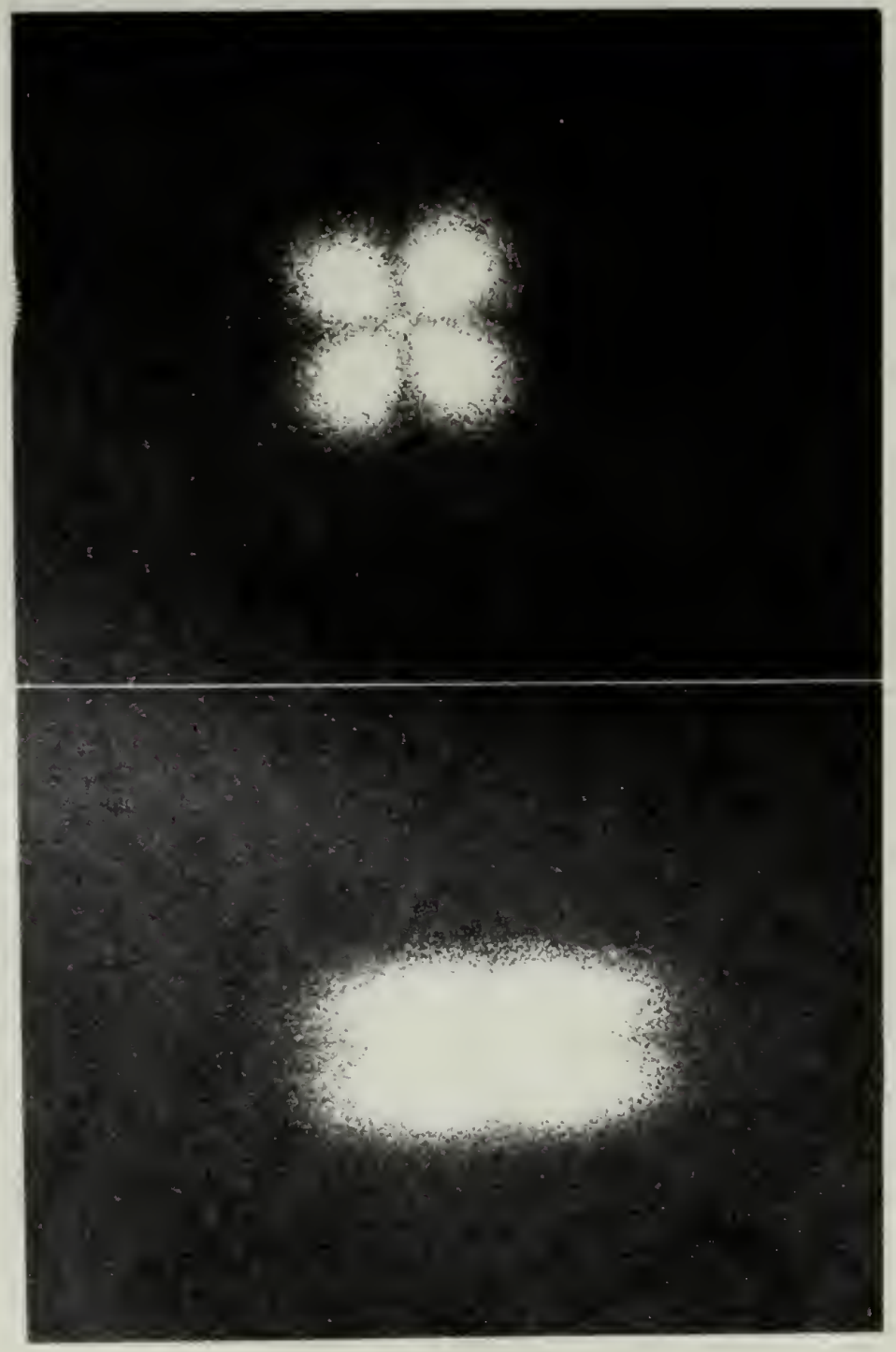

(a)

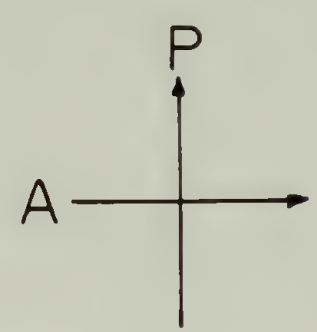

$\lambda = 1.0$

(b)

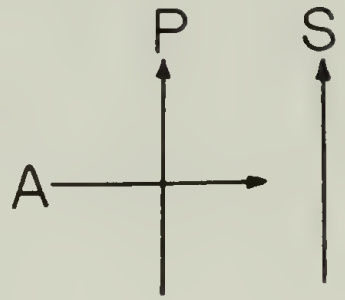

$\lambda = 1.4$

Fig. 8

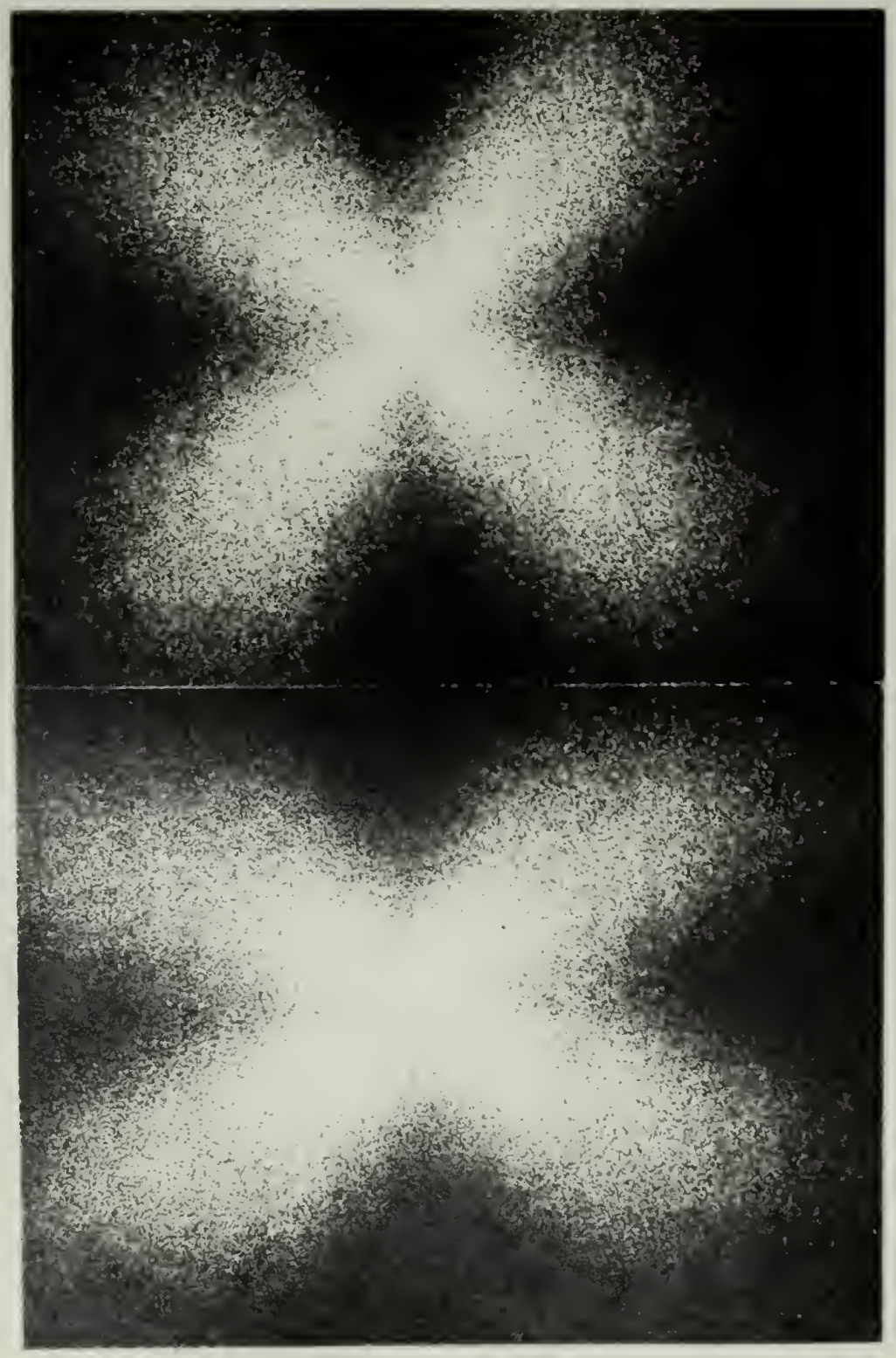

HDPE220/27007

(a)

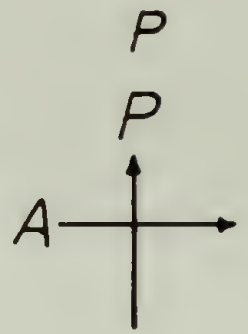

λ=1.0

(b)

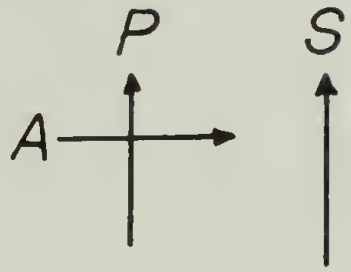

λ=1.2

Fig. 9

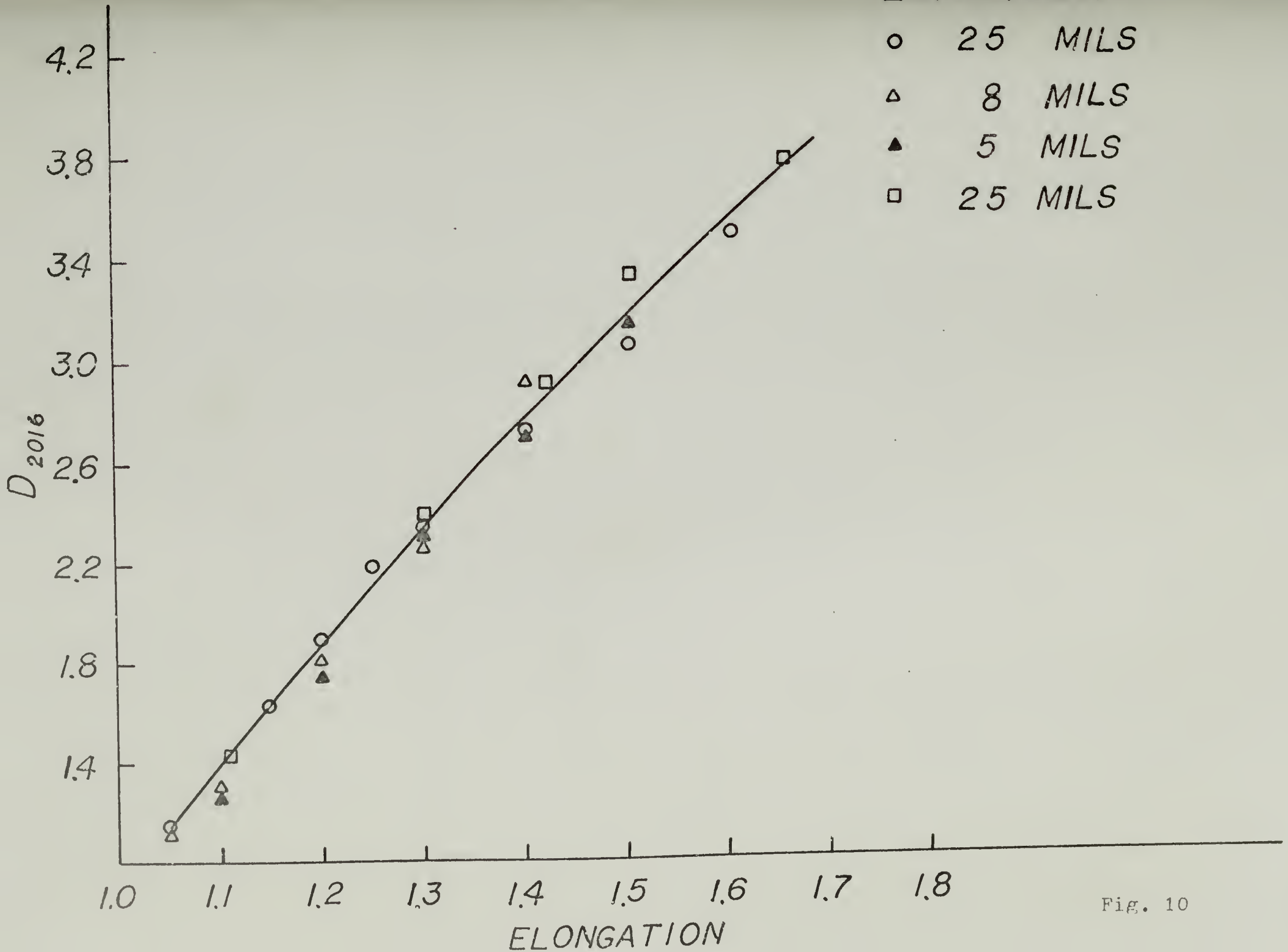
LDPEM 8011
25 MILS
8 MILS
5 MILS
25 MILS
4.2
3.8
3.4
3.0
2.6
2.2
1.8
1.4
D 2016
1.0
1.1
1.2
1.3
1.4
1.5
1.6
1.7
1.8
ELONGATION

Fig. 10

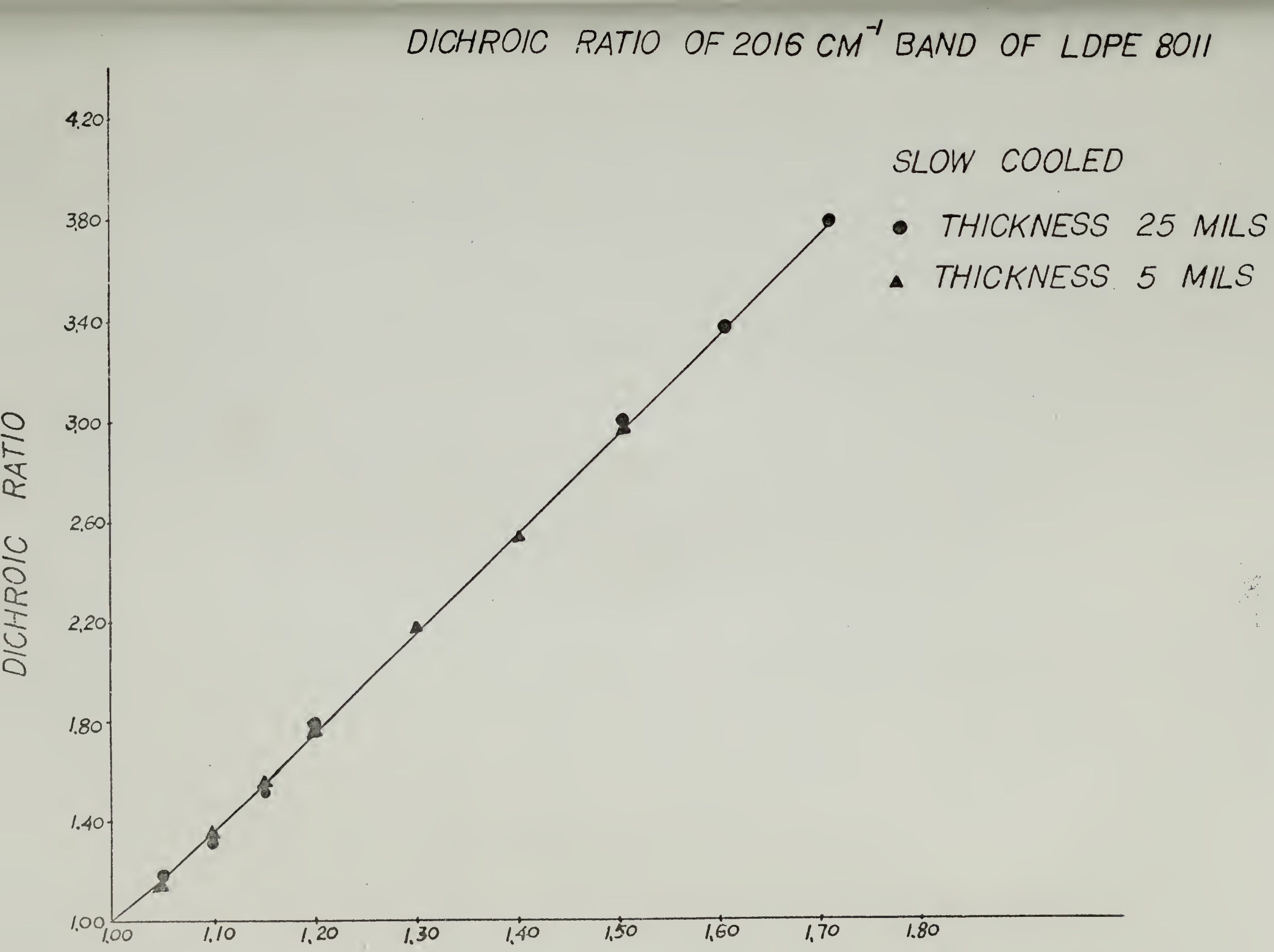
DICHROIC RATIO OF 2016 CM⁻¹ BAND OF LDPE 8011
SLOW COOLED
THICKNESS 25 MILS
THICKNESS 5 MILS
DICHROIC RATIO
4.20
3.80
3.40
3.00
2.60
2.20
1.80
1.40
1.00
1.00
1.10
1.20
1.30
1.40
1.50
1.60
1.70
1.80

Fig. 11

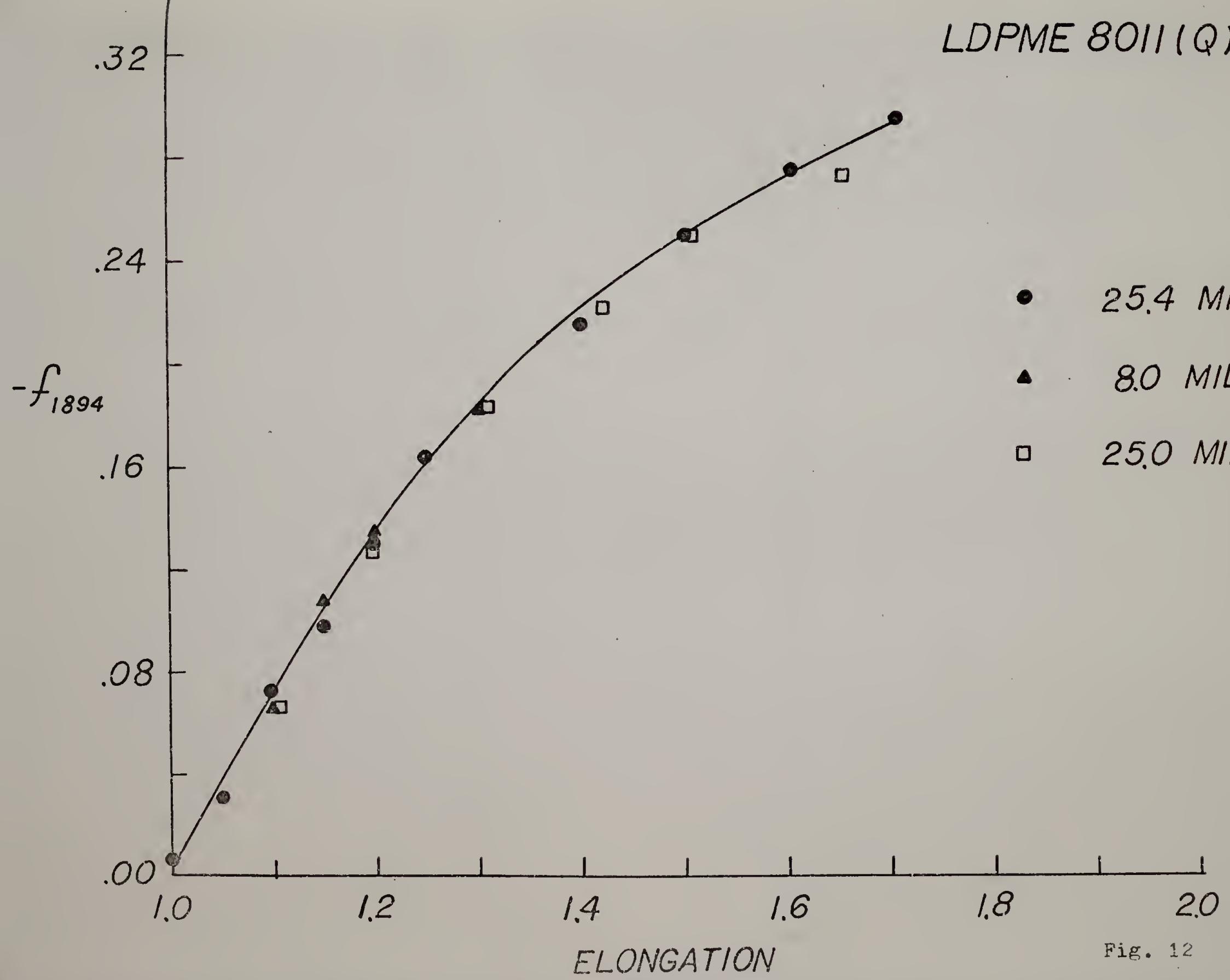
LDPME 8011(Q)
25.4 MILS
8.0 MILS
25.0 MILS
$-f_{1894}$
.32
.24
.16
.08
.00
1.0
1.2
1.4
1.6
1.8
2.0
ELONGATION

Fig. 12

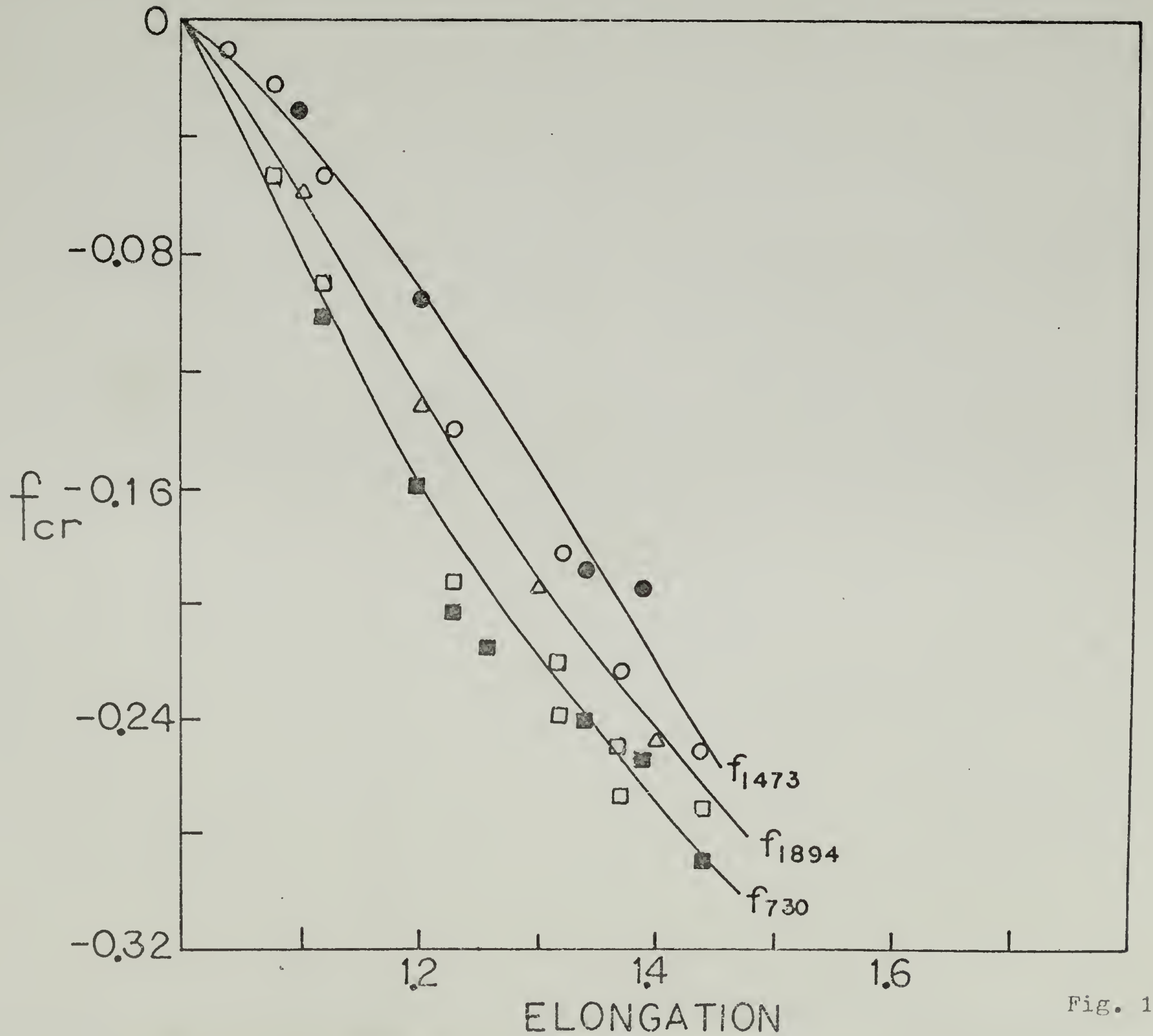

Fig. 13

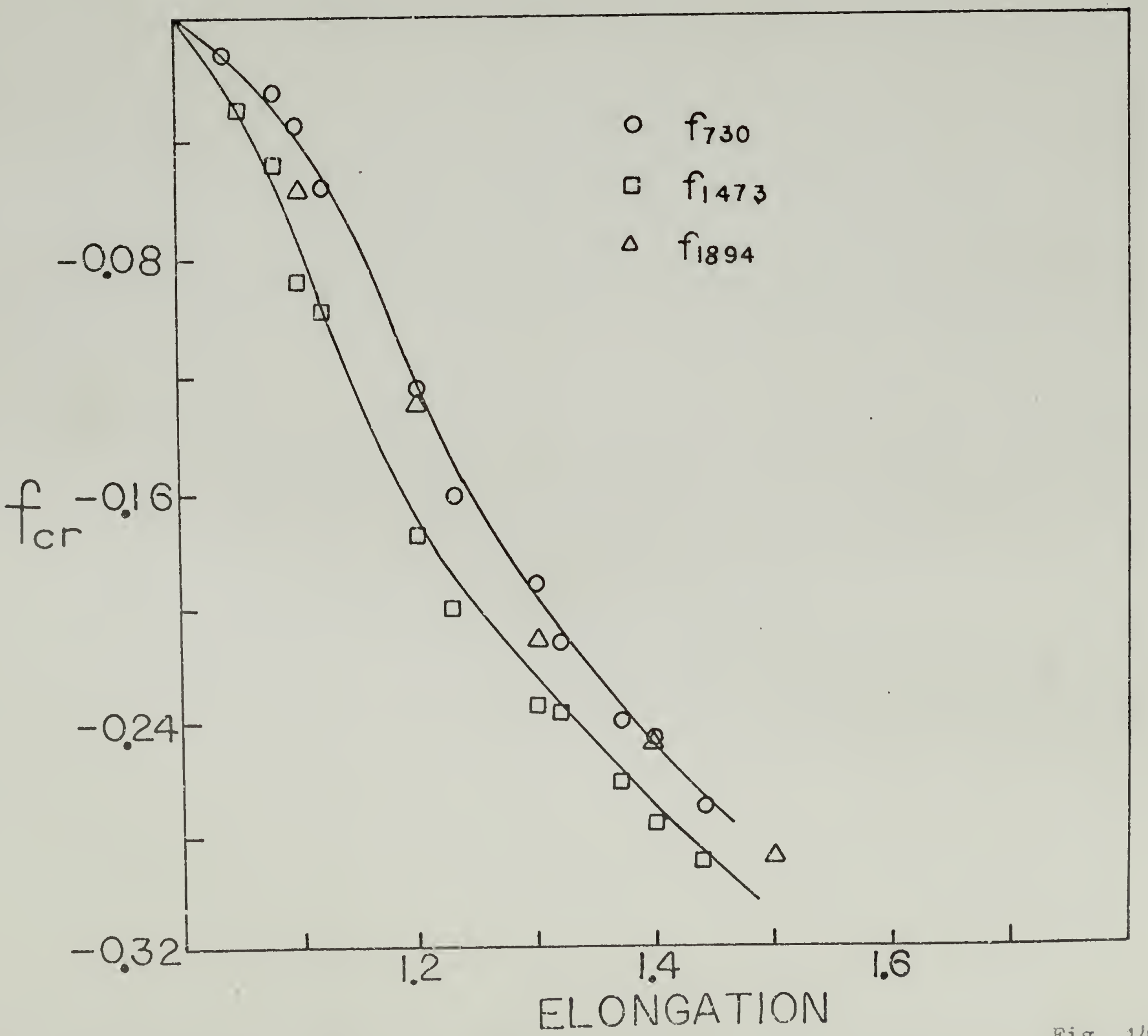

Fig. 14

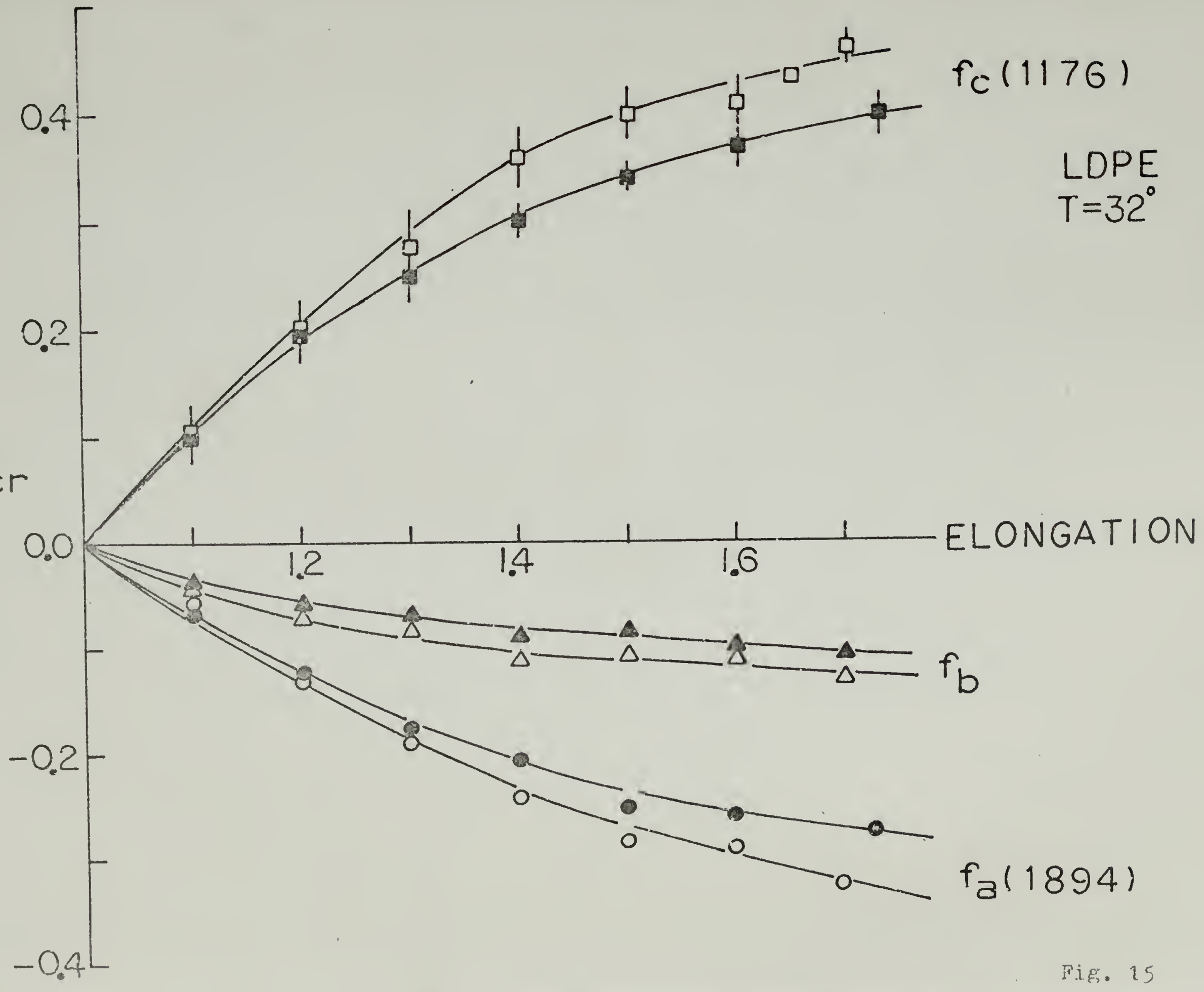
0.4
0.2
0.0
-0.2
-0.4
f_{cr}
1.2
1.4
1.6
ELONGATION
f_c(1176)
LDPE
T=32°
f_b
f_a(1894)

Fig. 15

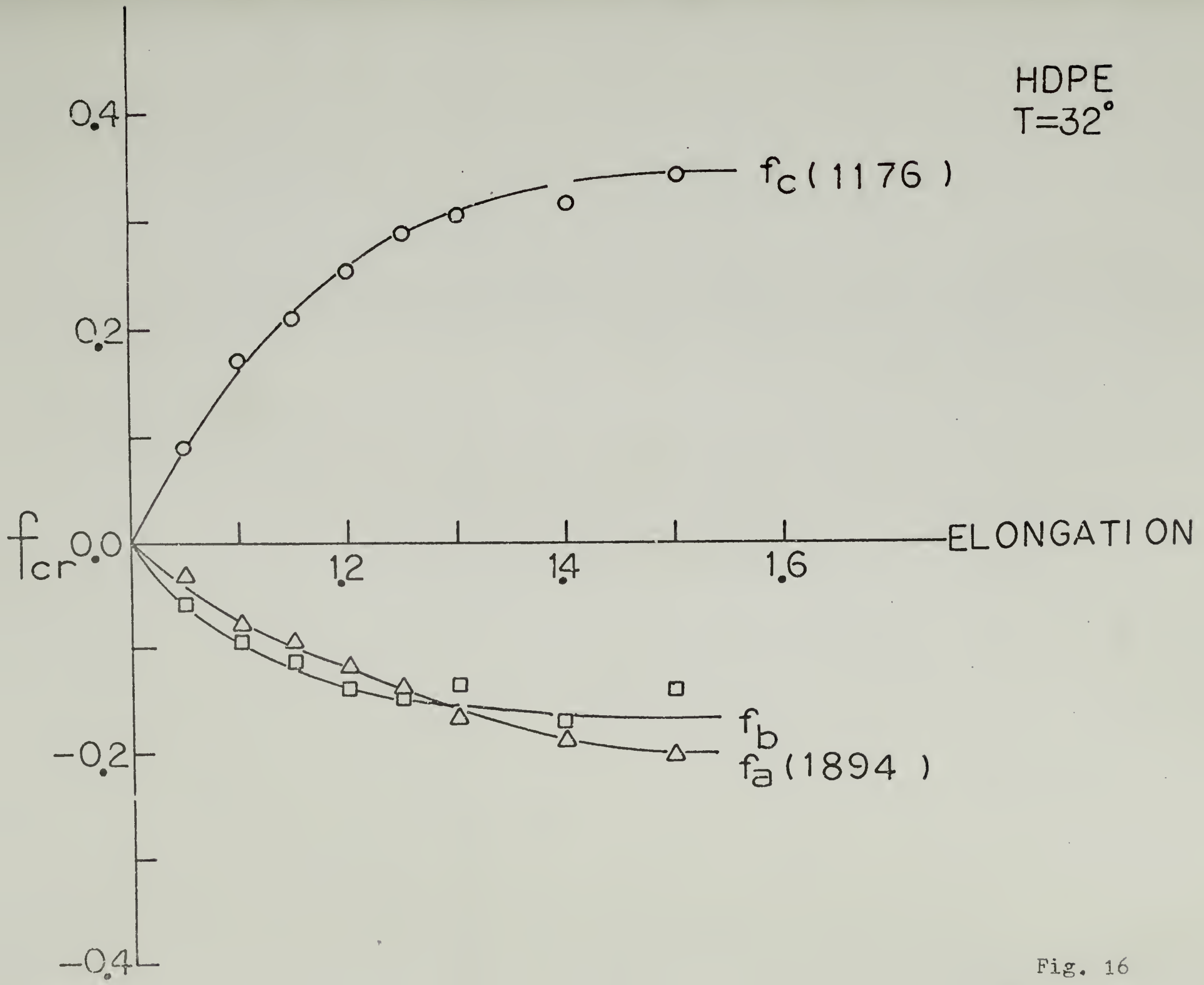
HDPE
T=32°
0.4
0.2
0.0
-0.2
-0.4
f_{cr}
1.2
1.4
1.6
ELONGATION
f_c (1176)
f_b
f_a (1894)

Fig. 16

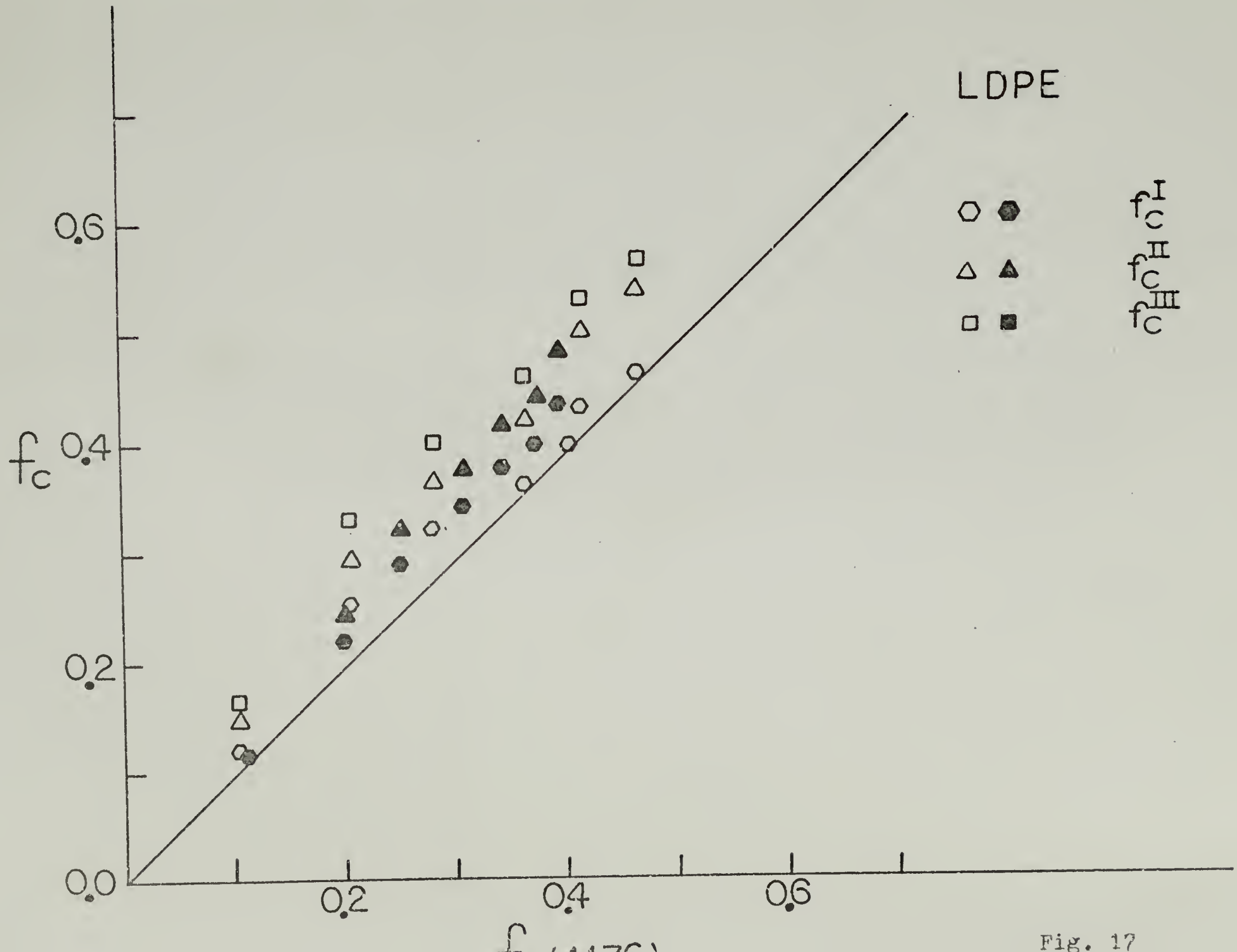

Fig. 17

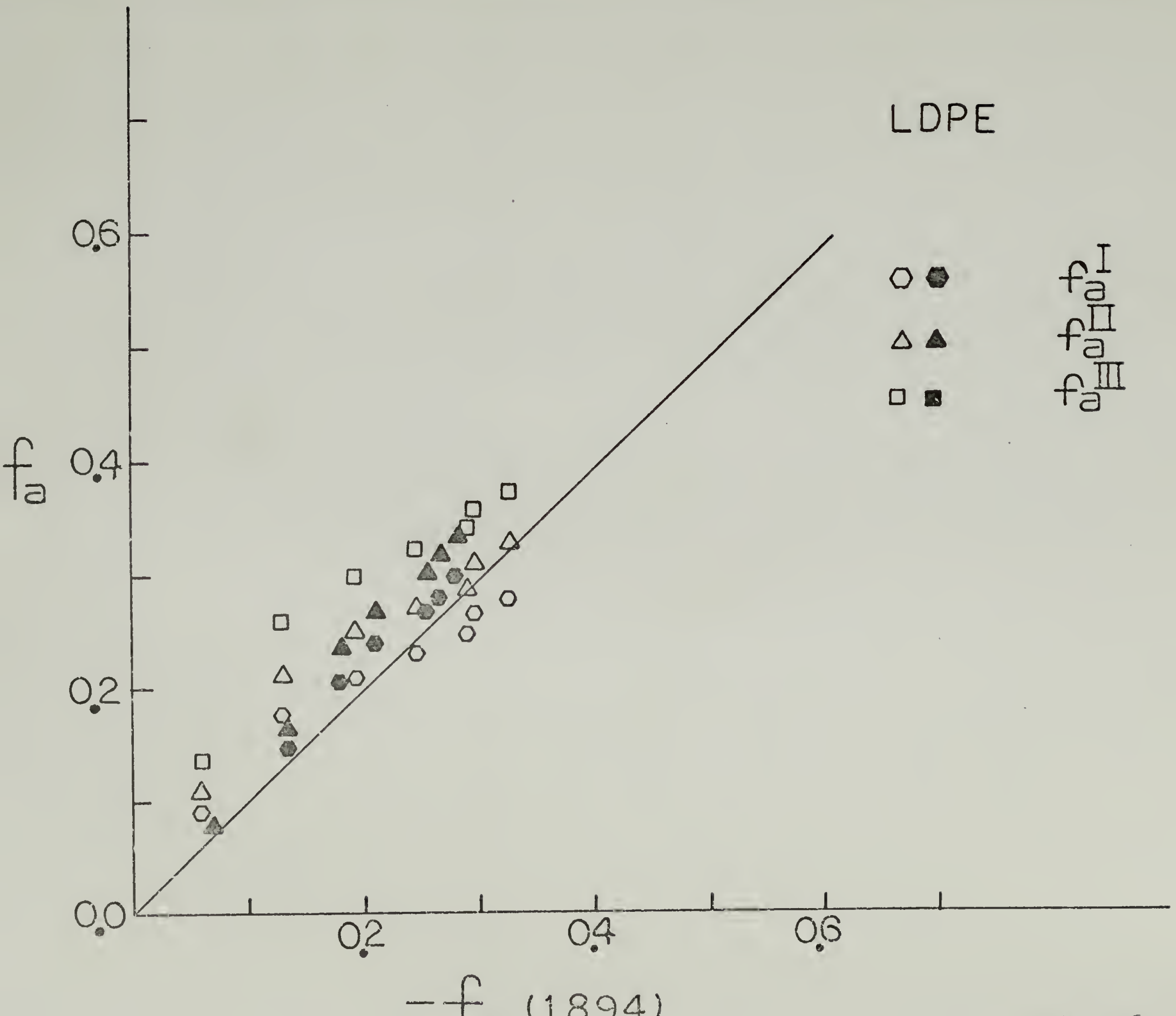

Fig. 18

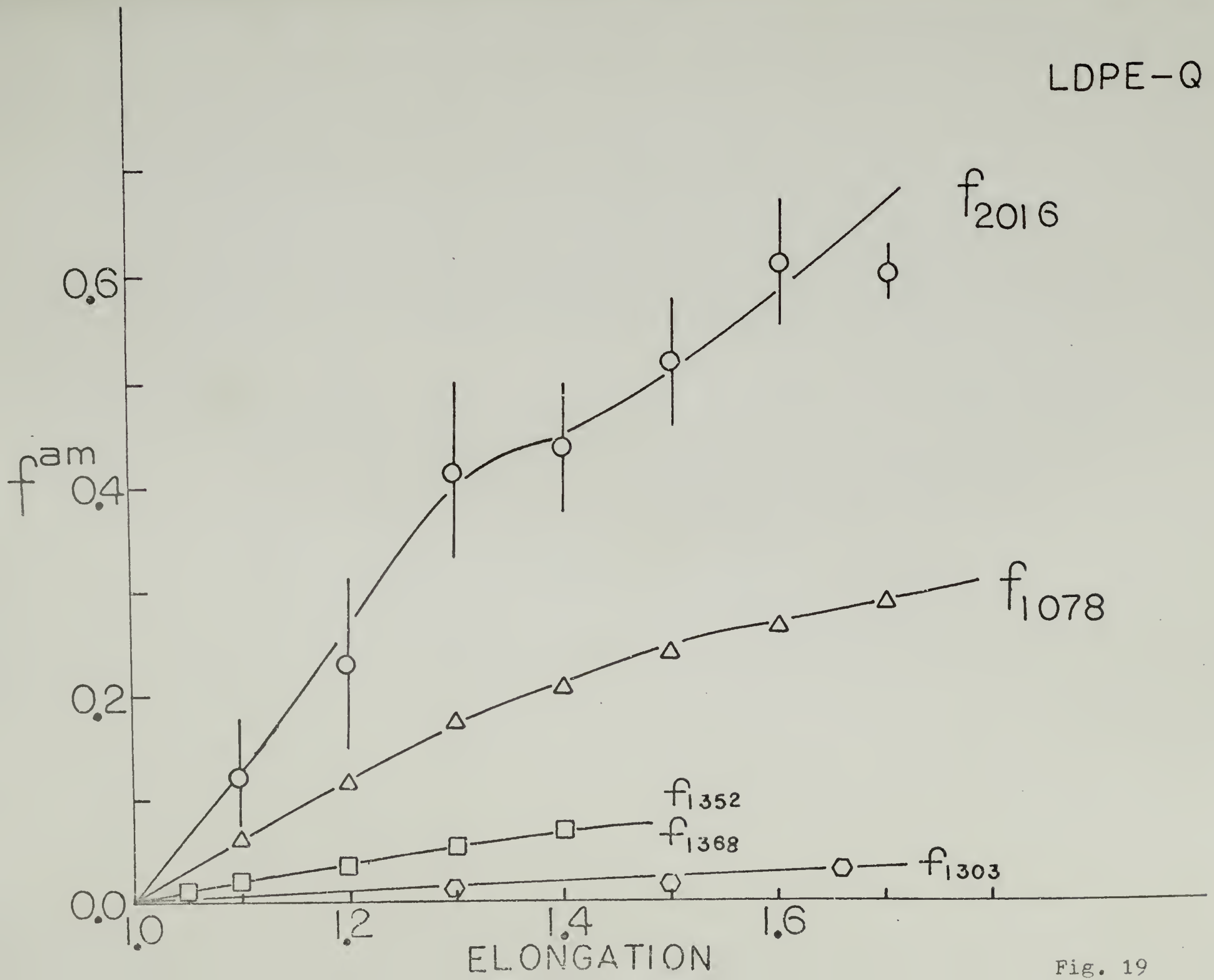
LDPE-Q
f_{2016}
f_{1078}
f_{1352}
f_{1368}
f_{1303}
f^{am}
0.0
0.2
0.4
0.6
1.0
1.2
1.4
1.6
ELONGATION

Fig. 19

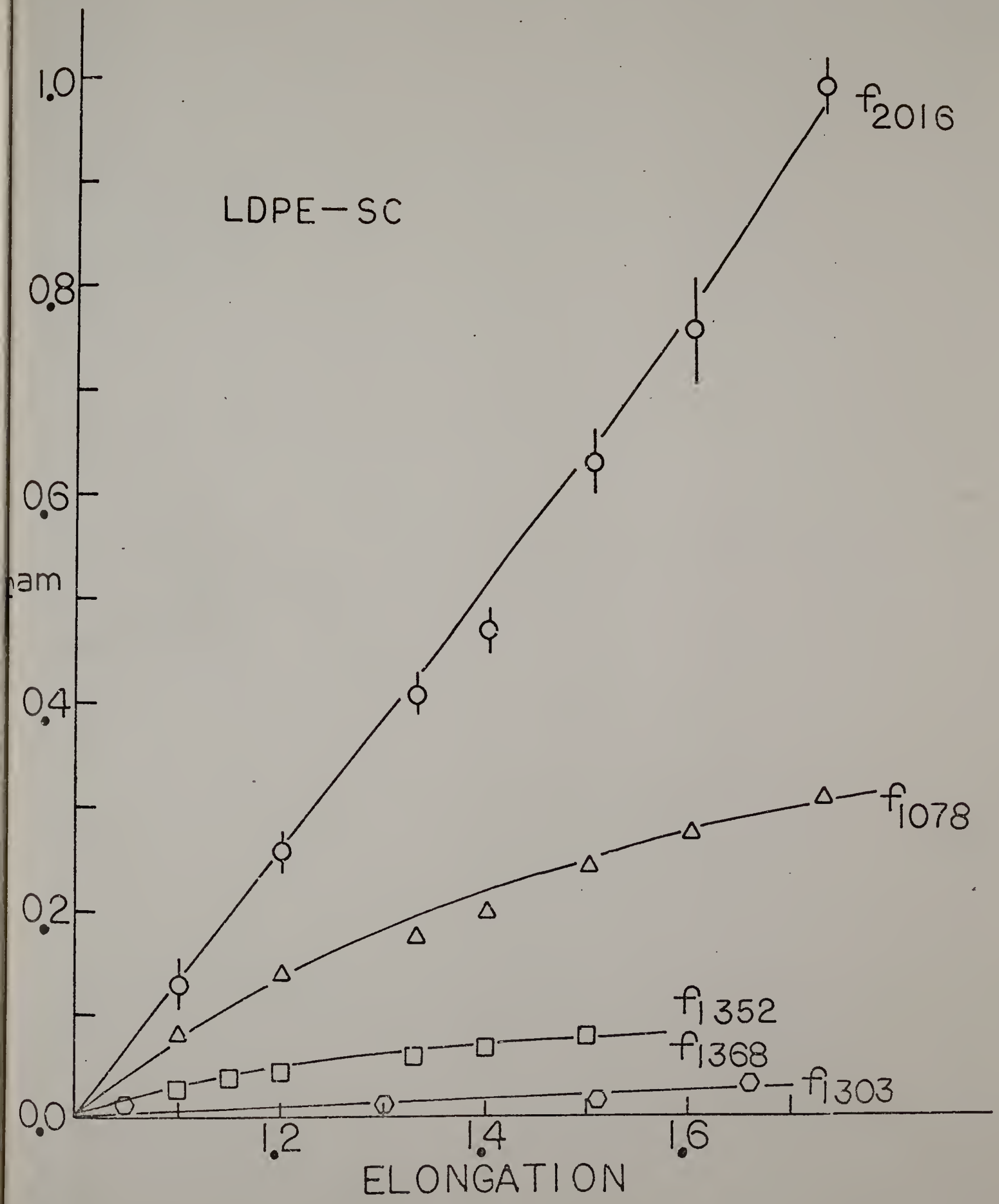
LDPE—SC
1.0
0.8
0.6
0.4
0.2
0.0
1.2
1.4
1.6
ELONGATION
f_{2016}
f_{1078}
f_{1352}
f_{1368}
f_{1303}

Fig. 20

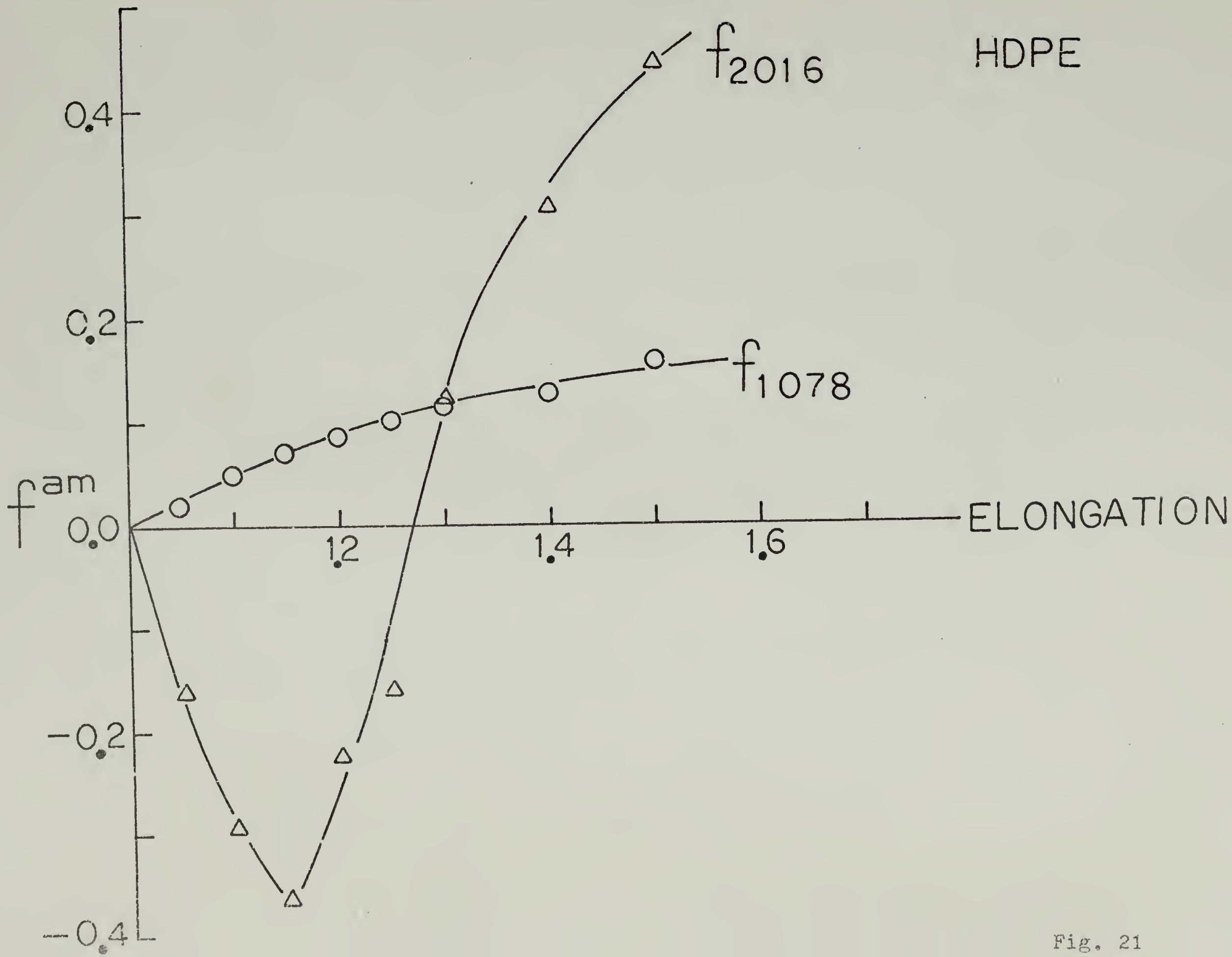

Fig. 21

AZIMUTHAL ANGLE Fig. 22

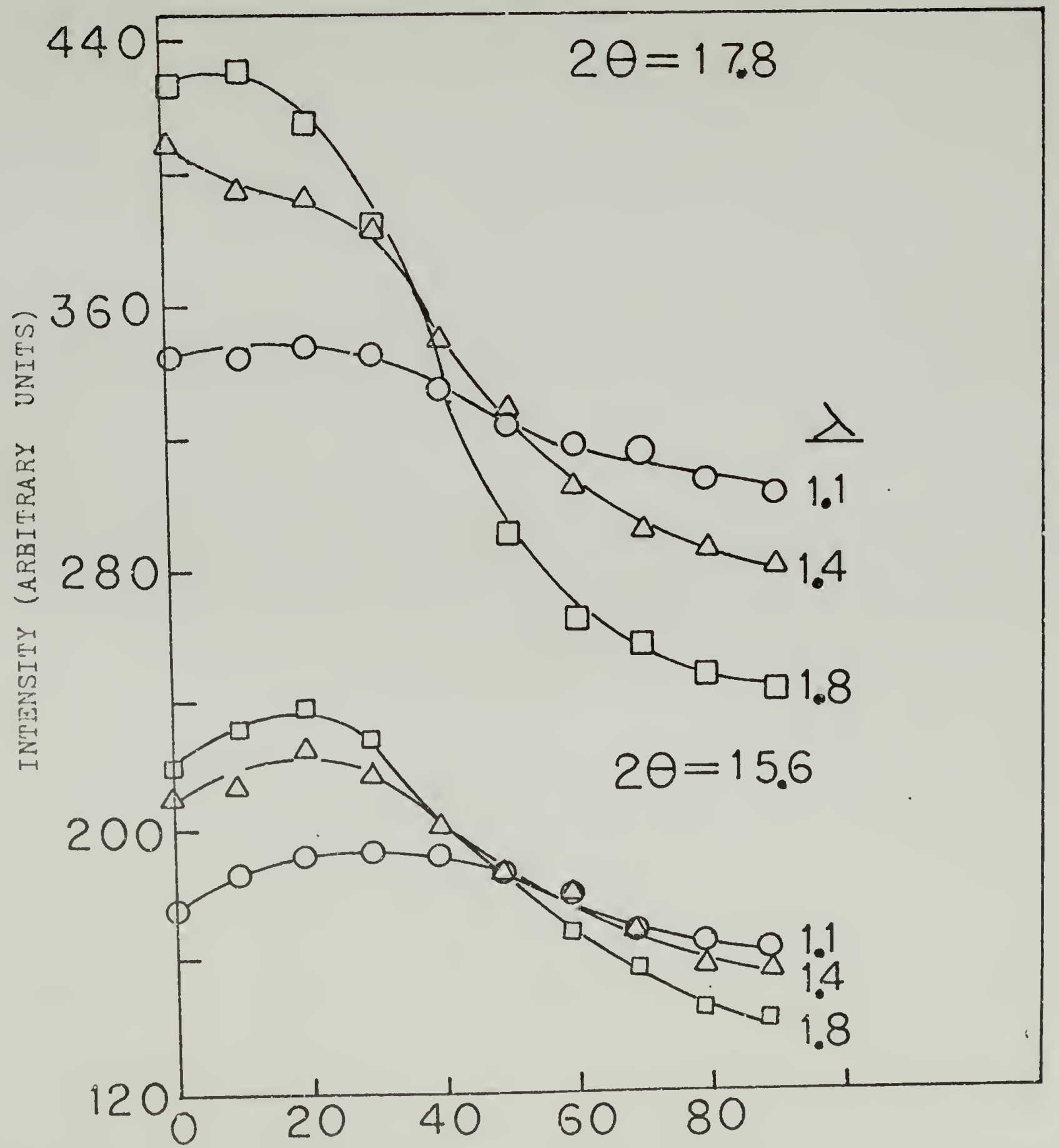

Fig. 22

LDPE-Q

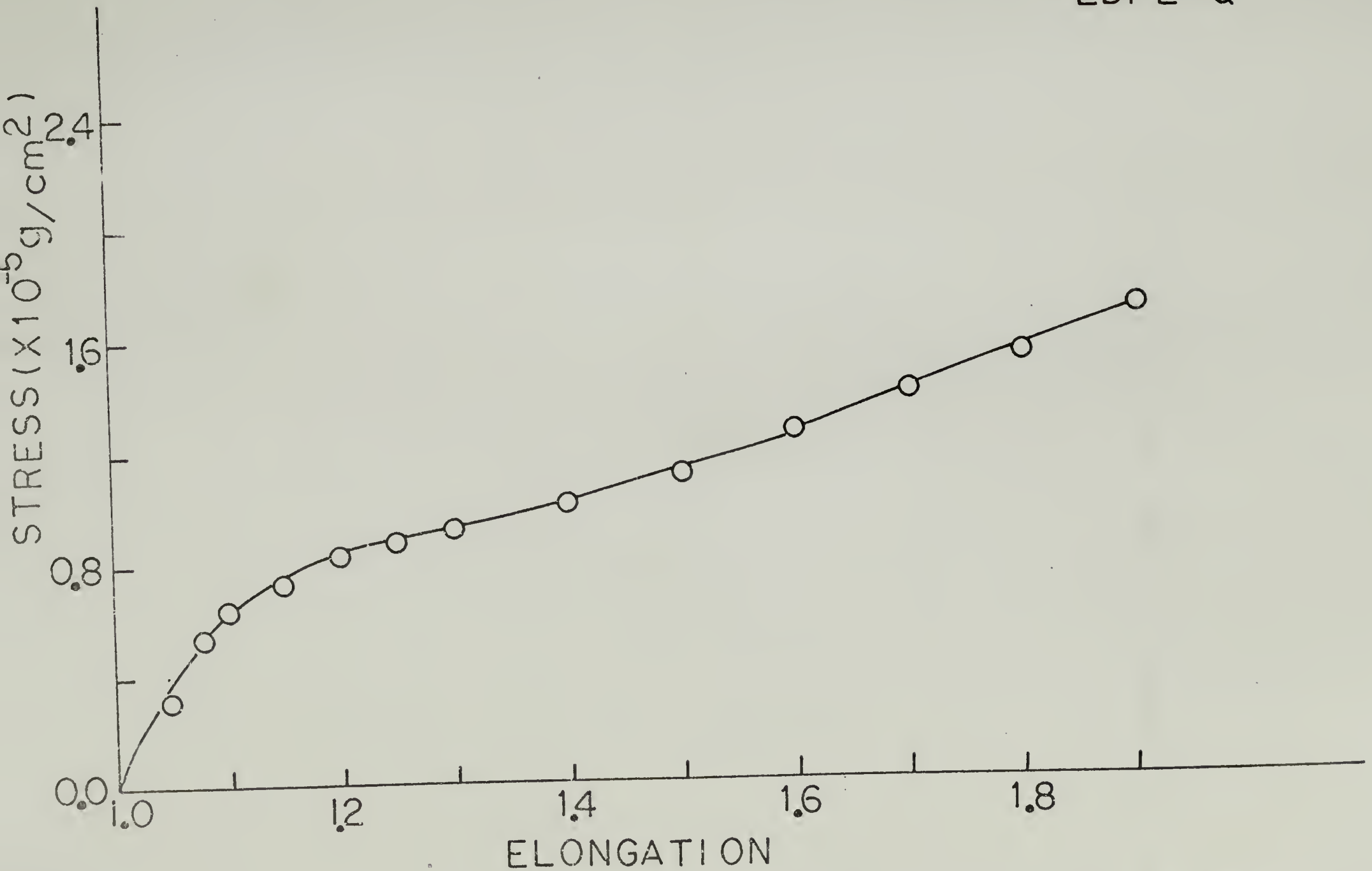

Fig. 23

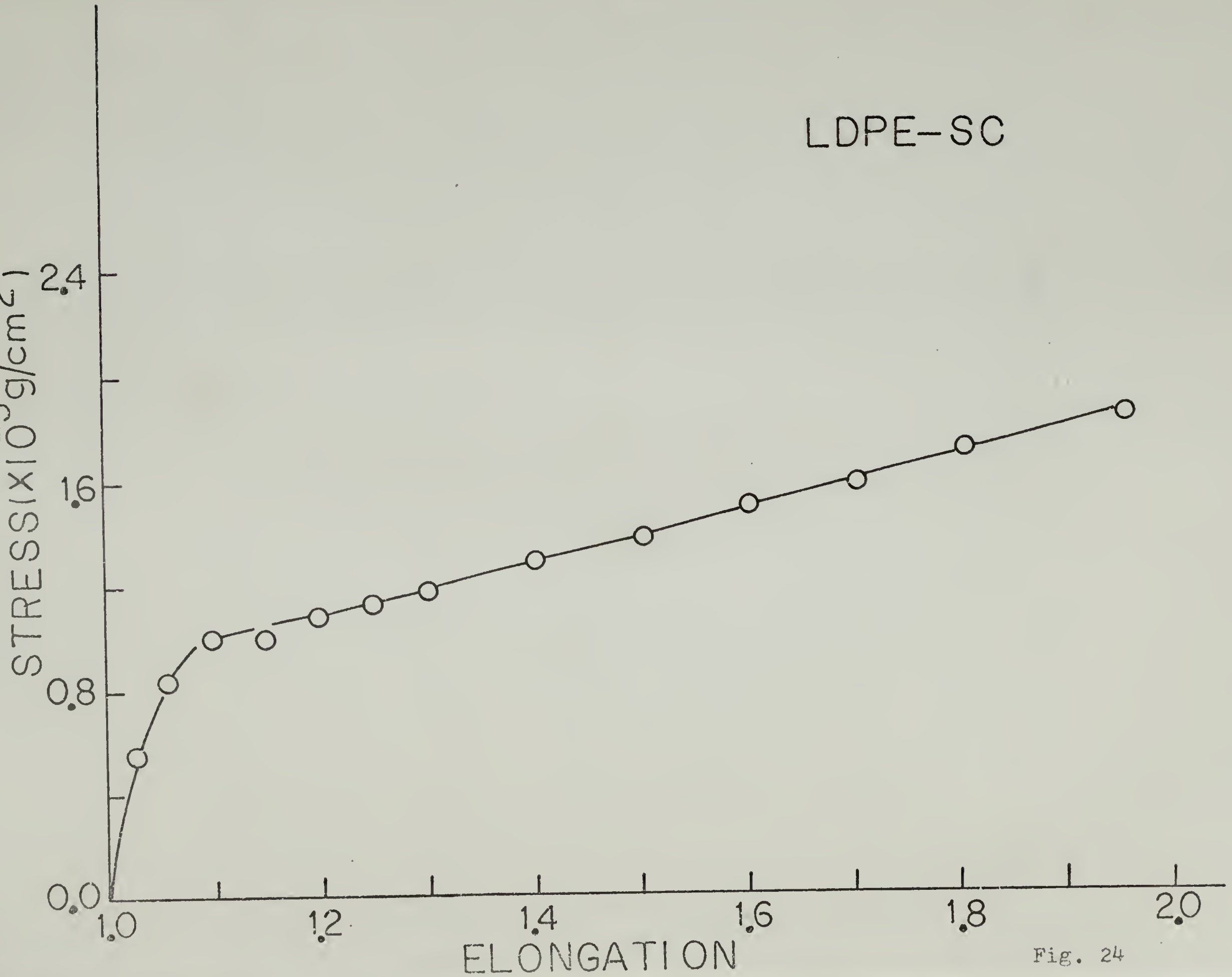
LDPE-SC
STRESS ($\times 10^{-5}$ g/cm^2)
2.4
1.6
0.8
0.0
1.0
1.2
1.4
1.6
1.8
2.0
ELONGATION

Fig. 24

HDPE

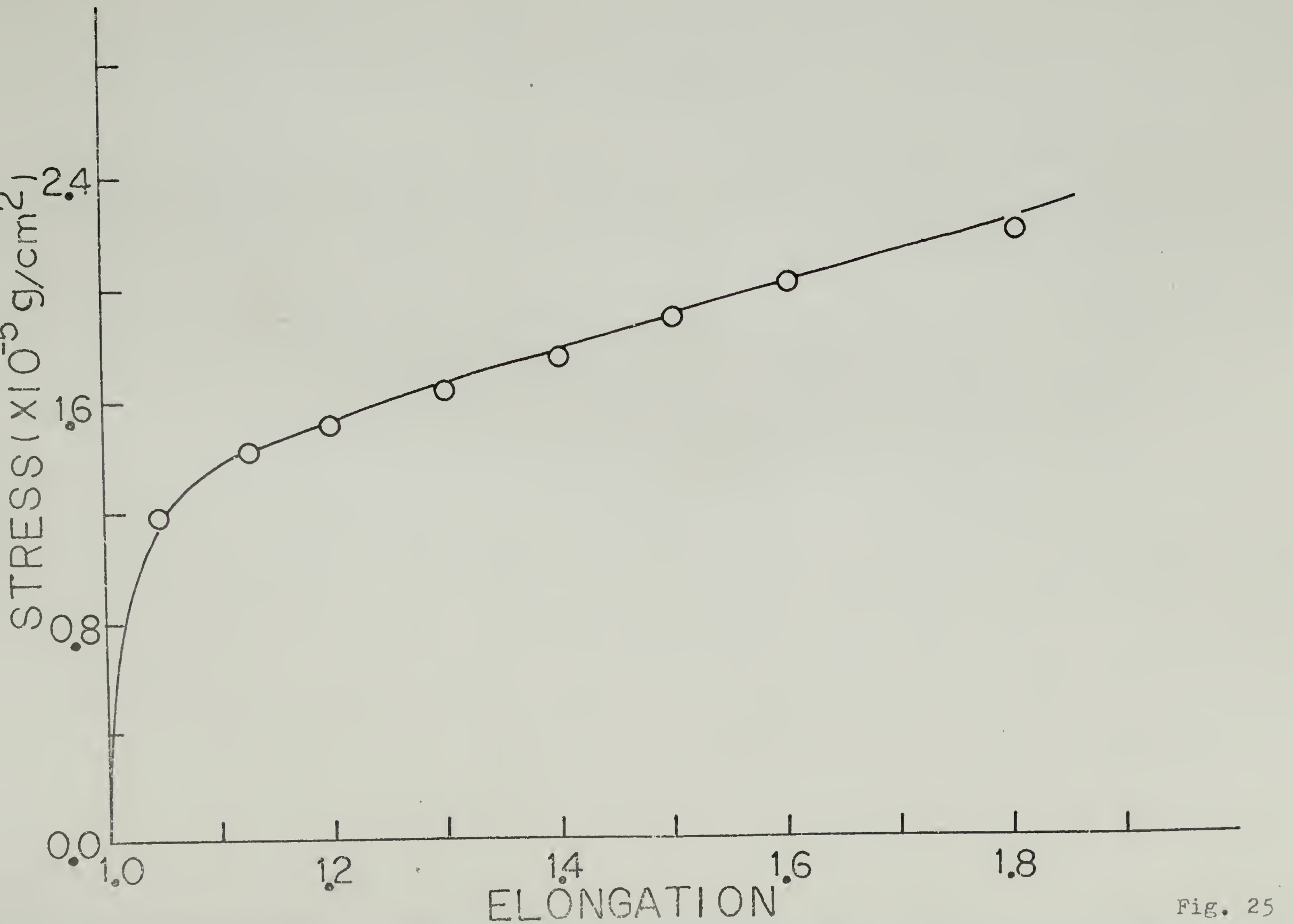

Fig. 25

CHAPTER VI

CHANGES IN INFRARED DICHROISM AND BIREFRINGENCE DURING RELAXATION OF LOW DENSITY POLYETHYLENE

SYNOPSIS

Quenched low density polyethylene was stretched at rates of less than 500 % sec^{-1} and higher than 1100 % sec^{-1}. The changes in infrared dichroism and in birefringence were measured during and after stretching. It was found that for samples stretched at rates less than 500 % sec^{-1} the molecular orientation, as shown by infrared dichroism and birefringence, could follow the strain without any delay, but for samples stretched at rates in the range of 1100 % sec^{-1} and 1400 % sec^{-1}, the molecular orientation lagged the strain by about 10 msec for samples stretched about 40 %.

The stress relaxation for samples stretched at a rate of 380 % sec^{-1} was measured. It was concluded that molecular orientation was not associated with stress relaxation. Various mechanisms of stress relaxation were discussed.

INTRODUCTION

Deformation of a crystalline polymer produces a change in orientation of the crystalline phase and of the amorphous phase, and may cause deformation within the crystals, too. The time and temperature dependence of crystal orientation of polyethylene has been extensively investigated (1-13), and it has been demonstrated

that the crystal orientation is a composite process in which spherulite deformation and various crystal reorientation processes occurring within the spherulite are involved. A phenomenological theory has been developed (14) to account for the macroscopic crystalline orientation functions of polyethylene in terms of various deformation processes, assuming affine deformation of the spherulite.

These deformation processes may be dependent on stretching rate; thus a finite time is required for crystal orientational change to take place. Consequently, if the polymer is stretched at a high rate so that the structural changes such as the crystal orientation can not follow the strain change, the orientation function will reflect the time-dependent effect. This effect has been observed for polyethylene using the x-ray technique (9) and infrared dichroism (15). Experimental studies of dichroism changes during polymer relaxation were carried out using modifications of commercial infrared spectrometers (15) and were consequently limited to the study of changes occurring in time periods longer than several seconds which were considerally longer than those accessible by other techniques. One of the purposes of the present work is to study the dichroism changes following rapid stretching.

The stress is indicative of the resistance of polymer chains in complying with the imposed strain. Orientation of the struc-

tural elements such as crystal and molecular chain in the amorphous phase in response to the strain will relieve the excessive stress bearing upon some parts of the molecules. If the structural changes such as those of crystal orientation cannot follow the strain, large strains may concentrate on the tie chains because they interconnect the lamellae. Bond rupture may occur in these tie chains which results in stress relaxation, too.

This part of the thesis presents the work investigating the molecular orientation following rapid stretching at different rates using infrared dichroism and birefringence technique. In order to correlate the molecular orientation and stress relaxation, the stress relaxation at 380 % sec^{-1} strain rate was measured. This strain rate was the highest one attainable by the equipment used.

EXPERIMENTAL

The Q-sample of low density polyethylene (LDPE) was used. The preparation and characterization of this sample were presented in the previous Chapter. The SC-sample and the HDPE samples were not used because these samples were too stiff, and it was difficult to stretch these samples up to 20 % which was necessary to have a significant change in dichroic ratio because of the high noise of the fast response detector used.

The polarized infrared studies were carried out with a fast-

response dichroism apparatus constructed for this purpose. The detailed description of this instrument was presented elsewhere (16-17). Dichroism changes of the absorption bands 1894 cm^{-1}, 1473 cm^{-1}, 1368 cm^{-1} and 1352 cm^{-1} following stretching were studied. The assignments of these absorption bands were presented in Table II of Chapter 5. The base lines used for calculating the absorbance were indicated by the solid lines in Fig. 2 of Chapter 5. The bands 2016 cm^{-1} and 1078 cm^{-1} were not included in this investigation because for the former band the orientation function of C-axis of the crystal, f_c, measured under the exact same conditions was not available for resolving this composite band (see eq. 19 of Chapter 5), and for the latter band the sensitivity of the detector was such that the measurement was not possible. The slit width was set at 0.8 mm for the bands 1894 cm^{-1} and 1473 cm^{-1}, and at 1.2 mm for the bands 1368 cm^{-1} and 1354 cm^{-1}.

Fig. 1 shows the amplified output of the detector displayed on a storage oscilloscope screen; Fig. 1a shows the oscilloscope trace for a undeformed sample and Fig. 1b shows that during and following stretching. The zigzag trace occurs because of the rotation of the chopping wheel which alternately diverts the beam through a horizontally and a vertically oriented wire-grid infrared polarizers each 2.3 msec. The alternate peaks are of different height because of the machine polarization. There is

an overall periodicity in transmitted intensity resulting from the 12 sectors per revolution of the chopping wheel which shows some variation in reflectivity from one sector to the next. In order to correct for this difference, it is necessary to identify the sector. This is done by referring to the position of the missing signal in Fig. 1, obtained by blocking one of the apertures of the chopping wheel. The superposed linear trace on Fig. 1b is the output from a potentiometer whose setting varies with the distance between clamps of the stretching device and serves as a measure of sample elongation. The stretching is seen to occur linearly with time.

The absorbance is obtained from the true transmittance, which is the ratio of the measured transitted intensity to the baseline intensity at the same frequency. The baseline intensity from the identical sector is obtained from the corresponding transmitted intensity without a sample multiplied by the baseline transmittance. The baseline transmittance was directly measured from the ratio of the transmitted intensity at the frequency on one side of the absorption band, as indicated in Fig. 2 of Chapter 5, to the transmitted intensity without a sample at the same frequency. This procedure of calculating the true transmittance simultaneously corrects the effects of variation in reflectivity of the chopping wheel sectors and the machine polarization of monochromater grating.

For the band 1473 cm^{-1}, a very thin sample (0.003 cm in thickness) has to be used, and the baseline transmittance was determined from the spectrum on the same type of sample obtained with a conventional spectrophotometer. Possible changes in baseline transmittance due to stretching of the sample was neglected. For the measurement of other bands, the baseline transmittance of the undeformed sample and that of the deformed sample were measured. Possible changes in baseline transmittance due to change in sample thickness, etc., caused by stretching were assumed to follow a linear relationship and were obtained by interpolation.

The birefringence was measured using the polarized light-transmission technique. A Ne-He laser (Spectra Physics) was used as light source and the sample was stretched between two crossed polars with the stretching direction at 45° to the polarization direction of the polars. The output of the 1P21 photomultiplier tube was displayed on a storage oscilloscope screen. The fraction of the incident light which is transmitted, T, for a sample of thickness d and birefringence Δ between $\pm 45^{\circ}$ crossed polars is

$$T = \sin^2(\pi d \Delta/\lambda)\, e^{-\tau d} + T_o \qquad (1)$$

where λ is the wavelength of light in vacuum, τ is the turbidity of the sample which represents light lost from the incident beam due to scattering, and T_o is the transmittance in the absence of macroscopic birefringence, which represents the transmittance of the sample resulting from locally birefringent regions such as spherulites. It was observed that the changes in the turbidity due to stretching were relatively small, thus the characteristic square sine curve of T vs. elongation (time in this case) was preserved. From the maxima and minima of the curve of T vs. time, the birefringence was determined as a function of time.

The stress relaxation was carried out using a table model instron (Instron Engineering Corp., Model TM). The sample was stretched at a rate of 380 % sec^{-1} to predetermined total elongation and was then held at constant length while the stress was being recorded.

RESULTS AND DISCUSSION

(1) Sample Stretched At A Rate Less Than 500 % Sec^{-1}

Fig. 2 shows the dichroic ratio of the 1473 cm^{-1} band as a function of time. The sample was stretched 25 % at a rate of 400 % sec^{-1}. The datum points were scattered considerably in the transient region, this is because the absorption of this band is quite high and the weak transmitted intensity results

in very high noise to signal ratio. At longer times, the dichroic ratios were obtained by averaging all the dichroic ratios measured during the time of the oscilloscope trace (0.2 sec.), thus the precision of the data is much better than that in the transient region.

Fig. 3 shows the dichroic ratio of the 1894 cm^{-1} band during and following stretching. The sample was stretched 42 % at a rate of 420 % sec^{-1}.

As discussed in Chapter 5, the absorption bands 1473 cm^{-1} and 1894 cm^{-1} arise from the vibration mode of CH_2 group in the crystal and their transition moments lie in the direction of a-axis of the unit cell. Thus the dichroism changes of these two absorption bands indicate the orientation of the crystal a-axis. The dichroism of these two absorption bands appears to remain constant after the stretching was completed, as shown by Fig. 2-3. This means that the orientation of the a-axis of the crystal can follow the strain without any delay at the strain rate of about 420 % sec^{-1}. We were not able to obtain the orientation of the crystal c-axis from the dichroism of the absorption band 1176 cm^{-1} under the same conditions because of low sensitivity of the detecting system.

The orientation in the amorphous phase following stretching is shown by Fig. 4, in which the dichroism changes of the band 1368 cm^{-1} was plotted against time. The film was stretched

38 % at a rate of 470 % sec^{-1}. One can see that after the stretching was completed, there was no apparent change in the dichroism.

Fig. 5 shows the oscilloscope trace of birefringence change during and after stretching. Fig. 5a has a time scale of 20 msec/div and the upper trace of Fig. 5b is at a sweep rate of 0.1 sec/div and the lower trace of Fig. 5b at a sweep rate of 1sec/div. It is clearly shown that the birefringence remained constant after the stretching was completed. The birefringence changes against time is plotted in Fig. 6 for samples stretched at rates of 270 % sec^{-1} (λ = 1.20) and 470 % sec^{-1} (λ = 1.40). The vertical dotted lines indicated the time when stretching was completed.

Fig. 7 shows the stress relaxation for films stretched at 380 % sec^{-1}. Fig. 7a shows film stretched 18 % and Fig. 7b stretched 30 %. The stress relaxation can be divided into two regions of fast decay and slow decay. Most of the stress relaxed within the first three seconds, then it was followed by a slow relaxation.

The results from infrared dichroism and birefringence show no molecular orientation change after the stretching was completed. Thus molecular orientation is not associated with the stress relaxation.

Wool and Statton (18) studied the molecular mechanics of highly oriented polypropylene during stress relaxation and creep

using the polarized infrared technique. They concluded that the stress-transfer from non-aligned chains to aligned chains and the rupture of very highly overstressed aligned chains were responsible for the fast stress decay, and the disorientation and the helix distortion (in case of polypropylene) were responsible for the slow decay.

The sample has 46 % crystalline material and the crystalline lamellae aggregate to form superstructure. The lamellae may be connected to each other through direct crystal-crystal contact, as a result of a branching growth of the crystal, and through tie chains in the amorphous phase. As the sample is deformed, in the amorphous phase the tie chains will extended, and in the crystalline phase such deformation mechanisms like deformation in the intermosaic regions (19), changes in crystal lattice (20), dislocation in the crystal (21), and [001] (100) slip and (110) and (310) twinning (22) have been reported to occur. All these processes may be time-dependent and thus may be related to stress relaxation.

As the sample is rapidly deformed, some of the tie chains may be fully extended and sustain very high stress. These chains are the ones most likely to be broken. From the fact that the birefringence remained constant after stretching indicates that, if chain rupture did occur, these were probably only few tie chains being ruptured, thus the birefringence of the sample

It is also likely that after the stretching some tie chains become highly extended, the stress may be relieved by the translational motion along the c-axis (which may involves the [001](100) slip, for instance) in the crystalline region. This will not change the crystal orientation nor the birefringence and will increase the orientation of the tie chains connected through the lamellae to those highly extended tie chains. The number of such tie chains involved may not be very large, thus its effect on the orientation function measured by infrared dichroism using the bands 1368 cm^{-1} or 1354 cm^{-1} is not detectable, because these bands have very low dichroism and measure the orientation of all the chains in the amorphous phase including loops and cilia.

When the sample is rapidly stretched, the anchored points of the tie chains on the lamellae are moved to new positions. However, the configurations of the tie chains may not be readily adjusted to the new states, thus some of the bonds in these tie chains will be distorted to bear excessive stress. The adjustment of the configurations of the tie chains to the new states through internal motions will result in stress relaxation. The internal motions may have a distribution of relaxation times and some of them may have quite long relaxation times. This can then explain the slow decay of the stress. This process presumably occurs within the same tie chain and will not significantly affect the birefringence. This is because in the beginning

when the bonds are distorted, the deformation birefringence will contribute to the total birefringence; as the chains reorient, the deformation birefringence decreases while the birefringence arising from reorientation increases, thus the total birefringence remains constant but there is a stress relaxation.

Other mechanisms which may account for the relaxation without significantly changing molecular orientation may be those of changes in crystal lattice (20) and deformation in the intermosaic regions (19). Only slight changes in crystal lattice will result in substantial reduction in stress without changing the crystal orientation and the deformation in the intermosaic regions will have the similar effects. Conceivably these processes are all time-dependent and may be associated with the stress relaxation. Furthermore other mechanisms like dislocation assisted slip (21) and twinning (22) may also be associated with the stress relaxation.

(2) Sample Stretched At A Rate Higher Than 1000 % Sec^{-1}

Fig. 8 indicates the dichroic ratio of the band 1894 cm^{-1} and Fig. 9 that of the band 1354 cm^{-1} as a function of time following stretching. The films were stretched about 60 % at a rate of about 1400 % sec^{-1}.

Fig. 10 shows the oscilloscope traces of birefringence changes following stretching. Fig. 10a has a sweep rate of

20 msec/div, and the upper trace of Fig. 10b has a sweep rate of 2 sec/div and the lower trace of Fig. 10b has a sweep rate of 0.1 sec/div. Fig. 11 shows the plot of birefringence change against time for the film stretched 45 % at a rate of 1200 % sec^{-1}.

It is not very certain that, from the results of Figs. 8-9, there were a further changes in the orientation of the crystals and the amorphous phase, because of the scattered datum points. On the other hand, the results from the birefringence relaxation, as shown in Fig. 11, clearly indicate that there was further increase in birefringence after the stretching was completed.

The birefringence was relaxed within about 10 msec and remained constant thereafter. For samples stretched at rates higher than 1100 % sec^{-1}, they all showed a time lag between the stretching completion and the reaching of the final birefringence. This is a clear indication that the molecular orientation can not follow the strain at such stretching rates. Such time-dependence of orientation has been observed in high speed x-ray relaxation (9). The effect was more pronounced in the x-ray relaxation because the sample was stretched at a rate of about 4000 % sec^{-1}, about four times faster than what used in this work.

CONCLUSIONS

It is observed that, for the quenched low density polyethylene, the molecular orientation can follow the strain for a sample

stretched at about 500 % sec^{-1} or so, and the molecular orientation lags the strain for a sample stretched at rates of 1100 % sec^{-1} or higher. Thus the rate-dependence of the molecular orientation is clearly demonstrated. Because of the poor precision of the present infrared dichroism technique, it is not certain whether the crystal orientation or the amorphous orientation or both are dependent on time.

By comparing the stress relaxation and molecular orientation during relaxation, it is concluded that molecular orientation is not the relaxation mechanism. It is suggested that bond rupture, translational motion of crystal c-axis, relaxation of tie chains to the conformations consistent with the new deformed state or various crystal deformations such as changes in crystal lattice, deformation in the intermosaic regions, dislocation assisted slip and twinning may be responsible for stress relaxation.

The results from the infrared dichroism are not able to confirm the results from the high-speed x-ray relaxation for these samples because of the present low precision of the infrared dichroism technique.

According to the band assignments (see Table II of Chapter 5), the band 2016 cm^{-1} from the amorphous phase may arise from bonds in a trans sequence conformation, such bonds may preponderantly reside in the tie chains, and the band 1078 cm^{-1} comes from the stretching of skeletal C-C bonds. Thus the dichroism changes

of these two bands during relaxation, particularly combining with the kind of dynamic polarized infrared studies employed by Wool and Statton, may provide valuable information concerning the molecular mechanics. Furthermore, dynamic x-ray studies of those various crystal deformation mechanisms supposedly associated with stress relaxation may unveil the important information concerning the role of the crystal in this regard.

REFERENCES

1. R. S. Stein, S. Onogi and D. A. Keedy, J. Polym. Sci., 57 801 (1962).
2. R. S. Stein, S. Onogi, K. Sasaguri and D. A. Keedy, J. Appl. Phys., 34 80 (1963).
3. R. Yamada and R. S. Stein, J. Appl. Phys., 36 3005 (1965).
4. A. Takeuchi and R. S. Stein, J. Polym. Sci., A2, 5 1079 (1967).
5. A. Tanaka, E. P. Chang, B. Delf, I. Kimura and R. S. Stein, J. Polym. Sci., A2, 11 1891 (1973).
6. S. Onogi, T. Asada, Y. Fukui and T. Fujisawa, J. Polym. Sci., A2, 5 1067 (1967).
7. I. Sato, M. Ushirokawa, T. Asada and S. Onogi, J. Polym. Sci., A2, 8 1195 (1970).
8. S. Onogi, T. Asada and Y. Fusui, J. Polym. Sci., A2, 8 1211 (1970).
9. R. S. Stein, R. S. Finkelstein, D. Y. Yoon and C. Chang, J. Polym. Sci., Symposium No. 46, 15 (1974).
10. T. Oda and R. S. Stein, J. Polym. Sci., B, 9 543 (1971).
11. T. Oda and R. S. Stein, J. Polym. Sci., 10 625 (1972).
12. R. S. Stein, R. S. Finkelstein and C. Chang, J. Appl. Polym. Sci.,
13. P. Erhardt and R. S. Stein, J. Polym. Sci., B, 3 553 (1965).
14. D. Y. Yoon and R. S. Stein, J. Polym. Sci., Polym. Phys. Ed., 12 2091 (1974).
15. Y. Fukui, T. Asada and S. Onogi, Polymer J., 3 100 (1972).

16. G. L. Wilks, Y. Uemura and R. S. Stein, J. Polym. Sci., A2, 9 2151 (1971).

17. Y. Uemura and R. S. Stein, J. Polym. Sci., A2, 10 1690 (1972).

18. R. P. Wool and W. O. Statton, J. Polym. Sci., Polymer Phys. Ed., 12 1575 (1974).

19. T. Kajiyama and M. Takayanagi, J. Macromol. Sci.-Phys., B 10 (1), 131 (1974).

20. I. Sakurada, T. Ito and K. Nakamae, J. Polym. Sci., Part C, 15 75 (1966).

21. B. W. Cherry and P. L. McGinley, Appl. Polym. Symposium, No. 17, 59 (1971).

22. I. L. Hay and A. Keller, J. Polym. Sci., Part C, No. 30, 289 (1970).

CAPTIONS FOR FIGURES

1. Oscilloscope trace of the variation of the transmitted signal with time. Fig. 1a shows that of a undeformed sample and Fig. 1b shows that during and following the 60 % stretching of a 25-mil quenched low density polyethylene film at 23°C. The time scale is 20 msec/div. The superposed smooth trace on Fig. 1b indicates the strain change.
2. Variation of dichroism with time at 1473 cm^{-1} during and following stretching of a film of quenched low density polyethylene at 23°C. The film was stretched 25 % at a rate of 400 % sec^{-1}.
3. Variation of dichroism with time at 1894 cm^{-1} during and following stretching of a quenched low density polyethylene film at 25°C. The film was stretched 42 % at a rate of 420 % sec^{-1}.
4. Variation of dichroism with time at 1368 cm^{-1} during and following stretching of a quenched low density polyethylene film at 23°C. The film was stretched 38 % at a rate of 470 % sec^{-1}.
5. Oscilloscope trace of the output of 1P21 photomultiplier following birefringence changes during and after the stretching of a quenched low density polyethylene at 23°C. The sweep rate for Fig. 5a is 20 msec/div and 0.1 sec/div and 1 sec/div for the upper trace and for the lower trace of Fig. 5b, respectibely.

6. Variation of birefringence with time during and following stretching of a quenched low density polyethylene. The upper curve shows the results from a film stretched 40 % and at a rate of 470 % sec^{-1} and the lower curve that from a film stretched 20 % at a rate of 270 % sec^{-1}.
7. Stress relaxation for two quencehd low density polyethylene films. The one was stretched 18 % at a rate of 380 % sec^{-1} and the other was stretched 30 % at the same rate. The stress was not corrected for change in sample cross-section due to stretching.
8. Variation of dichroism at 1894 cm^{-1} during and following stretching of a quenched low density polyethylene film at 23°C. The sample was stretched 65 % at a rate of 1400 % sec^{-1}.
9. Variation of dichroism at 1354 cm^{-1} during and following stretching of a quenched low density polyethylene film at 23°C. The sample was stretched 60 % at a rate of 1360 % sec^{-1}.
10. Oscilloscope trace of the output of 1P21 photomultiplier following birefringence changes during and after the stretching of a quenched low density polyethylene at 23°C. The sweep rates are 20 msec/div, 2 sec/div and 0.1 sec/div for Fig. 10a, the upper trace of Fig. 10.6 and the lower trace of Fig. 10b, respectively.
11. Variation of birefringence with time during and following stretching of a quenched low density polyethylene film. The sample was stretched 45 % at a rate of 1150 % sec^{-1}.

LDPEM 8011(Q)

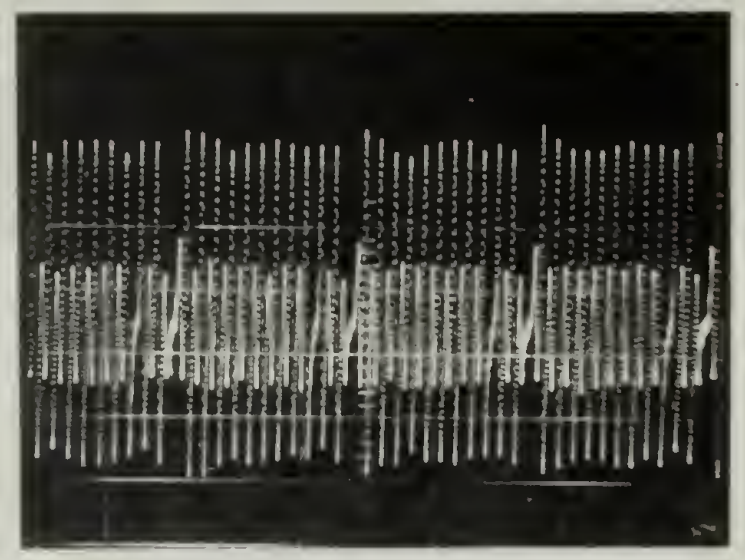

(a) $\lambda = 1.0$
20 msec/div

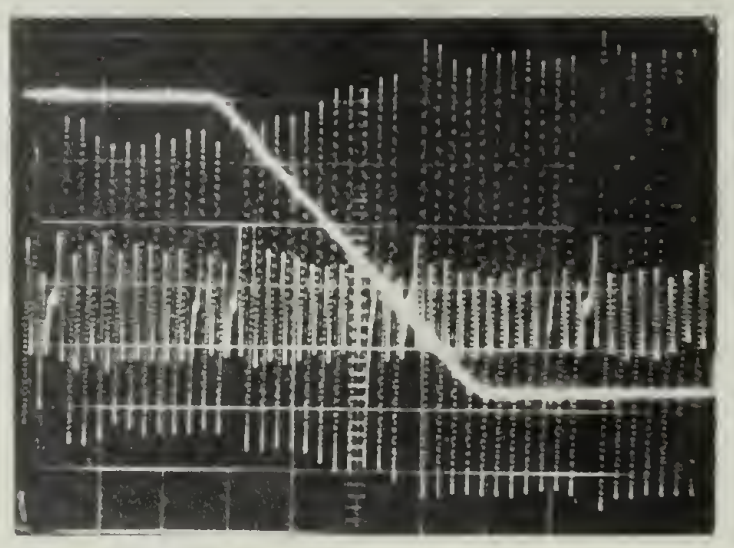

(b) $\lambda = 1.6$
20 msec/div

Fig. 1

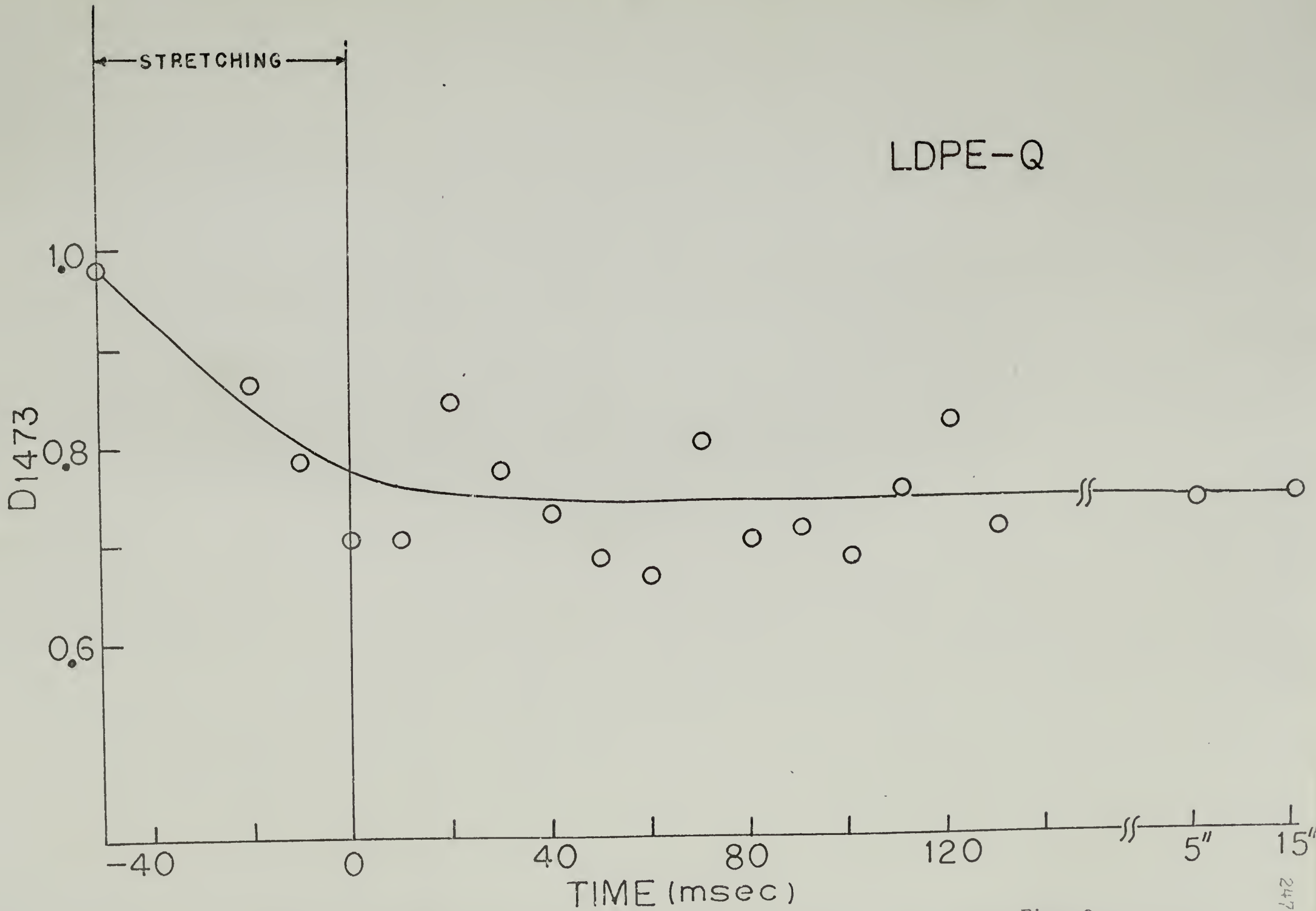

Fig. 2

LDPEM 8011(Q)
T = 25°C
STRAIN RATE = 420%SEC^{-1}
1894 CM^{-1}(C)

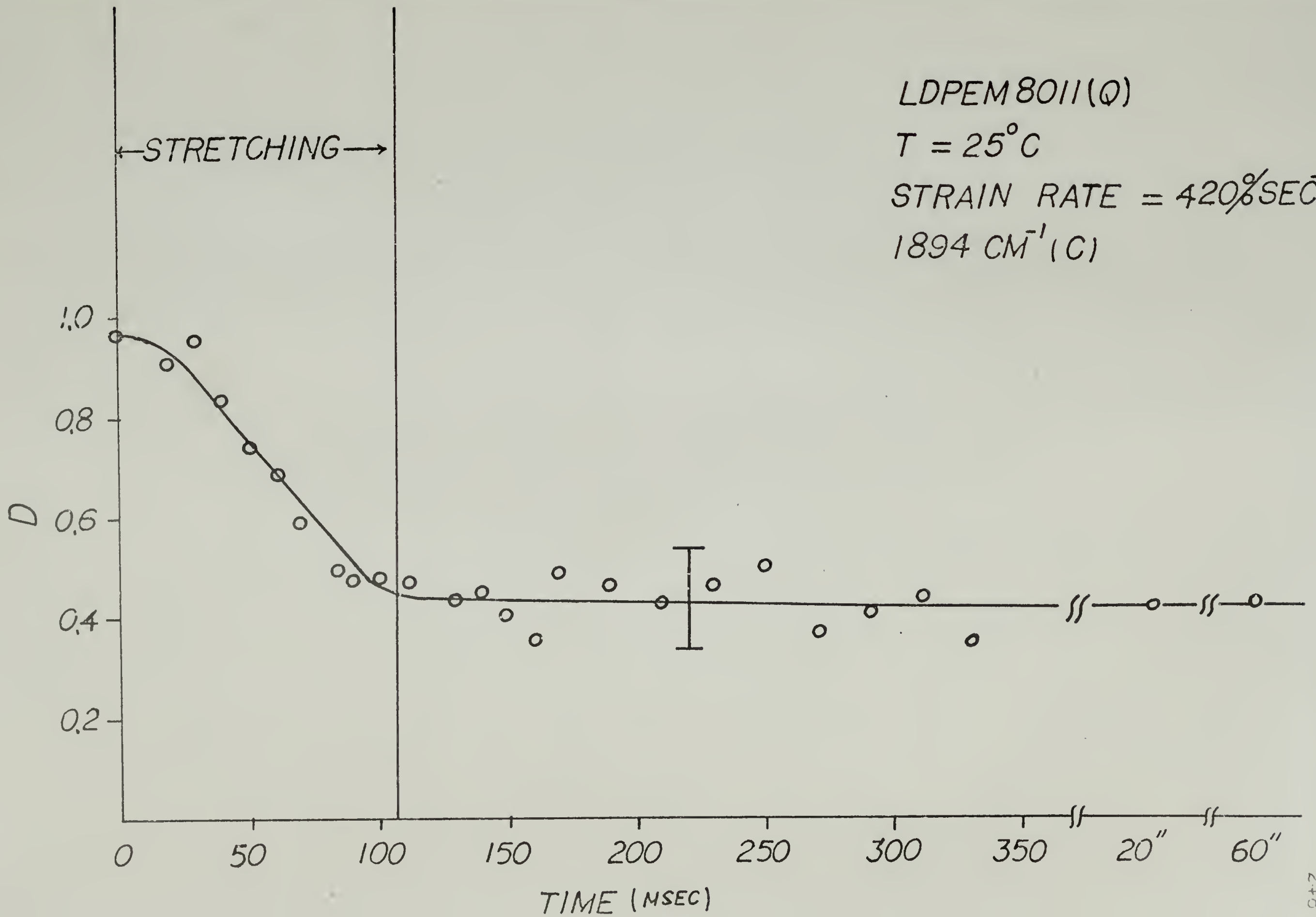

LDPEM 8011

$T = 23^{\circ}C$

$\lambda = 1.38$ (470% SEC^{-1})

STRETCHING

D_{1368}

1.2

1.0

0.8

0 40 80 120 160 200 5 20 30 60

TIME (msec)

249

Fig. 4

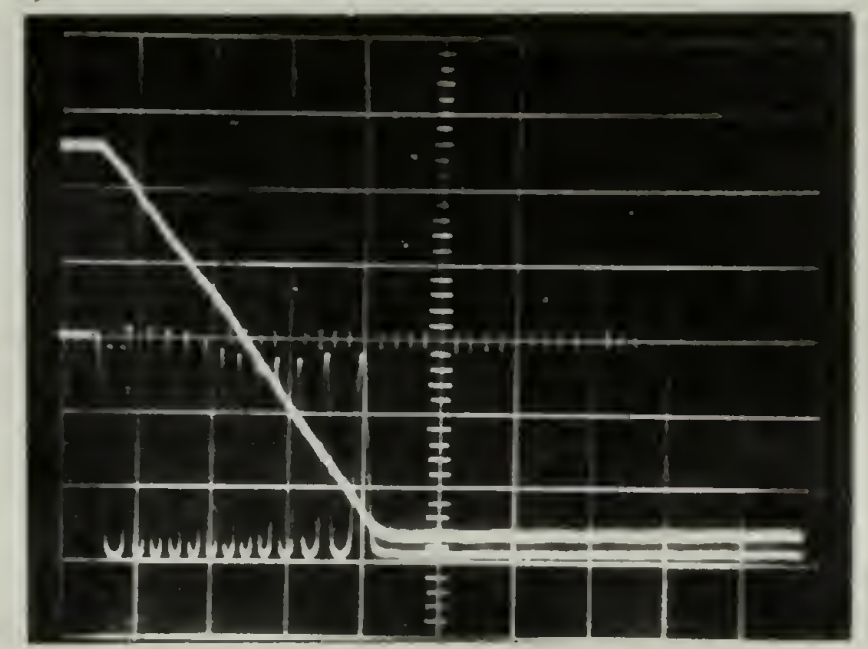

(a)

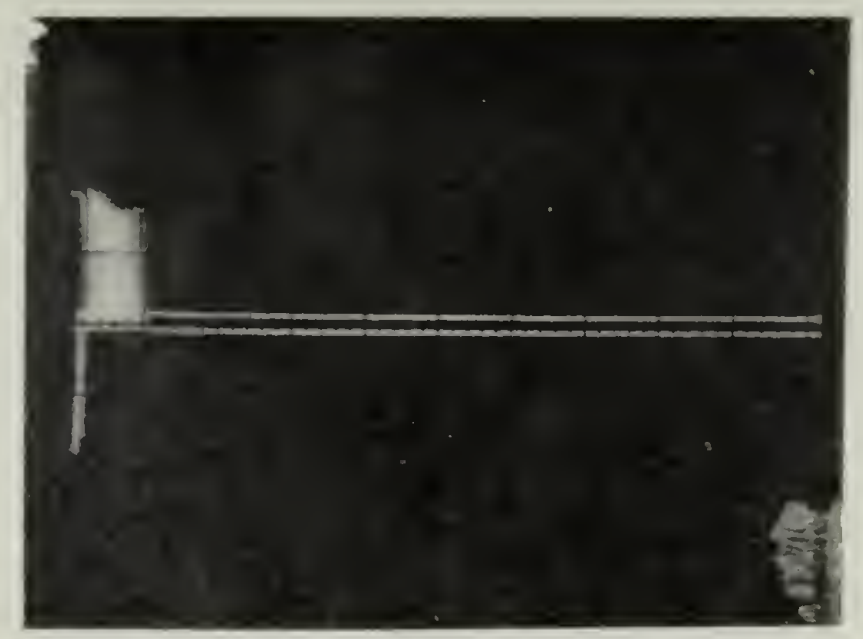

(b)

Fig. 5

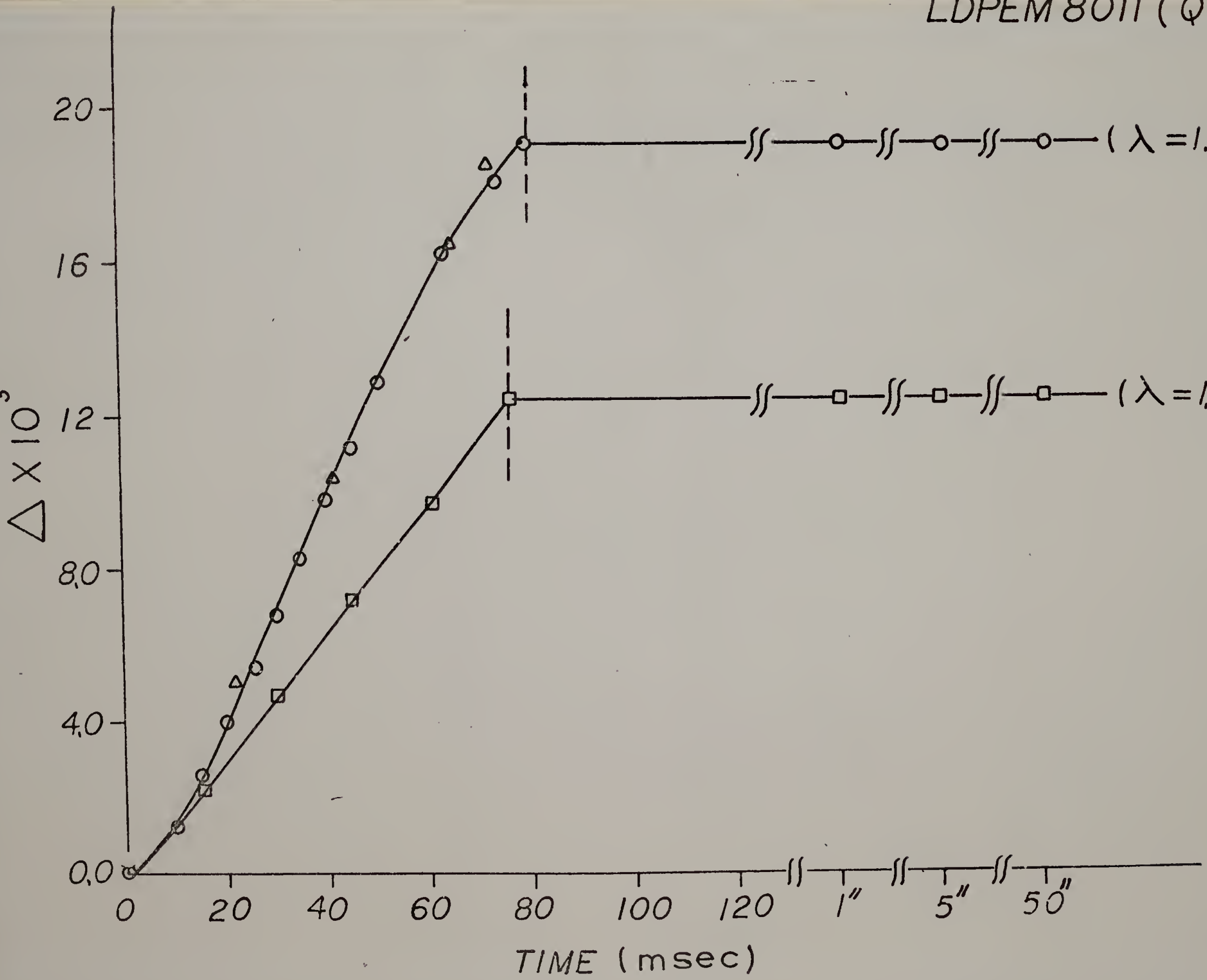
20
16
12
8.0
4.0
0.0
$\triangle X \times 10^3$
(λ = 1.40)
(λ = 1.20)
0
20
40
60
80
100
120
1"
5"
50"
TIME (msec)

Fig. 6

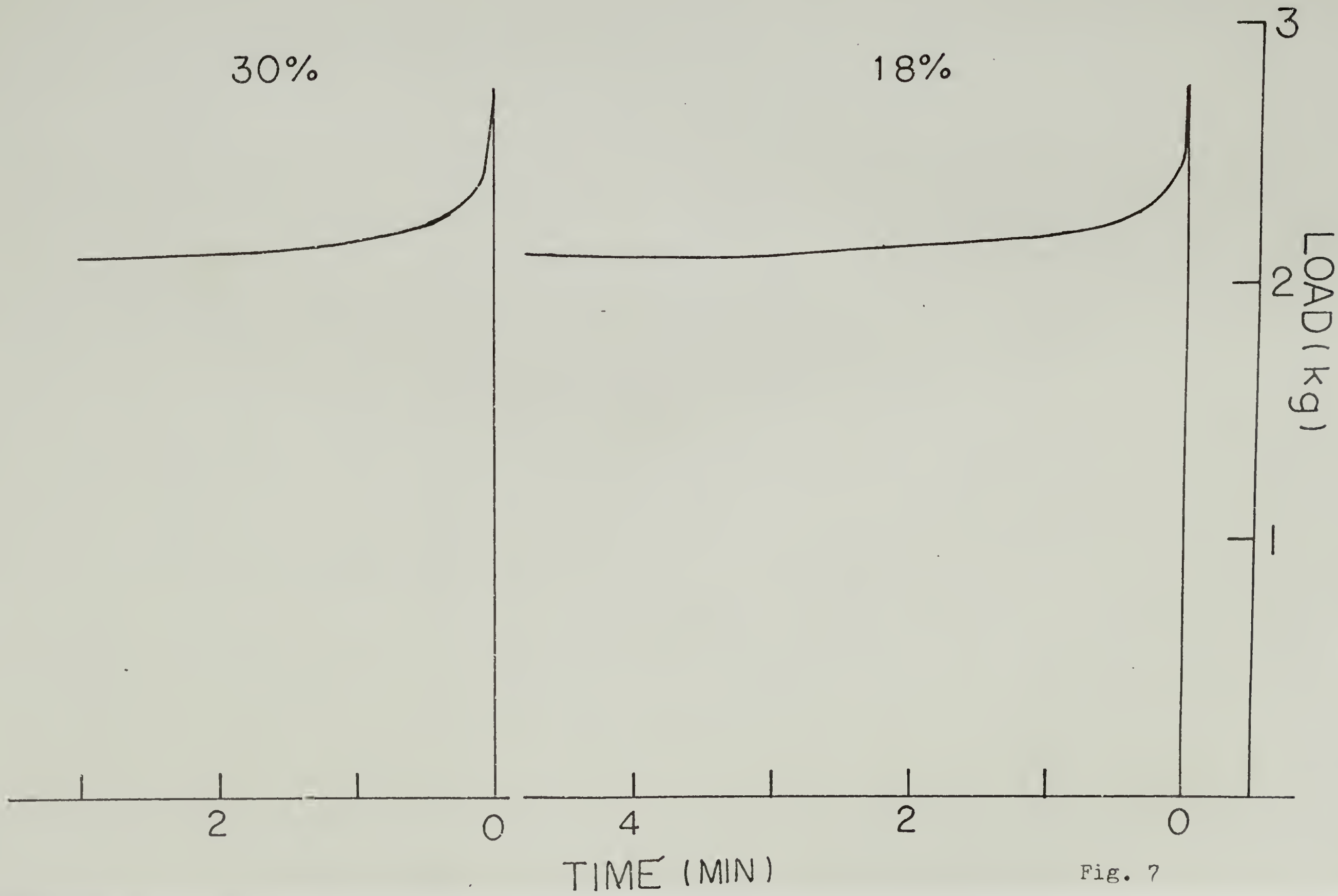

Fig. 7

LDPEM8011

STRAIN RATE = 1400% SEC^{-1}

TEMP = 23°C

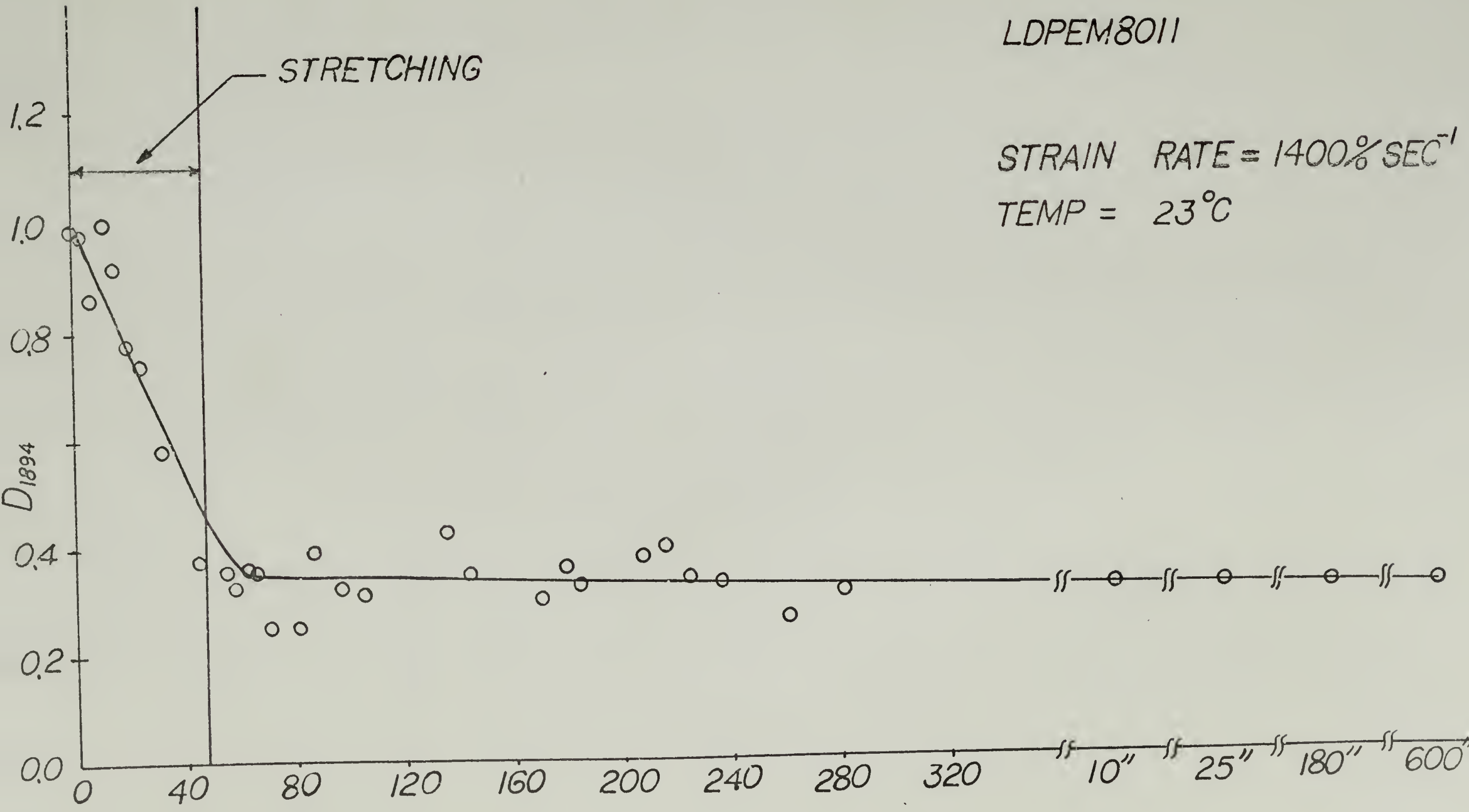

Fig. 8

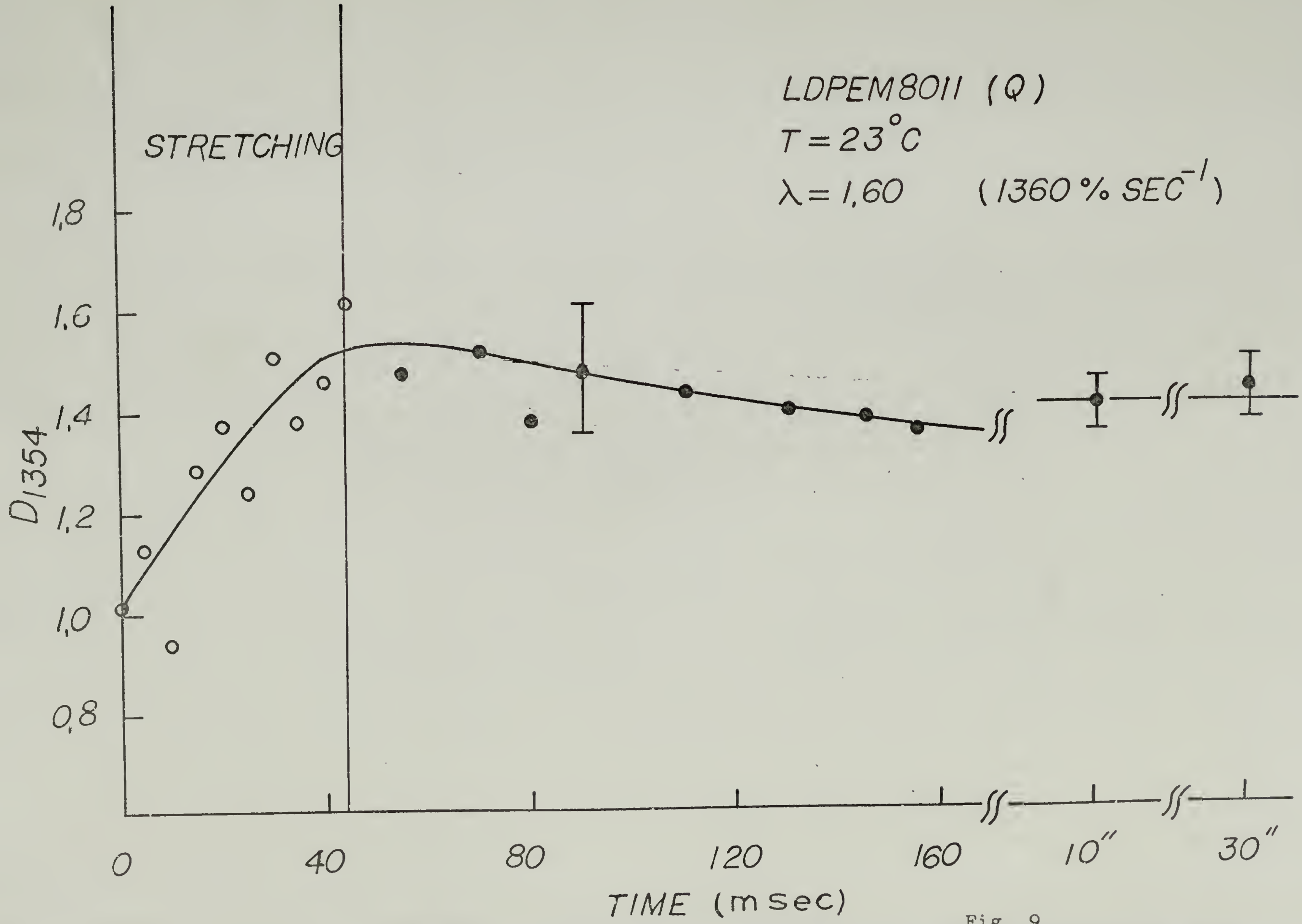
STRETCHING
LDPEM8011 (Q)
T = 23°C
λ = 1,60 (1360 % SEC⁻¹)
D1354
1,8
1,6
1,4
1,2
1,0
0,8
0
40
80
120
160
10″
30″
TIME (msec)

Fig. 9

(a)

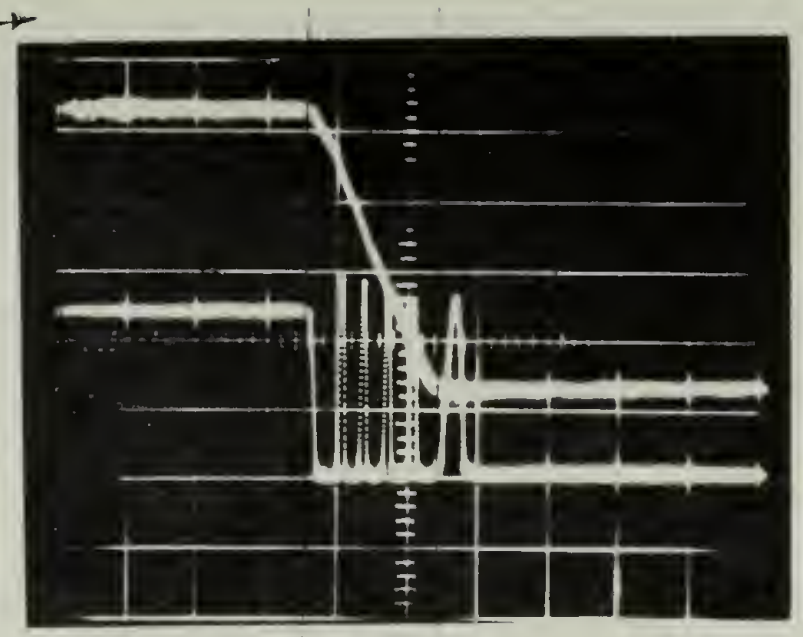

(b)

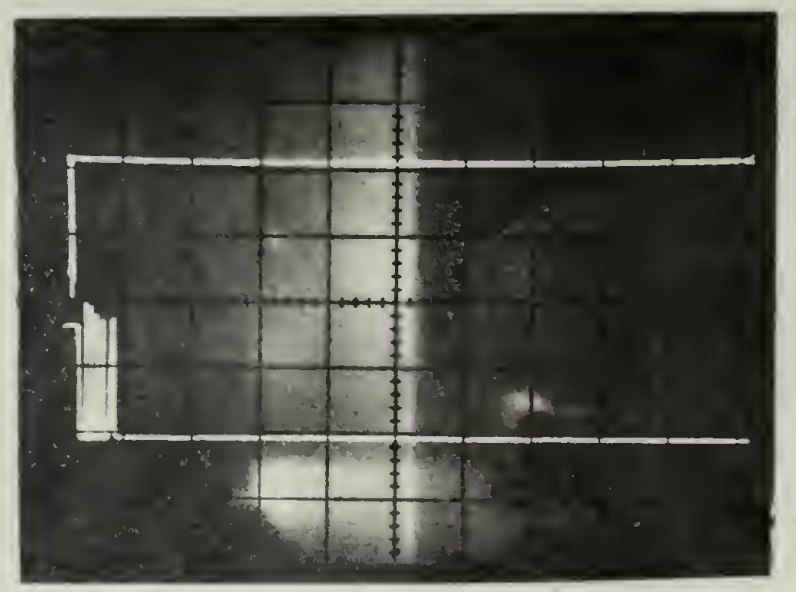

20 msec/div
$\lambda = 1.45$ (1150% sec^{-1})

Fig. 10

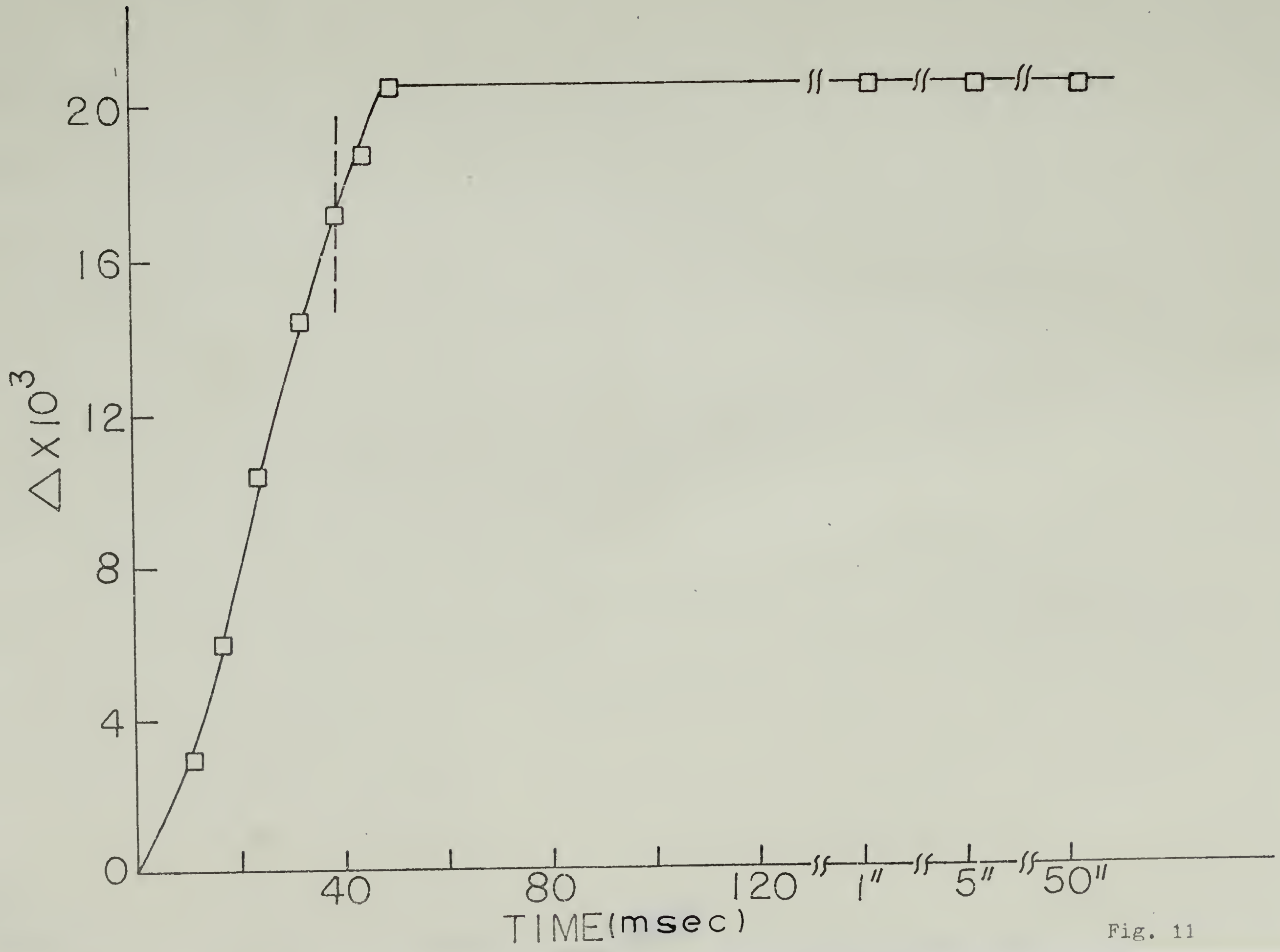

Fig. 11